Homo-Oligomerization of the Activating Natural Killer Cell Receptor NKp30 Ectodomain Increases its Binding Affinity for Cellular Ligands

TECHNISCHE
UNIVERSITÄT
DARMSTADT

GEORG SPEYER HAUS
INSTITUTE FOR TUMOR BIOLOGY
AND EXPERIMENTAL THERAPY

Vom Fachbereich Biologie
der Technischen Universität Darmstadt

zur Erlangung des akademischen Grades eines

Doctor rerum naturalium

genehmigte Dissertation von

Diplom Chemikerin Julia Herrmann
aus Altdöbern

1. Referentin:	Prof. Dr. B. Süß
2. Referent:	Prof. Dr. B. Laube
3. Referent:	Prof. Dr. J. Koch
Tag der Einreichung:	14. August 2014
Tag der mündlichen Prüfung:	07. Oktober 2014

Darmstadt 2014
D 17

Die vorliegende Arbeit wurde unter der Leitung von Prof. Dr. J. Koch in der Arbeitsgruppe "NK Cell Biology" am Georg-Speyer-Haus, Institut für Tumorbiologie und experimentelle Therapie, Paul-Ehrlich-Straße 42-44, 60596 Frankfurt am Main angefertigt.

Die Betreuung seitens der Technischen Universität Darmstadt erfolgte durch Prof. Dr. B. Süß vom Fachbereich Biologie, Schnittspahnstraße 10, 64287 Darmstadt.

Contents

List of Tables

List of Figures

1 Introduction

1.1 Innate and Adaptive Immunity

The immune system of vertebrates is a complex network of biological structures (different organelles, cell types, molecules) and processes within an organism to maintain normal homeostasis and protect against disease[a]. Thus, the most essential attribute of the immune system is to discriminate between self and non-self. Along this line, it is important to mount efficient immune responses since vertebrates permanently encounter harmful environmental influences such as microbes (bacteria, viruses, fungi, and parasites) or degenerated self-cells. These immune responses can be assigned to either the innate or the adaptive (also known as acquired) immunity. Notably, innate immunity already existed in invertebrates and hardly changed during evolution, whereas only jawed vertebrates possess an adaptive immune system [2]. Innate immunity is characterized by fast pathogen control within minutes or hours upon encounter due to pattern recognition. By contrast, jawed vertebrates are able to additionally mount adaptive immune responses within days or weeks due to highly specialized antigen receptors specific to individual pathogens. The generation of an immunological memory furthermore enables a faster and more efficient immune response upon second encounter of the same pathogen. According to their function, the cells of the immune system can be classified to the innate or the adaptive immunity. All leukocytes of the myeloid lineage such as granulocytes (eosinophils, basophils, neutrophils), macrophages, mast cells, and myeloid dendritic cells (DCs) as well as the some cell lines of lymphoid origin such as natural killer (NK) cells and lymphoid DCs are assigned to the innate immune system. B and T lymphocytes belong to the major leukocytes of the acquired immunity due to their adaptability against specific pathogens by somatic recombination of antigen-receptor genes.

The first lines of defense against pathogens are the skin and the mucosal epithelia within airways and gut displaying physical and chemical barriers. Microbes breaching these barriers despite low pH and antimicrobial peptides encouter humoral factors in the blood such as plasma proteins of the complement system or phagocytes leading to an immediate innate immune response. Surface structures of invading bacteria trigger the activation of the zymogens of the complement system inducing a cascade of proteolytic reactions. Beside cytolysis of bacteria via pore formation induced by the membrane attack complex, opsonization with complement fragments leads to the recruitment of and recognition by phagocytes. Upon identification of the site of infection, e.g. macrophages resident in the nearby tissue recognize opsonized bacteria by complement-specific surface receptors and directly engulf the pathogen. Moreover, these macrophages secrete pro-inflammatory cytokines and chemokines to recruit further immune cells such as neutrophils and monocytes out of the blood stream. Notably, during the respiratory burst, phagocytes produce reactive oxygen species (NO, H_2O_2, O_2^-) to intracellularly degrade the pathogen. Additional blood clotting within the blood vessels close to the site of infection reduces the risk of pathogen expansion within the body.

[a] Unless otherwise denoted, "Innate and Adaptive Immunity" was reviewed in Janeway *et al.* (2012) [1].

Beside the complement system, a limited number of invariant, germline encoded receptors (pattern recognition receptors, PRRs) such as mannose receptors, toll-like receptors, or scavenger receptors on macrophages, neutrophils and DCs recognizes pathogen-associated molecular patterns (PAMPs), which are present on many microbes but not on self-cells. These receptors bind simple molecules and regular patterns of molecular structures such as mannose-rich oligosaccharides, peptidoglycans or lipopolysaccharides of the bacterial cell wall. In addition, damage-associated molecular patterns (DAMPs), such as nuclear or cytosolic proteins of the body released outside the cell or exposed on the cell surface, are recognized and induce noninfectious inflammatory immune responses due to tissue injury or tumor formation. Notably, upon viral infection, secretion of cytokines such as interferons is induced, which results in recruitment and activation of NK cells. This granular lymphocyte population of the innate immune system expresses a large repertoire of germline encoded activating and inhibitory receptors. In general, immune cells such as NK cells are self-tolerant due to a prevalence of inhibitory signals transduced upon binding to self-cells. By contrast, interaction with a virus-infected or malignantly transformed cell results in killing of the target cell, which is induced by a shift of the equilibrium to activating signals.

Immature dendritic cells (iDCs) form a crucial link between the innate and the adaptive immune system. Upon phagocytosis of the microbe at the site of infection, iDCs migrate via the lymph system to nearby peripheral lymphoid organs (e.g. lymph nodes, spleen, tonsils, mucosa) for maturation and initiation of the adaptive immune response by presenting antigens to naive T lymphocytes. Antigen presenting cells (APCs) such as DCs as well as T and B lymphocytes represent the major cellular components of the adaptive immune system. Though B and T cells arise both from the bone marrow, B cells mature at their point of origin whereas T lymphocytes migrate to the thymus for education before congregating in the lymphoid tissue throughout the body. As humoral part of the adaptive immunity, the B cell recognizes after clonal selection of the B cell receptor (BCR) a native antigen in its soluble form or presented on the surface of pathogens. Notably, the BCR is a momoneric membrane-anchored immunoglobulin M (IgM). Upon antigen binding, IgM is internalized and the antigen is processed for peptide presentation via major histocompatibility complex (MHC) class II molecules on the B cell surface. These peptide-MHC II complexes are recognized by T helper cells, which secrete chemokines that stimulate further B cell proliferation. Additionally, B cells differentiate to plasma cells secreting large amounts of soluble pentameric IgMs with the same antigen specificity into the bloodstream. In the course of the immune response, further Ig subtypes such as e.g. IgG, IgA or IgE are expressed (class switching), which differ in their constant regions. Antibodies bound to the pathogens surface or their products drastically boost the immune response by i) blocking the access to the host cell (neutralization), ii) induction of antibody-dependent cellular cytotoxicity (ADCC) via CD16 on NK cells, iii) activation of the classical complement pathway by interaction of the first complement protein with the constant regions of the bound antibodies, or iii) opsonization of the pathogens and bacterial toxins, thereby activating other immune cells such as T lymphocytes. After positive selection two main populations of T cells persist, which differ in their surface expression of the coreceptors cluster of differentiation (CD) 4 (T helper cells) and CD8 (cytotoxic T lymphocytes, CTLs). The clonal selection is again accomplished by the T cell receptor (TCR) via antigen-MHC complex recognition. Notably, the TCR is related to immunoglobulins, but displays a quite distinct structure and recognition properties. In contrast to the BCR, the T cell receptor function is dependent on the interaction with its coreceptor CD4 or CD8 for recognition of either MHC class II or MHC class I molecules, respectively. T helper cells bind antigen-MHC II complexes via the TCR

and CD4 molecules resulting in activation of phagocyting macrophages or cytotoxic T lymphocytes (T_H1 cells) and the support of B cell proliferation (T_H2 cells). By contrast, CTLs are activated by recognition of antigen-MHC I complexes on virus-infected or malignantly transformed cells by the TCR in combination with its coreceptor CD8. Upon secretion of enzymes and cytolytic proteins such as granzymes or perforin, lysis of the target cell and apoptosis via the Fas/Fas-ligand system are induced. Notably, some of the active B and T lymphocytes remain within the body as memory cells. On a second encounter with a distinct pathogen, these already differentiated cells can induce a much faster and therefore more effective immune response.

Similar to the T lymphocytes of the adaptive immune system, the NK cells of the innate immunity induce cell lysis and apoptosis of target cells. There are several reports that demonstrate the central role of NK cells in immunosurveillance [3], especially in the control and clearance of malignantly transformed cells [4–8]. Furthermore, the physiological significance of NK cells was supported by observations of patients with NK cell deficiencies suffering from severe recurrent systemic and life-threatening virus infections [9–11]. Beside their cytotoxic effector function, NK cells also act as immune regulators by secreting chemokines or cytokines and directly interacting with other immune cells such as DCs, macrophages, T cells and endothelial cells [12–14], thereby bridging the innate and the adaptive immunity. However, killing by NK cells as well as triggering of an adaptive immune response are affected by diverse immune escape strategies of malignantly transformed or virus-infected cells [15, 16].

1.2 Natural Killer Cells

In the 1970s, natural killer cells were described as large granular lymphocytes of the innate immune system from uninfected individuals with an essential contribution to the initial immune response. Within minutes, these immune cells perform spontaneous cytotoxicity to some nonantibody-coated transformed and tumor cells in culture [17–24]. Moreover, this cytotoxic activity is drastically increased upon exposure to interferon (IFN)-α and IFN-β, Interleukin (IL)-2, IL-12 or IL-15, which are produced by macrophages and DCs in early infections. Beside immunosurveillance of tumors as well as combating microbial and viral infections, NK cells also play important roles in transplantation, autoimmunity, allergic diseases and pregnancy [25]. Therefore, patients without NK cells in the peripheral blood or with functional defectives in NK cell activity are susceptible to severe recurrent systemic and life-threatening infections such as herpesvirus infections, fungal infections, human papilloma virus (HPV)-related cancers, and leukemia [9, 10, 26–28]. Although many diseases, drugs, infections, and physiologic states can affect NK cell numbers, function, or both, NK cell deficiencies are inherent. Therefore, possible therapeutic approaches are e.g. application of prophylactical antiviral drugs [10, 29], stimulation of the immune system, HPV vaccination, induction of NK cell cytotoxic function by systemic administration of cytokine therapies such as IFN-α [30], and hematopoietic stem cell transplantation [31, 32].

NK cells develop from the same progenitor cells as T and B lymphocytes ($CD34^+$ hematopoietic cells) in the bone marrow [33] and differentiate dependent on DCs, monocytes, and neutrophils mainly in thymus, spleen, liver, tonsils and lymph nodes [33–36]. They comprise approximately 10-15 % of peripheral blood lymphocytes, have a life span of two weeks in circulation and can be divided into subsets according to morphology, sites and pathways of development as well as the expression pattern of CD surface molecules [33, 37]. In general, NK cells are characterized by a variable expression of the neural cell

adhesion molecule (CD56) as well as the FcγRIIIA receptor (CD16) [33]. Furthermore, the natural cytotoxicity receptor (NCR) NKp46, which is expressed in man and mice, is strictly NK specific and therefore represents a reliable marker for human (and murine) NK cell identification. Notably, while the NCRs NKp46 and NKp30 are present in both resting and activated NK cells, the third member of the NCR family NKp44 is expressed only in cytokine-activated NK cells [38]. Based on the relative levels of CD56 surface expression, two major subsets can be divided, and related to a distinct localization and function within the body. $CD56^{dim}$/$CD16^{bright}$ cells comprise >90 % of peripheral blood NK cells, secrete low levels of cytokines, and have a high cytolytic capacity [33, 39]. This cytotoxic activity is mediated by CD16, which is a receptor for direct lysis of some targets by human NK cells [40] or can induce ADCC by recognition of antibody-decorated target cells [41]. By contrast, $CD56^{bright}$/$CD16^{dim}$ cells are predominant (>90 %) in secondary lymphoid organs and execute immune regulatory functions. On the one hand, NK cells bridge the innate and the adaptive immunity by killing of immature and tolerogenic DCs to ensure a functional DC population. On the other hand, they secrete cytokines such as tumor necrosis factor (TNF)-α and IFN-γ to enhance inflammation in tissues, induce differentiation of helper T cells into T_H1 and T_H2 cells and maturation of antigen-loaded DCs, which efficiently activate effector cells of the adaptive immune system [42]. In turn, due to IL-2, IL-12 and IL-15 production of DCs upon phagocytosis, NK cells start proliferation, secrete larger amounts of cytokines, have a reduced threshold to trigger NK cell cytotoxicity, and therefore display a higher cytolytic potential [43]. The three main functions of NK cells are: i) promotion and regulation of immunity by costimulatory and regulatory mechanisms upon contact with DCs, macrophages and T cells [12–14], ii) production of chemokines or cytokines such as IFN-γ to promote direct anti-disease effects and to further induce or regulate immunity [13, 14], and iii) mediation of contact-dependent killing of target cells by activating receptors as an innate immune defense or by recognition of IgG-opsonized cells via CD16 to enable ADCC [41, 44, 45]. Interestingly, it was demonstrated in mice that beside their innate properties NK cells also display acquired immunity characteristics. Due to clonal-like expansion upon virus infection, long-lived memory NK cells develop, which reside in multiple organs and are ready for a robust secondary response [46–50].

NK cells share a common killing mechanism with $CD8^+$ T lymphocytes by using effector molecules such as perforin and granzymes for induction of target cell apoptosis via the Fas ligand or TRAIL (TNF-related apoptosis-inducing ligand) signaling [51–53]. However, NK cells perform their effector functions upon recognition of malignantly transformed and virus-infected cells within minutes and without prior sensitization [54–60]. Notably, self-MHC class I molecules are recognized by inhibitory NK cell receptors to restrain the NK cell activity and protect uninfected host cells. Many viruses have evolved strategies to prevent the infected host cell from presenting peptides to virus-specific CTLs by specifically downregulating MHC class I molecules. Therefore, the absence or downregulation of MHC class I molecules (missing-self regocnition) can make infected cells more susceptible to NK cell lysis [61, 62]. Furthermore, activating NK receptors directly recognize particular microbial and viral antigens or stress-induced ligands upon malignant transformation (induced-self recognition) on the target cell surface, thus representing an important paradigm by which NK cells combat disease [45, 63, 64]. Additionally, certain therapeutic monoclonal antibodies (mAbs) can enable NK cell cytotoxicity by ADCC [65]. Other than T lymphocytes, NK cells are able to recognize multiple diverse ligands, which are not related in sequence and structure, despite the expression of invariant surface receptors [66, 67]. The highly sophisticated mechanisms, which regulate the cytolytic activity, mainly depend on the balance between inhibitory and

activating signals transduced into the NK cell upon receptor-ligand interaction [68–70].

NK cell cytotoxicity followes a coordinated series of events: i) contact with the target cell, ii) adhesion, and iii) formation of an activating immunological synapse (IS). The formation of a cleft between the NK cell and its target cell at the interface protects neighboring cells from exposure to lytic effector molecules and is dependent on the ordered rearrangement of molecules within the immune cell [57, 71]. Upon interaction with a healthy cell, the formation of an inhibitory synapse promotes detachment and prevents the release of the granula. Since the IS formation is transient, highly organized and occupies only small areas of the cell surface, more than one IS might form at the same time [71, 72]. Interestingly, only a minority of NK cells (∼20 %) is responsible for the majority of killing events, which is possibly due to their ability of performing multiple consecutive lytic hits [72–74].

1.3 Regulation of Natural Cytotoxicity

NK cell-mediated cytotoxicity is an effective mechanism to protect the host from microbial or virus infections and malignantly transformed cells by induction of target cell apoptosis within minutes upon encounter. To prevent killing of healthy cells, the cytolytic process is tightly regulated by sophisticated mechanisms mainly dependent on the balance between opposite signals from germline-encoded inhibitory and activating natural killer cell receptors (NKRs). These surface receptors accumulate within the immunological synapse to engage respective ligands and mediate downstream signaling (Fig. 1) [60,75,76]. The control mechanism to ensure self-tolerance is mainly based on the recognition of MHC class I proteins by inhibitory NK cell receptors since peptide-presenting MHC class I molecules are present in large numbers on healthy cells (Fig. 1A) [77]. Self-tolerance and functional competence are attained during education in the bone marrow by binding to cognate MHC class I molecules and subsequent signaling via the ITIMs of the inhibitory NK cell receptors [78]. Thus, a prerequisite for the license to kill is the expression of at least one inhibitory surface receptor specific for self-MHC class I molecules [79]. As a consequence of malignant transformation or virus infection, MHC class I molecules are often downregulated leading to NK cell activity due to decreased binding of inhibitory NK cell surface receptors (missing-self recognition [61, 62], Fig. 1B). Additionally, upregulation or expression of stress-induced activating ligands (induced-self recognition [80, 81]) results in NK cell activation despite inhibitory signaling (Fig. 1C). In both conditions, the target cell is eliminiated through NK cell-mediated cytotoxicity or the production of pro-inflammatory cytokines [75].

There are two main categories of inhibitory NK cell surface receptors defined in humans: (i) the CD94/NKG2A heterodimer recognizing human leukocyte antigen (HLA)-E, thereby enabling the NK cell to sense the presence of appropriate expression of MHC class I molecules, since HLA-E mostly binds leader peptides derived from MHC class I proteins [82–84], and (ii) the killer-cell immunoglobulin-like receptors (KIRs), which recognize different allelic groups of HLA-A, -B or -C molecules [85–87] (Fig. 2). Additionally, the leukocyte Ig-like receptors (LILRs), evolutionary related to the KIR family, are also expressed by NK cells and recognizes a large spectrum of classical and non-classical HLA I molecules [88, 89], but their importance for NK cell functions has yet to be defined. Mouse NK cells also have two categories of inhibitory MHC class I receptors: (i) the CD94/NKG2A receptor complex with functions similar to the human receptor [90], and (ii) diverse family members of Ly49 molecules, which are phenotypically unrelated to KIRs [91–93].

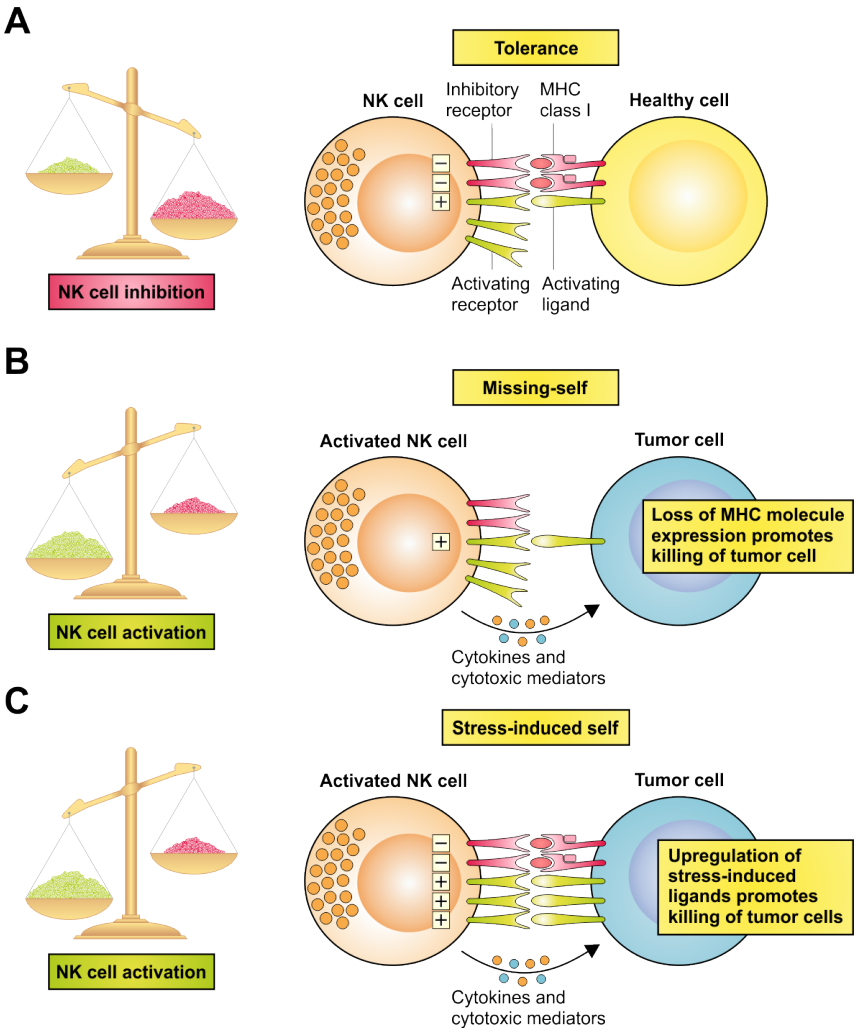

Fig. 1: Recognition of tumor cells by natural killer cells

(A) Natural killer (NK) cells are tolerant to healthy host cells, as the strength of the activating signals they receive on encountering these cells is dampened by the engagement of inhibitory receptors. (B) Tumor cells may lose expression of MHC class I molecules. NK cells become activated in response to these cells, as they are no longer held in check by the inhibitory signals delivered by MHC class I molecule engagement. This is known as ”missing-self” triggering of NK cell activation. (C) In addition, NK cells are selectively activated by ”stressed” cells, which upregulate activating ligands for NK cells and thereby overcome the inhibitory signaling delivered by MHC class I molecules. This is known as ”stress-induced self” triggering of NK cell activation. In both conditions, NK cell activation leads to tumor elimination directly (through NK cell-mediated cytotoxicity) or indirectly (through the production of pro-inflammatory cytokines, such as interferon-γ). (Modified from [75].)

Among human NK cell receptor families, only the KIR gene family is highly polymorphic and comprises 15 genes and two pseudogenes. Related to the function performed, the cytoplasmic domains of KIRs can feature either a short (activating KIRs) or a long (inhibitory KIRs) tail, denoted with “S” or “L” in the nomenclature, respectively. Inhibitory KIRs are type I transmembrane glycoproteins of the Ig superfamily, which are further discriminated by the presence of two (KIR2DL) or three (KIR3DL) Ig domains within their extracellular part followed by a transmembrane region and the characteristic long intracellular tail comprising two immunoreceptor tyrosine-based inhibition motifs (ITIMs, Fig. 2) [67].

Upon ligand binding, the tyrosine within the ITIM consensus sequence (I/L/V/SxYxxL/V, where x represents any amino acid and slashes separate alternative amino acids) becomes phosphorylated by a kinase of the Src (sarcoma) family, which then binds SHP-1 or SHP-2 (Src homology (SH)-2-domain contain-

ing protein tyrosine phosphatase). Subsequent dephosphorylation of molecules involved in downstream signaling of activating receptor results in blocking of activating signal transduction cascades [66, 76, 94].

Independently of their state of activation, NK cells express functional toll-like receptors (TLRs) to rapidly respond invading pathogens and synergize with chemokine- or cytokine-mediated signals to activate NK cell function [95]. As other innate immune cells express the same TLRs, NK cells interact with the same pathogen-derived products such as bacterial lipoprotein, flagellin or single- or double stranded RNA [67]. To overwhelm inhibitory signals, specific activation signals are mainly mediated by the engagement of activating receptors with non-HLA class I proteins, which are expressed upon cellular stress [68].

The major human activating NK cell receptors are the C-type lectin-like superfamily member NKG2D [96] and the heterologous NCRs NKp30, NKp44 and NKp46 (Fig. 2) [97–101]. NKG2D is a type II transmembrane glycoprotein, which is constitutively expressed as homodimer on all mouse and human NK cells, T cells and NKT cells [96, 102]. In humans, this NK cell receptor recognizes stress-induced ligands with structural homology to MHC class I molecules, MICA and MICB (MHC class I chain-related gene A/B) and the ULBPs (unique long 16-binding proteins) [77, 80]. Since activating NK cell receptors do not comprise any functional activating tyrosine phosphorylation motif within their cytoplasmic tail, they associate with signaling adaptor molecules via oppositely charged amino acids within their transmembrane domains (TMDs). NKG2D associates with DNAX-activation protein (DAP) 10 dimers [102], which are phosphorylated at the tyrosine residue within their YINM-motif upon ligand binding. Subsequently, this phosphotyrosine recruits the p85 subunit of PI3K (phosphatidylinositol-3-kinase) or Grb2 (growth factor receptor-bound protein 2) [103], which then transduce the signal intracellularly by the MAP (mitogen-activated protein) kinase cascade and the JAK/STAT (janus kinase/signal transducers and activators of transcription) pathway resulting in NK cell cytotoxicity [70].

Similar to NKG2D, the NCR family members are primarily expressed on NK cells but also on distinct T cell subsets [104–108]. NKp30 and NKp46 are constitutively expressed on all NK cell subsets [109–111], whereas NKp44 is exclusively found on activated NK cells, thus displaying a marker for cytolytic activity of NK cells [60, 112]. Notably, NKp46 is the only NCR with a functional orthologue in mice [113]. The NCRs are a heterogeneous group of type I transmembrane glycoproteins, which belong to the Ig superfamily. They are comprised of an extracellular ligand binding domain (LBD), a flexible membrane proximal stalk region, a TMD and a short cytosolic tail. The ectodomains of the NCRs are phenotypically characterized by two C2-type domains (NKp46), one V-type domain (NKp44) or one I-type domain (NKp30) [114–117]. Due to the lack of intracellular activating signaling motifs, the NCRs have to associate with accessory signaling proteins via oppositely charged amino acid residues within the plasma membrane. Most signaling adaptor proteins contain immunoreceptor tyrosine-based activaing motifs (ITAMs, consensus sequence D/ExxYxx[L/I]X_{6-8}Yxx[L/I]) within their cytoplasmic domains. NKp30 and NKp46 interact with CD3ζ and FcϵRIγ homo- or heterodimers, whereas NKp44 associates with DAP12 homodimers for subsequent activating signal transduction upon ligand engagement [97–100]. The adaptor proteins contain several tyrosines, which are targeted by kinases of the Src family. Upon tyrosine phosphorylation, Syk kinases and ZAP-70 (zeta-chain-associated protein kinase 70) are recruited and activated, which then phosphorylate key enzymes of downstream signaling cascades leading to NK cell activation and the release of cytotoxic granules [76, 118].

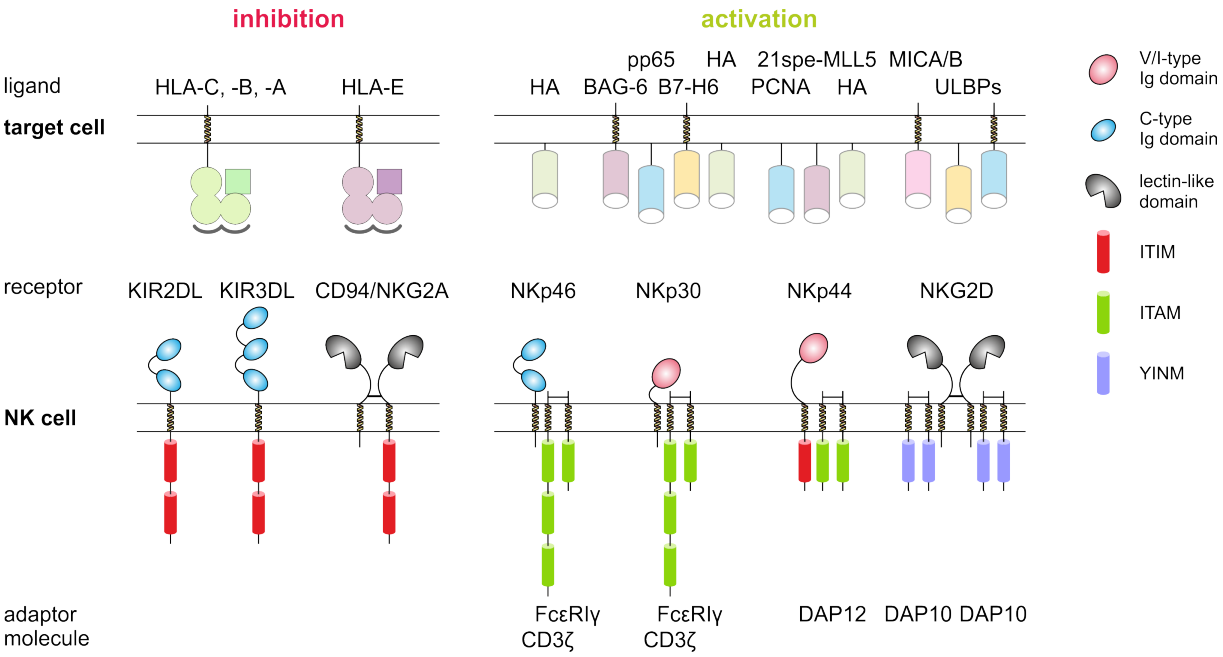

Fig. 2: Human inhibitory and activating natural killer cell receptors and their corresponding ligands

This is a simplified representation of the major natural killer cell receptors (NKRs) and their identified ligands involved in natural cytotoxicity. The major inhibitory NKRs are the KIR family members KIR2DL and KIR3DL, and the heterodimer CD94/NKG2A. KIRs belong to the Ig superfamily and possess two (KIR2DL) or three (KIR3DL) Ig-like domains in their extracellular region. Their cognate ligands are the human leukocyte antigen (HLA)-A, -B or -C molecules. CD94/NKG2A belongs to the C-type lectin family, contains two lectin-like domain in its extracellular region and binds to HLA-E molecules. All inhibitory receptors have two immunoreceptor tyrosine-based inhibitory motifs (ITIMs) within their cytoplasmic tail for inhibitory signal transduction. The major activating NKRs are NKG2D and the members of the natural cytotoxicity receptor (NCR) family NKp30, NKp44 and NKp46. The NCRs belong to the Ig superfamily and contain either one (NKp30 and NKp44) or two (NKp46) Ig-like domains in their extracellular regions. All of the NCRs bind to viral hemagglutinins (HA). Additionally, the human cytomegalovirus (HCMV) tegument protein pp65, the BCL2-associated anthanogene 6 (BAG-6) and a structural homologue of the B7 family (B7-H6) were described as ligands for NKp30. Recently, the proliferating cell nuclear antigen (PCNA) and the mixed-lineage leukemia-5 variant 21spe-MLL5 were discovered as novel ligands for NKp44 on tumor cells. The disulfide-linked homodimer NKG2D belongs to the C-type lectin family, contains two lectin-like domains in its extracellular region and binds to MICA and MICB (MHC class I chain-related gene A/B) and to ULBPs (unique long 16-binding proteins). Since none of the activating receptors possesses functional activating tyrosine phosporylation motifs within their cytoplasmic tail, they associate with signaling adaptor molecules via oppositely charged amino acids in their transmembrane domains. NKp30 and NKp46 associate with a CD3ζ/FcϵRIγ heterodimer, whereas NKp44 interacts with DNAX-activation protein (DAP) 12. These adaptor molecules contain immunoreceptor tyrosine-based activating motifs (ITAMs) within their cytoplasmic tails. By contrast, NKG2D uses a different pathway of activation with two DAP10 molecules, which possesses two YINM motifs for activating signal transduction. (Modified from [119].)

Several studies demonstrate the diversity of NCR ligands and report of cellular and pathogen-derived ligands, which are not expressed on healthy cells. All NCRs recognize heparin/heparan sulfate [120–124] and bacterial structures [125–127]. Furthermore, NKp44 and NKp46 bind to viral hemagglutinins (HAs) of influenza virus, sendai virus or new castle disease virus, whereas vaccinia virus HA is an other ligand of NKp30 and NKp46 [63, 128–132]. Additionally, the human cytomegalovirus (HCMV) tegument protein pp65, the BCL2-associated anthanogene 6 (BAG-6, also known as BAT3) and the B7 family member (B7-H6) were described as ligands for NKp30 [133–136]. Recently, the proliferating cell nuclear antigen (PCNA) and the mixed-lineage leukemia-5 variant 21spe-MLL5 were discovered as novel ligands for NKp44 on malignantly transformed cells [137, 138]. Moreover, a so far unknown cellular NKp44L is

expressed during HIV-1 infection that correlates with both progression of $CD4^+$ T cell depletion and the increase of viral load [139]. However, due to the broad impact of the NCRs on immunosurveillance, it is likely that there are other cellular ligands, especially for NKp46, which remain to be discovered [67, 140].

NK cell activity largely depends on the natural cytotoxicity receptors NKp30 (NCR3, CD337), NKp44 (NCR2, CD336) and NKp46 (NCR1, CD335), as reduced NCR expression is associated with different forms of cancer such as acute myeloid leukemia (AML) [141–144]. Especially, reduced NKp30 expression has clinical implications in patients with AML [144–146], cervical cancer, and high grade squamous intraepithelial lesions (HGSIL) [141] as well as gastrointestinal sarcoma (GIST) [147]. Longitudinal analyses of AML patients showed that an NKp30 downregulation on NK cells during leukemia development resulted in an $NKp30^{dull}$ phenotype leading to an impaired natural cytotoxicity against leukemia cells [144–146]. The same effect together with enhanced HPV-16 infections due to NKp30 downregulation was observed in cervical cancer and HGSIL patients. Moreover, due to a retrospective analysis of GIST patients, the reduced survival was associated with a predominant expression of an immunosuppressive splice variant of NKp30 (isoform c) [147]. Within the activating NK cell receptors, NKp30 displays a unique role since it is the only receptor involved in tumor immunosurveillance by NK cells as well as shaping the adaptive immune response, primarily by the NK-DC cross-talk [148, 149].

1.4 Natural Cytotoxicity Triggering Receptor 3 (NCR3, NKp30)

In 1999, Pende and colleagues identified a novel triggering receptor of roughly 30 kDa, which is involved in natural cytotoxicity [101]. Despite any sequence homology between NKp30, NKp44 and NKp46, these surface proteins have been grouped to the family of natural cytotoxicity receptors according to the following features: (i) their expression is mostly restricted to NK cells, (ii) monoclonal antibody (mAb)-mediated crosslinking triggers and mAb-mediated masking inhibits NK cell cytotoxicity, and (iii) they specifically recognize non-HLA ligands [150]. Identified as third member of the NCR family, NKp30 was also named natural cytotoxicity receptor 3 (NCR3).

From an evolutionary point of view, the three NCR family members putatively emerged in another order with NKp46 (NCR1) as first and NKp44 (NCR2) as latest member, while NKp30 evolved in between. This progressive NCR appearance may reflect an increase in the complexity and the fine-tuning of the innate immune response [151], further confirmed by the fact that most orthologues of NK cell receptors are not present beyond the mammalian branching [152]. While NKp30 is expressed as a functional protein on human and primate (*Macaca fascicularis* and *Pan troglodytes*) NK cells, chimpanzee NK cells express NKp30 only upon activation similar to NKp44 [101, 151, 153]. Moreover, NKp30 was found to be expressed as a functional protein on certain rat NK cell subsets [154–156]. However, in mice it is only a pseudogene leading to a truncated non-functional protein with exception of the mouse strain *Mus caroli*, where NKp30 was found as a potential soluble protein [157–159].

The human NKp30 gene *1C7* is located on chromosome 6. According to phylogenetic analyses of different mammalian species, the nucleic acid sequences of the NKp30 genes are highly conserved except in exon 4, which encodes the intracellular domain. In humans, there are six transcript variants (a-f) resulting from alternative splicing of exon 2 (encoding the extracellular domain) and exon 4 (Fig. S1, see the appendix 7.1.1) [160], thus differing in the length of the extracellular and intracellular domains.

Isoforms a-c consist of the complete ectodomain of NKp30, whereas isoforms d-f lack amino acids 66-99[b] within the ligand binding domain of NKp30. Additionally, the intracellular domains of the isoforms differ in their length and amino acid composition. Isoforms a and e contain the longest (36 aa) and isoforms b and d harbor the shortest (12 aa) intracellular domain, whereas the cytoplasmic tail of the isoforms c and f consist of 25 aa. All splice variants are translated into cell surface proteins with different expression levels and tissue distribution. Notably, the NKp30a-c containing the longest extracellular domain are most abundant and ubiquitously distributed [159]. According to their structural heterogeneity, the transcripts adopt different NK cell functions. Activation by isoforms a and b results in stimulation of the immune system, whereas NKp30c is immunosuppressive [147]. Although the first functional NKp30 protein identified was isoform b (190 aa), the ”canonical” sequence refers to the longest isoform a (201 aa).

NKp30 is a 201 amino acids (aa) long type I transmembrane protein comprised of (i) a leader sequence for plasma membrane targeting, (ii) an extracellular ligand binding domain (LBD), (iii) a flexible membrane-proximal stalk domain connecting the LBD to (iv) a single TMD, which contains a positively charged arginine, and (v) a short cytoplasmic tail without tyrosine phosphorylation motif (Fig. 3A and B). For signaling, NKp30 associates with CD3ζ and FcϵRIγ homo- or heterodimers (although there is no published experimental evidence regarding an association between NKp30 and FcϵRIγ) [101, 161]. This interaction is mediated by the arginine (R143) within the TMD of NKp30 and a negatively charged aspartic acid residue within the TMD of the adaptor molecules.

NKp30 plays a pivotal role for the elimination of parasites, malignantly transformed and virus infected cells, and even some healthy cells [140]. While there are still some unknown ligands [3], the following NKp30 ligands were identified: (i) heparin/heparan sulfate molecules [120, 123, 124], (ii) the viral HCMV tegument protein pp65 [133], (iii) viral hemagglutinins [130], (iv) *Pf* EMP1 (*Plasmodium falciparum* erythrocyte membrane protein 1) as well as (i) the cellular proteins B7-H6 [134] and BAG-6 [135, 136]. Beside its influence on NK cell cytotoxicity against pathogens and non-self cells, NKp30 also displays immune regulatory functions. By binding of NKp30 to BAG-6, which is expressed on the plasma membrane of immature (but not mature) DCs, NK-dependent activation of DCs mediated by TNF-α and IFN-γ release as well as NK cell killing of immature DCs are induced [135, 149]. BAG-6 is a multifunctional protein mainly located in the nucleus, which is known to be involved in p53-DNA repair and apoptosis [162, 163]. However, it is also present in various tissues, on the plasma membrane of malignantly transformed cells as well as on exosomes and as a soluble protein upon cellular stress [136, 164]. A recent study identified a sub-domain within the C-terminal half of BAG-6 as inhibitory ligand being sufficient for receptor docking and inhibition of NKp30-dependent NK cell cytotoxicity. Therefore, soluble BAG-6 represents an important tumor antigen and might be part of a tumor immune escape strategy reminiscent of the NKG2D ligands ULBP2 and ULBP3 [164–166]. Furthermore, all three NCRs recognize viral hemagglutinins [63, 128, 130, 132]. These interactions are particularly affected by *N*-linked glycosylation of NKp30 or sialic acids attached to galactose of NKp46 and NKp44 [130, 167]. However, whereas the interaction of NKp46 with hemagglutinins of the poxvirus family (such as vaccinia virus) results in NK cell activation, binding to NKp30 leads to NK cell inhibition [130]. Another known viral ligand for NKp30 leading to NK cell inhibition is the HCMV tegument protein pp65, which is not secreted but released from infected cells upon lysis. Despite a direct receptor-ligand interaction, there is a mechanistical difference to BAG-6-dependent inhibition of NK cell cytotoxicity. Whereas BAG-6 inter-

[b] Amino acid annotation refers to the ”canonical” NKp30 sequence (isoform a) depicted in Fig. 3.

acts with the NKp30 ectodomain, pp65 splits up the interaction between NKp30 and its adaptor proteins, thus decreasing the activation state of the NK cell [133, 168]. Another pathogen-derived NKp30 ligand is *Pf*EMP1, which is presented on the surface of erythrocytes infected with the parasite *Plasmodium falciparum* [125]. Additionally, there are controversial experimental studies discussing heparin/heparan sulfate as potential NCR ligands with varying binding affinities dependent on receptor glycosylation or as coreceptors in complex with other ligands [120, 123, 124, 169]. Most important for structural analyses and investigation of key features for ligand binding and signaling so far is the second cellular ligand B7-H6 [117, 170]. It is a type I transmembrane glycoprotein that is believed to be exclusively expressed upon tumor transformation [134]. Similar to the ligands of the other major activating NK cell receptor NKG2D, B7-H6 ectodomain shedding from the surface of different tumor cells by metalloproteases was demonstrated as tumor immune escape mechanism [171]. However, by contrast to NKG2D, the known ligands for NKp30 are not related in sequence and structure.

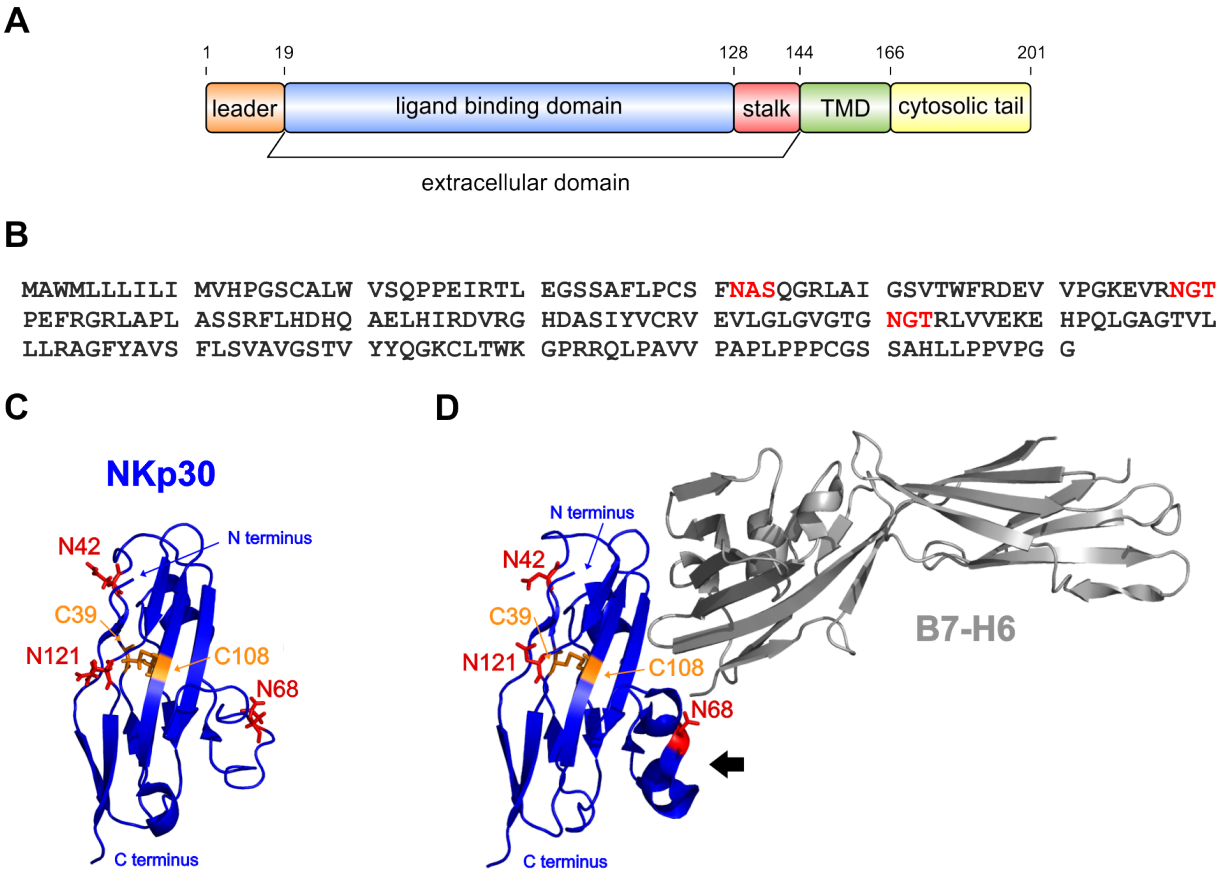

Fig. 3: Domain organization, amino acid sequence and crystal structure of human NKp30

(A) Domain organization of NKp30. The NKp30 amino acid sequence can be subdivided into five domains: a leader sequence for plasma membrane targeting (orange), an extracellular ligand binding domain (blue), a flexible stalk domain (red) connecting the ligand binding domain with a single transmembrane domain (TMD, green), and a short cytosolic tail (yellow). The first amino acid of each domain is indicated[c]. (B) Amino acid sequence of NKp30 isoform a. Consensus sequence for *N*-linked glycosylation motifs are depicted in red. (C) Unbound crystal structure of the NKp30 ectodomain containing amino acids 18-130 (blue); PDB 3NOI[d]. (D) B7-H6 (gray)-bound crystal structure of the NKp30 ectodomain containing amino acids 19-130 (blue); PDB 3PV6[d]. The arrow indicates the area that undergoes reorganization due to ligand binding. (C/D) Cystein residues forming a disulfide bond (orange) and asparagines within consensus motifs for *N*-linked glycosylation (red) are depicted with corresponding amino acid annotation. N- and C-termini are indicated. Structural illustrations were made with PyMol software. (Modified from [119].)

In 2011, the ligand binding domain of NKp30 (corresponding to the isoforms a-c) was crystallized in an unbound (PDB: 3NOI [116]) and a B7-H6-bound state (PDB: 3PV6 [117]), which is unique amongst the NCR family (Fig. 3C and D). Consistently, both crystal structures display an I-type Ig-like domain. However, upon interaction with B7-H6, there is a slight conformational reorganization of the NKp30 LBD underneath the binding pocket. Since NKp30 ligands are diverse, it remains unclear whether the identified interface displays a common binding site or whether other ligands would occupy different binding pockets.

The ligand binding domain of NKp30 is *N*-linked glycosylated at three asparagines (N42, N68 and N121, Fig. 3B). Surprisingly, binding studies with glycosylation-deficient variants of NKp30 revealed that engagement of NKp30 and B7-H6 is mainly dependent on glycosylation of N42, which is located outside the binding pocket. Moreover, glycosylation of N42 and N68 is essential for efficient intracellular signaling. By contrast, for binding of NKp30 to BAG-6 N68 was critical, whereas glycosylation at positions N42 and N121 had less impact. On the one hand, the degree of glycosylation could provide a switch to modulate the ligand binding properties of NKp30, and on the other hand this further suggests the presence of different ligand binding sites [170]. Beside *N*-linked glycosylation, the same study identified the flexible stalk domain of NKp30 as an important feature for ligand recognition and related signaling. The stalk domain is rich in hydrophobic amino acids, which might promote the formation of NKp30 oligomers, thereby leading to an increased apparent affinity for the ligand due to increased avidity. This idea could at least partially explain the observation that some cell lines are killed by NK cells but fail to bind NKp30-Ig proteins without a functional stalk domain [40, 128, 170].

1.5 Oligomerization of Natural Killer Cell Receptors

NK cell activity largely depends on the NCRs NKp30, NKp44 and NKp46. Mechanistic details are still unknown on how these germline-encoded surface receptors are able to recognize multiple ligands like viral hemagglutinins or proteins from cellular, bacterial or parasitical origin, which are not related in sequence or structure [63, 125, 172]. As suggested from the structures of the NCRs, monovalent receptor ligand interactions are expected. In 2003, Augugliaro and colleagues demonstrated that there would be a selective cross-talk between the NCRs. A polyclonal NK cell population was stimulated with anti-NKp30 monoclonal antibodies and cell lysates were immunoprecipitated not only with the NKp30 mAb, but also with the other anti-NCR antibodies. Notably, anti-NKp44 and anti-NKp46 mAb stimulated NK cells were analysed in the same way. Controls included immunoprecipitates with mAb directed to CD16 or p50.3 (KIR2DS4) molecules that are known to associate with CD3ζ and DAP12, respectively. Surprisingly, individual activation of one NCR led to tyrosine phosphorylation of the adaptor molecules of all NCRs, whereas the same adaptor proteins associated with other receptors were not activated [173]. If nearby adaptor molecules became phosphorylated due to close neighborhood of kinases within the immunological synapse or if a specific interaction between the NCRs amplified activating signals, remained unclear. However, NK cell killing requires the formation of a complex immunological synapse between the target cell and the NK cell that is highly organized in time and space [44, 174, 175], which argues for concerted lateral interactions of receptors at the plasma membrane of the NK cell engaged with a target cell.

[c] The amino acid sequence refers to accession number O14931 found at the UniProt database (http://www.uniprot.org).
[d] The PDB accession number refers to the RCSB Protein Data Bank (http://www.rcsb.org).

Beside complex formation of different NCRs to amplify activating signaling, there are also speculations on NKp46 homo-oligomerization on the NK cell surface to enable multivalent interactions with trimeric influenza virus hemagglutinin complexes [63]. Hemagglutinin neuraminidases of newcastle disease virus form dimers and tetramers on the viral surface. Therefore, oligomeric ligand structures suggest homo- or heteromeric NCR association [176–178], but to date there is no evidence for preformed or ligand-induced receptor oligomerization. Notably, it is known that IL-2 activation of NK cells leads to an up-regulation of NCR expression, especially NKp44 and NKp30 (Fig. S2), and thereby increases cellular cytotoxicity [68, 179–184].

Beside variable ligand binding affinities due to modulation of the glycosylation state of the NKp30 ligand binding domain, formation of *de novo* binding interfaces by homo-oligomerization could be an additional mechanism how the NK cell is able to recognize multiple different ligands. Many laboratories have shown that cell surface detection of NKp30 on NK cell lines or primary NK cells with NKp30-specific monoclonal antibodies gives rise to a dotted rather than a homogeneous plasma membrane staining suggesting preformed clusters of NKp30. Interestingly, there are further hints from a structural point of view suggesting a self-association of the NCR ectodomains. In this context, Bezouška and co-workers [185] have shown that a fraction of the NKp30 ectodomain expressed in *Escherichia coli* forms oligomers as detected by size exclusion chromatography. However, the authors have not analyzed this fraction of NKp30 in more detail. Moreover, although both structures show NKp30 as a monomer, Sun and co-workers [116] observed a crystallographic dimer of NKp30 arguing for a potential intrinsic capability of NKp30 to oligomerize. Similarly, Bordo and co-workers [114] discussed a saddle-shaped dimer within the crystal structure of NKp44 that is exclusively expressed on activated NK cells. Along these lines, Porgador and co-workers [186] showed that the membrane proximal domain of NKp46 (NKp46D2) mediates ligand-induced dimerization of NKp46 in the membrane and contributes to NKp46-mediated lysis by NK cells. By contrast, the activating NK cell receptor NKG2D assembles a composite binding site for the interaction with its corresponding cellular ligands by homo-dimerization [187, 188]. Similarly, the natural killer cell receptor KIR2DL2 dimerizes with both receptor ectodomain molecules in the same orientation via two different interaction sites. Therefore, Snyder and co-workers [189] suggested formation of KIR2DL2 oligomers within the plasma membrane by alternating dimerization. In addition, self-assembly of activating KIR2DS1 was shown to be concentration-dependent. Although local concentration and oligomerization might even be fostered by ligand-induced assembly of a condensed immunological synapse between the NK cell and its target cell, receptor oligomerization prior to ligand induction would most likely lead to faster activation of signaling.

1.6 Objectives

Previous studies have shown that dimerization or oligomerization of NK cell surface receptors is a potent mechanism to achieve functional receptor complexes with enhanced ligand binding affinity or *de novo* formed interaction sites [189, 190]. Furthermore, Augugliaro and co-workers described a selective cross-talk between NKp30 and the other NCRs NKp44 and NKp46 within the plasma membrane of NK cells [173, 189]. They could demonstrate that an engagement of NKp30 resulted in efficient amplification of the activation signaling cascade associated with the other NCRs. However, in this study, the exact mechanism of signal transmission between the NCRs and whether this interaction could cause structural

rearrangements of the NKp30 ectodomains remained unclear. Therefore, the aim of this thesis was to investigate self-assembly of the human activating NK cell receptor NKp30 as possible key mechanism to enhance its ligand binding affinity for corresponding ligands by increased avidity.

1. Dotted patterns in confocal immunofluorescence analyses of anti-NKp30 antibody decorated primary NK cells suggest individual NKp30 complex formation on the surface of natural killer cells. Notably, NKp30 surface expression as well as the fluorescence intensity of the dotted pattern increase upon cytokine activation of the NK cells. So far, it remains unknown whether NKp30 alone is able to form functional receptor complexes or whether NKp30 complex formation is due to association with other upregulated surface receptors such as NKp44 and NKp46. In this thesis, different mammalian or insect cells should be investigated to identify a suitable expression host for the generation of a minimal NK cell mimic. Full-length NKp30 alone or in combination with NKp44 and NKp46 should be constitutively expressed in a non-immunological background to enable the individual characterization of NKp30 self-association or NCR assembly as well as a putative cross-stimulation in more detail.

2. In general, binding interfaces between NK cell surface receptors and their ligands are located within the extracellular part of the receptor. Suggesting an NKp30 self-assembly or functional cross-talk between all NCRs, it is evident to recombinantly express the ectodomain of NKp30 for molecular investigations. For this purpose, expression and purification schemes should be established to obtain large amounts of soluble NKp30 ectodomain proteins. As basis for *in vitro* studies to functionally characterize as well as to perform structural analyses, the NKp30 ligand binding domain should be produced in *E. coli*. Another approach should be based on the expression of soluble and post-translationally modified NKp30 ectodomain proteins produced in insect cells to investigate the oligomeric state of NKp30. Furthermore, the ligand binding capacity as well as the structure of the oligomeric species should be characterized by size exclusion chromatography, ELISA and electron microscopy.

3. In a previous study, bivalent NKp30 ectodomain proteins fused to a human IgG1-Fc part were used to elucidate the NKp30 stalk domain as well as the glycosylation status as key features to modulate NKp30-dependent NK cell cytotoxicity [170]. Accordingly, in this thesis, insect cell-derived NKp30 ectodomain proteins with and without the stalk domain should be generated. Furthermore, an antibody, which recognizes a specific epitope within the ligand binding domain, should be purified from rabbit blood serum after peptide-immunization. The antigen-specificity should be verified by peptide SPOT arrays, whereas the suitability of the anti-NKp30 antibody for biochemical and cellular applications should be demonstrated by immunoblot analyses, ELISA as well as cell decoration assays. This novel anti-NKp30 antibody, which binds to both NKp30 ectodomain variants to the same extent, should allow for the investigation of the individual impact of the stalk domain on ligand binding activity and oligomerization of NKp30.

2 Materials and Methods

2.1 Materials

2.1.1 Chemicals, Consumables and Instruments

Unless otherwise denoted, all used chemicals were obtained in p. a. quality from the companies AppliChem (Darmstadt, Germany), Carl Roth GmbH (Karlsruhe, Germany), Life Technologies (Carlsbad, California, USA), Lonza (Basel, Switzerland), Roche (Mannheim, Germany) or Sigma-Aldrich GmbH (Saint Louis, Missouri, USA). The cell culture chemicals were obtained from Carl Roth GmbH (Karlsruhe, Germany), Life Technologies (Carlsbad, California, USA), Mirus Bio (Madison, Wisconsin, USA) or PAA (Cölbe, Germany). All consumables used for cell culture, molecular biology and protein biochemistry were obtained from the companies Bio-Rad Laboratories (Hercules, California, USA), Carl Roth GmbH (Karlsruhe, Germany), Greiner Bio-One (Kremsmünster, Austria), Merck Millipore (Darmstadt, Germany), Miltenyi Biotec (Bergisch Gladbach, Germany), Sarstedt AG & Co (Nümbrecht, Germany), Thermo Fisher Scientific Inc. (Waltham, Massachusetts, USA) or Whatman (Dassel, Germany). Unless otherwise denoted, all instruments were common lab equipment.

2.1.2 Enzymes, Inhibitors, Antibiotics, and Additives

Enzyme	**Supplier**
Cre recombinase	New England Biolabs
DreamTaq polymerase	Thermo Fisher Scientific
FastAP thermo sensitive alkaline phosphatase	Thermo Fisher Scientific
FastDigest restriction endonucleases	Thermo Fisher Scientific
Phusion polymerase	Thermo Fisher Scientific
PNGase F	New England Biolabs
Protein Deglycosylation Mix	New England Biolabs
T4 DNA ligase	Thermo Fisher Scientific

Inhibitor	**Supplier**
complete protease inhibitor cocktail	Roche
tunicamycin	Sigma-Aldrich

Antibiotic	**Supplier**
Ampicillin	AppliChem
Chloramphenicol	Roth
Gentamycin	Life Technologies
Kanamycin	Roth
Penicillin/Streptomycin	Life Technologies
Spectinomycin	AppliChem
Tetracycline	AppliChem
Zeocin	Life Technologies

Additive	**Supplier**
FCS	PAA
X-gal	Sigma-Aldrich
L-Glutamine	PAA
HEPES	Life Technologies
Human serum	PAA
Interleukin-2 (Proleukin S)	Novartis
IPTG	Roche
β-Mercaptoethanol	Life Technologies
NEAA	Life Technologies
Pluronic F-68	Sigma-Aldrich

2.1.3 Antibodies, Isotype Controls and Cell Staining Reagents

Primary Antibody/Isotype Control		**Supplier**
anti-mouse CD4, GK1.5, APC-conjugated	(rat IgG2b)	eBioscience
anti-His, HIS-1, HRP-conjugated	(mouse IgG2a)	Sigma-Aldrich
anti-gp64 (FastPlax Titer Kit)	(mouse IgG)	Merck Millipore
anti-human MICA, polyclonal	(goat IgG)	R&D Systems
anti-human NKp30, polyclonal	(goat IgG)	R&D Systems
anti-human NKp30, peptide immunized (NH_2-CPGKEVRNGTPEFRGR-COOH)	(rabbit IgG)	BioScience/PepScience, this thesis
anti-human NKp30, 210845	(mouse IgG2a)	R&D Systems
anti-human NKp30, P30-15	(mouse IgG1)	BioLegend
anti-human NKp30, P30-15, APC-conjugated	(mouse IgG1)	BioLegend
anti-human NKp30, Z25, PE-conjugated	(mouse IgG1)	Beckman Coulter
anti-human NKp44, Z231, PE-conjugated	(mouse IgG1)	Beckman Coulter
anti-human NKp46, BAB281, PE-conjugated	(mouse IgG1)	Beckman Coulter

Secondary Antibody		**Supplier**
anti-goat IgG, HRP-conjugated	(donkey IgG)	Jackson ImmunoResearch
anti-human IgG-Fc, DyLight649-conjugated	(goat IgG)	Jackson ImmunoResearch
anti-human IgG-Fc, HRP-conjugated	(goat IgG)	Sigma-Aldrich
anti-mouse IgG, HRP-conjugated	(goat IgG)	Sigma-Aldrich
anti-mouse IgG, Alexa546-conjugated	(goat IgG)	Life Technologies
anti-mouse IgG, Alexa647-conjugated	(goat IgG)	Life Technologies
anti-rabbit IgG, HRP-conjugated	(goat IgG)	Sigma-Aldrich
anti-rabbit IgG, APC-conjugated	(goat IgG)	Life Technologies

Isotype Control	**Supplier**
mouse (BALB/c) IgG1, MOPC-21, APC-conjugated	BioLegend

Cell Staining	**Supplier**
DAPI	AppliChem

2.1.4 Kits

Kit	**Supplier**
Gel Filtration Calibration Kit LMW and HMW	GE Healthcare
GeneJET Gel Extraction Kit	Thermo Fischer Scientific
GeneJET Plasmid Miniprep Kit	Thermo Fisher Scientific
NK Cell Isolation Kit, human	Miltenyi Biotec GmbH
NucleoBond Xtra Midi/Maxi	Macherey-Nagel

2.1.5 Bacterial Strains and Culture Media

Strain	**Genotype**	**Supplier**
BL21(DE3) [191]	B strain derivative: F- *omp*T *hsdS*$_B$ (r_B-m_B-)*gal dcm* (DE3)	Life Technologies
BW23473 [192–194]	K-12 strain derivative: Δ*lac*-169 *rpo*S(Am) *rob*A1 *cre*C510 *hsd*R514 *uid*A(Δ*Mlu*I)::*pir*$^+$ *endA*$_{BT333}$ *rec*A1	Life Technologies
DH5α [195, 196]	K-12 strain derivative: F-Θ80*lac*ZΔM15 *lac*ZYA-) Δ(*arg*F U169 *rec*A1 *and*A1 *hsd*R17 (r_K-m_K+) *pho*A *sup*E44 λ- *thi*-1 *gyr*A96 *rel*A1	Life Technologies
DH10EmBacY [197, 198]	B strain derivative: F-*mcr*A Δ(*mrr-hsd*RMS-*mcr*BC) Θ80*lac*ZΔM15 Δ*lac*X74 *rec*A1 *end*A1 *ara*D139 Δ(*ara leu*)7697 *gal*U *gal*K *rps*L *nup*G λ- *ton*A + helper plasmid for Tn7 transposon enzyme + *yfp* reporter gene (Kan^{R}Tet^{R}Cam^R)	I. Berger[e]
Origami 2 (DE3) [199, 200]	K-12 strain derivative: Δ(ara-leu)7697 Δ(*lac*X74) Δ*pho*A *Pvu*II *pho*R *ara*D139 *ahp*C *gal*E *gal*K *rps*L F'[*laq*+ *laq*Iq *pro*] (DE3) *gor*522::Tn10 *trx*B (Str^{R}Tet^R)	Life Technologies

For the cultivation of bacteria, *lysogeny broth* (LB) medium [201] and agar with the low salt formulation of Lennox [202] were purchased from Carl Roth. The cryo culture medium is made of 50 % (v/v) LB medium and 50 % (v/v) sterile glycerol.

2.1.6 Cell Lines and Culture Media

2.1.6.1 Unmodified Cell Lines

Unless otherwise denoted, all used cell lines were either purchased from the American Type Culture Collection (ATCC), the *Deutsche Sammlung von Mikroorganismen und Zellkulturen* (DSMZ) or the European Collection of Cell Cultures (ECACC).

Cell Line	Characteristics	Supplier
HEK293	human embryonic kidney cells	ATCC (CRL-1573)
A5	murine $CD4^+$ T cell hybridoma, 14.3.d TCR β chain	A. Diefenbach [203]
Ba/F3	murine pro B cells	DSMZ (ACC 300)
High Five (Hi5)	ovarian tissue cells from *Trichoplusia ni*	Life Technologies
Jurkat	human T cell lymphoma	ATCC (TIB-152)
MiaPaCa-2	human pancreatic cancer cells	ATCC (CRL-1420)
NK-92MI	human natural killer cells	ATCC (CRL-2408)
*Sf*9	ovarian tissue cells from *Spodoptera frugiperda*	Life Technologies

2.1.6.2 Gene-Modified Cell Lines

Cell Line	Characteristics	Supplier
HEK293-30-His	codon-optimized human NKp30 full-length protein containing a C-teminal His-tag; GFP protein expression under IRES control	this thesis
HEK293-mock	no NKp30 insertion; GFP protein expression under IRES control	this thesis
HEK293T/T17	human embryonic kidney cells, large T antigen expression	ATCC (CRL-11268)
HEK293T-30-His	codon-optimized human NKp30 full-length protein containing a C-teminal His-tag; GFP protein expression under IRES control	this thesis
HEK293T-mock	no NKp30 insertion; GFP protein expression under IRES control	this thesis
A5-GFP	GFP protein expression under control of three NF-AT binding sites of the *Il*2 gene	A. Diefenbach [203, 204]
A5-30FL-His	codon-optimized human NKp30 full-length protein containing a C-terminal His-tag; GFP protein expression under control of three NF-AT binding sites of the *Il*2 gene	K. Oberle[f]/ J. Hartmann [170]

[e]The *E. coli* strain DH10EmBacY was kindly provided by I. Berger, European Molecular Biology Laboratory, Grenoble, France.

Cell Line	Characteristics	Supplier
A5-mock	no NKp30 insertion; GFP protein expression under control of three NF-AT binding sites of the *Il*2 gene	K. Oberle[f]/ J. Hartmann [170]
Ba/F3-B7-H6	human B7-H6 full-length protein; intracellular GFP expression; puromycin resistance	A. Cohnen[g] [170]
Ba/F3-mock	no B7-H6 insertion; intracellular GFP expression; puromycin resistance	A. Cohnen[g] [170]
Jurkat-30-His	codon-optimized human NKp30 full-length protein containing a C-teminal His-tag; GFP protein expression under IRES control	this thesis
Jurkat-mock	no NKp30 insertion; GFP protein expression under IRES control	this thesis

2.1.6.3 Culture Media

DMEM

Dulbecco's modified Eagle medium (DMEM) was supplemented with 25 mM glucose, 10 % (v/v) FCS (PAA), 50 U/ml penicillin, 50 μg/ml streptomycin, 10 μg/ml gentamicin, 5.5 mM L-glutamine, 1 mM sodium pyruvate, 0.1 M MEM non-essential amino acids, 10 mM HEPES, and 5.5 mM β-mercaptoethanol. DMEM was used for the cultivation of A5-GFP cells.

Express Five

Express Five SFM (Gibco) was supplemented with 18 mM L-glutamine and used for the cultivation of Hi5 insect cells.

Insect Xpress

Insect Xpress medium (Lonza) was supplemented with 0.2 % (v/v) Pluronic F-68 and used for the cultivation of *Sf* 9 insect cells.

RPMI-1

RPMI 1640 was supplemented with 10 % (v/v) FCS (PAA), 100 U/ml penicillin, 100 μg/ml streptomycin, and 2 mM L-glutamine. RPMI-1 was used for the cultivation of HEK293, HEK293T and Jurkat cells.

RPMI-2

RPMI 1640 was supplemented with 10 % (v/v) FCS (PAA), 100 U/ml penicillin, 100 μg/ml streptomycin, 2 mM L-glutamine, and 5.5 mM β-mercaptoethanol. RPMI-2 was used for the cultivation of Ba/F3 cells.

RPMI-3

RPMI 1640 was supplemented with 15 % (v/v) FCS (PAA), 100 U/ml penicillin, 100 μg/ml streptomycin, and 2 mM L-glutamine. RPMI-3 was used for the clonal isolation of gene-modified HEK293 cells.

[f] The cell line was kindly generated by K. Oberle in the lab of A. Diefenbach, Institute of Medical Microbiology and Hygiene at the University of Freiburg, Germany.

[g] The cell line was kindly generated and provided by A. Cohnen in the lab of C. Watzl, Leibniz Research Centre for Working Environment and Human Factors, Dortmund, Germany.

RPMI-4

RPMI 1640 was supplemented with 10 % (v/v) FCS (PAA), 10 % (v/v) horse serum (PAA), 100 U/ml penicillin, 100 μg/ml streptomycin, 1 mM sodium pyruvate, and 4 mM L-glutamine. RPMI-4 was used for the cultivation of NK-92 cells.

X-Vivo

X-Vivo10 was supplemented with 5 % (v/v) human serum (PAA), and 1000 U/ml IL-2. X-Vivo was used for the cultivation of primary human natural killer cells.

2.1.7 Buffers

Unless otherwise denoted, all buffers and solutions were prepared with deionized water, and the pH was adjusted with HCl or NaOH.

Buffer/Solution	**Formulation**	
Agarose Gel Electrophoresis (2.3.6)		
TAE Buffer	40 mM 1 mM 1.14 % (v/v)	Tris EDTA acetic acid
EtBr solution	10 % (w/v)	ethidium bromide (EtBr)
EtBr stain	1 % (v/v)	EtBr solution in TAE buffer
Competent Bacteria (2.2.2)		
TFB I buffer	30 mM 10 mM 50 mM 100 mM 15 % (v/v) adjust to pH 6.8	potassium acetate $CaCl_2$ $MnCl_2$ RbCl glycerol with acetic acid
TFB II buffer	10 mM 75 mM 10 mM 15 % (v/v) adjust to pH 6.8	MOPS $CaCl_2$ RbCl glycerol with KOH
Deglycosylation Assay (2.5.4)		
10x glycoprotein denaturation buffer	5 % (v/v) 400 mM	SDS DTT
10x G7 reaction buffer	500 mM adjust to pH 7.5	Na_3PO_4
10x NP-40	10 % (w/v)	NP-40

Buffer/Solution	Formulation	
ELISA (2.5.9)		
PBS-T	0.05 % (v/v)	Tween20 in PBS
7.5 % BSA/PBS	7.5 % (w/v)	albumin fraction V in PBS
1 % BSA/PBS	1 % (w/v)	albumin fraction V in PBS
Flow Cytometry (2.4.12), CLSM (2.4.13), Signaling Reporter Assay (2.4.15)		
FACS buffer	2 % (v/v)	FCS in PBS
5 % BSA/FACS	5 % (w/v)	albumin fraction V in FACS buffer
FACS-fix	1 % (w/v)	formalin in FACS buffer
mounting medium	4.8 g 12 g 12 ml 24 ml	Mowiol 4-88 glycerol H_2O 0.2 M Tris pH 8.5
DAPI stain	10 μg/ml	DAPI in mounting medium
Immunoblotting (2.5.7), Peptide Spot Array (2.5.8)		
transfer buffer	192 mM 25 mM 20 % (v/v)	glycine Tris EtOH (pure)
TBS-T	50 mM 150 mM 0.1 % (v/v)	Tris NaCl Tween20
blocking buffer	2 % (w/v)	milk powder in TBS-T
coumarin solution	90 mM	*p*-coumaric acid in DMSO
luminol solution	250 mM	luminol in DMSO
ECL I solution	100 mM 396 μM 5 mM	Tris pH 8.5 coumarin luminol
ECL II solution	100 mM 0.02 % (v/v)	Tris pH 8.5 H_2O_2

Buffer/Solution	Formulation	
Immunoprecipitation (2.5.5)		
PBS-T	0.01 % (v/v)	Tween20 in PBS
PBS-TT	0.5 % (v/v)	Triton X-100 in PBS-T
DB storage buffer	0.01 % (v/v) 0.09 % (w/v)	Tween20 NaN_3 in PBS
lysis buffer	20 mM 150 mM 2 mM 10 mM 10 % (v/v) 10 % (v/v) 1 mM	Tris pH 7.4 NaCl EDTA NaF Triton X-100 glycerol PMSF
lysis-T buffer	0.01 % (v/v)	Tween20 in lysis buffer
elution buffer (IP)	100 mM 0.01 % (v/v) 0.5 % (v/v) adjust to pH 2.7	glycine Tween20 Triton X-100
Inhibition of Glycoprotein Synthesis (2.4.11)		
tunicamycin	1 mg/ml	tunicamycin in DMSO
Isolation of Primary NK Cells (2.4.10)		
PBS/EDTA	2 mM	EDTA in PBS
Protein Purification (2.5.1), Size Exclusion Chromatography (2.5.2)		
dialysis buffer (IMAC)	50 mM 500 mM 10 mM adjust pH 8.0	Tris NaCl imidazole at 4 °C
wash buffer (IMAC)	50 mM 500 mM 20 mM adjust pH 8.0	Tris NaCl imidazole at 4 °C
elution buffer (IMAC)	50 mM 500 mM 250 mM adjust pH 8.0	Tris NaCl imidazole at 4 °C
regeneration buffer (IMAC)	100 mM 500 mM	EDTA pH 8.0 NaCl
Ni^{2+} solution (IMAC)	100 mM	$NiSO_4$

Buffer/Solution	Formulation	
Protein Purification (2.5.1), Size Exclusion Chromatography (2.5.2)		
Tris buffer	50 mM 150 mM adjust pH 8.0	Tris NaCl at 4 °C
PI mix	0.5 tablet/ml in PBS or	complete protease inhibitor cocktail Tris buffer
collection buffer (protein A)	1 M	Tris pH 8.8
elution buffer (protein A)	100 mM	glycine pH 2.7
regeneration buffer (protein A)	20 mM 0.05 % (w/v) adjust pH 7.4	NaH_2PO_4 NaN_3 20 mM Na_2HPO_4
storage buffer (protein A)	0.01 % (v/v)	NaN_3 in PBS
SDS-PAGE (2.5.6)		
SDS running buffer	25 mM 192 mM 0.1 % (w/v)	Tris glycine SDS
5x SDS sample buffer (non-reducing)	300 mM 10 % (w/v) 50 % (v/v) 0.005 % (w/v)	Tris pH 6.8 SDS glycerol bromophenolblue
5x SDS sample buffer (reducing)	300 mM 10 % (w/v) 50 % (v/v) 0.005 % (w/v) 25 % (v/v)	Tris pH 6.8 SDS glycerol bromophenolblue β-mercaptoethanol
Transfection of Mammalian Cells (2.4.5), Lentiviral Particle Production (2.4.7)		
TA-trans	18 mM	polyethylenimine, branched in H_2O (cell culture grade)
TA-glucose	5 % (w/v)	glucose in H_2O (cell culture grade)
sucrose solution	20 % (w/v)	sucrose in PBS
RPMI/Gln	2 mM	L-glutamine in RPMI 1640
RPMI/FCS	100 U/ml 100 μg/ml 5 % (v/v)	penicillin streptomycin FCS (PAA) in RPMI/Gln

2.1.8 Oligonucleotides

All oligonucleotides (primers) were synthesized by the company Sigma-Aldrich, and their calculated melting temperatures (T_M) are indicated. The numbers refer to an intralaboratory primer database. Nucleotides matching the annealing sequence are written in capital letters, whereas introduced nucleotides are indicated by lowercase. Endonuclease recognition sites within the primer sequences are underlined. Introduced His-tags are double underlined. Start and stop codons are depicted in bold.

No.	Name	Sequence (5'→3')	T_M [°C]
001	NKp30 seq for	AGGGAAGGAGGTGAGGAATG	64.2
002	NKp30 seq rev	TAGAATCCAGCCCGAAGGAG	65.3
010	NKp44 seq for	GAATCTACCGCCCTTCTGAC	62.5
011	NKp44 seq rev	AGGGACAGGGATGGTAGATG	62.7
015	NKp46 seq for	CCTGGACCCGAAGTGATCTC	65.9
016	NKp46 seq rev	CCAGGCATGGTTGTTATAGG	61.7
038	pET16b seq for	AGCCAACTCAGCTTCCTTTC	62.4
039	pET16b colony rev	GGGAATTGTGAGCGGATAAC	63.1
041	pFastBac1 seq for	ATTCATACCGTCCCACCATC	63.3
043	pFastBac1 colony rev	TAGGCTCAAGCAGTGATCAG	60.7
049	pGEX-4T-1-F	TATAGCATGGCCTTTGCAGG	57.3
050	pGEX-4T-1-R	CGGGAGCTGCATGTGTC	57.6
052	pIRES-GFP seq for	TGACGCAAATGGGCGGTAGG	72.1
053	pIRES-GFP seq rev	AAGCGGCTTCGGCCAGTAAC	69.4
059	pMal-p5X seq for	GATGTCCGCTTTCTGGTATG	62.0
060	pMal-p5X seq rev	CGTTCACCGACAAACAACAG	64.2
061	LeGO-iG2 seq for	ATGACCCTGCGCCTTATTTG	65.9
064	MultiBac colony for	CGGGTGATCAAGTCTTCGTC	64.6
074	StuI NKp30 for	aaggcctt**ATG**GCCTGGATGCTGTTGCTCATATC TTG	81.5
075	NKp30-His STOP XbaI rev	gctctaga**TCA**GTGATGGTGATGGTGATGGTGAT GGTGATGGC	85.0
077	BamHI NKp44 for	cgcggatcC**ATG**GCCTGGCGAGCCCTACACCCAC TGCTACTG	91.5
079	NKp44-His STOP XbaI rev	gctcta**gaT**CAGTGATGGTGATGGTGATGGTGAT GGTGATGC	83.9
080	BamHI NKp46 for	cgggatcC**ATG**TCTTCCACACTCCCTGCCCTGCT CTG	87.3
081	NKp46-His STOP StuI rev	aaggcctt**TCA**GTGATGGTGATGGTGATGGTGAT GGTGATGAAGAG	85.8
117	EcoRI NKp30LBD$_{tr}$ for	ccggaattcCTCTGGGTGTCCCAGCCCCCTGAG	86.3
118	NKp30LBD$_{tr}$ STOP XhoI rev	ccgctcgag**tca**CCCTGTCCCGACACCAAGGCCC AGCAC	92.0

No.	Name	Sequence (5'→3')	T_M [°C]
119	NKp30LBD$_{tr}$ STOP HindIII rev	cccaagctt**tca**CCCTGTCCCGACACCAAGGCCC AGCAC	89.7
153	SacII/NdeI/BamHI NKp30opt for	tccccgcgggggaattccatatgcgcggatcc**AT** **G**GCCTGGATGCTGCTGCTGATTCTGATTATG	96.6
236	NKp30opt-His STOP PacI/NdeI/SacII rev	tccccgcgggggaattccatatgccttaattaa**t** **ca**gtgatggtgatggtgatggtgatggtgatgTC CGCCTGGGACTGGGGG	97.3
249	NKp30opt-His STOP NotI rev	ttttccttttgcggccgctttttttcctt**tca**gtg atggtgatggtgatggtgatggtgatgTCCGCCT GGGACTGGGGGCAGCAGATGAGCAGATGAGCC	99.4

2.1.9 Plasmids and Proteins

2.1.9.1 Plasmids

Unless otherwise denoted, all plasmids used were amplified using the *Escherichia coli* (*E. coli*) strain DH5α. Indicated numbers refer to an intralaboratory plasmid database. The corresponding plasmid maps (7.2) are provided in the appendix.

No.	Expression Plasmid (*E. coli*)	Selection	Supplier
101	pUC57-NKp30-His	Amp^R	GenScript
102	pUC57-NKp44-His	Amp^R	GenScript
103	pUC57-NKp46-His	Amp^R	GenScript
108	pUC57-NKp30LBD$_{tr}$-TEV-His	Amp^R	GenScript
109	pUC57-His-TEV-NKp30LBD$_{tr}$	Amp^R	GenScript
114	pUC57-gp67ss-NKp30LBD-Stalk-TEV-His	Amp^R	GenScript
117	pUC57-NKp30opt	Amp^R	GenScript
127	pUC57-gp67ss-NKp30LBD-TEV-His	Amp^R	GenScript
1901	pET16b-His-TEV-NKp30LBD$_{tr}$	Amp^R	this thesis
1902	pET16b-NKp30LBD$_{tr}$-TEV-His	Amp^R	this thesis
2105	pGEX-4T-1-NKp30LBD$_{tr}$	Amp^R	this thesis
3301	pMAL-p5X-NKp30LBD$_{tr}$	Amp^R	this thesis

No.	Expression Plasmid (Mammalian Cells)	Selection	Supplier
48	pIRES2-EGFP	Kan^R/GFP	Clontech
4805	pIRES2-NKp30opt-His-EGFP	Kan^R/GFP	this thesis
813	pcDNA3.1-TNFss-B7-H6-hIgG1-Fc	Amp^R/Neo^R	A. Cohnen[h]

[h]The plasmid was kindly provided by A. Cohnen in the lab of C. Watzl at the Leibniz Research Centre for Working Environment and Factors, Dortmund, Germany.

No.	Expression Plasmid (Lentiviral Particles)	Selection	Supplier
49	LeGO-iG2	Amp^R/GFP	[205]
4901	LeGO-NKp30opt-His-iG2	Amp^R/GFP	this thesis

No.	Packaging Plasmid (Lentiviral Particles)	Selection	Supplier
30	pCMV-ΔR8.91	Amp^R	[206]
31	pMD2.G	Amp^R	[207]

No.	Expression Plasmid (Insect Cells)	Selection	Supplier
308	pFastBac1-gp67ss-NKp30LBD-Stalk-TEV-His	Amp^R/$Gent^R$	this thesis
315	pFastBac1-gp67ss-NKp30LBD-TEV-His	Amp^R/$Gent^R$	this thesis

No.	Multigene Transfer Vector (Insect Cells)	Selection	Supplier
401	pFL-NKp30-His	Amp^R/$Gent^R$	J. Hartmann[i]
501	pSPL-NKp44-His[j]	$Spec^R$	S. Beyer[k]
601	pUCDM-NKp46-His[j]	Cam^R	J. Hartmann[i]
2007	pFL-NKp30-His/pSPL-NKp44-His/ pUCDM-NKp46-His	Amp^R/$Gent^R$/ $Spec^R$/Cam^R	J. Hartmann[i]

2.1.9.2 Proteins

Indicated numbers refer to the plasmid haboring the corresponding DNA sequence. The theoretical molecular mass (MW) of monomeric proteins without secretion sequence or post-translational modification are denoted. The corresponding protein sequences (7.3) are listed in the appendix.

No.	Expression in *E. coli*	MW kDa	Supplier
1901	His-TEV-NKp30LBD$_{tr}$	13.9	this thesis
1902	NKp30LBD$_{tr}$-TEV-His	13.9	this thesis
2105	GST-NKp30LBD$_{tr}$	37.9	this thesis
3301	MBP-NKp30LBD$_{tr}$	58.1	this thesis
	MICA*04-His	32.0	S. Weil[l]

No.	Expression in Mammalian Cells	MW kDa	Supplier
4805/4901	NKp30opt-His	22.9	this thesis
813	B7-H6-Ig	52.9	this thesis[h]

[i] The plasmid was kindly provided by J. Hartmann in the lab of J. Koch at the Georg-Speyer-Haus, Frankfurt am Main, Germany.
[j] This multigene transfer vector was amplified using the *E. coli* strain BW23473.
[k] The plasmid was kindly provided by S. Beyer in the lab of J. Koch at the Georg-Speyer-Haus, Frankfurt am Main, Germany.
[l] The protein was kindly provided by S. Weil in the lab of J. Koch at the Georg-Speyer-Haus, Frankfurt am Main, Germany.

No.	Expression in Insect Cells	MW kDa	Supplier
401	NKp30-His	22.9	this thesis[i]
501	NKp44-His	32.0	this thesis[k]
601	NKp46-His	35.9	this thesis[i]
2007	NKp30-His/NKp44-His/NKp46-His		this thesis[i]
308	NKp30LBD-Stalk-His	16.6	this thesis
315	NKp30LBD-His	15.0	this thesis

2.2 Methods of Microbiology

2.2.1 Cultivation of Bacteria

All of the used *E. coli* strains were either K-12 strain or B strain derivatives. K-12 strains were originally developed as cloning hosts and mainly used for plasmid amplification *in vitro*. They are usually *rec*A mutants. The *rec*A mutation keeps *E. coli* hosts from recombining homologous sequences of DNA in genomic clones. In contrast, for gene overexpression *E. coli* strains with *rec*A function (e.g. BL21 (DE3)) were used.

E. coli cultures were grown in LB medium overnight at 37 °C and 200 rpm in a bacteria shaker. For the cultivation on LB agar plates, the bacteria suspension was applied onto the plates prior to overnight incubation at 37 °C. To select for resistent bacteria, the LB medium or LB agar was supplemented with the relevant antibiotics and additives listed in Tab. 1 [198].

Tab. 1: Antibiotics and additives for selection of resistant bacteria

Antibiotic/Additive	Stock concentration	End concentration	Solvent
Ampicillin	100 mg/ml	100 μg/ml	H_2O
Chloramphenicol	34 mg/ml	30 μg/ml	70 % (v/v) EtOH
Gentamycin	50 mg/ml	10 μg/ml	H_2O
Kanamycin	50 mg/ml	50 μg/ml	H_2O
Spectinomycin	50 mg/ml	50 μg/ml	H_2O
Tetracycline	10 mg/ml	10 μg/ml	70 % (v/v) EtOH
Zeocin	100 mg/ml	100 μg/ml	H_2O
IPTG	280 mg/ml	120 μg/ml	H_2O
X-gal	20 mg/ml	500 μg/ml	DMSO

Cultivated bacteria suspensions can be stored for up to one week and bacteria plates for up to one month at 4 °C. For long-term storage of bacterial strains glycerol stocks are recommended. 1.5 ml of bacteria suspension were centrifuged for 5 min at 500x g. The bacteria cell pellet was resuspended in 1 ml of cryo culture medium consisting of 50 % (v/v) sterile glycerol and 50 % (v/v) LB medium supplemented with the respective antibiotics and stored at -80 °C.

2.2.2 Generation and Transformation of Rb-Competent Bacteria

The easiest way to amplify plasmid DNA is by cellular replication in *E. coli*. Via a process called transformation bacteria take up surrounding plasmid DNA. Since this process does not occur naturally in *E. coli* strains, the bacteria have to be pretreated to become competent for the introduction of foreign DNA. Chemically competent bacteria were generated by the $CaCl_2$/RbCl method [208]. 100 ml of LB medium were inoculated with 2 ml of an *E. coli* suspension culture and incubated at 37 °C and 200 rpm in a bacteria shaker until reaching an OD_{600}=0.4-0.6. After incubation on ice for 10 min, the culture was centrifuged (2,000x g, 10 min, 0 °C). The bacteria cell pellet was resuspended in 7.5 ml of sterile filtered, ice cold TFB I buffer and incubated for 1 h on ice. After centrifugation (3,000x g, 10 min, 0 °C), the bacteria pellet was resuspended in 2 ml of sterile filtered, ice cold TFB II buffer. 50 μl aliquots were shock frozen in liquid nitrogen and stored at -80 °C.

To transform Rb-competent *E. coli*, one aliquot of bacteria was thawed on ice. Approximately 50 ng of plasmid DNA or 10 μl of ligation reaction (2.3.3) were added and mixed gently prior to incubation on ice for 20 min. After a heat shock (90 s, 42 °C), the cells were incubated on ice for 3 min. 500 μl of LB medium were added to the transformation reaction and incubated at 37 °C and 600 rpm for 60 min. The bacteria suspension was plated on LB agar supplemented with the respective antibiotics and additives (Tab. 1) and incubated overnight at 37 °C.

2.3 Methods of Molecular Biology

2.3.1 Plasmid Preparation

Plasmid DNA was prepared from bacteria suspension cultures using the GeneJET Plasmid Miniprep kit (mini preparation) or the NucleoBond Xtra Midi/Maxi kit (midi or maxi preparation). The basic principle of these kits is the alkaline lysis of the bacteria cells, neutralization and subsequent precipitation of proteins and genomic DNA. Plasmid DNA bound to silica gel membranes in the presence of a high concentration of chaotropic salts is eluted by water or an appropriate buffer.

For purification of low amounts of plasmid DNA (mini preparation), 3 ml of LB selection medium (Tab. 1) were inoculated with one bacteria colony and incubated overnight at 37 °C and 200 rpm. 2 ml of bacteria suspension were pelleted (14,000x g, 30 s, 4 °C) and used for the preparation of plasmid DNA according to the manufacturer's instructions. The plasmid DNA was eluted with 50 μl of pre-warmed H_2O (50 °C).

To extract larger amounts of plasmid DNA (midi or maxi preparation) 100-1000 ml of LB selection medium (Tab. 1) were inoculated with one bacteria clone or a 2 ml preparative culture of one bacteria clone prior to overnight incubation at 37 °C and 200 rpm. The suspension culture was harvested (9000x g, 5 min, 4 °C), and the bacteria cell pellet was used for the plasmid preparation according to the manufacturer's instructions. Precipitated and dried plasmid DNA was reconstituted in 0.1-1 ml of pre-warmed H_2O (50 °C). Throughout this thesis, all plasmid DNA preparations were performed according to the high copy protocol. The concentration of isolated plasmid DNA was determined photometrically (2.3.8).

2.3.2 Polymerase Chain Reaction

The polymerase chain reaction (PCR) is a method to exponentially and specifically amplify deoxyribonucleic acid (DNA) sequences from different origins such as plasmid or genomic DNA *in vitro* [209, 210]. This method is based on the ability of thermostable DNA polymerases to synthesize a new strand of DNA by using single stranded DNA (template) and oligonucleotides (primers), complementary to the offered template DNA, as an initiation point. Under appropriate reaction conditions, the primers hybridize to the template DNA, and the DNA polymerase amplifies the DNA fragment in sense (forward) or anti-sense (reverse) orientation by adding nucleotides onto the pre-existing 3'-OH group of the oligonucleotides. PCR is a thermal cycling process that starts with denaturation by high temperature, which leads to the dissociation of the double-stranded DNA. Lowering to moderate temperature enables the primers to hybridize to the complementary single-stranded template DNA (annealing). Elongation of the annealed primers is initiated by an increase to the working temperature of the DNA polymerase. Since the elongation products are also used as templates in the next cycles, there is an exponential increase of amplified DNA fragment mainly dependent on the number of cycles. By respective primer engineering (e.g. introduction of endonuclease restriction sites, point mutations, or addition of nucleotides) PCR can further be used to alter the amplified sequence or to append new sequence information. Moreover, colony PCR is an application by which to quickly determine if bacteria clones contain the gene of interest by investigating bacterial cells instead of plasmid DNA. Since it is not necessary to amplify the whole gene of interest and moreover, one to five colonies can be used as template in one reaction, it is possible to analyze huge sets of clones in a short time.

In this thesis, the thermostable DNA polymerases *Phusion* and *DreamTaq* were used. The *Phusion* polymerase is able to reduce the error rate by its 3'-5' exonuclease activity (also known as proof-reading) and was therefore used for preparative DNA amplification for subsequent cloning. In contrast, the *DreamTaq* polymerase has no proof-reading activity and was used for analytical approaches. For optimal reaction conditions, the annealing temperature and the elongation time had to be adjusted for each individual PCR dependent on the primer melting temperature (T_M) and the extension time, respectively. Generally, an annealing temperature about 5 °C below the lowest primer melting temperature T_M (at best at 55 °C) was used. The elongation time depended on the length of the amplified DNA fragment and the used DNA polymerase (*Phusion*: 15 s/kb at 72 °C; *DreamTaq*: 1 min/kb at 72 °C). The deoxyribonucleosidtriphosphate (dNTP) mix containing 10 mM of each dNTP (dATP, dCTP, dGTP, dTTP) was obtained from Thermo Scientific, all buffers and additives were supplied with the respective polymerase. After the preparative amplification for subsequent cloning, the DNA fragments were purified using the GeneJET Gel Extraction kit (2.3.7.2), and the DNA concentration of the isolated fragments was determined photometrically (2.3.8). To investigate a huge set of clones by colony PCR, subsequent colony PCRs were performed using one to five colonies within one reaction. After identification of reaction mixtures containing the PCR fragments of the desired size, the corresponding colonies were again analyzed using only one colony per reaction to obtain single positive clones. PCR reactions containing the amplified DNA fragment were identified by agarose gel electrophoresis (2.3.6). Standard reaction mixtures and PCR protocols for preparative (Tab. 2) and analytical PCR (Tab. 3) are depicted.

Tab. 2: Standard reaction mix and protocol for a PCR with the *Phusion* polymerase

Reaction mix		**PCR protocol**			
20 ng	template DNA				
0.5 μM	forward primer	98 °C	30 s		initial denaturation
0.5 μM	reverse primer	98 °C	10 s		denaturation
0.2 mM	dNTP mix	55 °C	15 s	35x	annealing
3 % (v/v)	DMSO	72 °C	30 s		elongation (for <2 kb)
2.5 mM	$MgCl_2$	72 °C	5 min		final elongation
1x	GC buffer	16 °C	∞		
0.02 U/μl	*Phusion*				
ad to 100 μl	with H_2O				

Tab. 3: Standard reaction mix and protocol for a colony PCR with the *DreamTaq* polymerase

Reaction mix		**PCR protocol**			
1-5	bacterial colonies				
1 μM	forward primer	98 °C	30 s		initial denaturation
1 μM	reverse primer	98 °C	10 s		denaturation
0.2 mM	dNTP mix	55 °C	15 s	25x	annealing
2.5 % (v/v)	DMSO	72 °C	30 s		elongation (for <500 bp)
1x	green buffer	72 °C	5 min		final elongation
0.025 U/μl	*DreamTaq*	16 °C	∞		
ad to 25 μl	with H_2O				

2.3.3 Enzymatic Restriction, Dephosphorylation, and Ligation of DNA

2.3.3.1 Enzymatic Restriction of DNA

Restriction endonucleases are able to bind DNA and are commonly classified into three types. These differ in their structure and whether they cut their DNA substrate at their recognition site, or if the recognition and cleavage sites are separated from one another. For molecular cloning, conventional type II restriction endonucleases are used since they recognize and cleave the DNA at the same site. Most of these enzymes only require Mg^{2+} as cofactor. The recognition sites are usually palindromic, 4-8 nucleotides in length and differ for every restriction endonuclease. According to the position of the double-stranded cut, restriction endonucleases can produce either blunt ends (no nucleotide overhang) or sticky ends (with nucleotide overhang). Unless otherwise noted, all DNA restrictions were performed according to the manufacturer's instructions using FastDigest restriction endonucleases from Thermo Scientific. All used enzymes with their recognition sequences and cutting patterns are listed in Table 4.

Tab. 4: Recognition sequences and cutting patterns of applied type II restriction endonucleases
Cutting sites are indicated by vertical lines.

Enzyme	Recognition Sequence
*Bam*HI	5'…G|GATCC…3' 3'…CCTAG|G…5'
*Eco*RI	5'…G|AATTC…3' 3'…CTTAA|G…5'
*Hin*dIII	5'…A|AGCTT…3' 3'…TTCGA|A…5'
*Not*I	5'…GC|GGCCGC…3' 3'…CGCCGG|CG…5'
*Sal*I	5'…G|TCGAC…3' 3'…CAGCT|G…5'
*Stu*I	5'…AGG|CCT…3' 3'…TCC|GGA…5'
*Xba*I	5'…T|CTAGA…3' 3'…AGATC|T…5'
*Xho*I	5'…C|TCGAG…3' 3'…GAGCT|C…5'

For a preparative restriction reaction (Tab. 5), 1-5 μg of DNA were used. In general, double digests were performed using the supplied FastDigest buffer. The reaction mixtures were incubated for 25 min at 37 °C, followed by enzyme inactivation for 10 min at 80 °C. The restriction samples were either first subjected to agarose gel electrophoresis (2.3.6) or directly purified using the GeneJET Gel Extraction kit (2.3.7). For analytical restriction reactions (Tab. 5), 0.5-1 μg of DNA were used. For all enzyme combinations, the supplied FastDigest green buffer was applied. The reaction mixtures were incubated for 10 min at 37 °C, followed by enzyme inactivation for 10 min at 80 °C. The restriction samples were analyzed by agarose gel electrophoresis (2.3.6).

Tab. 5: Standard restriction reaction for preparative and analytical applications
For preparative reactions the 10x FastDigest buffer and for analytical reactions the 10x FastDigest green buffer were used.

	Preparative Restriction	Analytical Restriction
DNA	1-5 μg	0.5-1 μg
restriction buffer	5 μl	2 μl
restriction enzyme I	2.5 μl	0.5 μl
restriction enzyme II	2.5 μl	0.5 μl
ad with H_2O	to 50 μl	to 20 μl

2.3.3.2 Enzymatic Dephosphorylation of DNA

Enzymatic restriction of DNA generates phosphorylated 5' ends and hydroxylated 3' ends. For ligation of two DNA fragments (2.3.3.3) only one phosphorylated 5' end is required. To enhance ligation specificity by reducing the recircularisation capability of the vector DNA, the 5' ends of the linearized vector DNA were enzymatically dephosphorylated by an alkaline phosphatase. The phosphorylated 5' end for DNA ligation is provided by the insert DNA. A standard dephosphorylation mix consisted of 1-5 μg of linearized vector DNA, 5 μl of 10x FastAP buffer (supplied with the enzyme), and 1 μl of FastAP thermosensitive alkaline phosphatase. The sample was adjusted to 50 μl with H_2O and incubated for 10 min at 37 °C, followed by enzyme inactivation for 5 min at 75 °C. The dephosphorylated DNA was purified with the GeneJET Gel Extraction kit (2.3.7.2).

2.3.3.3 Enzymatic Ligation of DNA

DNA ligases facilitate the joining of two DNA strands by catalyzing the formation of a phosphodiester bond between a 5' phosphate and a 3' hydroxyl group under consumption of ATP. The joining of DNA is usually performed by ligation of double-stranded nucleic acid molecules digested with the same restriction endonucleases. Since the ligation process is initiated by the annealing of the respective DNA fragments, the ligation efficiency decreases with less nucleotide overhang. To improve the ligation efficiency especially for blunt-end ligations, the reactions could be carried out by overnight incubation with an increasing temperature gradient from 0 °C to room temperature. One of the most frequently used DNA ligases in molecular biology is the T4 DNA ligase isolated from the bacteriophage T4.

For the ligation of two DNA fragments a three-fold molar excess of insert to vector DNA was applied. The total amount of DNA for one ligation reaction was limited to 100 ng, therefore generally 50 ng of vector DNA were used. The required amount of insert DNA for one ligation reaction was calculated according to the following equation:

$$insert\,DNA\,(ng) = \frac{molar\,excess \times insert\,DNA\,(bp) \times vector\,DNA\,(ng)}{vector\,DNA\,(bp)}$$

A standard ligation reaction (Tab. 6) was incubated for 60 min at 22 °C in a thermoblock (Eppendorf), followed by enzyme inactivation for 10 min at 65 °C. The 10x T4 DNA ligase buffer was supplied with the enzyme (Thermo Scientific). The ligated DNA was either used directly for transformation of competent bacteria (2.2.2) or stored at -20 °C.

Tab. 6: Standard DNA ligation reaction
The amount of required insert DNA was calculated for each reaction.

	DNA Ligation
insert DNA	molar excess of vector DNA
vector DNA	50 ng
10x T4 ligase buffer	2 μl
T4 DNA ligase	5 U
ad with H_2O	to 20 μl

2.3.4 Multigene Transfer Vector Assembly by *In Vitro* Cre fusion

Multiprotein interaction studies in a heterologous expression system are challenging due to the low efficiency of simultaneous introduction of two or more foreign DNAs. Moreover, conventional protein expression methods do not provide enough flexibility to alter the multiprotein composition after biochemical analyses. To address this, Berger and colleagues [197] introduced the MultiBac system, a modular baculovirus-based system specifically designed for eukaryotic multiprotein expression. Two years later, new transfer vectors and a combination of DNA recombination-based methods were published [198], which further facilitate the generation of multigene cassettes for protein co-expression (Fig. 4). The genes of interest are inserted into a suite of compatible donor and acceptor transfer vectors by conventional cloning. These progenitor constructs are then joined in the desired combination by Cre-*loxP* recombinase-mediated *in vitro* plasmid fusion. Acceptor and donor plasmids all contain the *loxP* imperfect inverted

repeat. In contrast to the donor plasmids, the acceptor plasmids and their derivatives additionally contain elements of the Tn7 transposon. Therefore, derivatives of one acceptor plasmid can be fused to one or two donor plasmids creating multigene plasmid dimers or trimers, respectively. The integration of the resulting multigene expression cassettes into the MultiBac baculovirual genome (bacmid), which relies on Tn7 transposition, is carried out *in vivo* in *E. coli* cells suitable for this purpose.

In this thesis, the DNA sequences encoding for the three NCRs NKp30, NKp44 and NKp46, each fused to a C-terminal deca-histidine tag (His-tag), were integrated into one MultiBac bacmid for the recombinant co-expression in insect cells. The DNA sequence encoding for NKp30-His was cloned into the acceptor plasmid pFL, whereas the sequences encoding for NKp44-His and NKp46-His were introduced into the donor plasmids pSPL and pUCDM, respectively (7.2). The vector assembly to the multigene plasmid trimer pFL-30-His/pSPL-NKp44-His/pUCDM-NKp46-His was generated by *in vitro* fusion (Fig. 4).

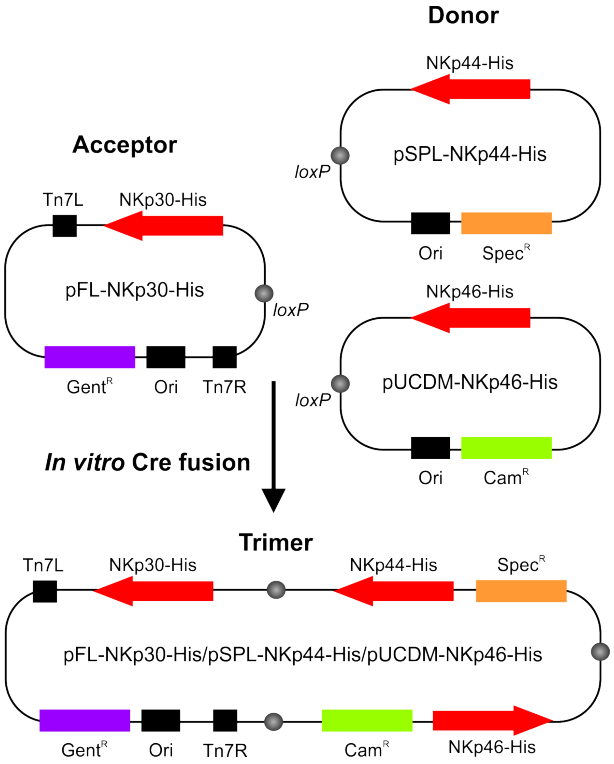

Fig. 4: Multigene transfer vector assembly by *in vitro* Cre fusion.

The acceptor plasmid pFL-NKp30-His and the donor plasmids pSPL-NKp44-His and pUCDM-NKp46-His, which all contain the *loxP* imperfect inverted repeat (gray circles), were fused *in vitro* to one multigene plasmid trimer using the Cre recombinase. Therefore, the generated multigene plasmid trimer contains NKp30-His, NKp44-His, and NKp46-His (red arrows) as well as the respective antibiotic resistance genes (Gent^R, violett box, Spec^R, orange box, and Cam^R, green box). Expression cassettes in between the Tn7 transposition sequences (black square, Tn7R $\rightarrow$ Tn7L) are integrated into the MultiBac baculovirus genome. Adapted from Fitzgerald *et al.* (2006) [198].

The plasmid fusion reaction was set up in a 10 μl reaction mix with individual donor and acceptor plasmid amounts of $\approx$ 500 ng and 1 U of Cre recombinase using the supplied buffer (New England Biolabs). The reaction mixture was incubated for 30 min at 37 °C in a thermoblock (Eppendorf), followed by enzyme inactivation for 10 min at 70 °C. 1-5 μl of the Cre recombinase reaction products were directly used for transformation of competent bacteria (2.2.2). Positive transformants were selected based on the resistance marker combination.

Tab. 7: Standard Cre recombinase reaction

	DNA Ligation
H_2O	2 μl
10x Cre recombinase reaction buffer	1 μl
Acceptor plasmid (500 ng)	2 μl
Donor plasmid A (500 ng)	2 μl
Donor plasmid B (500 ng)	1 μl
Cre recombinase	1 μl

Tab. 8: Features of the MultiBac acceptor and donor plasmid derivatives.

Vector	**Marker**	**Host Strain**	**Element**	**Usage**
pFL	Amp^R Gent^R	DH5α	*loxP*, TnL7, TnLR	acceptor for plasmid fusions, integration in MultiBac Tn7 site
pSPL	Spec^R	BW23473	*loxP*	donor for plasmid fusions, integration in MultiBac *loxP* site
pUCDM	Cam^R	BW23473	*loxP*	donor for plasmid fusions, integration in MultiBac *loxP* site

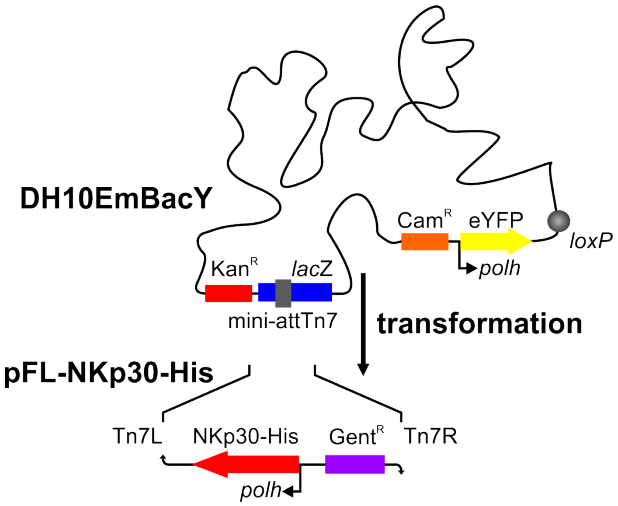

Fig. 5: Integration of the NKp30-His expression cassette into the DH10EmBacY genome

Upon transformation of *E. coli* DH10EmBacY with the acceptor plasmid pFL-NKp30-His, the expression cassette in between the Tn7 transposition sequences Tn7R and Tn7L is integrated into the bacmid genome via the mini-attTn7 site. Since the mini-attTn7 site is located within the *lacZ* gene, successful transposition can be identified by blue-white selection. *E. coli* DH10EmBacY has stably integrated the gene encoding eYFP (yellow box) as protein expression marker. Both, eYFP and NKp30-His expression are under the control of a polyhedrin promoter polh. Adapted from Berger *et al.* (2004) [197].

2.3.5 Generation of Bacmid DNA

The baculovirus expression vector system (BEVS) is used in research for the production of high levels of properly post-translationally modified (folding, disulfide bond formation, oligomerization, glycosylation,

acylation, proteolytic cleavage), biologically active and functional recombinant proteins [211,212]. Baculoviruses are rod-shaped dsDNA viruses found mainly in insects. The most common baculovirus used for expression studies is *Autographa californica multicapsid nucleopolyhedrovirus* (AcMNPV), which relies on the lepidopteran species *Spodoptera frugiperda* and *Trichoplusia ni* as host insects. AcMNPV particles surround themselves with a protective matrix consisting of the protein polyhedrin, which is under the control of the extremely strong and late promoter polh, resulting in up to 50 % of all cellular protein at the end of the baculovirus life cycle. However, in cell culture the polyhedrin coat is not essential for virus propagation and thus heterologous proteins can be expressed under the control of the polh promoter [213]. Therefore, the gene of interest is transferred from a donor plasmid to cloned AcMNPV-DNA (bacmid) in *E. coli* DH10Bac via specific transposition with the use of a helper plasmid (Fig. 5), also known as Bac-to-Bac system [214]. This recombinant baculovirus-DNA can replicate in *E. coli* and is infectious for lepidopteran cells. In this thesis, *E. coli* DH10EmBacY was used. Berger and colleagues stably introduced the gene encoding eYFP into the bacmid genome under control of the polyhedrin promoter polh, which is used as protein expression marker [197, 198]. To introduce the donor plasmid containing the gene of interest, *E. coli* DH10EmBacY were transformed using 100 ng of plasmid DNA adjusted with deionized, sterile filtered (0.22 μm) water to a final volume of 5 μl. Therefore, a 50 μl aliquot of cells was thawed on ice, gently mixed with plasmid DNA (without pipetting), and incubated for 30 min on ice. The heat shock was performed for 45 s at 42 °C prior to incubation on ice for 2 min. 900 μl of LB medium were added, and the transformation mix was incubated for 4 h at 37 °C and 600 rpm. A dilution series of the bacteria suspension (pure, 1:10, 1:100, 1:1,000) was plated on LB agar supplemented with the respective antibiotics and additives (Kan, Tet, Gent, IPTG, X-gal, listed in Tab. 1), and incubated for 24-48 h at 37 °C to perform blue-white selection. Blue colonies contained the donor plasmids, whereas white colonies integrated the gene of interest into the bacmid genome. To ensure correct discrimination between blue and white colonies, one blue colony (negative control) and up to ten white colonies were replated on LB selection agar and incubated again for 24 h at 37 °C. 4 ml of LB medium supplemented with the appropriate antibiotics (Kan, Tet, Gent) were inoculated with one white colony and incubated overnight at 37 °C and 200 rpm in a bacteria shaker. The cells were pelleted (9,000x g, 5 min, 4 °C), and stored at -20 °C or transferred into a 2 ml reaction tube for bacmid preparation. Therefore, 300 μl of solution 1 to 3 of the NucleoBond Xtra Midi/Maxi kit were used according to the manufacuter's instructions. After neutralization, the suspension was centrifuged (14,000x g, 10 min, 4 °C) two to three times, each time transferring the supernatant into a new reaction tube. The bacmid DNA was precipitated from the cleared lysates by mixing with 700 μl of isopropyl alcohol, pelleted (14,000x g, 10 min, 4 °C), washed with 500 μl of 70 % (v/v) EtOH (pure), and thereby transferred into a new 1.5 ml reaction tube. The DNA pellet was dried and gently reconstituted using the appropriate amount (50-100 μl) of pre-warmed (50 °C) deionized, sterile filtered (0.22 μm) water. Intensive pipetting was avoided to prevent fragmentation of the large genomic bacmid DNA. The concentration of isolated bacmid DNA was determined photometrically (2.3.8). Bacmid DNA was stored at 4 °C until it was used for transfection.

2.3.6 Agarose Gel Electrophoresis

Agarose gel electrophoresis is a method for separation and analysis of DNA (or RNA) molecules based on their size. DNA molecules are negatively charged due to their phosphate backbone. Therefore, they migrate from the cathode to the anode after applying an electric current in the agarose gel. Since poly-

merized agarose acts as a molecular sieve, the migration speed of each DNA molecule is dependent on its size. Small DNA fragments migrate faster through the agarose matrix than large fragments, thereby separating from one another. The applied agarose concentration depends on the size of the DNA fragments to be analyzed; most agarose gels are made with between 0.7 % (w/v) (good resolution of large 5-10 kb DNA fragments) and 2 % (w/v) (good resolution of small 0.2-1 kb DNA fragments) agarose dissolved in electrophoresis buffer.

In this thesis, 0.8 % (w/v) agarose gels were used for separation of fragments >1 kb, whereas 1.2-2 % (w/v) agarose gels were applied for smaller DNA fragments. The gels were produced by adding the respective amount of agarose in TAE buffer. After heating, the emulsion in a microwave oven until the solid agarose dissolved, the agarose solution was casted into a tray to polymerize. Unless DNA samples did not already contain *DreamTaq* green buffer (2.3.2) or FastDigest green buffer (2.3.3), DNA samples were supplemented with 6x DNA loading dye (Thermo Scientific) and applied to the agarose gel. GeneRuler 1 kb Plus DNA ladder (Thermo Scientific) was used as size standard. The electrophoresis was performed at 160 V for approximately 45 min in a WIDE MINI-SUB cell GT chamber (Bio-Rad) filled with TAE buffer. Since ethidium bromide (EtBr) intercalates between DNA strands and can be visualized under UV light (254 nm), agarose gels were incubated for 15 min in EtBr stain. DNA fragments were detected and photographically documented using a Gel Doc 2000 gel documentation system (Bio-Rad).

2.3.7 Isolation of DNA from Agarose Gels, Purification of DNA

2.3.7.1 Isolation of DNA from Agarose Gels

After the separation by agarose gel electrophoresis (2.3.6), DNA fragments can be isolated from the gel matrix for subsequent cloning. Since long exposure with short-wave (high intensity) UV light can damage the DNA, agarose gels used for DNA isolation were exposed with long-wave (low intensity) UV light (302 nm). After electrophoretic separation, the agarose gel was cut as close as possible around the respective DNA fragment to decrease impurities or the loss of DNA, and transferred into a 2.0 ml tube. The purification was performed using the GeneJET Gel Extraction kit according to the manufacturer's instructions. The DNA containing agarose fragment was melted in a buffer with high concentration of a chaotropic salt, which allows for the binding of the DNA to silica gel membranes. To elute the DNA from the silica gel membrane, 50 μl of H_2O (50 °C) were used, followed by the determination of the DNA concentration (2.3.8).

2.3.7.2 Purification of DNA

To prepare the DNA for subsequent applications, enzymes and disturbing buffer components after PCR (2.3.2), restriction (2.3.3.1), or dephosphorylation (2.3.3.2) were removed using the GeneJET Gel Extraction kit according to the manufacturer's instructions. The DNA fragments bind to silica gel membranes in the presence of a chaotropic salt. Thus, all enzymes are removed while the DNA is retained and can be eluted with water or appropriate buffers. DNA fragments derived from restriction or dephosphorylation reactions were eluted in 50 μl of pre-warmed H_2O (50 °C). DNA fragments from PCR reactions were eluted in one-fifth of the original volume. The concentration of purified DNA fragments was determined photometrically (2.3.8).

2.3.8 Determination of DNA Concentration

The spectrophotometric quantitation of nucleic acids, which is based on the absorbance of UV light (A_{max} = 260 nm) by the purine and pyrimidine bases of the DNA, is performed to determine the purity and the average concentration of DNA present in a mixture. Using the Lambert-Beer law it is possible to relate the amount of light absorbed to the concentration of the absorbing molecule. The ratio of the absorbance 260/280 nm is commonly used to assess the purity of the DNA, since aromatic amino acids of proteins absorb UV light at 280 nm. Pure DNA possesses a value of roughly 1.8.

In this thesis, the spectrophotometric quantitation of DNA was performed with a NanoDrop ND 1000 (PeqLab Biotechnologie). To assess the DNA concentration and purity, the UV absorbance spectrum between 220 nm and 300 nm of 1-2 μl of isolated DNA either from plasmid preparation (2.3.1), DNA purification (2.3.7.2), or agarose gel extraction (2.3.7.1) was measured. H_2O was used as blank, since all DNA samples were dissolved in water.

2.3.9 Nucleic Acid Sequencing

Nucleic acid sequencing was performed by sequencing service from the company GATC Biotech (Cologne, Germany) using the chain-termination method developed by Sanger [215]. For this purpose, sequencing samples containing 5 μl of DNA (80-100 ng/μl) and 5 μl of the respective primer (5 pmol/μl) were prepared in a 1.5 ml reaction tube. A standard sequencing run is able to sequence up to 600 bp of the DNA sample proceeding from the primer binding region.

2.3.10 Cloning Strategies

For the following cloning processes, the full-length sequence of the human *NCR3* gene or variants were synthesized *de novo* either with wild type (wt) or codon-optimized (opt, indicated) codon usage by the company GenScript. The synthesized genes were delivered in pUC57 plasmids and served as templates for PCR amplification (2.3.2) or subsequent cloning (2.3.3). All used oligonucleotides with their corresponding numbers are listed (2.1.8), and the generated constructs were verified by nucleotide sequencing (2.3.9). The corresponding plasmid maps (7.2) and protein sequences (7.3) are listed in the appendix.

2.3.10.1 Full-Length NKp30-His Constructs for Expression in Mammalian Cell Lines

To investigate self-assembly of NKp30 or interaction with other cell surface molecules, full-length NKp30 with a C-terminal deca-histidine tag (His-tag) for detection was generated for the transient introduction into NKp30 negative mammalian cell lines. For this purpose, the primer combinations 153/236 (listed in 2.1.8) and pUC57-NKp30opt (plasmid 117, listed in 2.1.9.1) as template were used to introduce endonuclease recognition sites as well as the His-tag by PCR (2.3.2). The amplified DNA fragment was enzymatically digested using *Sac*II (2.3.3.1). After purification (2.3.7.2) of the digested and dephosphorylated (2.3.3.2) expression vector pIRES2-EGFP (Clontech, 5308 bp), the purified NKp30opt-His encoding DNA fragment (689 bp) was enzymatically ligated (2.3.3.3) generating pIRES-NKp30-His-EGFP (plasmid 4805). Positive clones with correct insert orientation were identified by colony PCR using the primer combinations 052/236 or 153/053. For nucleotide sequencing (2.3.9), the primers 052 and 053 were applied.

For stable integration of the full-length NKp30-His by lentiviral particles into NKp30 negative mammalian cell lines, the NKp30-His encoding DNA fragment was introduced into the transfer vector LeGO-iG2 ([205]). Therefore, the primer combinations 153/249 and pUC57-NKp30opt (plasmid 117) as template were used to introduce endonuclease recognition sites as well as the His-tag by PCR. The amplified DNA fragment was enzymatically digested using *Bam*HI and *Not*I. After purification of the digested and dephosphorylated transfer vector LeGO-iG2 (7771 bp), the purified NKp30opt-His encoding DNA fragment (653 bp) was enzymatically ligated generating LeGO-NKp30optHis-iG2 (plasmid 4901). Positive clones were identified by colony PCR using the primer combination 061/053. For nucleotide sequencing, the same oligonucleotides were applied.

2.3.10.2 Constructs for Co-Expression of NKp30, NKp44, and NKp46 in Insect Cells

Multiprotein interaction studies in a heterologous expression system are challenging due to the low efficiency of simultaneous introduction of two or more foreign DNAs. To analyze the possible cross-talk between the NCRs NKp30, NKp44, and NKp46 in a non-immunological background, the MultiBac system was applied to introduce the genetic information of all three NCRs simultaneously into insect cells using baculoviral particles. For this purpose, monomeric acceptor (pFL-NKp30-His (plasmid 401)) and donor plasmids (pSPL-NKp44-His (plasmid 501), pUCDM-NKp46-His (plasmid 601), listed in 2.1.9.1) were generated prior to combination via *in vitro* Cre fusion (2.3.4). To generate the MultiBac acceptor plasmid pFL-NKp30-His, the primer combinations 074/075 (listed in 2.1.8) and pUC57-NKp30-His (plasmid 101) as template were used to introduce endonuclease recognition sites by PCR. The amplified DNA fragment was enzymatically digested using *Stu*I and *Xba*I (2.3.3.1). After purification of the digested and dephosphorylated (2.3.3.2) transfer vector pFL ([197,198], 5410 bp), the purified NKp30-His encoding DNA fragment (641 bp) was enzymatically ligated. Positive clones were identified by colony PCR using the primer combination 001/002. To generate the MultiBac donor plasmids pSPL-NKp44-His and pUCDM-NKp46-His, the primer combinations 077/079 or 080/081, respectively, as well as the appropriate template pUC57-NKp44-His (plasmid 102) or pUC57-NKp46-His (plasmid 103) were used to introduce endonuclease recognition sites by PCR. The amplified DNA fragment was enzymatically digested using *Bam*HI and *Xba*I or *Bam*HI and *Stu*I. After purification of the digested and dephosphorylated transfer vectors pSPL (2786 bp) and pUCDM (2947 bp) [197,198], the purified NKp44-His (867 bp) and NKp46-His (954 bp) encoding DNA fragments were enzymatically ligated. Positive clones were identified by colony PCR using the primer combination 010/011 or 015/016, respectively. For nucleotide sequencing, the oligonucleotides 064 and 001, 010 or 015 were applied (2.3.9).

2.3.10.3 NKp30 Ligand Binding Domain Constructs for the Expression in *Escherichia coli*

The 3D structure of the NKp30 ligand binding domain had not been solved until 2011 [116,117]. Therefore, a *de novo* model of the NKp30 ligand binding domain, based on structural homologies, was calculated using the protein structure prediction service PHYRE (**P**rotein **H**omology/Analog**Y** **R**ecognition **E**ngine [216]). Based on this model predicting the globular ligand binding domain of NKp30 from amino acid M1 to G120 (NKp30 protein sequence listed in 7.3), a truncated version of the NKp30 ligand binding domain (30LBD$_{tr}$) lacking eight amino acids at the C-terminus was used for these expression and purification analyses. To obtain large amounts of protein for biochemical approaches, 30LBD$_{tr}$ was expressed in *E. coli*. The *E. coli* BL21 (DE3) strain was especially constructed for high-level protein expression

of recombinant proteins. Moreover, inducibility by IPTG could minimize the toxic effects of some recombinant proteins. To identify optimal expression and purification conditions of the 30LBD$_{tr}$ protein, variants with an N- or C-terminal deca-histidine tag (His-tag), and an additional glycine-serine linker flanked TEV cleavage site for optional removal of the His-tag were synthesized by GenScript (pUC57-NKp30EC-TEV-His (plasmid 108) and pUC57-His-TEV-NKp30EC (plasmid 109), listed in 2.1.9.1). After enzymatic restriction of the plasmids 108 and 109 using *Nco*I and *Xho*I (2.3.3.1), the DNA fragments encoding His-30LBD$_{tr}$ and 30LBD$_{tr}$-His (both 380 bp) were isolated from agarose gels after separation (2.3.6 and 2.3.7.2). The expression vector pET-16b (Merck Millipore) was digested (*Nco*I and *Xho*I, 5643 bp) and dephosphorylated (2.3.3.2) prior to ligation of the inserts (2.3.3.3) generating the plasmids pET16b-His10-TEV-NKp30EC (plasmid 1901) and pET16b-NKp30EC-TEV-His10 (plasmid 1902), respectively. Positive clones were identified by colony PCR (2.3.2) using the primer combination 038/039 (listed in 2.1.8).

To increase the solubility of the 30LBD$_{tr}$ protein during protein expression, larger purification tags such as GST (glutathion-S-transferase, encoded by the vector pGEX-4T-1, GE Healtcare) or MBP (maltose binding protein, encoded by the vector pMAL-p5X, New England Biolabs) were fused at the N-terminus. For this purpose, the primer combinations 118/119 or 117/119, respectively, and pUC57-NKp30EC-TEV-His (plasmid 108) as template were used to introduce endonuclease recognition sites and amplify 30LBD$_{tr}$ encoding fragments by PCR. These amplified DNA fragments were enzymatically digested using *Eco*RI and *Xho*I or *Eco*RI and *Hin*dIII, respectively. After purification of the digested and dephosphorylated expression vectors pGEX-4T-1 (4954 bp) and pMAL-p5X (5729 bp), the purified 30LBD$_{tr}$ encoding DNA fragments (both 315 bp) were enzymatically ligated with the respective vector fragment generating the GST-30LBD$_{tr}$ (pGEX-4T-1-NKp30EC (plasmid 2105)) and MBP-30LBD$_{tr}$ (pMal-p5X-NKp30EC (plasmid 3301)) encoding expression plasmids. Positive clones were identified by colony PCR using the primer combinations 049/050 and 059/060, respectively. For nucleotide sequencing (2.3.9), the same oligonucleotides were applied.

2.3.10.4 NKp30 Ectodomain Constructs for the Expression in Insect Cells

Previous studies concerning ligand binding and signaling were performed with bivalent Ig fusion proteins exhibiting post-translational modifications such as glycosylation. This modification may provoke a conformational change of the NKp30 ectodomain when compared to the non-glycosylated NKp30 ectodomain produced in *E. coli* and most probably increases the protein stability in solution. However, these fusion proteins display an antibody-like architecture. This forced dimerization could have a boosting or even impeding influence on the interaction of NKp30 with its binding partners. Moreover, not only the ligand binding domain alone but also the membrane proximal stalk domain could participate in interaction events. Therefore, variable monovalent NKp30 ectodomain constructs with and without the NKp30 stalk domain were generated for the expression in insect cells (30Stalk-His: amino acids L19-R143, 30LBD-His: amino acids: L19-E128). Both NKp30 ectodomain variants were N-terminally fused to a gp67 secretion sequence, and had a C-terminal deca-histidine tag (His-tag) with an additional glycine-serine linker flanked TEV cleavage site for optional removal of the His-tag. The constructs pUC57-gp67ss-NKp30LBD-Stalk-TEV-His (plasmid 114, listed in 2.1.9.1) and pUC57- gp67ss-NKp30LBD-TEV-His (plasmid 127) were synthesized by GenScript. After enzymatic restriction of the plasmids 114 and 127 using *Xho*I and *Hin*dIII (2.3.3.1), the DNA fragments encoding 30Stalk-His and 30LBD-His

(576 and 531 bp) were isolated from agarose gels after separation (2.3.6 and 2.3.7.2). The baculovirus expression vector pFastBac1 (Life Technologies) was digested (*Xho*I and *Hin*dIII , 4758 bp) and dephosphorylated (2.3.3.2) prior to ligation of the inserts (2.3.3.3) generating the plasmids pFastBac1-gp67ss-NKp30LBD-Stalk-TEV-His (plasmid 308) and pFastBac1-gp67ss-NKp30LBD-TEV-His (plasmid 315), respectively. Positive clones were identified by colony PCR (2.3.2) using the primer combination 041/043 (listed in 2.1.8).

2.4 Methods of Cell Biology

2.4.1 Protein Production in *Eschericia coli*

E. coli is one of the most widely used expression host for recombinant protein production. Overexpression of the gene of interest in this system is facilitated by a high copy-number of the plasmid DNA introduced by transformation or by increased binding strength of the promoter region, thereby assisting transcription. In general, a combination of both is applied by high copy-number plasmids containing the strong *lac* promoter upstream the gene of interest. Upon successful transformation of *E. coli* with the expression vector, recombinant protein production can be induced by the lactose analog isopropyl β-D-1-thiogalactopyranoside (IPTG).

In this thesis, the bacteria strains *E. coli* BL21 (DE3) and Origami (DE3) were applied for recombinant 30LBD$_{tr}$ protein production. Therefore, an aliquot of bacteria cells was transformed with the respective plasmid DNA (2.2.2) prior to inoculation of an appropriate volume of LB selection medium for overnight incubation under standard conditions (2.2.1). For recombinant protein expression, fresh LB selection medium was inoculated with 1/10 Vol of the preparative culture and incubated under standard conditions following the optical density at 600 nm (OD_{600}). At an OD_{600} of 0.6, recombinant gene expression was induced by addition of 1 mM IPTG to the bacteria suspension. 4 h post IPTG induction, bacteria cells were harvested by centrifugation (5,000x g, 20 min, 4 °C). Bacteria cell pellets were stored at -20 °C or used directly.

To visualize time-dependent recombinant protein expression by SDS-PAGE (2.5.6) and immunoblot analyses (2.5.7), samples corresponding to an OD_{600} of 1 were taken prior to and every hour post IPTG induction. After centrifugation of these samples (300x g, 5 min, 4 °C), the supernatant was discarded, and the bacteria cell pellet was resuspended in 100 μl of PBS. To distinguish between soluble and aggregated recombinant proteins (inclusion bodies), the samples were sonicated for 5 min at high power using a Bioruptor Standard (Diagenode). Inlusion bodies and soluble recombinant proteins were separated by centrifugation (14,000x g, 10 min) prior to SDS-PAGE and immunoblot analyses.

2.4.2 Cultivation of Cell Lines

2.4.2.1 Maintenance of Insect Cells

*Sf*9 or Hi5 insect cells were cultivated in suspension culture under serum-free conditions in the appropriate medium (2.1.6.3) at 27 °C and 90 rpm in an incubation shaker (Multitron Standard, HT Infors, Bottmingen, Switzerland). To passage insect cells, the cell number was determined using a counting chamber (Neubauer counting chamber improved (bright-lined), Carl Roth). The cell viability was assessed by trypan blue staining. Insect cells were passaged three times a week to maintain mid-log phase

of growth ($2x10^6$ to $4x10^6$ cells/ml) and seeded between $3x10^5$ to $5x10^5$ viable cells/ml.

Sf 9 suspension cultures were utilized for virus amplification. For this purpose, the cells were diluted to a cell density of $7x10^5$ cells/ml in a volume of 25 to 50 ml (250 ml-shaker flask) prior to infection and cultivated under standard conditions. Hi5 suspension cultures were utilized for protein production. For this purpose, the cells were diluted to a cell density of $7x10^5$ cells/ml in a volume of 150 to 500 ml (2 l-shaker flask) prior to infection and cultivated under standard conditions.

For long term storage, cryo cultures were prepared and kept in liquid nitrogen or at -80 °C. For this purpose, cells being in a logarithmic growth-phase were used. Insect cells were pelleted (200-300x g, 5 min, 4 °C), resuspended in an appropriate volume of freezing medium (45 % (v/v) conditioned medium, 45 % (v/v) fresh medium, 10 % DMSO, sterile filtered) to achieve a cell density of 2-$3x10^7$/ml. 1 ml-aliquots of the cell suspension were prepared in cryogenic vials, transferred in a freezing container (Mr. Frosty, Nalgene) and incubated at -80 °C. After 24 h, the vials were stored in the gas phase of liquid nitrogen or remained at -80 °C.

To initiate an insect cell culture, a cryogenic vial of cells was thawed in a 37 °C water bath and immediately transferred into 30 ml of fresh, prewarmed (27 °C) medium. To remove cytotoxic DMSO, the cells were pelleted (200-300x g, 5 min), reconstituted in 30 ml fresh medium and seeded into a 250 ml-shaker flask.

2.4.2.2 Maintenance of Mammalian Cells

Mammalian cell lines were cultivated in the appropriate medium (2.1.6.3) in a cell culture incubator (ATP Line CB, Binder GmbH) at 37 °C, 5 % CO_2 and saturated water atmosphere. The cells were passaged 2-3 times a week to maintain optimal growth conditions. For this purpose, adherent cells were washed once with PBS prior to trypsin (1x trypsin/EDTA, PAA) or accutase (PAA) treatment. An appropriate fraction of detached cells was seeded into a new cell culture flask with fresh medium. To passage suspension cells, the cell number was determined using a counting chamber (Neubauer counting chamber improved (bright-lined), Carl Roth). After counting, the appropriate fraction of cells was pelleted (200-300x g, 3 min), reconstituted in fresh medium and seeded into a new culture flask.

For long term storage of cells, cryo cultures were prepared and kept in liquid nitrogen or at -80 °C. For this purpose, cells being in a logarithmic growth-phase were used. Detached adherent cells or suspension cells were pelleted (200-300x g, 3 min, 4 °C), resuspended in an appropriate volume of freezing medium (45 % (v/v) conditioned medium, 45 % (v/v) fresh medium, 10 % DMSO, sterile filtered (0.22 μm)). Aliquots of the cell suspension were prepared in cryogenic vials, transferred in a freezing container (Mr. Frosty, Nalgene) and incubated at -80 °C. After 24 h, the vials were stored in the gas phase of liquid nitrogen or remained at -80 °C.

To recover the cells from long term storage, a cryogenic vial of cells was thawed at 37 °C and immediately transferred into 10 ml of fresh, prewarmed medium. To remove cytotoxic DMSO, the cells were pelleted (200-300x g, 3 min), reconstituted in fresh medium and seeded into an appropriate culture flask.

2.4.3 Production of Baculovirus Particles

Baculovirus particles are used to introduce foreign DNA into lepidopteran cells such as *Spodoptera frugiperda* or *Trichoplusia ni*, especially for recombinant protein production from higher eukaryotes. Characteristic for the infection cycle is the generation of two different virion types: at early time points

(6-8 h after infection), there is the budded virus (BV) located at the plasma membrane and at later time points (18 h after infection), there is occlusion-derived virus (ODV) found in the nucleus. BV is infectious in cell culture, since the virus enters into the host cell via receptor-mediated endocytosis. Gp64 (also known as gp67), a membrane fusion protein, is essential for the entry of BV into the cell [217].

For baculovirus particle production, *Sf*9 insect cells were transfected with recombinant bacmid DNA in a 6-well plate according to the manufacturer's instructions using the TransIT-LT1 transfection reagent (Mirus Bio). Therefore, 1x10^6 cells per 6-well were seeded in a final volume of 3 ml of Insect Xpress medium (2.1.6.3) and incubated for approximately 30 min at 27 °C to adhere. 5 μg of bacmid DNA were added to 250 μl of Insect Xpress medium in a 1.5 ml reaction tube and mixed gently. 15 μl of pre-warmed (room temperature) TransIT-LT1 were added, mixed gently and incubated for 15-30 min at room temperature. The transfection mixture was distributed dropwise all over the 6-well. 60 h after transfection, the initial virus-containing supernatant (V_0) was collected and used directly for infection of an *Sf*9 suspension culture or stored at 4 °C. 3 ml of fresh medium were added to the 6-well and incubated for further 72 h at 27 °C. To investigate the transfection efficiency, the cytosolic YFP expression was analyzed. Therefore, the supernatant was discarded, the cells were gently washed by rinsing with PBS, resuspended in 500 μl of PBS, and transferred into a 1.5 ml reaction tube. The cell suspension was sonicated for 5 min at high power using a Bioruptor Standard (Diagenode). After centrifugation (14,000x g, 10 min), 150 μl of the YFP containing cell lysate were transferred into a 96-well plate (solid black flat bottom, Corning) to measure the YFP fluorescence intensity (excitation: 485 nm, emission: 520 nm) using a FluoStar Optima device (BMG Labtech). To amplify the virus stock, an *Sf*9 suspension culture (7x10^5 cells per ml in 25 ml) was infected using the total V_0 from one 6-well (approximately 3 ml). Suspension cultures of infected cells were split every 24 h until cell proliferation arrest occurred. 48 h after proliferation arrest, the amplified virus-containing supernatant (V_1) was collected (300x g, 5 min), sterile filtered (0.22 μm), and stored in a dark 50 ml tube at 4 °C.

2.4.4 Protein Production in Insect Cell Lines

Protein expression in insect cell lines was applied since the produced proteins exhibit post-translational modifications similar to mammalian producer cells. In this thesis, on the one hand insect cells were functionalized with either full-length NKp30 alone or in combination with full-length NKp44 and NKp46. On the other hand, the NKp30 ectodomain variants 30Stalk-His and 30LBD-His were produced by secretion into the cell culture supernatant due to an N-terminal glycoprotein (gp) 67 secretion signal. Therefore, High Five insect cell suspension cultures with 7x10^5 cells per ml were infected with 1 ml of V_1 (2.4.3) per 100 ml. After 72 h of incubation under standard conditions (2.4.2.1), the functionalized insect cells were applied to further analyses such as flow cytometry (2.4.12) and CLSM (2.4.13). To purify the secreted 30Stalk-His and 30LBD-His proteins from the cell culture supernatant, the cells were pelleted (1,000x g, 10 min, 4 °C). The supernatant was sterile filtered (0.22 μm), supplemented with 0.025 % (v/v) sodium azide and stored at 4 °C. To remove the baculovirus particles prior to purification by IMAC (2.5.1.1), the protein containing supernatants were ultracentrifuged (100,000x g, 2 h, 4 °C). Moreover, L-glutamine was decreased from the expression medium by dialysis to minimize unfavorable occupation of binding places during protein purification. Therefore, up to 200 ml of the supernatant were transferred into a dialysis tube, which was incubated overnight at 4 °C in stirred 5 l of dialysis buffer (2.1.7).

2.4.5 Transfection of Mammalian Cell Lines

Transfection is the process of deliberately introducing foreign DNA or RNA into eukaryotic cells. There are various methods to introduce nucleic acids into cells, which can be categorized into physical (e.g. electroporation) or chemical (e.g. calcium phosphate precipitation or lipofection) treatment. For some applications of transfection, it is sufficient if the introduced genetic material is only transiently expressed. Thus, the foreign DNA will be diluted through mitosis following cell division or degraded. In contrast, a stable transfection assures that the transfected DNA remains in the genome of the cell and its daughter cells. Stable integration of a co-transfected marker gene (e.g. resistance to a certain toxin) into the genome leads to a selection advantage and the survival of the respective cells. After applying the selection pressure for an appropriate time, only the stably transfected cells remain and can be further cultivated.

In this thesis, the chemical transfection with polyethylenimine (PEI) was used. PEI is a highly branched and positively charged organic polymer with primary, secondary and tertiary amino groups. It binds to the negatively charged phosphate groups of the nucleic acid backbone, and thereby condenses DNA into positively charged particles. It facilitates the attachment to the cell surface leading to endocytosis of the foreign DNA [218,219]. Once inside the cell, protonation of the amines results in an influx of counter-ions and increase of the osmotic potential. Due to osmotic swelling of the endosomes, the bursting vesicles release the polymer-DNA complex into the cytoplasm. After unpacking from the complex, the DNA is free to diffuse to the nucleus.

For transient transfection of HEK293T cells, $1x10^7$ cells were seeded into a T175 culture flask with 20 ml of prewarmed RPMI-1 medium 24 h before transfection. Immediately before the transfection, the medium was replaced by 13 ml of prewarmed RPMI/Gln medium. The transfection mix consists of two solutions (solution A and B). To prepare solution A, 65 μg of DNA was supplemented with 310 μl of TA-glucose. Solution B consists of 65 μl of TA-trans and 310 μl of TA-glucose. Both solutions were intensively mixed for 1 min at maximum speed (Vortex Genie 2, Scientific Industry). After incubation for 10 min at room temperature (RT), solution A was added to solution B, intensively mixed for 1 min and again incubated for 10 min at RT. The transfection mix was supplemented with 1 ml of RPMI/Gln medium, mixed and added directly to the cells. After 4-6 h, the medium was replaced by 25 ml of prewarmed RPMI/FCS medium.

2.4.6 Protein Production in Mammalian Cell Lines

Protein expression in mammalian cell lines was applied since the produced proteins exhibit post-translational modifications (PTMs) similar to their natural producer cells. Common PTMs are methylation, phosphorylation, glycosylation and disulfide bond formation. In this thesis, B7-H6-Ig fusion protein was produced by secretion into the cell culture supernatant due to an N-terminal tumor necrosis factor (TNF) secretion signal. Therefore, HEK293T cells were transiently transfected with the pcDNA3.1(+)-TNFss-B7-H6-hIgG1-Fc plasmid (2.4.5). After 72 h of incubation under standard conditions, the cell culture supernatant was collected and centrifuged (1,000x g, 10 min, 4 °C) to remove remaining cells and cell debris. The supernatant was sterile filtered (0.22 μm), supplemented with 0.025 % (v/v) sodium azide and stored at 4 °C. The secreted protein was purified from the supernatant by protein A affinity purification (2.5.1.2).

2.4.7 Production and Concentration of Lentiviral Particles

Viral particles are a common tool in the field of molecular biology to deliver genetic material into cells *in vitro* or *in vivo*. In this thesis, human immunodeficiency virus (HIV)-1-derived lentiviral particles were used for the stable introduction of the genes encoding recombinant NKp30-His and, moreover, the green fluorescent protein (GFP) as marker for gene expression into HEK293 cells. Lentivirus is a genus of viruses of the *retroviridae* family, which has the unique ability to infect both dividing and non-dividing cells. Since these particles are created from a pathogenic virus, they are Gene-modified to be replication-incompetent. For the production of infectious particles, viral genes are segregated onto three different plasmids: (i) a transfer plasmid (harboring the transgene), (ii) a packaging plasmid (encoding for viral structural proteins and enzymes), and (iii) an envelope plasmid (encoding for envelope proteins). Transient co-transfection of these three types of plasmids into HEK293T cells (triple transfection) ensures the assembly of lentiviral particles containing only the transgene of choice but no gene for viral replication. Moreover, triple transfection allows for rapid change of tropism or virus type by applying another envelope or packaging plasmid.

Generation of lentiviral particles was achieved by triple transfection of HEK293T cells with LeGO-iG2-NKp30-His opt or LeGO-iG2 as mock control (transfer plasmid), pCMV-ΔR8.91 (packaging plasmid) harboring the HIV-1 genes *gag* and *pol*, and pMD2.G (envelope plasmid) encoding the vesicular stomatitis virus (VSV)-G envelope protein. Transfection was performed in T175 culture flasks based on the PEI method (2.4.5). In contrast to a single transfection approach, solution A contains 70.5 μg of DNA in total (35 μg of transfer plasmid, 23 μg of packaging plasmid, and 12.5 μg of envelope plasmid). To obtain sufficient lentiviral particles from one transfection, two T175 culture flasks of HEK293T cells were transfected. 4-6 h after transfection, the medium was replaced by 25 ml of prewarmed RPMI-1 medium. 72 h later, the cell culture supernatant containing the lentiviral particles was collected and sterile filtered (0.45 μm). 5 ml of the supernatant were either used directly for transduction (2.4.8) or stored at -80 °C in 1 ml-aliquots. To obtain more concentrated lentiviral particles, 30 ml of the remaining supernatant were transferred into a sterile thinwall polyallomer tube (Beckman Coulter) and layered with below 5 ml of sucrose solution. After ultracentrifugation (100,000x g, 2 h, 4 °C; Optima L-70, SW32Ti, Beckman Coulter), the pellet was resuspended in 1 ml of appropriate medium. Aliquots of 500 μl were stored at -80 °C.

2.4.8 Transduction of Mammalian Cell Lines

Lentiviral particles can mediate the efficient delivery, integration and stable expression of transgenes. This method called transduction is commonly used for cell lines that are hard to transfect. Another benefit of transduction with lentiviral particles is the stable integration of the delivered transgene into the genome of the transduced cell, generating stable transgene expressing cell lines.

For transduction of HEK293T cells with LeGO-iG2-NKp30-His opt or LeGO-iG2 as mock control, about $3x10^5$ cells were seeded into a single well of a 6-well plate. The next day, the medium was replaced by 1 ml of prewarmed RPMI/Gln medium supplemented with 8 μg/ml protamine sulfate per well. The cationic polymer protamine sulfate enhances the transduction efficiency by neutralizing the charge repulsion between the lentiviral particles and the cell surface [220]. Immediately before centrifugation, 1 ml of fresh or thawed lentiviral particle suspension (2.4.7) was added to one well of cells. To force lentiviral particles onto the cells, the plate was centrifuged for 1 h at 1,800x g and 32 °C. After incu-

bation of the cells under standard conditions for 6-12 h, the supernatant was replaced by 2 ml of fresh, prewarmed RPMI-1 medium. After 24 h, single cell clones were isolated (2.4.9) and the transduction efficiency was assessed by GFP expression analyses using a fluorescence microscope (Eclipse TE 300, Nikon Instruments, Melville, USA).

2.4.9 Clonal Isolation of Gene-modified Cell Lines

Though transduction with lentiviral particles (2.4.8) is a very efficient method to introduce foreign DNA, not every single cell stably integrates the transduced DNA into the host genome. Even if the integration was successfull, there can be single cells expressing only low amounts of the transgene. If there is no selection pressure due to the transgene (resistance to a toxin), these cells obtain a selection advantage and could overgrow the culture, thus losing the transgene expression at all over time. Therefore, gene-modified single cell clones with high expression of the transgene have to be isolated. In this thesis, a limiting dilution approach in a 96-well plate was performed. The 96-well plate was prepared with 100 μl of prewarmed RPMI-3 medium per well. 1x10^5 cells in 100 μl of prewarmed RPMI-3 medium were seeded into the first well of the 96-well plate, gently mixed, and 100 μl of this cell suspension were transferred into well below. This step was repeated up to the last well of the row. The remaining 100 μl of cell suspension were discarded. With an 8-channel micropipette, 100 μl of prewarmed RPMI-3 were added to the first row, gently mixed, and 100 μl of cell suspension were again transferred into the next wells. This step was repeated up to the last row. Finally, 100 μl of prewarmed RPMI-3 were added to each well, following cell cultivation under standard conditions. After 24 h, wells with only one single cell, which expresses the transgene (GFP), were identified by fluorescence microscopy (Eclipse TE 300, Nikon Instruments, Melville, USA). These gene-modified single cell clones were cultivated until an appropriate cell number for subsequent analyses was reached.

2.4.10 Isolation and Cultivation of Primary Natural Killer Cells

Primary Natural Killer (pNK) cells can be isolated from peripheral blood, bone marrow, and umbilical cord blood via density gradient centrifugation using ficoll medium. Ficoll is a neutral, highly-branched, hydrophilic polymer of sucrose that dissolves readily in aqueous solution. It is placed at the bottom of a conical tube, and blood is then slowly layered above. After centrifugation the following layers are visible (from top to bottom): blood plasma and other constituents, an intermediate layer of peripheral blood mononuclear cells (PBMCs) and platelets called buffy coat, ficoll, and a pellet comprising erythrocytes and granulocytes. To exclude red blood cell trapping, which could partly remain in the PBMC fraction, the anticoagulant ethylene diamine tetra acetic acid (EDTA) is supplemented during the washing steps. Primary NK cells are isolated using a kit developed for the untouched isolation of NK cells from human PBMCs. Non-NK cells, i.e. T cells, B cells, stem cells, dendritic cells, monocytes, granulocytes, and erythroid cells, are magnetically labeled by using a cocktail of biotin-conjugated antibodies and the NK Cell MicroBead Cocktail. Isolation of highly pure NK cells is achieved by depletion of magnetically labeled cells.

In this thesis, primary human natural killer cells were isolated from buffy coats (kindly provided by H. Bönig, DRK, Frankfurt, Germany) by ficoll gradient (Biozol). Therefore, the buffy coat was diluted 1:3 to 1:4 with PBS/EDTA, and transferred into conical tubes prior to applying ficoll (15 ml). After centrifugation (400x g, 15 min, 4 °C, no deceleration, low acceleration), the intermediate layers of two tubes

were transferred into one new tube, thereby reducing the working volume. After subsequent washing with PBS/EDTA (300x g, then two times 200x g, 15 min, 4 °C) under stepwise reduction of the working volume, the pNK cells were isolated by negative selection from the residing PBMCs using the NK Cell Isolation Kit (Miltenyi Biotec). The cells were seeded at 1.5-2x10^7 cells/ml in X-Vivo medium (2.1.6.3) and cultivated under standard conditions for up to 10 days. The cell density was adjusted every three days by adding new medium with fresh IL-2 for activation. After 7 days, the pNK cells were prepared for flow cytometry (2.4.12) or CLSM analyses (2.4.13).

2.4.11 Inhibition of Protein Glycosylation

To inhibit protein glycosylation during protein synthesis in eukaryotic cells, tunicamycin was used. Tunicamycin is a mixture of homologous nucleoside antibiotics that blocks the synthesis of all *N*-linked glycoproteins and causes cell cycle arrest. Glycosylation inhibition during protein synthesis was performed to validate the suitability of insect cells to perform *N*-linked glycosylation at the three identified acceptor sites (N42, N68, N121 [170]) by comparison with the native non-glycosylated NKp30 ectodomain with respect to their molecular mass.

For this purpose, insect cells were infected with baculovirus encoding for 30Stalk-His (2.4.4) 1 h prior to addition of 1 μg/ml tunicamycin, and maintained under standard conditions. 72 h post infection, the cell culture supernatant was harvested (1,000x g, 10 min, 4 °C), sterile filtered (0.22 μm), supplemented with 0.025 % (v/v) sodium azide and stored at 4 °C. The secreted protein was purified from the supernatant by IMAC (2.5.1.1).

2.4.12 Flow Cytometry

Flow cytometry is a laser-based technology that is employed in cellular approaches such as cell counting, cell sorting or biomarker detection according to the cellular shape, surface expression of proteins or intrinsic fluorophore expression. The method is based on the detection of light scattering as well as fluorescence features of a single cell solution. The light scattering is dependent on the size and granularity of the cells, wheras fluorescence results from intrinsic fluorophore expression or labeling of proteins with fluorophore-conjugated antibodies.

Flow cytometry analyses were performed on a FACSCantoII system (BD). For this purpose, 4x10^5 suspension cells per sample were harvested (200x g, 3 min, 4 °C), washed with 1 ml FACS buffer (200x g, 3 min, 4 °C), and incubated with 50 μl of 5 % (w/v) BSA/FACS for 15 min on ice. To investigate surface NKp30-His expression on adherent cell lines upon transfection or lentiviral transduction, cells were detached with accutase (NKp30 is trypsin sensitive) prior to washing and incubation with 5 % (w/v) BSA/FACS. The cells were washed prior to appropriate antibody or recombinant protein incubation (Tab. 9). All proteins or antibodies were diluted in FACS buffer as shown in Tab. 10. For one sample, 40 μl of antibody or recombinant protein solution were used. Control cells were incubated with 40 μl of FACS buffer. To specifically block protein interactions, cells or recombinant proteins were pre-incubated with the respective blocking antibody for 1 h on ice. The cells were incubated with unconjugated proteins, antibodies or protein-antibody complexes at least for 1 h on ice. After each antibody or recombinant protein incubation step, all samples were washed twice prior to incubation with the appropriate fluorophore-conjugated antibodies for at least 15 min on ice in the dark. The cells were washed twice and fixed in 300 μl FACS-fix. The samples were either used directly for flow cytometry analyses or kept

overnight at 4 °C in the dark (for up to one week). Approximately 5x10^4 cells per sample were analyzed using FACSDiva 6.0 software (BD). To determine the rate of unspecific staining, samples decorated with isotype control or detection antibodies only were analyzed.

Tab. 9: Recombinant protein and antibody combinations for flow cytometry and CLSM analyses

Protein expression was detected by antibody or recombinant protein staining. Unlabeled antibodies were detected by secondary fluorophore-conjugated antibodies.

Recombinant Protein/Antibody	Antigen/Isotype	Detection Antibody
B7-H6-Ig	human IgG	anti-human IgG-Fc, DyLight649-conjug.
30Stalk-His	NKp30	anti-human NKp30, pep. immun.
30LBD-His	NKp30	anti-human NKp30, pep. immun.
anti-human NKp30, 210845	mouse IgG2a	anti-mouse IgG, Alexa647-conjug.
anti-human NKp30, pep. immun.	rabbit IgG	anti-rabbit IgG, APC-conjug.
anti-human NKp30, Z25, PE-conjug.	mouse IgG1	anti-mouse IgG, Alexa546-conjug.
anti-human NKp44, Z231, PE-conjug.	mouse IgG1	anti-mouse IgG, Alexa546-conjug.
anti-human NKp46, BAB281, PE-conjug.	mouse IgG1	anti-mouse IgG, Alexa546-conjug.

Tab. 10: Dilutions for recombinant proteins and antibodies for flow cytometry and CLSM analyses

Antibodies and recombinant proteins were diluted in FACS buffer according to the manufacturer's recommendation or tested in this thesis.

Recombinant Protein/Antibody	Antigen/Isotype	Dilution
B7-H6-Ig	human IgG	50 μg/ml
30Stalk-His	NKp30	50-75 μg/ml
30LBD-His	NKp30	50-75 μg/ml
anti-human NKp30, 210845	mouse IgG2a	25-250 μg/ml
anti-human NKp30, pep. immun.	rabbit IgG	50 μg/ml
anti-human NKp30, Z25, PE-conjug.	mouse IgG1	1:20
anti-human NKp44, Z231, PE-conjug.	mouse IgG1	1:20
anti-human NKp46, BAB281, PE-conjug.	mouse IgG1	1:20
anti-mouse IgG, Alexa647-conjug.	goat IgG	1:200
anti-rabbit IgG, APC-conjug.	goat IgG	1:100
anti-human IgG-Fc, DyLight649-conjug.	goat IgG	7.5 μg/ml
anti-mouse IgG, Alexa546-conjug.	goat IgG	1:200

2.4.13 Confocal Laser Scanning Microscopy

Immunohistochemistry is a common method to detect intracellular antigens or biomarkers on the cell surface by specific antibody binding. Due to fluorophore-conjugated antibodies, proteins can be visualized by immunofluorescence microscopy. Simultaneous staining with antibodies againts biomarkers within different cellular compartments allows protein localization within the cell. In this thesis, the confocal TCS-SP5 laser scanning microscope (CLSM, Leica) was used. In contrast to an epifluorescence microscope, a CLSM is able to generate optical sections of the sample resulting in a better transverse resolution of the fluorescent image and the determination of the cellular localization of the respective antigens [221]. For this purpose, cells were decorated with unconjugated proteins, antibodies or protein-

antibody complexes and further stained with fluorophore-conjugated antibodies as described for flow cytometry analyses (2.4.12). The following steps were performed at room temperature in the dark. After fixation, 50 μl of the sample were centrifuged (200x g, 3 min, 4 °C), washed with FACS buffer, pelleted, and the supernatant was discarded. The remaining cell pellet was resuspended in 7 μl of DAPI stain (nuclear stain), and transferred onto the microscope slide. By applying the cover slip (12 mm in diameter), the cell suspension was distributed avoiding air bubbles. Prepared microscope slides were stored for up to four weeks at 4 °C in the dark. Fluorescent images were obtained using a HCX PL APO Lbd. Bl 63x/1.4-0.6 oil objective, a diode laser (405 nm) to detect DAPI (emission: 410-550 nm), an argon laser (488 nm) to detect GFP (emission: 490-580 nm) or YFP (emission: 515-615 nm), and a HeNe laser (633 nm) to detect APC (emission: 635-750 nm) or DyLight649 (emission: 660-720nm). Analyses of the fluorescent images were performed with the LAS-AF lite 2.0 software.

2.4.14 Quantification of Cell Decoration

Images of single B7-H6 transduced Ba/F3 cells decorated with 30Stalk-His and 30LBD-His proteins (2.4.13) were quantitatively analyzed using the cell image analysis software CellProfiler [222]. NKp30 ectodomain protein clusters (diameter of 4-40 pixel) were identified on grayscale images of the APC channel by pixel intensity (thresholding method: kapur global, correction factor: 2). The cluster area was determined as actual number of pixels in the region. Statistical significance was determined by the Mann-Whitney test using the Prism 5 software (Graph Pad): not significant (n.s.), >0.05; *, p = 0.01-0.05; **, p = 0.001-0.01; ***, p < 0.001.

2.4.15 Signaling Reporter Assay

A signaling reporter assay is a rapid, sensitive and quantitative approach to assess the activation of receptor signal transduction pathways due to ligand binding. Upon induction of the signaling pathway, the activity of downstream transcription factors is analyzed by reporter gene expression. A well-established signaling pathway is the initiation of interleukin-2 expression during T cell activation. Signaling of the T cell receptor complex activates the transcription factor NF-AT (nuclear factor of activated T cells), which binds to NF-AT binding sites within the promoter region of the *IL*-2 gene, thereby initiating gene expression. Within the TCR complex, the CD3ζ chains are responsible for signal transduction. In this thesis, the A5-GFP reporter cell line (mouse T cell hybridoma) was used, which constitutively expresses the CD3ζ chains. The *IL*-2 gene was substituted by a GFP reporter gene that is under the control of the IL-2 promoter, which harbors three NF-AT binding sites [203, 204]. To analyze NKp30-dependent signaling, the A5-GFP cells were retrovirally transduced with the NKp30 full-length receptor or control vector [170]. Thus, ligand-induced NKp30-dependent signaling via CD3ζ can be investigated due to subsequent GFP expression.

To investigate the NKp30 signal transduction capacity after B7-H6 ligand binding, the following effector (A5-30FL-His) to target (Ba/F3-B7-H6) ratios were applied: 2:1, 1:1, and 0.5:1. Both cell lines were washed with FACS buffer (200x g, 3 min), and 7.5x10^7 Ba/F3-B7-H6 cells were resuspended in 1.5 ml of DMEM medium without gentamycin (DMEM/-). 100 μl of target cells (corresponding to 2.5x10^5) were mixed with 5x10^5, 2.5x10^5, or 1.25x10^5 effector cells in a final volume of 200 μl DMEM/- medium. After co-incubation for 16 h (37 °C, 5 % CO_2 and saturated water atmosphere), the cells were pelleted (200x g, 3 min) and incubated for 1 h with 100 μl of APC-conjugated anti-mouse CD4 antibody

(0.2 μg/ml in FACS buffer) to discriminate the effector from the target cells. To validate appropriate NKp30 expression, the cells were incubated for 1 h with 100 μl of APC-conjugated anti-human NKp30 antibody (0.02 μg/ml in FACS buffer). The GFP expression of $CD4^+$ reporter cells was determined by flow cytometry. As signaling control, reporter cells were incubated for 16 h without target cells or in the presence of 50 ng/ml PMA (phorbol 12-myristate-13-acetate) and 750 ng/ml ionomycin (constitutive stimulation of NF-AT [223]). To investigate the concentration-dependent signal inhibition capacity of the NKp30 ectodomain proteins, Ba/F3-B7-H6 target cells were pre-incubated with graded amounts of 30Stalk-His (3.1 and 6.2 μM) or 30LBD-His proteins (2.7, 5.4, 10.8 and 21.6 μM) for 1 h at 37°C prior to co-incubation with A5-30FL-His effector cells at a 1:1 ratio. As reference, Ig fusion proteins (30Stalk-Ig: 2.5 μM, Ifnar2-Ig: 2 μM, [170]) were used. To validate signal inhibition by blocking the effector-target cell interaction, A5-30FL-His reporter cells were pre-incubated with an anti-human NKp30 blocking antibody (0.25 μM).

2.5 Methods of Protein Biochemistry

2.5.1 Protein Purification from Cell Culture Supernatant or Rabbit Serum

Protein purification methods are applied to isolate the protein of choice from a complex mixture. For this purpose, recombinantly expressed proteins are often tagged with short amino acid sequences to allow for affinity purification. In this thesis, all recombinantly expressed proteins contain a specific signaling motif at the N-terminus to facilitate secretion into the cell culture supernatant, thereby reducing the content of disturbing components which bind unspecifically to the affinity matrix during protein purification. The basic principle of affinity purification is protein absorption to a purification matrix, washing away contaminants, elution of the protein, and regeneration of the matrix. In this thesis, different affinity-based chromatographic methods were applied for protein purification by gravity flow: (i) the NKp30 ectodomain proteins (30Stalk-His and 30LBD-His) contain a C-terminal deca-histidine tag, by which the proteins can be purified via immobilized metal ion affinity chromatography (IMAC); (ii) the secreted recombinant ligand B7-H6 is fused C-terminal to a human IgG1-Fc part (B7-H6-Ig), and can thus be purified via the affinity to protein A; and (iii) the antibodies within the rabbit antiserum after peptide immunization can be purified after binding to this peptide, which is coupled to a sepharose resin.

2.5.1.1 Immobilized Metal Ion Affinity Chromatography

Immobilized metal ion affinity chromatography (IMAC) is based on the specific chelate formation of amino acids such as histidines or cysteines to metal ions. In this thesis, Ni^{2+} ions are complexed by nitrilotriacetic acid (Ni-NTA), which is cross-linked to agarose beads (Protino Ni-NTA agarose, Macherey-Nagel). The soluble NKp30 ectodomain variants 30Stalk-His and 30LBD-His are fused to a C-terminal deca-histidine tag to allow for high-affinity binding to the Ni-NTA matrix, and thereby specific protein purification.

For this purpose, an appropriate amount of Ni-NTA agarose (binding capacity up to 50 mg/ml) was applied onto an Econo-Pac column (Bio-Rad) including a bed support frit (30 μm, polyethylene), washed with 10 column volumes (CV) deionized water, and equilibrated with 10 CV wash buffer to reduce unspecific protein binding. After adding the appropriate amount of Ni-NTA agarose beads to the dialysed NKp30 ectodomain protein containing cell culture supernatant (2.4.4), the suspension was incubated for

at least 3 h at 4 °C on a tilt/roller mixer. To avoid loss of protein activity, all of the following purification steps were performed on ice and with ice cold buffers. To collect the Ni-NTA agarose beads, the suspension was again applied onto the Econo-Pac column. The flow-through was stored at 4 °C. The collected Ni-NTA agarose beads were washed with 10 CV of wash buffer, collecting the last milliliter in a reaction tube. To elute the protein from the Ni-NTA agarose beads by high concentrations of the competitor molecule imidazole, 20 CV of elution buffer were applied and collected in 1 ml fractions. Regeneration of Ni-NTA agarose beads was performed by washing with 10 CV of deionized water prior to applying 5 CV of regeneration buffer to remove the complexed Ni^{2+} ions. The Ni-NTA agarose beads were again washed with 10 CV of deionized water prior to recharging with 2 CV of Ni^{2+} solution. The regenerated Ni-NTA agarose beads were washed again with deionized water prior to resuspension in 20 % (v/v) of EtOH for storage at 4 °C. To analyze the purification process, 50 μl of each purification step (input, flow-through, wash, and elution fractions) were subjected to SDS-PAGE (2.5.6) and immunoblot analyses (2.5.7).

To concentrate the purified protein, all elution fractions were combined and applied to an Amicon Ultra-15 centrifugal filter unit (Merck Millipore) with 3 kDa molecular weight-cut off (MWCO). The elution suspension was concentrated to 1 ml (5,000x g, >60 min, 4 °C), and washed three times with 5 ml of Tris buffer. Finally, the protein suspension was concentrated to 0.3-1 ml, transferred into a 1.5 ml reaction tube and supplemented with 4 % (v/v) PI mix. After protein concentration determination (2.5.3), the protein suspension was either stored at 4 °C for up to one month or supplemented with 25 % (v/v) of glycerol for long-term storage at -20 °C.

2.5.1.2 Protein A Affinity Chromatography

The bacterial surface protein A binds specifically to the constant region of immunoglobulins from many mammalian species, most notably IgGs. Therefore, matrix-bound protein A was utilized to affinity purify IgG1-Fc (Ig) tagged proteins. For this purpose, an appropriate amount of rec-Protein A-Sepharose 4B Conjugate (protein A beads, Life Technologies) was washed twice with PBS (1,000x g, 3 min). For each 25 ml of supernatant, 10 μl of settled protein A beads were applied. After adding the appropriate amount of protein A beads to the sterile filtered Ig fusion protein containing cell culture supernatant (2.4.6), the suspension was incubated overnight at 4 °C on a tilt/roller mixer. To avoid loss of protein activity, all of the following purification steps were performed on ice. To collect the protein A beads, the suspension was applied onto an Econo-Pac column (Bio-Rad) including a bed support frit (30 μm, polyethylene). The flow-through was stored at 4 °C. The collected protein A beads were washed with 20 column volumes (CV) of PBS, collecting the last milliliter in a reaction tube. Elution of the protein was performed by pH shift. Adding collection buffer (1/10 of the volume of the elution fractions) into the collection tubes prior to elution facilitates neutralization of the pH within the protein suspension immediately after elution from the beads. To elute the protein from the protein A beads, 10 CV of elution buffer were applied and collected in 0.5 ml fractions. Regeneration of protein A beads was performed by adding 10 CV of regeneration buffer onto the beads. The protein A beads were transferred into a reaction tube and washed once again with PBS. The settled beads were suspended in storage buffer and stored at 4 °C. To analyze the purification process, 50 μl of each purification step (input, flow-through, wash, and elution fractions) were subjected to SDS-PAGE (2.5.6) and immunoblot analyses (2.5.7).

To concentrate the purified protein, all elution fractions were combined and applied to an Amicon Ultra-4 centrifugal filter unit (Merck Millipore) with 50 kDa molecular weight-cut off (MWCO). The elution suspension was concentrated to 1 ml (7,500x g, 5-10 min, 4 °C), and washed three times with 4 ml of PBS to exchange the buffer. Finally, the protein suspension was concentrated to 0.3-1 ml, transferred into a 1.5 ml reaction tube and supplemented with 4 % (v/v) PI mix. After protein concentration determination (2.5.3), the protein suspension was either stored at 4 °C for up to one month or supplemented with 25 % (v/v) of glycerol for long-term storage at -20 °C.

2.5.1.3 Immunoaffinity Chromatography

Immunoaffinity chromatography is a method applied to purify antibodies from blood serum. This serum could be derived from an organism that was immunized with an antigen such as a peptide or recombinant protein. When the peptide antigens are produced synthetically, a terminal cysteine residue is added at either the N- or C-terminus of the peptide. This cysteine residue contains a sulfhydryl and/or amine functional group which allows the peptide to be easily conjugated to a carrier protein (e.g. Keyhole Limpet Hemocyanin (KLH)). The same peptide is also immobilized onto a solid support such as agarose or sepharose resin through the cysteine residue and is then used as an affinity ligand in purifications of antibodies from the antiserum. Elution of the antibodies is most often achieved using a low pH buffer such as it is described for Protein A chromatography (2.5.1.2). In this thesis, an anti-NKp30 antibody with a defined epitope (amino acids P62 to R75) situated within the NKp30 ligand binding domain was generated. Therefore, two rabbits were immunized with the peptide NH_2-CPGKEVRNGTPEFRGR-COOH (Bioscience, Göttingen) to obtain the antiserum. The same peptide was used for the immunoaffinity chromatography. Peptide loading as well as antibody purification steps were performed on ice and with ice-cold buffers. The sepharose resin (1 ml), which was stored in isopropanol, was washed in a first step with 20 column columes (CV) of 0.1 M HCl. For optimal peptide loading, the matrix was adjusted to pH 8.5 by washing with 20 CV of ice-cold PBS (pH 8.5). 4 mg of peptide were resolved in 50 μl of DMSO and adjusted to 1 ml with ice-cold PBS (pH 8.5). The peptide suspension was incubated with the sepharose resin overnight at 4 °C on a tilt/roller mixer. Peptide binding onto the matrix was checked by determination of the protein concentration of the flow-through. To block residual binding places, the matrix was incubated for 1 h with 15 ml of 1 M Tris (pH 8.8) at 4 °C on a tilt/roller mixer, and then equilibrated with 10 CV of PBS (pH 8.5). 25 ml of the rabbit antiserum were centrifuged (9,000x g, 30 min, 4 °C) and sterile filtered (0.45 μm) to remove cellular components and larger protein aggregates prior to incubation with the peptide-loaded sepharose resin overnight at 4 °C on a tilt/roller mixer. The matrix was washed with 20 CV of PBS (pH 8.5) and 20 CV of PBS (pH 4.6) to reduce unspecific binding. 300 μl of ice-cold 1 M Tris (pH 8.8) were added into ten reaction tubes prior to collection of 700 μl elution fractions using ice-cold 100 mM glycine (pH 2.7). The sepharose resin was neutralized with ice-cold PBS, and stored in PBS supplemented with 3 mM NaN_3 at 4 °C.

To concentrate the purified peptide-specific antibodies, all elution fractions were combined and applied to an Amicon Ultra-4 centrifugal filter unit (Merck Millipore) with 50 kDa molecular weight-cut off (MWCO). The elution suspension was concentrated to 1 ml (7,500x g, 5-10 min, 4 °C), and washed three times with 4 ml of PBS to exchange the buffer. Finally, the protein suspension was concentrated to 0.3-1 ml, transferred into a 1.5 ml reaction tube and supplemented with 4 % (v/v) PI mix. After protein concentration determination (2.5.3), the protein suspension was stored in 30 μl aliquots at -20 °C.

2.5.2 Size Exclusion Chromatography

Size exclusion chromatrography or gel filtration allows for separation of analytes on the basis of their size or hydrodynamic volume using porous beads in a column [224]. The separation is dependent on the pore size of the beads as well as the buffer conditions. An important value is the retention volume (V_r) of the separated analyte molecules, which is determined by UV absorption at 280 nm. Small molecules are retained by easy entering pores, and thereby increasing V_r. Conversely, larger analytes spend less, if any, time in the pores and are eluted quickly. Analytes, which are not retained, are eluted with the free volume outside of the particles, also known as void volume (V_0). The void volume is known to be approximately 1/3 of the column volume and can be determined by using Blue Dextran 2000 (molecular mass of ∼2000 kDa, GE Healthcare). There is a limited range of molecular mass that can be separated by each column. Therefore, it could be necessary to use several columns with different pore sizes in tandem to fully resolve the sample having a broad molecular mass range. To estimate the retention volume/molecular size of the protein(s) of interest, commercially available calibration standards (highly purified, well-characterized, globular proteins) are used.

In this thesis, prepacked analytical Superdex 200 10/300 GL (24 ml, fractionation range: $1x10^4$ to $6x10^5$ Da) and Superose 6 10/300 GL (24 ml, fractionation range: $5x10^3$ to $5x10^6$ Da) columns were used in an Äkta Prime FPLC system (GE Healthcare). All buffers and solutions were prepared at 4 °C and sterile filtered (0.22 μm) to remove particles and air bubbles. Both columns were stored in 20 % (v/v) of EtOH. Therefore, they were washed with 1.5 CV of deionized water prior to equilibration with 1.5 CV of Tris buffer (pH 8.0). Concentrated protein samples were injected via an appropriate sample loop. Size exclusion chromatography was performed in Tris buffer (pH 8.0) with flow rates of 0.5 ml/min and 0.3 ml/min, respectively. Elution fractions were collected according to the following application. Molecular weight and void volume determination was carried out according to the manufacturer's instructions using the Gel Filtration LMW and HMW Calibration Kits (GE Healthcare). The respective retention volumes are shown in Tab. 11. For the long-term storage, the columns were washed with 1.5 CV of deionized water prior to 20 % (v/v) of EtOH.

Tab. 11: Retention volumes (V_r) of the calibration standards on Superdex 200 and Superose 6 column
Respective standard proteins were mixed and applied to SEC using Tris buffer.

Calibration Standard		Molecular Weight	Superdex200	Superose6
Blue Dextran 2000	V_0	2,000 kDa	8 ml	8 ml
Thyroglobulin	T	669 kDa	8 ml	13.7 ml
Ferritin	F	440 kDa	10.0 ml	15.2 ml
Aldolase	Ald	158 kDa	13.6 ml	16.8 ml
Conalbumin	C	75 kDa	15.2 ml	17.0 ml
Ovalbumin	O	44 kDa	17.0 ml	18.2 ml
Ribonuclease A	R	13.7 kDa	19.9 ml	

2.5.3 Determination of Protein Concentration

Proteins in solution absorb ultraviolet (UV) light with absorbance maxima at 280 nm (aromatic rings of amino acids) and 200 nm (peptide bonds). The secondary, tertiary and quaternary structure can affect the absorbance, therefore factors such as pH or ionic strength can alter the absorbance spectrum. The

spectrophotometric quantification of proteins is based on the Lambert-Beer law relating the amount of absorbed light to the amount of protein in the mixture. For this purpose, 2 μl of a protein solution were measured at 280 nm using the NanoDrop ND 1000 (PeqLab Biotechnologie) device. The corresponding buffer solution was used as blank.

2.5.4 Enzymatic Protein Deglycosylation

Glycosylation is one of the most common post-translational modifications of proteins to facilitate correct folding, stability, and function. Oligosaccharides can be attached either at asparagine residues (*N*-linked glycosylation) or serine or threonine residues (*O*-linked glycosylation) on the core protein. To asses if a protein is glycosylated, enzymatic deglycosylation is performed. Treatment with specific glycosidases provides complete sugar removal without protein degradation. Peptide-*N*-Glycosidase (PNGase) F is an amidase that cleaves between the innermost *N*-Acetylglucosamine (GlcNAc) and asparagin residues of high mannose, hybrid, and complex oligosaccharides from *N*-linked proteins [225]. PNGase F treatment of glycoproteins is the most effective method for removing almost all *N*-linked oligosaccharides. However, oligosaccharides containing a fucose α1-3-linked to the glycan core are restitant to PNGase F, which can occur on some plant, insect and mammalian glycoproteins [226, 227]. In contrast, *O*-linked glycans were removed stepwise by a series of exoglycosidases such as *O*-Glycosidase, α(2-3,6,8)-Neuraminidase, β(1-4)-Galactosidase, and β-*N*-Acetylglucosaminidase. This combination of enzymes will not remove all *O*-linked oligosaccharides but should remove many common oligosaccharide structures.

In this thesis, enzymatic deglycosylation assays were performed using PNGase F (New England Biolabs) for removal of only *N*-linked oligosaccharides, and an enzyme mix (New England Biolabs) for removal of *N*- and *O*-linked glycosylation. All enzymes were supplied with buffers. A standard deglycosylation mix was performed according the manufacturer's instructions. Therefore, 5 μg of purified protein were mixed with 1 μl of 10x glycoprotein denaturation buffer and adjusted to a final volume of 10 μl with deionized water. To denature the protein and thereby provide better accessibility for the glycosidases, the protein solution was incubated for 10 min at 100 °C. After cooling down, the reaction mixture was supplemented with 2 μl of NP-40, 2 μl of G7 reation buffer, 1 μl PNGase F (500 U) or protein deglycosylation mix, and adjusted to a final volume of 20 μl with deionized water. The reaction mix was incubated at 37 °C for 4 h, followed by incubation overnight at 4 °C to ensure complete oligosaccharide removal. Potential reduction in molecular mass was investigated by SDS-PAGE (2.5.6) and immunoblot analyses (2.5.7).

2.5.5 Immunoprecipitation

Immunoprecipitation (IP) is a biochemical method to isolate and concentrate a protein of interest from a protein solution mixture by applying specific antibodies. These protein solutions could be obtained by total cell lysis or preparation of specific cellular fractions such as crude membranes and cytosolic fractions prior to IP. For this purpose, 1x10^7 cells were harvested (200x g, 3 min) and washed once with PBS (200x g, 3 min). Cell pellets were either stored at -20 °C or immediately used for cell lysis. Therefore, the cell pellet was resuspended in 200 μl of lysis buffer, incubated for 20 min on ice mixing the suspension every 5 min, and centrifuged for 30 min at 20,000x g and 4 °C. The supernatant containing the solubilized proteins was transferred into a low protein binding reaction tube (Kiskers Biotech) and supplemented with 10 μg of anti-human NKp30 (P30-15) antibodies. After incubation for 4 h at 4 °C on a

tube rotator (LD 79, Labinco BV), 2 μl of 1 % (v/v) of Tween20 were added to the solution. To isolate the antibody-bound proteins from the solution, magnetic beads coupled with Protein A (Dynabeads Protein A, Life Technologies) were applied. For one sample, 50 μl of the Dynabeads Protein A suspension was used. The beads were washed twice with 1 ml of lysis-T buffer utilizing a magnetic separation rack (New England Biolabs). The beads were reconstituted in the reaction mixture containing the antibody-bound proteins and incubated overnight at 4 °C on a tube rotator. The beads were washed three times with PBS-TT and transferred into a new low protein binding reaction tube. To elute the bound proteins by applying a pH shift, the beads were reconstituted in 50 μl of elution buffer and incubated for 1 min at room temperature. The eluate suspension was transferred into a new low protein binding reaction tube containing 3 μl of collection buffer to neutralize the pH, and subjected to SDS-PAGE (2.5.6) and immunoblot analyses (2.5.7). The remaining magnetic beads were washed twice with 1 ml of PBS-T, resuspended in 50 μl of DB storage buffer and stored at 4 °C.

2.5.6 Sodium Dodecyl Sulfate Polyacrylamide Gel Electrophorsis

Sodium dodecyl sulfate polyacrylamide gel electrophoresis (SDS-PAGE) is an analytical method in biochemistry, which allows the separation of protein mixtures according to their molecular mass after applying an electric current. The most common procedure to separate molecules between 5 to 250 kDa is the discontinuous SDS-PAGE. This method relies on the concentration of the proteins on a barrier between stacking and resolving gel due to different pH and pore sizes [228]. The basic principle of the method is to shield the native charge of denatured proteins by hydrophobic interaction with the anionic detergent sodium dodecyl sulfate (SDS). The generated negatively charged micelles migrate from the cathode to the anode after applying an electric current in the polyacrylamide gel. Since the gel acts like a molecular sieve, similar to agarose gels (2.3.6), denatured SDS treated protein mixtures are separated dependent on their size. Additional treatment with the reducing agents β-mercaptoethanol and/or dithiothreitol (DTT) reduces disulfide bonds within proteins, promoting further protein denaturation.

To prepare protein samples for SDS-PAGE, protein solutions were mixed with the appropriate amount of either reducing or non-reducing 5x SDS sample buffer (to a final concentration of 1x SDS sample buffer). Samples containing reducing sample buffer were additionally supplemented with 200-300 mM DTT (final concentration). All samples were heated, either for 5 min at 95 °C (purified protein sample) or 30 min at 37 °C (total cell lysates), and centrifuged for 5 min at 20,000x g. An appropriate amount of the sample was applied to a polyacrylamide gel (Tab. 12) including a PageRuler variant (Thermo Scientific) as size standard. The electrophoresis was performed at 200 V for approximately 60-90 min (according to the pore size) in a Mini-PROTEAN II electrophoresis cell (Bio-Rad) filled with SDS running buffer according to Laemmli [228]. Polyacrylamid gels were either subjected to coomassie staining or to immunoblot analysis (2.5.7).

Tab. 12: SDS polyacrylamide gel composition

Dependent on the molecular mass of proteins to be separated, different acrylamide concentrations were used. APS and TEMED start polymerization, and are therefore added last. The instruction refers to the preparation of two gels (100 x 100 x 1 mm).

		Resolving Gel		Stacking Gel
Component		**12 %**	**15 %**	**5 %**
30 %	acrylamide	4.0 ml	5.0 ml	1.0 ml
	H_2O	3.3 ml	2.3 ml	4.0 ml
1.5 M	Tris pH 8.8	2.5 ml	2.5 ml	—
1.5 M	Tris pH 6.8	—	—	750 μl
20 %	SDS	50 μl	50 μl	30 μl
10 %	APS	100 μl	100 μl	60 μl
	TEMED	4 μl	4 μl	6 μl

To visualize proteins on polyacrylamide gels, PageBlue protein staining solution (Thermo Scientific) was applied according to the manufacturer's instructions. PageBlue is based on the coomassie brillant blue G-250 dye, which binds unspecifically to cationic and hydrophobic amino acid residues. The sentivity allows for detection of only 5 ng depending on the protein properties. To fix the proteins in the gel matrix, gels were incubated in 10 % (v/v) acetic acid for 10 min. Since SDS interferes with PageBlue staining, gels were additionally washed twice with water. Staining was performed for 1-2 h at room temperature. To reduce background staining, stained gels were washed twice with water.

2.5.7 Immunoblotting

The immunoblotting method, also known as western blotting, facilitates the transfer of proteins from a gel matrix onto a membrane (e.g. nitrocellulose or PVDF) prior to immunodetection by specific antibodies [229]. Therefore, a mixture of proteins is separated by SDS-PAGE according to their molecular mass (2.5.6). During the transfer onto the membrane, an electric current is applied to pull the proteins from the gel onto the membrane, maintaining the same organization as in the gel matrix. The blotted proteins are exposed on a thin surface layer and can be visualized by immunostaining, allowing specific detection of the protein of interest. The uniformity and overall effectiveness of transfer from the gel to the membrane can be checked by staining the membrane with Ponceau S dye, which can be easily removed by washing with deionized water. A common method to analyze immunoblots is enhanced chemiluminescence (ECL). For this purpose, horseradish peroxidase (HRP) enzymes are tethered to the protein of interest by applying HRP-coupled antibodies. HRP catalyzes the conversion of ECL substrate (based on *p*-coumaric acid and luminol) in the presence of hydrogen peroxide to a light emitting product, which can be detected and documented using photographic films.

To transfer proteins from SDS polyacrylamide gels onto nitrocellulose membranes, a Trans-Blot SD Semi-Dry transfer cell (Bio-Rad) was used according to the manufacturer's instructions. Therefore, two blotting papers (1.0 mm) and the nitrocellulose membrane were soaked with transfer buffer prior to assembly into a stack of blotting paper, membrane, SDS polyacrylamide gel, and blotting paper. After blotting at 15 V for 16 min (one blot) or 25 V for 30 min (four blots), the membranes were incubated in blocking buffer for 30 min at room temperature (RT) to prevent unspecific antibody binding. For specific

protein staining, membranes were incubated overnight at 4 °C with the appropriate antibody diluted in blocking buffer (Tab. 13). The membranes were washed three times for 5-10 min at RT with TBS-T to remove unbound antibodies. To detect unlabeled antibodies, the appropriate HRP-conjugated secondary antibody was applied and incubated for 2-4 h at RT prior to ECL detection. Therefore, membranes were washed again three times with TBS-T to remove unbound HRP-conjugated antibodies. For ECL detection, the membranes were incubated with ECL I solution for 5 min following incubation with ECL II solution for 1 min. The chemiluminescence signals were documented using Super RX medical X-ray film 100NIC (FujiFilm Europe GmbH).

Tab. 13: Antibody dilutions for immunoblot analyses

Antibodies were diluted in blocking buffer according to the manufacturer's recommendation or tested in this thesis.

Antibody	Antigen/Isotype	Dilution
anti-human NKp30, pep. immun.	rabbit IgG	1:500
anti-human NKp30, polyclonal	goat IgG	1:1,000
anti-rabbit IgG, HRP-conjug.	goat IgG	1:10,000
anti-goat IgG, HRP-conjug.	donkey IgG	1:30,000
anti-His, HIS-1, HRP-conjug.	mouse IgG2a	1:2,000
anti-human IgG-Fc, HRP-conjug.	goat IgG	1:10,000

2.5.8 Peptide Spot Array

Peptide arrays on cellulose membranes are synthesized with the unique SPOT technology, which allows for efficient and inexpensive antibody epitope mapping or protein-protein interaction studies. In this thesis, this method was applied to determine the epitope(s) of the antibodies purified from rabbit antiserum after peptide immunization. Therefore, peptide arrays of human NKp30 (18 amino acids, off-set by one amino acid) were synthesized by Fmoc chemistry at activated PEG spacers on cellulose membranes by automated parallel peptide synthesis on a MultiPep RS instrument (Intavis) [230, 231]. To use these membranes for binding experiments, they were rehydrated by incubation with pure ethanol and stepwise dilution with deionized water until there is no ethanol left. The membranes were washed three times with TBS-T for 5 min and incubated with the blocking solution for 1 h at room temperature (RT). Antibody incubation (anti-human NKp30, pep. immun.; anti-rabbit-IgG, HRP-conjug.) and ECL detection were performed as described for immunoblot analyses (13).

2.5.9 Enzyme-Linked Immunosorbent Assay

Enzyme-linked immunosorbent assay (ELISA) is an approach to assess the amount of substances or binding affinities by color change applying HRP-conjugated antibodies. The basic principle of an ELISA is to immobilize a protein on a solid support and incubate either with an interacting protein prior to or directly apply a specific antibody for detection. Notably, the absorbance (A) of a chromogenic substrate converted by HRP is proportional to the amount of specifically bound detection antibody. In a saturation binding experiment, the concentration (c) of the interacting protein/antibody is stepwise increased from blank (buffer control) up to complete occupation of all binding places on the immobilized protein.

Multiple washing steps ensure that only specifically bound proteins and/or antibodies are detected.

In this thesis, the Langmuir adsorption model is used to quantify specific binding as a function of the concentration at room temperature. Assuming one site specific binding, the equilibrium binding constant K_D (ligand concentration that binds to half the receptor sites at equilibrium) and the maximum number of binding sites B_{max} are determined according to the following equation using the Prism 5 software (GraphPad).

$$A = \frac{B_{max} \times c}{K_D + c}$$

To asses the ligand binding affinity of the soluble NKp30 ectodomain proteins to the recombinant ligand B7-H6-Ig, 0.5 μg of B7-H6-Ig were coated overnight at 4 °C into one well of a 96-well MICROLON microtiter plate (Greiner Bio-One) in a total volume of 100 μl of PBS. All further incubation and washing steps were performed at room temperature. The plate was washed four times with 300 μl of PBS-T per well. To inhibit unspecific protein binding, the plate was incubated with 300 μl of 7.5 % BSA/PBS per well for 1 h, and washed again four times with PBS-T. To apply graded amounts of soluble NKp30 ectodomain proteins, a 1:1 dilution series was generated using 1 % BSA/PBS covering a protein concentration range of 400 nM-1.6 nM as well as a blank (buffer control) for background subtraction. Notably, for determination of binding affinities, each data point represents the mean of triplicates whereas the identification of 30Stalk-His or 30LBD-His protein containing SEC fractions (500 μl) was performed in duplicates. 100 μl of each dilution or SEC fraction were applied to one well and incubated for 1 h. The plate was washed four times with PBS-T prior to incubation with 100 μl per well of an anti-human NKp30 antibody (Tab. 14) for 1 h.

Tab. 14: Antibody dilutions for ELISA

Antibodies were diluted in 1 % BSA/PBS according to the manufacturer's recommendation or tested in this thesis.

Antibody	Antigen/Isotype	Dilution
anti-human NKp30, 210845	mouse IgG2a	10 μg/ml
anti-human NKp30, pep. immun.	rabbit IgG	5 μg/ml
anti-human NKp30, polyclonal	goat IgG	0.5 μg/ml
anti-human MICA, polyclonal	goat IgG	0.5 μg/ml
anti-rabbit IgG, HRP-conjug.	goat IgG	1:10,000
anti-goat IgG, HRP-conjug.	donkey IgG	1:5,000
anti-human IgG-Fc, HRP-conjug.	goat IgG	1:50,000

The plate was washed four times with PBS-T and incubated with 100 μl per well of the respective HRP-conjugated detecion antibody for 1 h. The plate was washed four times with PBS-T prior to detection of bound antibodies using 100 μl per well of 1-Step Ultra TMB-ELISA solution (Pierce) according to the manufacturer's instructions. TMB (3,3',5,5'-tetramethylbenzidine) is a chromogenic substrate for HRP, turning blue upon oxidization. To stop the reaction, 50 μl per well of 1 N sulfuric acid was applied, and the color change to yellow was detected at 450 nm in a microplate reader (Kinetic-QCL, Anthos Labtech). As control protein, soluble MICA04-His (kindly provided by S. Weil in the lab of J. Koch at the Georg-Speyer-Haus, Frankfurt am Main, Germany) was used. To verify the specificity of the NKp30-B7-H6 interaction by ELISA, the dilution series was pre-incubated with an anti-human NKp30 blocking antibody

(67 nM, clone 210845) for 1 h at 4 °C prior to application of 100 μl of this antibody-protein-complex suspension per well as described for the protein dilution series.

2.5.10 Negative-Stain Electron Microscopy and 2D Class Averaging

Molecular transmission electron microscopy (TEM) in combination with image processing and reconstruction techniques provides 3D structure information such as composition, size, flexibility and heterogeneity on single biomacromolecules [232]. To sustain the native structure of the proteins or protein complexes during observation by TEM, the samples are fixed by rapid freezing for performing cryo electron microscopy at liquid helium temperature (0 K at 1 atm). Due to technical limitations, the negative-stain fixation method is applied more frequently. Upon adsorption on a solid support, the proteins are embedded using a heavy metal salt such as uranyl acetate, which contrasts the structure and conserves the structural information at moderate solution. To obtain information on the 3D structure, single particles are identified on digital images (2D). Due to complex calculations using classification algorithms, similar projections of the molecules are identified and summarized in 2D classes. Each of these classes represents a 2D projection of the investigated 3D complexes at a distinct solid angle. Upon characterization of the respective spatial directions, a 3D modell can be combined [232].

To analyze the geometry of the NKp30 ectodomain oligomers (in cooperation with K. Davies from the Department of Structural Biology at the Max Planck Institute of Biophysics, Frankfurt am Main, Germany), the elution fractions of the size exclusion chromatography (Superose 6 10/300 GL column) with the highest protein amount were chosen (2.5.2). The concentration of the oligomers was adjusted to 0.1 mg/ml with buffer (50 mM Tris, 150 mM NaCl, pH 8, 4°C). To obtain a suitable distribution of the oligomeric particles, the samples were diluted 1:4 (30Stalk-His) or 1:25 (30LBD-His) with the same buffer. 3 μl of sample were applied to glow-discharged EM grids (400 mesh) containing a continuous carbon support film. After 1 min, the samples were washed drop-wise with 20 μl of 1 % (w/v) uranyl acetate and then incubated with 3 μl of stain for a further minute. Excess stain was removed with filter paper (#4, Whatman). Electron microscopy was performed using a Tecnai Spirit electron microscope (FEI, Eindhoven, The Netherlands) operating at 120 kV. Images were acquired at a nominal magnification of 34,000x on a 4,096x4,096 pixel CCD (Ultrascan 4000, Gatan), which corresponds to a specimen pixel size of 0.36 nm.

To get a first impression of the structural heterogeneity of the oligomeric complexes, more than 6.000 single particles for both the 30Stalk-His and 30LBD-His proteins were isolated from 2D images to identify similar projections for averaging in 2D classes (calculations kindly perfomed by K. Davies from the Department of Structural Biology at the Max Planck Institute of Biophysics, Frankfurt am Main, Germany).

3 Results

So far, there is only little known about how the germline-encoded NK cell receptor NKp30 is able to recognize and interact with multiple ligands that are not related in sequence and structure. In this thesis, a cross-talk between NKp30 and the other NCRs or NKp30 self-assembly were assumed to be possible mechanisms to enhance ligand binding affinity for corresponding ligands by increased avidity. From various eukaryotic cell lines, insect cells were identified as appropriate expression host for analyses of single full-length NCRs or NCR combinations on the plasma membrane, representing a minimalistic NK cell mimic without immunological background. Furthermore, soluble variants of the NKp30 ectodomain were generated to investigate its oligomerization potential. Thereby, receptor homo-oligomerization was identified as a key mechanism to increase the ligand binding affinity of NKp30. The generation of all used full-length NCR and NKp30 ectodomain variants is described in detail in the ”Cloning Strategies” section (2.3.10) and therefore, it is not further mentioned in the ”Results” section. Parts of this thesis are published in Hartmann *et al.* (2012), Binici *et al.* (2013), and Herrmann *et al.* (2014) [166, 170, 233].

3.1 Functional Cooperation Between the NCRs

NKp30, one of the major activating NK cell receptors, recognizes multiple non-related ligands on various pathogens, malignantly transformed cells, virus-infected cells, and even immature dendritic cells, thereby bridging innate and adaptive immunity [3]. Interestingly, the molecular details of ligand recognition by NKp30 and the NCRs in general are poorly characterized. In 2003, Augugliaro and colleagues [173] could demonstrate a functional cross-talk between different NCRs within the plasma membrane of NK cells. They found that the engagement of a single NCR resulted in the activation of the signaling cascade associated with the other NCRs, which efficiently amplified activating signals. However, it is conceivable that this cross-talk could also cause structural rearrangements of the NCR ectodomains and thereby result in *de novo* formation of a composite binding site. Notably, an encounter of all three NCRs could only occur on activated NK cells due to IL-2 dependent induction of NKp44 expression [99, 100]. Moreover, upon IL-2 stimulation of NK cells not only NKp44 but a variety of activating NK cell receptors including NKp30 are upregulated on the plasma membrane [68, 179–184]. This was also demonstrated in this thesis by confocal laser scanning microscopy (CLSM) of freshly isolated (2.4.10) and IL-2 activated primary NK cells using an anti-NKp30 antibody (peptide immunized, Fig. 6). This increased local concentration of NKp30 on the NK cell surface could drive homo-oligomerization resulting in improved ligand recognition.

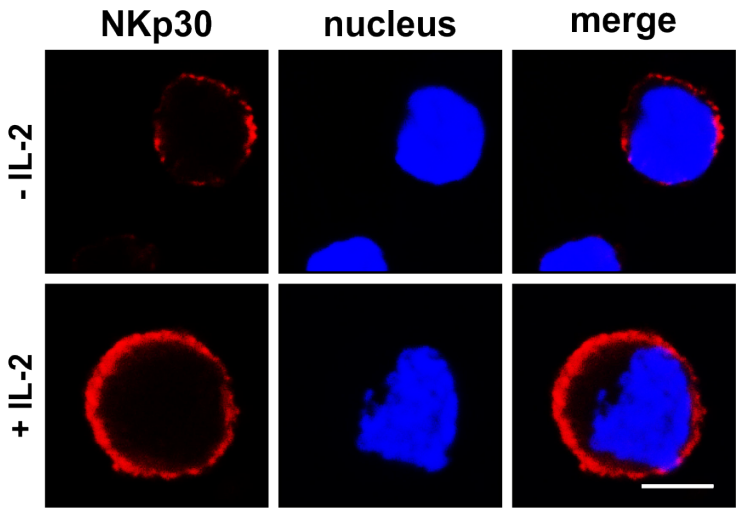

Fig. 6: Increased NKp30 surface expression by IL-2 activation of primary NK cells

Primary NK cells were isolated from buffy coat and activated with IL-2 for seven days. NKp30 surface expression of freshly isolated and activated primary NK cells was analyzed by confocal laser scanning microscopy (CLSM) using an anti-NKp30 antibody (NKp30, *red*; DAPI, *blue*; size bar corresponds to 5 μm).

Interestingly, the heterogeneous decoration pattern upon binding of a recombinant NKp30 ectodomain protein (30Stalk-Ig, detected by CLSM after decoration with FITC-coupled anti-hIgG1 antibodies) to NKp30 ligand expressing HEK293T cells indicates crowding of ligand molecules on the target cell surface (Fig. 7). Notably, ligand-induced receptor clustering is a common mechanism for receptor-mediated signaling in immune responses [234–236]. This strengthens the hypothesis of NKp30 homo-oligomerization for improved ligand recognition and increased binding affinity.

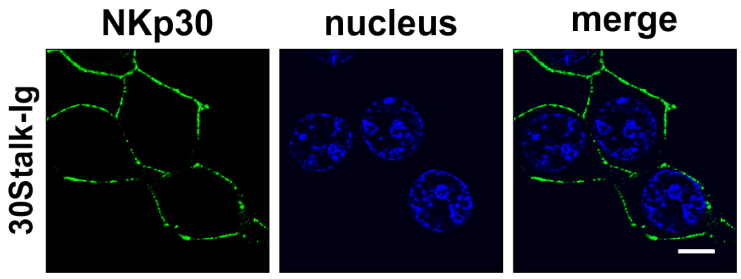

Fig. 7: Decoration pattern upon binding of 30Stalk-Ig proteins on NKp30 ligand positive HEK293T cells

Binding of 30Stalk-Ig proteins to HEK293T cells was analyzed by CLSM using an anti-hIgG1-Fc antibody (anti-hIgG1-Fc, *green*; To-Pro-3, *blue*; size bar corresponds to 8 μm, modified from [170]).

3.2 Insect Cells as Tool for Indivdiual Analyses of Recombinant Full-Length Natural Cytotoxicity Receptors

3.2.1 Full-Length NKp30 Surface Expression on Mammalian Cell Lines

Crowded ligand molecules on the target cell surface as well as an increased local receptor concentration on the plasma membrane upon IL-2 stimulation of primary NK cells indicate pre-clustering of NKp30 to facilitate specific ligand binding and efficient signal transduction for enhanced NK cell cytotoxicity. To investigate the homo-oligomerization potential of NKp30, different eukaryotic cell lines were analyzed with respect to recombinant receptor surface expression level.

For transient expression of the recombinant full-length NKp30 receptor fused to a C-terminal deca-histidine tag (NKp30-His), HEK293T cells were transfected with the construct pIRES2-NKp30opt-His-EGFP using the PEI transfection method (2.4.5). As mock control, HEK293T cells were transfected with empty vector. Due to an IRES element, all transfectants constitutively expressed cytosolic GFP. 72 h post transfection, the transfection efficiency (GFP expression) and the NKp30 surface expression (anti-NKp30, polyclonal) were monitored by flow cytometry (2.4.12) (Fig. 8). Based on the GFP expression, less than 50 % of the cells were transfected. Moreover, only moderate and inhomogeneous expression of surface NKp30-His was found on the plasma membrane of transfected HEK293T cells. Similar results were obtained by S. Weil (in the lab of J. Koch at the Georg-Speyer-Haus, Frankfurt am Main, Germany [237]). Notably, transfection of other eukaryotic cell lines such as the human pancreatic carcinoma cell line MiaPaCa-2 did not improve the transfection efficiency (data not shown).

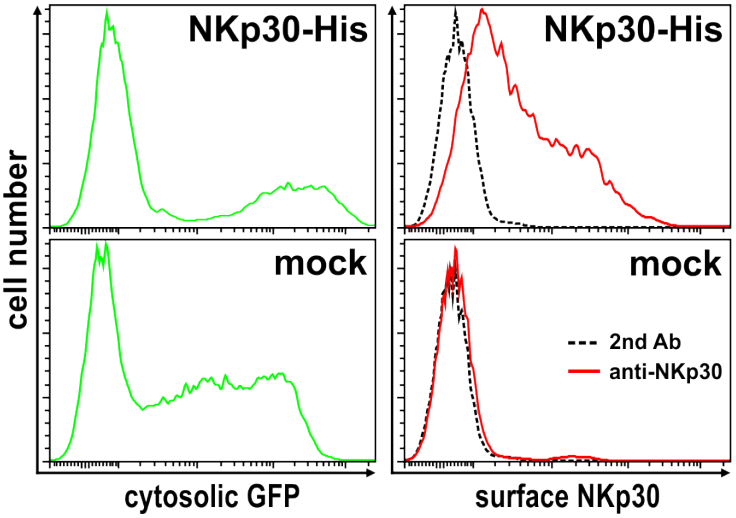

Fig. 8: Surface expression of NKp30-His on transfected HEK293T cells

HEK293T cells were transfected with pIRES2-NKp30opt-His-EGFP (NKp30-His) or pIRES2-EGFP (mock) plasmids. NKp30-His surface expression was analyzed 72 h post transfection by flow cytometry using an anti-NKp30 antibody (anti-NKp30, *red line*; antibody control, *dashed line*; cytosolic GFP, *green line*).

To increase the surface expression level of NKp30, HEK293 cells were transduced with lentiviral particles for stable integration of the introduced NKp30 DNA into the genome. For this purpose, lentiviral particles were produced by HEK293T cells upon triple transfection with the LeGO-NKp30opt-His-iG2 construct (encoding for NKp30-His) or empty vector (mock control) and two helper plasmids using the PEI method (2.4.7). 24 h post transfection, GFP expression was monitored by fluorescence microscopy (Fig. 9A). Notably, after transfection with the LeGO-NKp30opt-His-iG2 construct, less HEK293T cells survived suggesting that recombinant full-length NKp30-His might be cytotoxic. However, since the transfection efficiency was determined at 80-90 % for mock and 50 % for NKp30-His, lentiviral particles were harvested 72 h post transfection from the cell culture supernatants and used for transduction of HEK293 cells or stored. As this approach was a proof of concept, virus titers of lentiviral particles for NKp30-His and mock expression have not been adapted. Four weeks after lentiviral transduction of the HEK293 cells, GFP expressing single cell clones were isolated by limiting dilution to generate a cell line with high NKp30 surface expression. After seven weeks of proliferation, surface NKp30-His (anti-NKp30, polyclonal) and GFP expression of the remaining single cell clones (six clones for both NKp30-His and mock control) were investigated by flow cytometry. Dot plots of the clones with highest

NKp30-His surface and/or GFP expression are shown in Fig. 9B. Though stable integration obviously enhanced the GFP expression in the mock control (more than 90 % GFP positive cells), this was not the case for transduction with lentiviral particles encoding NKp30-His (51 % GFP positive cells). Moreover, only 10 % of these GFP positive cells expressed NKp30-His on the cell surface (anti-NKp30, polyclonal) implying difficulties with the receptor transport to or the stabilization on the plasma membrane.

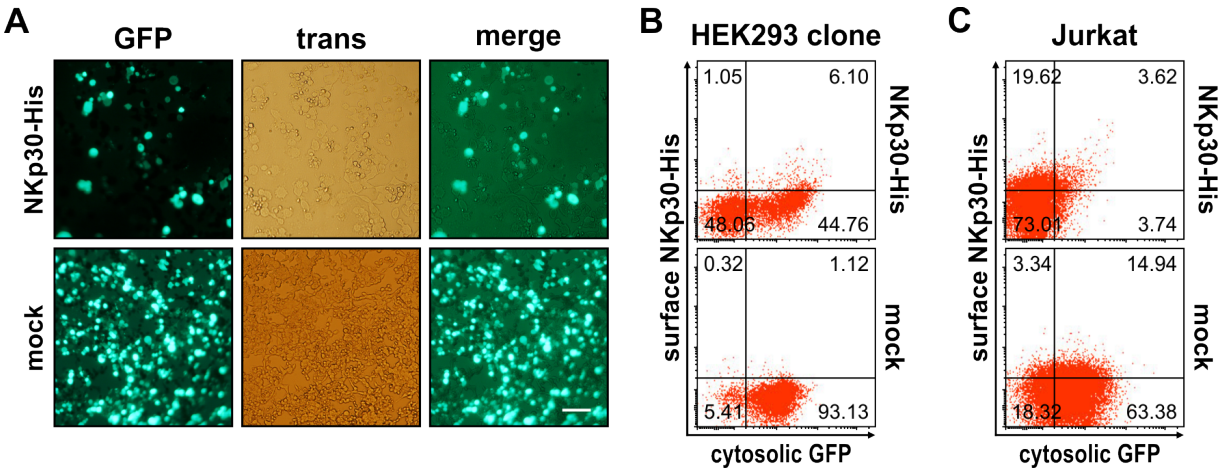

Fig. 9: Generation of NKp30-His expressing cells by lentiviral transduction

(A) HEK293T cells were transfected with LeGO-NKp30opt-His-iG2 (NKp30-His) or LeGO-iG2 (mock) and two helper plasmids for lentiviral particle production. After 24 h, the transfection efficiency was determined by fluorescence microscopy based on the number of cells expressing GFP (cytosolic GFP, *GFP*; transmitted light, *trans*). Size bar corresponds to 70 nm. (B) GFP expressing single HEK293 cell clones were isolated by limiting dilution four weeks after lentiviral transduction. After seven weeks of proliferation, NKp30-His surface expression was analyzed by flow cytometry using an anti-NKp30 antibody. Dot plots of cell clones with the highest GFP expression are shown. (C) One week after lentiviral transduction of Jurkat cells, NKp30-His surface expression was analyzed by flow cytometry using an anti-NKp30 antibody.

For intracellular signaling, NKp30 associates with its adapter protein CD3ζ via opposite charged amino acid residues within their transmembrane domains. However, it is still unknown whether CD3ζ could improve the NKp30 surface expression by assistance during the transport to or even by stabilization within the plasma membrane of the expression host. To provide this putative support, Jurkat cells (human T cell lymphoma cell line constitutively expressing CD3ζ) were transduced with the lentiviral particles for stable NKp30-His surface expression. Notably, the same preparation of lentiviral particles that was applied for the transduction of the HEK293 cells was used in this approach. One week after lentiviral transduction of the Jurkat cells, cytosolic GFP and surface NKp30-His expression were analyzed by flow cytometry using an anti-NKp30 antibody (polyclonal). Since HEK293 cells are much easier to transfect or transduce, a decrease of the transduction efficieny was expected. This assumption was confirmed by a lower percentage (77 %) of GFP expressing mock transduced Jurkat cells. Furthermore, after transduction with NKp30-His encoding lentiviral particles a very low transduction efficiency (7 % GFP positive cells) and thereby no relevant surface NKp30-His expression could be observed (Fig. 9C). Although NKp30 expression was observed in a HeLa cell line, which stably expresses recombinant CD3ζ [238], an association with the adapter protein CD3ζ in Jurkat cells did not enhance the NKp30-His surface expression. As mentioned above, the functional cross-talk between the NCRs concerning intracellular signaling was already demonstrated [173]. In this respect, NKp46 alone or in combination with NKp44 might stabilize NKp30 on the cell surface.

3.2.2 Co-Expression of Full-Length NCRs on the Plasma Membrane of Insect Cells

Since NKp30-His surface expression upon transfection or lentiviral transduction of mammalian cells was not sufficient and moreover, the constitutive expression of the adapter protein CD3ζ alone could not stabilize NKp30-His on the cell surface, all three recombinant NCRs were produced simultaneously and with comparable expression levels within one cell. For this purpose, the MultiBac expression system for insect cells was used. A multigene transfer vector was generated, which contained all the three genes encoding NKp30-His, NKp44-His and NKp46-His (2.3.4). Upon optimization of the transfection protocol (collaboration with I. Berger, European Molecular Biology Laboratory, Grenoble, France), baculovirus particles were produced (2.4.3) for the infection of *Sf* 9 insect cells (2.4.4). Transfection and infection efficiencies were monitored by intrinsic YFP expression of the insect cells (Fig. S3A and C, see 7.1.3). 96 h post baculoviral infection, recombinant NCR expression on the insect cell surface was analyzed by CLSM with NCR-specific antibodies in combination with a detection antibody (Alexa546-conjugated anti-mouse IgG antibody, Fig. 10). Strikingly, not only NKp30-His but also NKp44-His and NKp46-His were expressed on the surface of all YFP expressing cells.

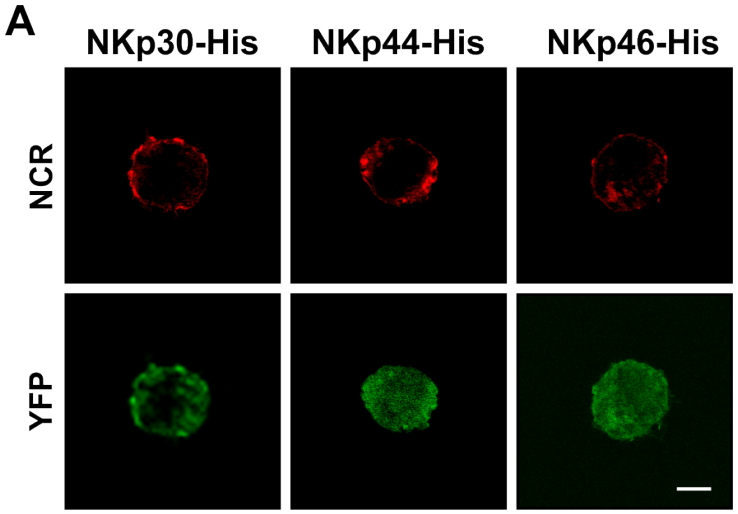

Fig. 10: Simultaneous NCR surface expression on insect cells post baculoviral infection

Sf 9 insect cells were infected with baculovirus particles encoding for NKp30-His, NKp44-His, and NKp46-His simultaneously. NCR surface expression was analyzed by CLSM using NCR-specific antibodies (anti-NKp30, anti-NKp44, anti-NKp46, *red*; cytosolic YFP, *green*; size bar corresponds to 10 μm).

Intriguingly, insect cells are capable of presenting all three recombinant NK cell receptors in combination on the cell surface. To clarify if recombinant NKp30-His surface expression on insect cells was due to an interaction with NKp46-His and/or NKp44-His or maybe resulted from changing the expression system, the NKp30-His surface level on insect cells functionalized only with the single recombinant NK cell receptor was analyzed.

3.2.3 Expression of Functional Full-Length NKp30 in Insect Cells

Based on the successful surface expression of all three NCRs, insect cells were infected with baculovirus particles encoding only NKp30-His. Notably, High Five insect cells were applied for further experiments due to their increased recombinant protein expression level. Transfection and infection efficiencies were again monitored by intrinsic YFP expression (Fig. S3A and B, see 7.1.3). 96 h post baculoviral infection

of High Five insect cells, full-length NKp30-His protein was detected by immunoblot analysis (anti-NKp30, polyclonal) after immunoprecipitation (anti-NKp30, clone P30-15) from lysates of NKp30-His infected but not from lysates of non-infected insect cells (Fig. 11A). NKp30-His (predicted molecular mass from primary sequence: 23 kDa) was detected as a protein band with an apparent molecular mass of roughly 30 kDa indicating post-translational modifications. In order to investigate whether NKp30-His was targeted to the insect cell surface, CLSM and flow cytometry analyses (anti-NKp30, clone P30-15) were performed (Fig. 11B and C). NKp30-His was exclusively found on the plasma membrane of infected insect cells. These data suggest that the overall folding of NKp30-His was correct since it had passed the endoplasmic reticulum (ER) quality control. Surprisingly, the expression level was significantly higher when compared to the NKp30-His surface expression of transfected or lentivirally transduced mammalian cell lines.

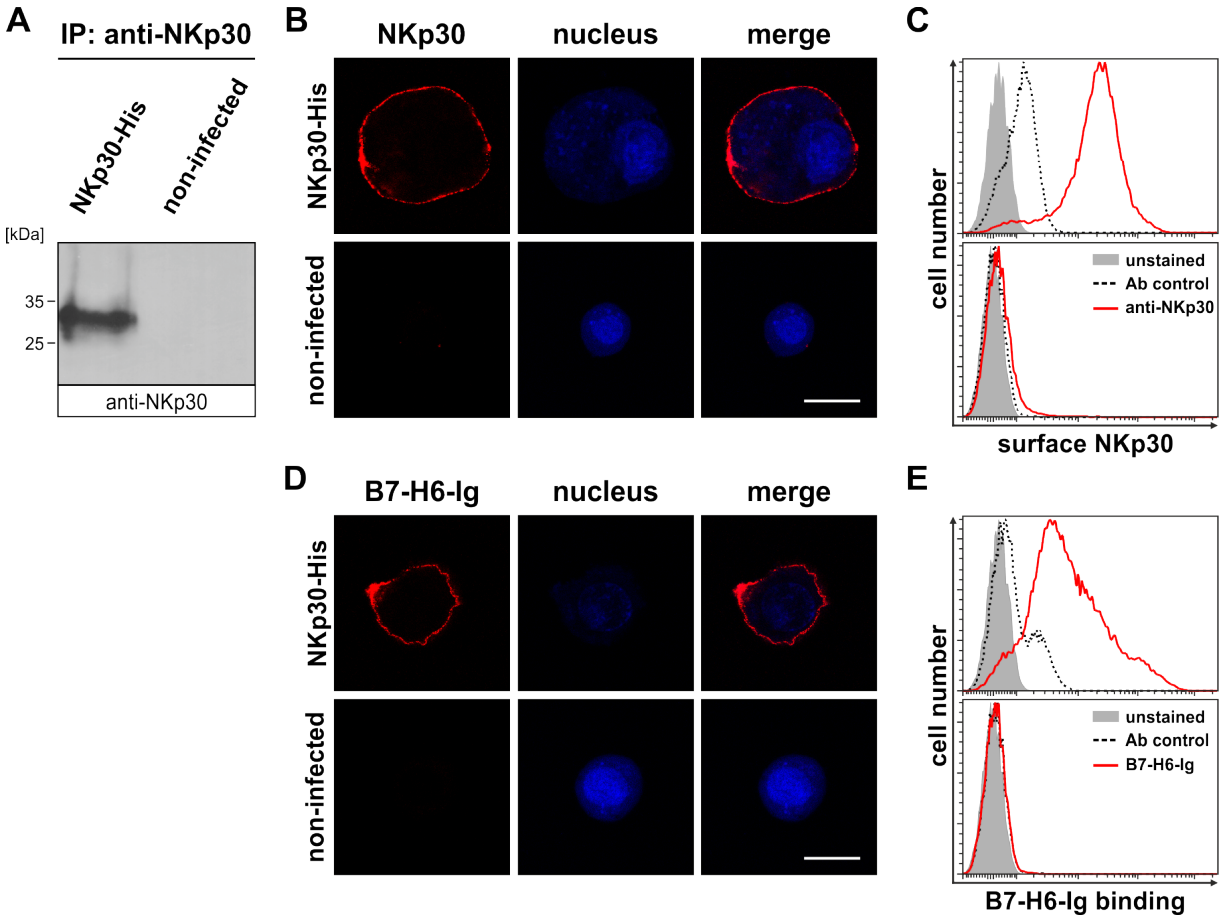

Fig. 11: Expression of functional NKp30-His on insect cells

High Five insect cells were infected with baculovirus particles encoding NKp30-His. (A) Immunoblot after immunoprecipitation of NKp30-His (anti-NKp30) from lysates of infected or non-infected insect cells. (B/C) Decoration of NKp30-His infected and non-infected insect cells with an anti-NKp30 antibody to analyze NKp30 surface expression by CLSM (anti-NKp30, *red*; DAPI, *blue*; size bar corresponds to 20 μm) and flow cytometry (unstained, *solid gray*; antibody control, *dashed line*; anti-NKp30, *red line*). (D/E) B7-H6-Ig fusion protein binding to NKp30-His infected and non-infected insect cells was analyzed by CLSM (B7-H6-Ig fusion protein, *red*; DAPI, *blue*; size bar corresponds to 20 μm) and flow cytometry (unstained, *solid gray*; antibody control, *dashed line*; B7-H6-Ig fusion protein, *red line*, modified from [233]).

In order to prove that NKp30-His adopts a ligand binding receptive conformation, decoration of NKp30-His infected and non-infected insect cells with recombinant B7-H6-Ig fusion protein was analyzed by CLSM and flow cytometry (DyLight649-conjugated anti-hIgG1-Fc, Fig. 11D and E). Strikingly, binding of the recombinant ligand B7-H6-Ig to NKp30-His was detected only at the plasma membrane of infected insect cells, demonstrating that NKp30-His expressed in insect cells is functionally equivalent to that derived from human expression hosts.

3.3 Soluble NKp30 Ectodomain Proteins for Investigation of the NKp30 Homo-Oligomerization Potential

Full-length NKp30-His presented on the surface of baculovirus-infected insect cells displays a functional equivalent to NKp30 derived from NK cells. Therefore, insect cells are a suitable expression host for investigation of recombinant NKp30-His. However, the baculovirus infection method is both beneficial and disadvantageous. Since in cell culture the polyhedrin coat is not essential for virus propagation, recombinant gene expression is under control of the extremely strong and late polyhedrin promoter facilitating high recombinant protein expression levels. However, to further spread baculovirus infection to the surrounding cells, occlusion bodies are released by viral cell lysis at approximately the same time point when high levels of full-length NKp30-His proteins are located within the plasma membrane (compare YFP expression level, Fig. S3B, see 7.1.3). Therefore, molecular investigation of NKp30 homo-oligomerization within an intact plasma membrane of infected insect cells would only be possible at early time points after infection. Since NKp30 self-assembly is assumed to occur at high local concentrations, these studies would be unreliable. Besides, not only ligand binding but also possible self-assembly or interaction with other surface molecules are expected to occur via the extracellular part of NKp30. Therefore, an individual investigation of the NKp30 ectodomain as soluble protein turned out to be more reasonable to identify putative interaction sites.

So far, bivalent NKp30 ectodomain proteins fused to an human IgG1-Fc part were produced in mammalian host cell lines and employed for cell decoration experiments to elucidate NKp30 target cell lines or novel cellular NKp30 ligands [124, 125, 133, 134, 136]. Furthermore, studies concerning ligand binding and signaling of NKp30 were performed with these bivalent NKp30-Ig fusion proteins exhibiting post-translational modifications. It was demonstrated that the stalk domain as well as the *N*-linked glycosylation of the acceptor sites N42, N68 and N121 within the NKp30 ectodomain are crucial for ligand binding [170]. However, these fusion constructs are constituted in an antibody-like architecture. This induced dimerization could have a boosting or even impeding influence on the NKp30 self-assembly or interaction with binding partners. To reveal the impact of the stalk domain on NKp30 self-assembly and its promoting influence on ligand binding, monovalent, post-translationally modified NKp30 ectodomain proteins with (30Stalk-His) and without (30LBD-His) membrane proximal stalk domain were produced. Since mammalian cells were again not applicable (H. Berberich, in the lab of J. Koch at the Georg-Speyer-Haus, Frankfurt am Main, Germany, data not shown [239]), insect cells were used due to their proven record of succes in expression of functional NKp30-His (3.2.3).

3.3.1 Expression of Soluble Variants of the NKp30 Ectodomain in Insect Cells

In 2011, the 3D structure of the NKp30 ligand binding domain was solved by two independent groups revealing a globular Ig domain comprising the amino acids L19 to E128 [116, 117]. Moreover, Mariuzza and colleagues determined the structure of NKp30 in complex with its ligand B7-H6 and validated the contacts by equilibrium binding of wild-type NKp30 and mutant versions to B7-H6 [117]. Interestingly, interaction studies with bivalent NKp30-Ig fusion proteins showed that the NKp30 ligand binding domain is sufficient for B7-H6 binding. Furthermore, these studies clearly demonstrated that the membrane proximal stalk domain significantly increases NKp30-B7-H6 binding [170], but the precise role of the NKp30 stalk domain on ligand binding remained obscure. A direct participation of the NKp30 stalk domain in B7-H6 binding was rather unlikely since this interaction would strongly decrease the flexibility of the stalk domain and thus increase its crystallizability. In contrast, an NKp30 ectodomain self-assembly to a larger complex via the stalk domain would be more reasonable, which results in enhanced ligand binding affinity by increased avidity. To confirm this hypothesis and compare ligand binding with previous studies, the construct design for the recombinant expression of the globular NKp30 ligand binding domain (30LBD-His, amino acids L19-E128) and the entire ectodomain of NKp30 including its stalk domain (30Stalk-His, amino acids L19-R143) was in analogy to the NKp30-Ig fusion proteins [170]. Notably, both constructs contain an N-terminal gp67 secretion sequence and a C-terminal deca-histidine tag for affinity purification.

To produce baculovirus particles encoding 30LBD-His or 30Stalk-His proteins, *Sf*9 insect cells were transfected with plasmid pFastBac1-gp67ss-NKp30LBD-TEV-His or pFastBac1-gp67ss-NKp30LBD-Stalk-TEV-His (2.4.3). Since both constructs are under the control of the extremely strong and late polyhedrin promoter, highest recombinant gene expression was observed at 72 h post infection of the High Five insect cells (2.4.4, compare YFP expression level, Figures S3D and E, see 7.1.3). Due to viral host cell lysis, at this time large amounts of baculovirus particles were present in the 30Stalk-His and 30LBD-His proteins containing cell culture supernatants, which might interfere with subsequent assays and therefore had to be removed. To investigate whether the baculovirus particles were depleted during affinity purification, samples prior to and post dialysis as well as post IMAC were collected (2.5.1.1). According to the glycoprotein 64 containing baculovirus envelope, baculovirus particles containing samples were identified by immunoblot analyses (anti-gp64, exemplarily shown for 30Stalk-His containing supernatant, Fig. 12A). Since baculovirus contaminations persisted during affinity purification, an ultracentrifugation step for virus depletion (2.4.4) prior to IMAC was added. Immunoblot analysis (anti-gp64) of supernatants containing 30Stalk-His proteins prior to and post ultracentrifugation confirmed complete removal of baculovirus contamination (Fig. 12B).

However, not only baculovirus particles but also large amounts of 30Stalk-His proteins were detected in precipitates from ultracentrifugation by immunoblot analysis (anti-NKp30, polyclonal, Fig. 12C). By contrast, 30LBD-His protein precipitation was not observed (data not shown). Interestingly, this drastically decreased amount of 30Stalk-His proteins by ultracentrifugation due to its intrinsic affinity to form higher molecular complexes indicated for the first time a potential relevance of the stalk domain for naturally occuring self-assembly of NKp30 ectodomains.

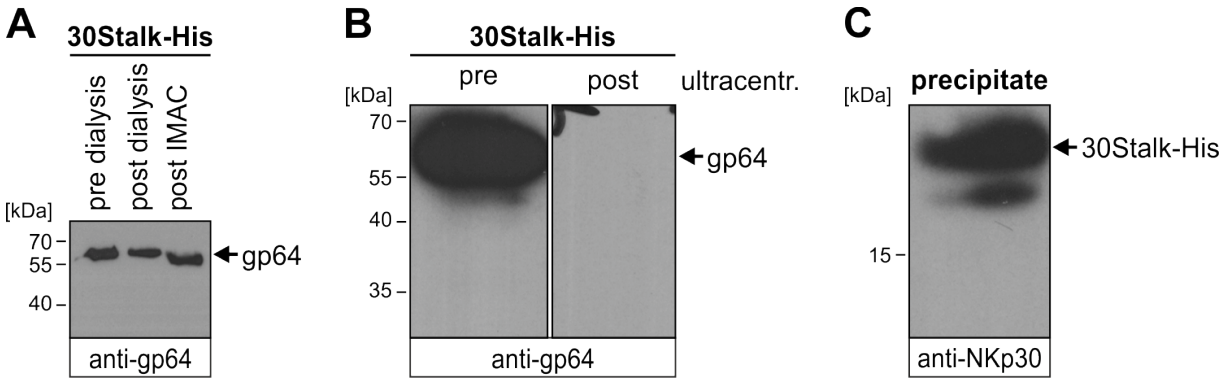

Fig. 12: Reduced yield of soluble 30Stalk-His proteins due to depletion of baculovirus particles

Infected insect cell culture supernatant contains secreted 30Stalk-His proteins and baculovirus particles. (A) 30Stalk-His containing aliquots from different purification steps were analyzed for baculovirus particle contamination by immunoblot (anti-gp64). Arrow, baculoviral glycoprotein 64 (gp64). (B) Aliquots of 30Stalk-His containing insect cell culture supernatants prior to and post ultracentrifugation were analyzed for baculovirus particle contamination by immunoblot (anti-gp64). Arrow, baculoviral glycoprotein 64 (gp64). (C) Precipitate from ultracentrifugation was analyzed for 30Stalk-His depletion by immunoblot (anti-NKp30). Arrow, 30Stalk-His proteins.

Generally, per litre insect cell culture supernatant more than 5 mg 30LBD-His proteins were obtained whereas only up to 1.5 mg 30Stalk-His proteins could be purified to homogeneity by IMAC as demonstrated by non-reducing SDS-PAGE and corresponding immunoblot analyses (anti-NKp30, polyclonal, Fig. 13). Since the volumes of cell culture supernatants for purification and aliquots for SDS-PAGE and immunoblot were equal for 30Stalk-His and 30LBD-His proteins, figure 13 illustrates the difference in total protein amount after purification. Notably, differences in the molecular mass (double or triple protein bands) reflect incomplete post-translational protein modification most likely due to a capacity overload of the glycosylation machinery.

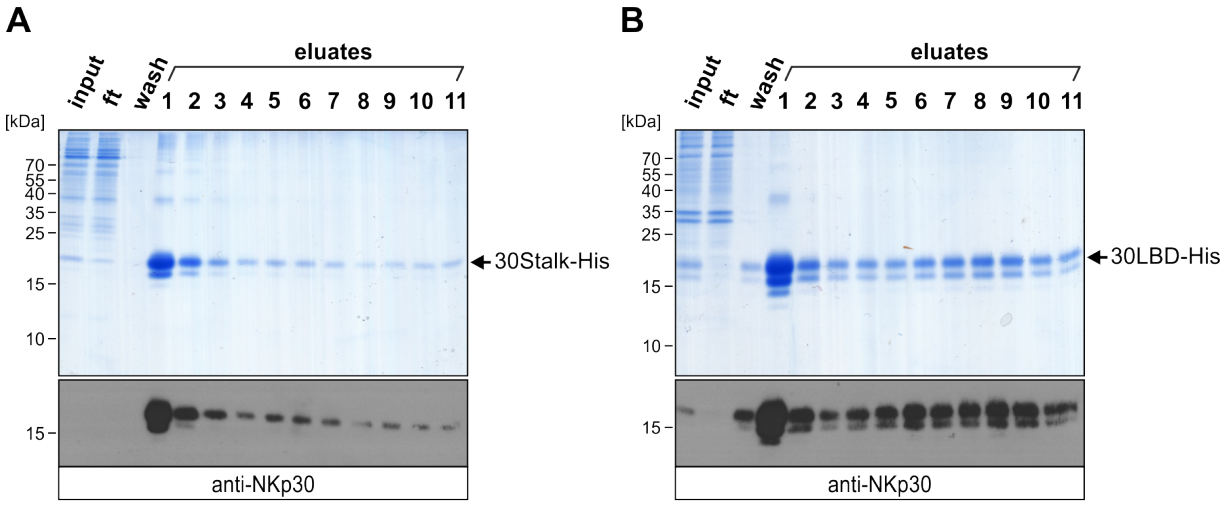

Fig. 13: Affinity purification of soluble variants of the NKp30 ectodomain produced in insect cells

(A/B) Non-reducing SDS-PAGE (coomassie-stained) and immunoblot (anti-NKp30) of aliquots (input, flow-through (ft), wash, and eluates) from purification after ultracentrifugation and dialysis of cell culture supernatants containing (A) the entire NKp30 ectodomain (30Stalk-His) and (B) the NKp30 ectodomain without stalk domain (30LBD-His). Arrow, fully glycosylated NKp30 ectodomain protein. (Modified from [233].)

Insect cells are able to perform post-translational modifications such protein glycosylation or formation of disulfide bonds between cystein residues. The ectodomain of NKp30 contains two cysteins (C39 and C108) which form an intramolecular disulfide bond [116, 117]. To exclude the formation of artificial intermolecular disulfide bonds, which might occur due to incomplete protein folding and exposure of reactive sulfhydryl groups, both NKp30 ectodomain proteins were investigated at reducing (+DTT) and non-reducing (-DTT) conditions. As shown by SDS-PAGE and corresponding immunoblot (anti-NKp30, polyclonal) analyses, there is no difference in the apparant molecular mass of the 30Stalk-His or 30LBD-His proteins at both conditions indicating correct protein folding and the absence of artificial intermolecular disulfide bonds (Fig. 14A). As expected from the results of full-length NKp30-His expression (3.2.3), the apparent molecular mass of the 30-Stalk-His (20 kDa vs. 16.6 kDa) and the 30LBD-His proteins (18 kDa vs. 15 kDa) differed from that predicted from primary sequence indicating post-translational modification. Glycosylation of the three acceptor sites for *N*-linked glycosylation within the ectodomain of NKp30 was investigated by reducing SDS-PAGE and immunoblot (anti-NKp30, polyclonal) analyses after enzymatic deglycosylation with PNGase F (cleavage of *N*-linked glycans) or with an enzyme mix (cleavage of *N*- and *O*-linked glycans, Fig. 14B).

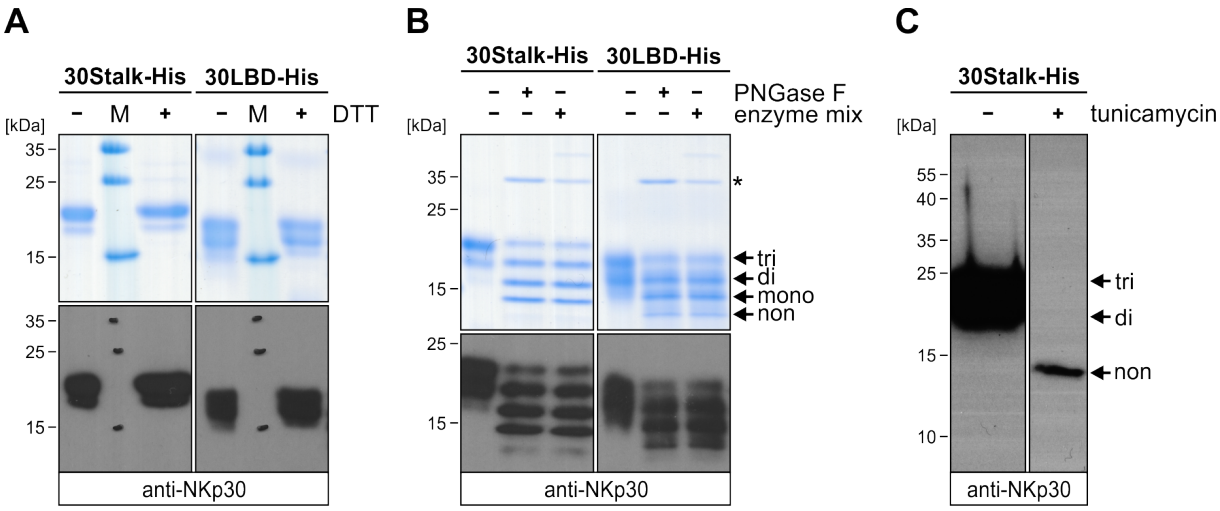

Fig. 14: Post-translational modifications of soluble NKp30 ectodomain proteins

(A) Non-reducing (-DTT) and reducing (+DTT) SDS-PAGE (coomassie-stained) and immunoblot (anti-NKp30, polyclonal) of purified 30Stalk-His and 30LBD-His proteins. (B) Reducing SDS-PAGE (coomassie-stained) and immunoblot (anti-NKp30, polyclonal) of untreated (30Stalk-His: lane 1, 30LBD-His: lane 4), PNGase F (30Stalk-His: lane 2, 30LBD-His: lane 5) or enzyme mix treated (30Stalk-His: lane 3, 30LBD-His: lane 6) NKp30 ectodomain proteins. Arrows, tri-, di-, mono- and non-glycosylated proteins. Asterisk, PNGase F. (C) Immunoblot (anti-NKp30, polyclonal) of purified 30Stalk-His protein without (lane 1) or with (lane 2) tunicamycin treatment 1 h post infection prior to protein expression to inhibit *N*-linked protein glycosylation. Arrows, tri-, di-, and non-glycosylated protein. (Modified from [233].)

For both, the 30Stalk-His and the 30LBD-His proteins, a distinct pattern of protein bands was observed due to incomplete deglycosylation corresponding to tri-, di-, mono- and non-glycosylated proteins. Notably, modification of the assay conditions, such as increasing the amount of enzyme or extending the incubation time, did not influence the relative amount of differentially glycosylated forms of NKp30. Most likely this is due to insect cell-specific glycosylation of proteins with an α1-3 fucose residue at the innermost *N*-acetylglucosamine (GlcNAc) residue of the glycoprotein, which is resistant to PNGase F cleavage. Therefore, tunicamycin was employed to inhibit the first step of *N*-linked glycosylation. Strik-

ingly, tunicamycin treatment of the insect cell culture 1 h post infection (2.4.11) quantitatively blocked *N*-linked glycosylation of the NKp30 ectodomain as shown by comparative immunoblot analysis (anti-NKp30, polyclonal) of purified 30Stalk-His proteins (Fig. 14C). Moreover, the reduction of the total protein amount (reflected by protein bands in figure 14C as well as YFP fluorescence intensities in figures S3D and F, see 7.1.3) as a consequence of imperfect protein folding and thus increased protein degradation underlines the impact of glycosylation on protein folding and stabilization in general. In conclusion, these studies show, that the ectodomain of NKp30 produced in insect cells is *N*-linked glycosylated at its three known acceptor sites (N42, N68, N121) in the absence of *O*-linked glycans and thus represents a molecular equivalent to the ectodomain of human NKp30 which can be employed for further studies.

3.3.2 An Antibody with Defined Specificity for the NKp30 Ligand Binding Domain

To date, several anti-human NKp30 antibodies are commercially available, which are suitable for different biochemical and cellular approaches. In general, these antibodies are not characterized extensively concerning their epitopes, blocking capacities and application possibilities. Hence, an antibody, suitable for diverse applications such as cell decoration assays, ELISA or immunoblot analyses, was generated. Due to a defined epitope (amino acids P62 to R75) situated within the NKp30 ligand binding domain (Fig. 15A), the antibody consequently binds to both 30Stalk-His and 30LBD-His proteins to the same extent. This peptide stretch is located outside of the NKp30-B7-H6 binding pocket with close proximity to the plasma membrane, which allows for the investigation of putative homo-oligomerization for enhanced ligand binding affinity by increased avidity. Notably, this sequence is of further interest, since it contains N68, one of the three known acceptor sites for *N*-linked glycosylation. NKp30 ectodomain glycosylation at position N68 was identified to be essential for efficient intracellular signaling upon engagement of B7-H6 [170].

To generate antibodies recognizing a defined epitope located within the NKp30 ligand binding domain, the antigenic peptide NH_2-CPGKEVRNGTPEFRGR-COOH was synthesized for immunization of two rabbits (BioScience/PepScience, Göttingen, Germany). Roughly 1 mg of peptide specific antibodies could be purified from 25 ml of rabbit antiserum by immunoaffinity chromatography (2.5.1.3). Multiple protein bands in reducing SDS-PAGE and corresponding immunoblot (anti-rabbit IgG) analyses of concentrated peptide antibody as well as aliquots from purification illustrated the heterogeneity of the purified rabbit IgG antibody subtypes (Fig. 16A). However, antigen-specificity was exemplarily demonstrated by immunoblot analyses of recombinant 30Stalk-His proteins (Fig. 16B). For reference, the same amount of 30Stalk-His proteins (2 μg) was detected with the polyclonal anti-NKp30 antibody. Higher signal intensities obtained for the polyclonal (goat) when compared to the peptide immunized anti-NKp30 antibody (rabbit) were either due to different antibody affinities or due to recognition of the entire NKp30 ectodomain, and thereby binding of more than one antibody molecule per 30Stalk-His protein.

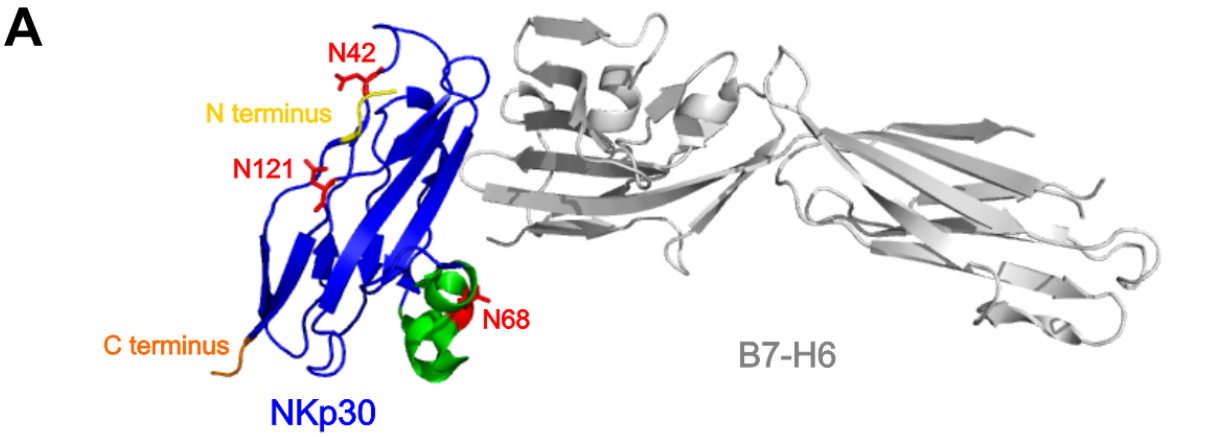

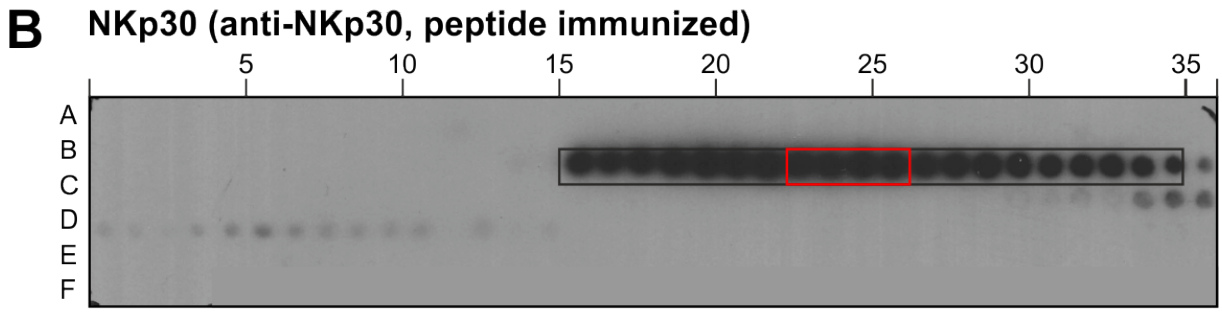

C

Spot	18mer peptide sequence	Spot	18mer peptide sequence
B16:	S-V-T-W-F-R-D-E-V-V-P-G-K-E-V-R-N-G	B26:	P-G-K-E-V-R-N-G-T-P-E-F-R-G-R-L-A-P
B17:	V-T-W-F-R-D-E-V-V-P-G-K-E-V-R-N-G-T	B27:	G-K-E-V-R-N-G-T-P-E-F-R-G-R-L-A-P-L
B18:	T-W-F-R-D-E-V-V-P-G-K-E-V-R-N-G-T-P	B28:	K-E-V-R-N-G-T-P-E-F-R-G-R-L-A-P-L-A
B19:	W-F-R-D-E-V-V-P-G-K-E-V-R-N-G-T-P-E	B29:	E-V-R-N-G-T-P-E-F-R-G-R-L-A-P-L-A-S
B20:	F-R-D-E-V-V-P-G-K-E-V-R-N-G-T-P-E-F	B30:	V-R-N-G-T-P-E-F-R-G-R-L-A-P-L-A-S-S
B21:	R-D-E-V-V-P-G-K-E-V-R-N-G-T-P-E-F-R	B31:	R-N-G-T-P-E-F-R-G-R-L-A-P-L-A-S-S-R
B22:	D-E-V-V-P-G-K-E-V-R-N-G-T-P-E-F-R-G	B32:	N-G-T-P-E-F-R-G-R-L-A-P-L-A-S-S-R-F
B23:	E-V-V-P-G-K-E-V-R-N-G-T-P-E-F-R-G-R	B33:	G-T-P-E-F-R-G-R-L-A-P-L-A-S-S-R-F-L
B24:	V-V-P-G-K-E-V-R-N-G-T-P-E-F-R-G-R-L	B34:	T-P-E-F-R-G-R-L-A-P-L-A-S-S-R-F-L-H
B25:	V-P-G-K-E-V-R-N-G-T-P-E-F-R-G-R-L-A	B35:	P-E-F-R-G-R-L-A-P-L-A-S-S-R-F-L-H-D

Fig. 15: Epitope of the ligand binding domain-specific anti-NKp30 antibody

(A) B7-H6 (gray) bound crystal structure of the NKp30 ligand binding domain (blue, amino acids L19-E130); PDB 3PV6. The peptide stretch used for immunization is shown in green. Asparagines within consensus motifs for *N*-linked glycosylation are depicted in red with corresponding amino acid annotation. N- (yellow) and C-terminus (orange) are indicated. The structural illustration was made with PyMol software. (B) Overlapping peptide arrays (18 amino acids long peptides, off-set by one amino acid) of human NKp30 were probed with purified anti-NKp30 antibody (peptide immunized) and detected with a rabbit-IgG-specific HRP-conjugated antibody. The identified interaction hot-spot is marked with a black box. The interaction hot-spot containing the entire peptide sequence used for immunization is marked with a red box. (C) Sequences of human NKp30 peptides identified as interaction hot-spots shown in B (green: sequence of peptide used for immunization; red: peptide spots containing the entire peptide sequence used for immunization).

In general, linear antibody epitopes comprise six to nine amino acids. Epitopes of monoclonal and polyclonal antibodies binding to linear peptide stretches can be identified by overlapping sequences from peptide spot arrays. To verify the recognition of the expected linear sequence within the NKp30 ectodomain, peptide spot arrays of human NKp30 (18 amino acids, off-set by one amino acid) were synthesized and probed with the purified anti-NKp30 peptide antibody (2.5.8). A binding region of 37 amino acids in length (peptide spots B16 to B35, Fig. 15B) was identified demonstrating the presence of three or more

antibody variants within the peptide purified antibody pool. These antibodies recognize different, probably overlapping epitopes with at least six amino acids of the selected region of the NKp30 ligand binding domain (see sequence of spot B35, Fig. 15C). N- and C-terminal truncations of this 37 amino acids long binding region could possibly narrow down but not definitely identify all distinct epitope sequences due to their putative overlap. However, the anti-NKp30 antibody variants obtained from peptide immunization specifically bind to the linear amino acid sequence of denatured NKp30 ectodomain proteins (Fig. 16B), and moreover recognize the epitope in its native conformation validated by detection of folded NKp30 ectodomain proteins in cell decoration and ELISA experiments (Fig. 17).

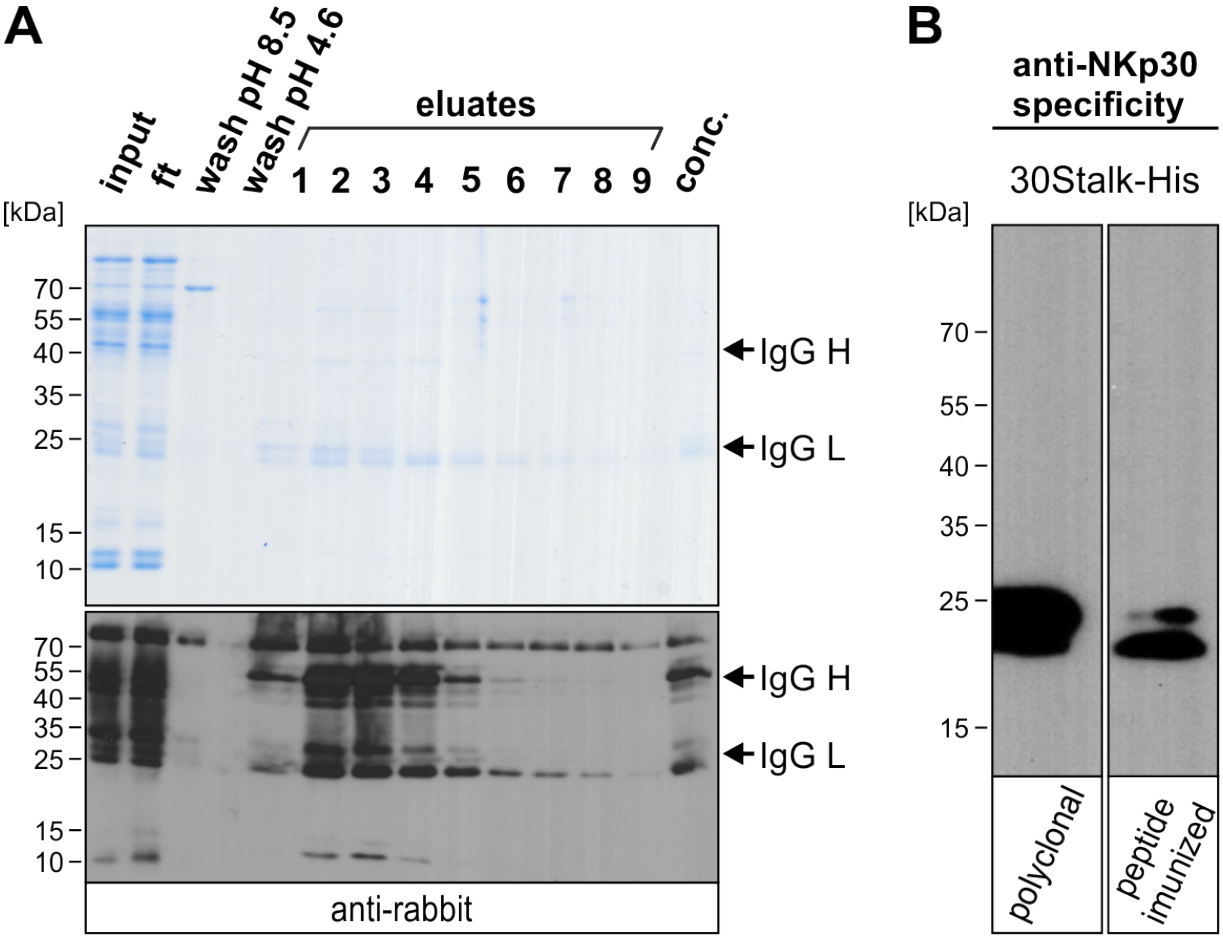

Fig. 16: Purification of and immunoblot with the ligand binding domain-specific anti-NKp30 antibody

(A) Non-reducing SDS-PAGE (coomassie-stained) and immunoblot (anti-rabbit IgG) of aliquots (input, flow-through (ft), washes, eluates, and concentrated (conc.)) from purification of rabbit antiserum after peptide immunization. Arrows, heavy and light chains of rabbit IgG. (B) Specificity of commercially available polyclonal (goat) and peptide immunized (rabbit) anti-NKp30 antibodies for the detection of 30Stalk-His proteins in immunoblot analyses.

3.4 Homo-Oligomerization of the NKp30 Ectodomain Increases the Binding Affinity for Its Cellular Ligand B7-H6

3.4.1 High Affinity Binding of the NKp30 Ectodomain Proteins to B7-H6

In order to examine the ligand binding properties of the soluble NKp30 ectodomain proteins and to study the contribution of the stalk domain to ligand binding, cell decoration experiments, signaling reporter cell assays, and ELISA were performed. For cell decoration experiments, NKp30 ligand-negative Ba/F3 cells stably transduced with the cellular NKp30 ligand B7-H6 and GFP (Ba/F3-B7-H6) or GFP only (Ba/F3-GFP) were incubated with 30Stalk-His and 30LBD-His proteins (2.4.12). Plasma membrane-attached NKp30 ectodomain proteins were visualized with anti-NKp30 antibody (peptide immunized) by CLSM. Specific binding of the 30Stalk-His and 30LBD-His proteins to B7-H6 on the plasma membrane of Ba/F3-B7-H6 cells was detected (Fig. 17A). In accordance with previous cell decoration studies with NKp30-Ig fusion proteins [170], binding of soluble 30Stalk-His proteins to plasma membrane B7-H6 was significantly stronger than that of 30LBD-His proteins. This observation was nicely reflected by flow cytometry measurements performed with these cells (Fig. 17B). Again, decoration of Ba/F3-B7-H6 cells with 30Stalk-His proteins led to much higher signal intensities when compared to 30LBD-His proteins. For reference, no binding of 30Stalk-His or 30LBD-His proteins to Ba/F3-GFP cells was observed. Importantly, the receptor ligand interaction was highly specific since it could be quantitatively competed with an anti-NKp30 blocking antibody (clone 210845).

As demonstrated by representative NKp30 stainings of Ba/F3-B7-H6 cells in Figure 17A, a distinct dotted pattern was observed upon decoration with the 30Stalk-His and 30LBD-His proteins suggesting formation of oligomeric receptor-ligand complexes. Quantitative analyses of a large number of cells (30Stalk-His: n=42; 30LBD-His: n=56) revealed an equal average number of clusters per cell (30Stalk-His: 53.4 $\pm$ 1.7 pixel; 30LBD-His: 53.1 $\pm$ 1.5 pixel) following binding of the NKp30 ectodomain proteins (Fig. 17C top). These data imply that the number of clusters is mainly dependent on the ligand concentration on the target cell. By contrast, the mean cluster size following binding of 30Stalk-His proteins (257.7 $\pm$ 16.9 pixel) was significantly increased when compared to the clusters induced by binding of 30LBD-His proteins (123.5 $\pm$ 6.5 pixel, Fig. 17C bottom). Thus, the investigation of receptor-ligand complexes on target cells decorated with soluble NKp30 ectodomain proteins strengthened the hypothesis that the stalk domain promotes formation of NKp30 ectodomain oligomers.

In order to test whether the soluble ectodomain variants of NKp30 can inhibit a productive NKp30-dependent NK cell-target cell interaction, signaling reporter assays were performed in the absence and presence of 30Stalk-His and 30LBD-His proteins (2.4.15). Therefore, the A5-30FL-His reporter cell line was employed as an effector cell, which couples NKp30/CD3ζ chain-dependent signaling to proportional GFP expression (Fig. 17D) [170]. Ba/F3-B7-H6 cells were used as target cells. The extend of signaling was measured by flow cytometry based on the percentage of GFP positive A5-30FL-His reporter cells (Fig. 17E). In the absence of blocking proteins, Ba/F3-B7-H6 cells induced robust NKp30-dependent signaling of the A5-30FL-His reporter cells, which could be inhibited by binding of an anti-NKp30 blocking antibody (clone P30-15) to the A5-30FL-His reporter cells (blocking control). Furthermore, signaling was decreased by decoration of the Ba/F3-B7-H6 cells with 30Stalk-Ig proteins but not influenced by a non-relevant control protein (Ifnar2-Ig).

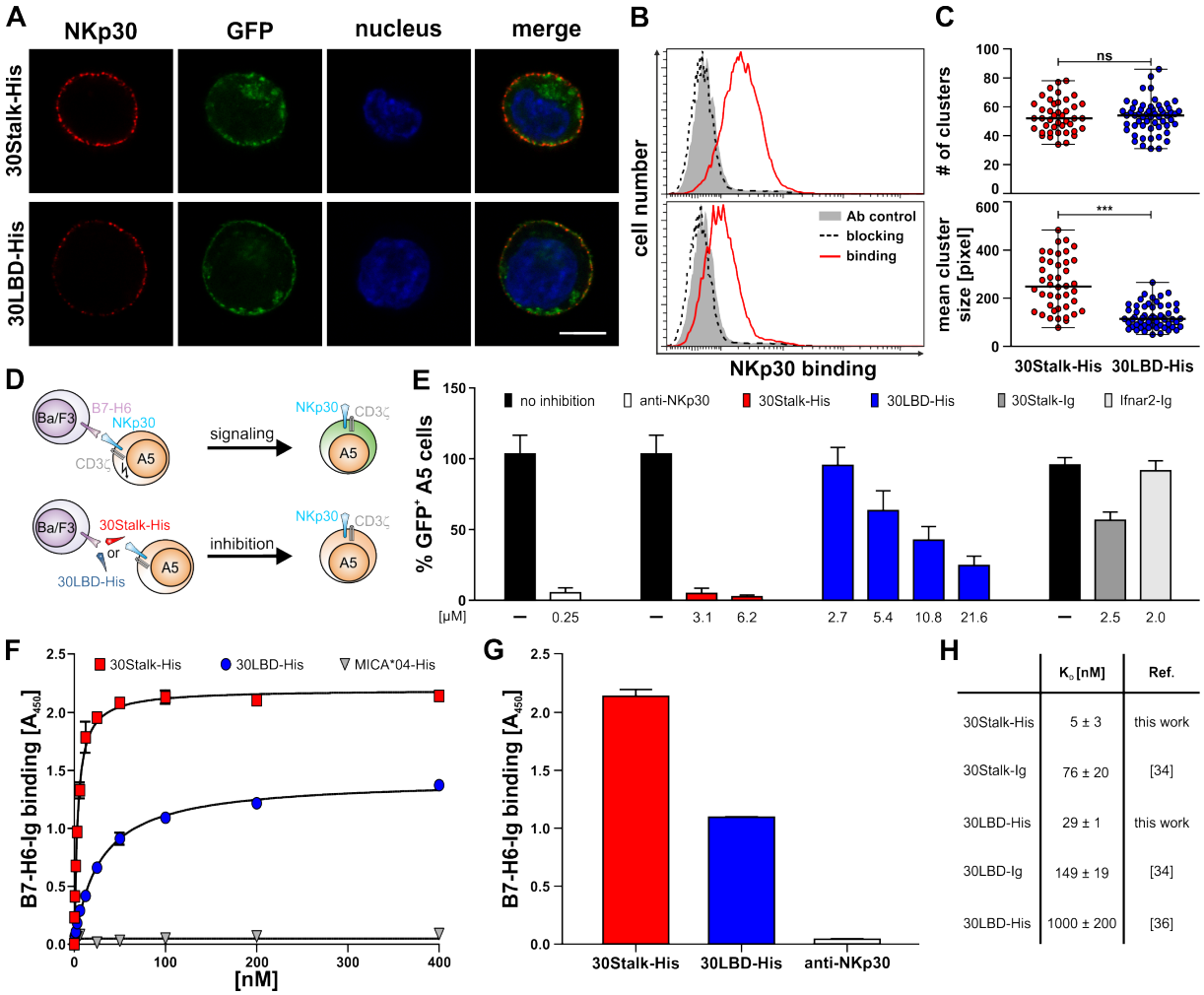

Fig. 17: High affinity binding of NKp30 ectodomain proteins to the cellular ligand B7-H6

(A) Binding of 30Stalk-His or 30LBD-His proteins to B7-H6 transduced Ba/F3 cells was monitored by an anti-NKp30 antibody via CLSM (anti-NKp30, *red*; GFP, *green*; DAPI, *blue*; size bar corresponds to 5 μm). (B) Binding of 30Stalk-His and 30LBD-His proteins (*red line*) and specific blocking with an anti-NKp30 antibody (*dashed line*) were analyzed by flow cytometry (antibody control, *solid gray*). (C) Quantification of clusters observed on B7-H6 transduced Ba/F3 cells after decoration with 30Stalk-His and 30LBD-His proteins. Data points represent the number of clusters (upper panel) and the mean cluster size (lower panel) on a large number of individual cells decorated with 30Stalk-His (*red*) or 30LBD-His (*blue*) proteins. Mann-Whitney test: ns, $p = 0.9914$; ***, $p < 0.0001$. (D) A5-30FL-His reporter cells were mixed with B7-H6 transduced Ba/F3 target cells. Upon NKp30-B7-H6 interaction, downstream signaling via CD3ζ results in GFP expression in the A5-30FL-His reporter cells. Pre-incubation of Ba/F3-B7-H6 target cells with 30Stalk-His or 30LBD-His protein blocks the effector-target interaction as indicated by the absence of GFP expression in the A5-30FL-His reporter cells. (E) The Ba/F3-B7-H6 target cells were pre-incubated with blocking proteins (30Stalk-His, *red*; 30LBD-His, *blue*; 30Stalk-Ig, *dark gray*; Ifnar2-Ig (control), *light gray*; concentrations indicated) prior to co-incubation (16 h) with A5-30FL-His reporter cells. As control, A5-30FL-His reporter cells were pre-incubated with an anti-NKp30 antibody (*white*) to inhibit signaling. For reference corresponding signaling without blocking protein (*black*) was normalized to 100 % GFP positive A5-30FL-His reporter cells. (F) Binding of graded amounts of 30Stalk-His (*red square*, K_D: 5 ± 3 nM), 30LBD-His (*blue circle*,K_D: 29 ± 1 nM) or MICA*04-His (control, *gray triangle*) proteins to recombinant B7-H6-Ig fusion protein analyzed by ELISA. Data were fit to a 1:1 Langmuir binding model to determine equilibrium binding constants (K_D). A representative of eight independent experiments is shown. (G) Binding of 30Stalk-His (100 nM, *red*) and 30LBD-His (100 nM, *blue*) proteins to recombinant B7-H6-Ig fusion protein analyzed by ELISA. Pre-incubation of the 30Stalk-His proteins with an anti-NKp30 antibody (*white*) specifically blocks the NKp30-B7-H6 interaction. Notably, analogous blocking was observed for the 30LBD-His proteins (not shown). A representative of five independent experiments is shown. (H) K_D values of different NKp30 ectodomain proteins. (Modified from [233].)

Strikingly, both the 30Stalk-His and 30LBD-His proteins were efficient competitors of NKp30-dependent signaling when bound to the Ba/F3-B7-H6 cells, indicating their ligand specificity. Importantly, quantitative blocking of the NKp30-B7-H6 interaction was achieved already at a concentration of 3.1 μM for the 30Stalk-His protein, whereas inhibition remained incomplete (75 %) for the 30LBD-His proteins even at a seven-fold higher concentration of 21.6 μM (Fig. 17E). In conclusion, these studies show that the ectodomain of NKp30 produced in insect cells specifically recognized its ligand B7-H6 on target cells with a strong contribution of its stalk domain to high-affinity binding.

To determine the apparent ligand binding affinities of the soluble 30Stalk-His and 30LBD-His proteins, ELISA experiments with recombinant B7-H6-Ig were performed (2.5.9). Therefore, B7-H6-Ig was immobilized and probed with graded amounts of 30Stalk-His and 30LBD-His proteins prior to detection of ligand-bound NKp30 with a polyclonal anti-NKp30 antibody. Both NKp30 variants bound specifically and dose-dependent to B7-H6-Ig with very low equilibrium binding constants (30Stalk-His: 5 $\pm$ 3 nM; 30LBD-His: 29 $\pm$ 1 nM, Fig. 17F, G and H). Surprisingly, these apparent binding affinities were higher than those published for the monovalent NKp30 ectodomain proteins refolded from *E. coli* inclusion bodies (1000 $\pm$ 200 nM, determined by SPR measurements), and even the bivalent 30Stalk-Ig (76 $\pm$ 20 nM, determined by SPR measurements) and 30LBD-Ig (149 $\pm$ 19 nM, determined by SPR measurements) fusion proteins (Fig. 17H [117,170]). Therefore, these data suggest that NKp30 might form higher molecular order complexes, which display a higher apparent ligand binding affinity by increased avidity of the oligomeric complex. Notably, the B_{max} values of the 30Stalk-His (1.58 $\pm$ 0.6) and the 30LBD-His proteins (1.01 $\pm$ 0.4) for binding to B7-H6-Ig were drastically different (Fig. 17F). The B_{max} is an indicator for the maximum number of ligand binding receptive receptors in the solution. Therefore, this observation argued for a stalk-dependent difference in the architecture of the oligomeric self-assembly of the 30Stalk-His and the 30LBD-His proteins, which might in turn lead to a different degree of avidity and apparent affinity to B7-H6-Ig. This hypothesis was also supported by the much stronger inhibition of NKp30/B7-H6-dependent signaling of A5-30FL-His reporter cells by the 30Stalk-His proteins when compared to the bivalent 30Stalk-Ig proteins (Fig. 17E).

3.4.2 NKp30 Ectodomain Proteins Self-Assemble Homo-Oligomers

In order to investigate the oligomeric state of NKp30, size exclusion chromatography (SEC) was performed using a Superdex 200 column (2.5.2). Surprisingly, an equilibrium of three major protein species in solutions of 30Stalk-His and 30LBD-His proteins corresponding to monomers, dimers and oligomers of soluble NKp30 were found. Interestingly, at the same protein concentration of both NKp30 ectodomain proteins, the relative content of oligomers was much higher for the 30Stalk-His when compared to the 30LBD-His proteins. Notably, the degree of oligomerization and the relative ratio of oligomers, dimers and monomers was dependent on the concentration of the protein solution, with a tendency to oligomer formation at higher protein concentrations. As demonstrated by figures 18A and B, the main fraction of separated 30Stalk-His proteins consisted of oligomers (approximately 75 %), whereas only 5 % dimeric and 20 % monomeric 30Stalk-His proteins were separated. By contrast, the different forms of the 30LBD-his proteins were distributed more equally with a tendency to stay monomeric (35 %) or form dimers (40 %), but only 25 % of the isolated 30LBD-His proteins were oligomers. With reference to SEC runs with a commercial calibration standard, the molecular mass of the oligomers was estimated at 360-440 kDa (elution volume 9.5 ml, corresponding to 18-22 30Stalk-His monomers) and 250-290 kDa (elution

volume 12 ml, corresponding to 14-16 30LBD-His monomers). Interestingly, even at higher protein concentrations the molecular mass of the oligomers remained constant demonstrating formation of defined oligomers rather than non-functional aggregates. Notably, after repeting SEC analyses of concentrated oligomeric, dimeric or monomeric 30Stalk-His and 30LBD-His protein peaks, the distribution of these NKp30 species was restored (data not shown).

Due to the intrinsic capacity of 30LBD-His and the drastically increased tendency of the 30Stalk-His proteins to oligomerize, two specific binding sites, located in the ligand binding domain and the stalk domain, are proposed for contribution to NKp30 self-assembly. So far, the results suggested an avidity-driven increase of the apparent affinity of the 30Stalk-His and 30LBD-His proteins (Fig. 17F), but the functional significance of the NKp30 ectodomain oligomers was uncertain. Therefore, fractions from SEC, containing 30Stalk-His or 30LBD-His proteins as determined by ELISA (anti-NKp30, polyclonal, Fig. 18C and D), were probed for binding to B7-H6-Ig in an ELISA setup described above. Strikingly, all of the oligomeric species (monomers, dimers and oligomers) of soluble NKp30 bound to B7-H6-Ig (anti-NKp30, polyclonal, Fig. 18E and F). In accordance with previous data, binding of 30Stalk-His to B7-H6-Ig was stronger than that of 30LBD-His, confirming the importance of the stalk domain for ligand binding. Moreover, an ELISA with separated 30Stalk-His oligomers, which were probed with recombinant B7-H6-Ig protein (detected with HRP-conjugated anti-hIgG-Fc antibodies), demonstrated again that NKp30 ectodomain oligomers had a very high apparent affinity for B7-H6 as indicated by the K_D (1.04 $\pm$ 0.21 nM) and B_{max} (1.12 $\pm$ 0.03) values. Notably, K_D and B_{max} values of 30Stalk-His dimers and monomers were not determined due to very low protein amounts after separation.

Figures 18E and F demonstrate the binding capacities of all oligomeric 30Stalk-His and 30LBD-His proteins. Since detection with polyclonal anti-NKp30 antibodies could result in different apparent signal intensities due to binding of more antibodies to one 30Stalk-His when compared to one 30LBD-His molecule, the same ELISA experiment was performed using the peptide immunized anti-NKp30 antibody ensuring similar binding properties for the detection of both NKp30 ectodomain proteins. Strikingly, only oligomeric but no dimeric or monomeric NKp30 ectodomain proteins were detected upon binding to immobilized B7-H6-Ig fusion proteins (Fig. 18G and H). Possibly, the affinity of monomeric and dimeric NKp30 ectodomain variants might be very low or the epitopes on dimeric and monomeric NKp30 ectodomain proteins were occupied by interacting ligand molecules. Thus, these results do not only confirm ligand binding capacities of the NKp30 ectodomain oligomers, but could further provide new insights into possible interaction sites for NKp30 dimer and even oligomer formation.

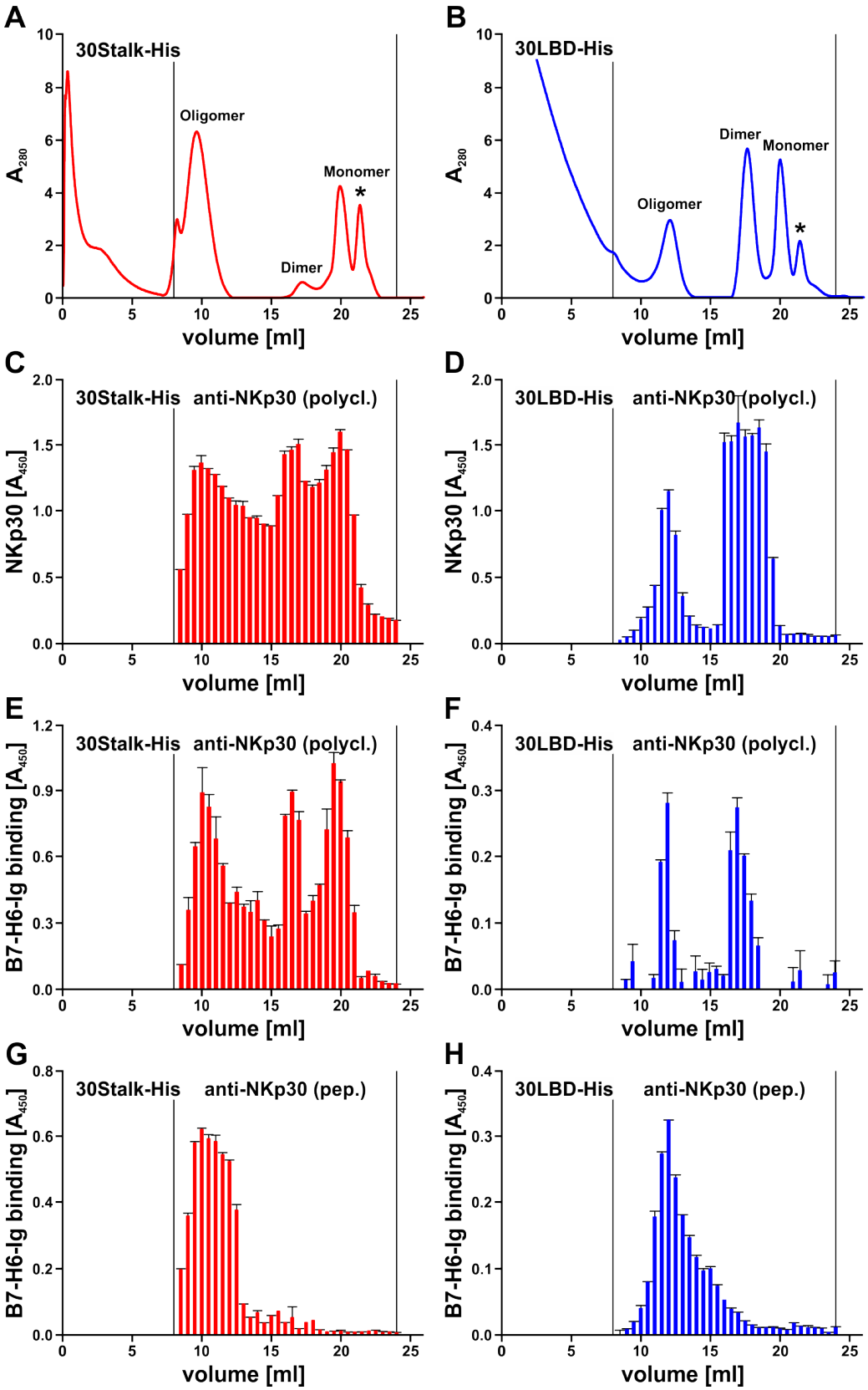

Fig. 18: The NKp30 ectodomain self-assembles oligomers, which bind to the ligand B7-H6

(A/B) Oligomers, dimers and monomers of (A) 30Stalk-His and (B) 30LBD-His were separated by size exclusion chromatography (Superdex 200 10/300 GL column). Asterisk, lower molecular mass compounds. (C/D) Elution fractions (500 μl) of size exclusion chromatography containing (C) 30Stalk-His and (D) 30LBD-His proteins were identified by ELISA with an anti-NKp30 (polyclonal) antibody. Binding of different oligomeric species of (E/G) 30Stalk-His and (F/H) 30LBD-His proteins to recombinant B7-H6-Ig fusion protein was validated by ELISA with anti-NKp30 antibodies (polyclonal, E/F; peptide immunized, G/H). (Modified from [233].)

3.4.3 Influence of the Stalk Domain on NKp30 Self-Assembly

In order to study the geometric arrangement of the oligomers formed by the 30Stalk-His and 30LBD-His proteins, the oligomers were isolated by SEC on a Superose 6 column for improved separation of large protein complexes (2.5.2). Although the individual peaks of the monomers and dimers could not be resolved on this column, again monodisperse peaks of the expected molecular mass for the NKp30 ectodomain oligomers were observed (Fig. 19A and C). After immobilization of the elution fractions corresponding to the peak maxima of the 30Stalk-His and 30LBD-His oligomers on EM grids, complexes were stained with uranyl acetate and subjected to EM (2.5.10).

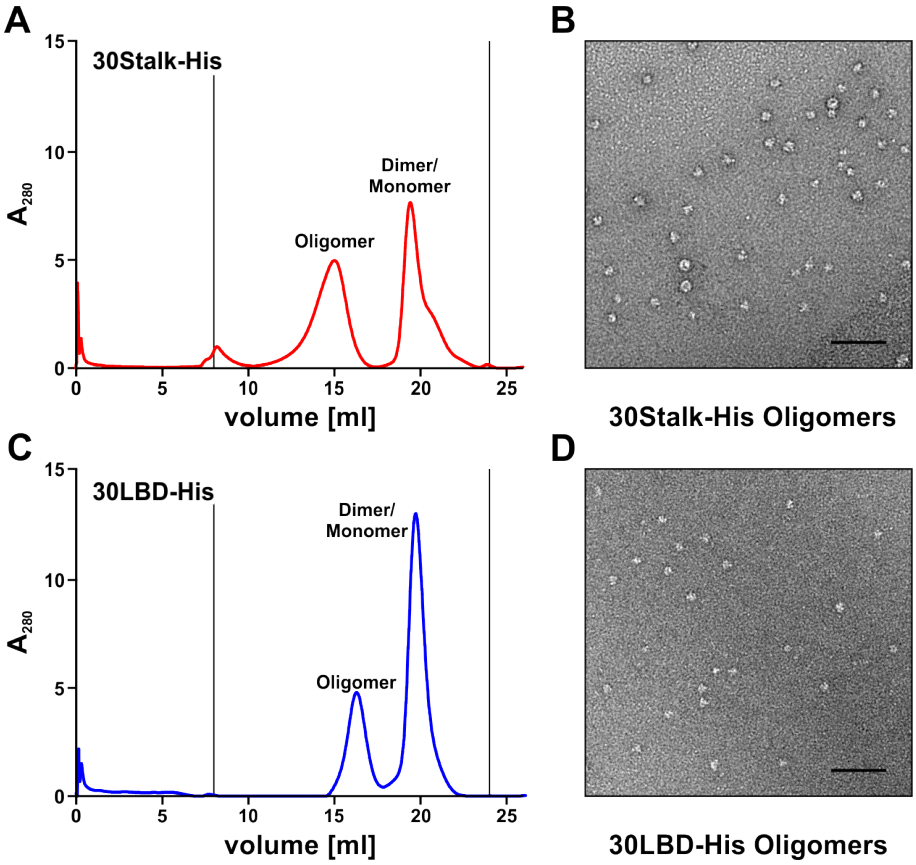

Fig. 19: The stalk domain modulates the geometric arrangement of the NKp30 ectodomain oligomers

(A) 30Stalk-His and (C) 30LBD-His oligomers were separated from the monomer/dimer fractions by size exclusion chromatography (Superose 6 10/300 GL column). 100 μl elution fractions were collected. (B/D) Geometry and 3D-arrangement of the (B) 30Stalk-His and (D) 30LBD-His oligomers were analyzed by electron microscopy using the oligomer elution fractions with the highest protein amount from size exclusion chromatography (see A/C). Size bars correspond to 100 nm. (Modified from [233].)

Strikingly, particles with a diameter of about 15 nm were observed for both NKp30 ectodomain proteins confirming formation of oligomers rather than non-functional aggregates. Interestingly, the 30LBD-His oligomers appeared more homogeneous than the 30Stalk-His oligomers (Fig. 19B and D). To identify groups of congruent oligomeric particles and thereby shed more light on the geometric arrangement of the 30Stalk-His and 30LBD-His oligomers, 2D class averaging was performed. Notably, the more definite the local positions of the monomers within an oligomeric particle the better would be the fine resolution of their geometric arrangement. For this purpose, more than 6.000 globular particles for both 30Stalk-His and 30LBD-His oligomers were analyzed. In preliminary experiments, a surprisingly large

number of rougly 120 different 2D classes was calculated for the 30LBD-His oligomers. Furthermore, 2D class averaging for 30Stalk-His oligomers was not possible at all, which might be due to more structural flexibility mediated by the stalk domain. Although the individual numbers of monomers within one oligomer were conserved for both 30LBD-His and 30Stalk-His proteins, a fixed position of the globular Ig domains within the oligomeric complexes was most probably inhibited by a local flexibility of the monomers. Since both 30LBD-His and 30Stalk-His oligomers displayed similar shapes without congruency, the precise orientation of the NKp30 ectodomain molecules within the oligomers remains unknown.

For the NK cell-target cell interaction a head-to-head (*in cis*) orientation is most plausible. However, based on decoration experiments with NKp30 ectodomain proteins and pNK cells analyzed by flow cytometry (2.4.12) and CLSM (2.4.13), a head-to-tail (*in trans*) orientation is an additional possibility. This interaction was strictly dependent on the stalk domain of NKp30 since no decoration of pNK cells was observed with 30LBD-His proteins (Fig. 20A and B). Notably, the specificity of the interaction of the 30Stalk-His proteins with NKp30 on the NK cell surface was validated by inhibition experiments with an anti-NKp30 blocking antibody (clone 210845, Fig. 20B). These findings are in accordance with the identification of a head-to-tail dimer in the crystal structure of the NKp30 ectodomain derived from *E. coli* [116]. However, it remains unclear whether this head-to-tail dimer is of physiological relevance or a product of crystallization. Taken together, these EM and pNK cell decoration experiments again demonstrate that the ectodomain of NKp30 has an intrinsic ability to form physiologically relevant oligomers. Furthermore, these results confirm the impact of the stalk domain on NKp30 self-association facilitating high-affinity interaction with corresponding ligands, thereby increasing NKp30-dependent NK cell cytotoxicity.

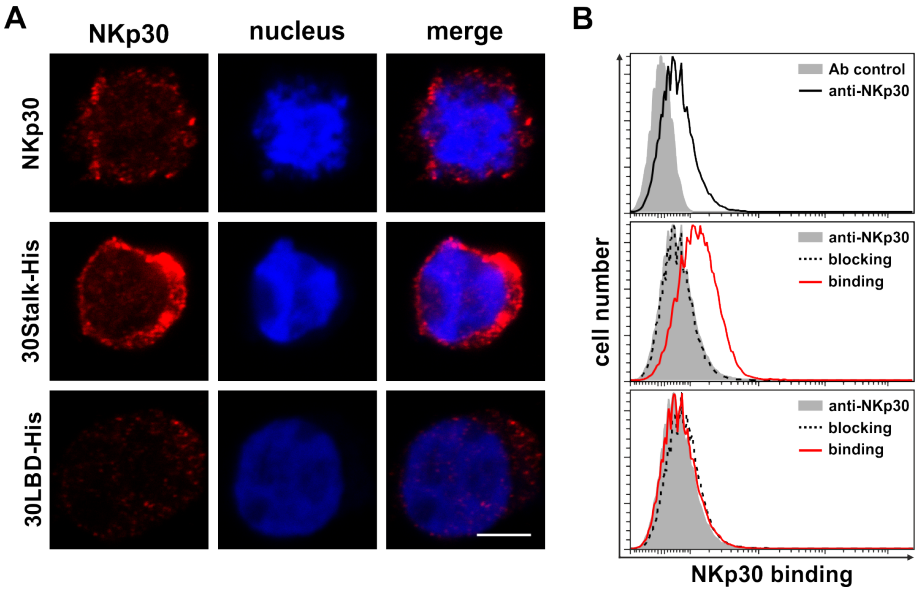

Fig. 20: The stalk domain of NKp30 is essential for recognition of NKp30 on NK cells *in trans*

(A) NK-92MI cells were decorated with an anti-NKp30 antibody, 30Stalk-His or 30LBD-His proteins. Binding of the NKp30 ectodomain proteins was detected with an anti-NKp30 antibody. The degree of surface staining was monitored by CLSM (anti-NKp30, *red*; DAPI, *blue*; size bar corresponds to 4 μm). (B) Quantification of surface decoration of primary NK cells by flow cytometry. Cells were stained with an anti-NKp30 antibody (*black line*) to quantify the level of NKp30 surface expression (antibody control, *solid gray*). Binding of 30Stalk-His and 30LBD-His proteins (*red lines*) on primary NK cells and specific blocking with an anti-NKp30 blocking antibody (*dashed lines*) were analyzed (NKp30 surface expression, *solid gray*, modified from [233].)

4 Discussion

The human activating NK cell receptor NKp30 plays an important role in immunosurveillance of malignantly transformed and virus-infected cells. For this purpose, NKp30 is able to recognize diverse ligands that are not related in sequence or structure. Previously, *N*-linked glycosylation of the ligand binding domain as well as the stalk domain of NKp30 were identified as important modules for engagement of cellular ligands and intracellular signal transduction to activate NK cell cytotoxicity [170]. Along this line, the molecular understanding of the NKp30 function in tumor immunosurveillance is instrumental in discovering novel access points to develop new tumor therapies. Therefore, structural modules and putative key mechanisms were investigated, which enable variations of the binding interfaces of NKp30 to enhance ligand binding affinity for corresponding ligands by increased avidity. Based on soluble NKp30 ectodomain variants comprising either the entire ectodomain or only the ligand binding domain, NKp30 self-assembly was identified as an important module to mediate high-affinity binding to the cellular ligand B7-H6. Moreover, the stalk domain was found to affect the three-dimensional arrangement and geometry within oligomeric NKp30 ectodomain particles. Two distinct sites for NKp30 ectodomain homo-oligomerization were identified, one present within the Ig domain of NKp30 and one within its membrane proximal stalk domain.

4.1 Modell: Homo-Oligomerization of the Activating NK Cell Receptor NKp30 to Enhance Specific NK Cell Cytotoxicity

Within this thesis, it was demonstrated for the first time that the ectodomain of NKp30 self-assembles oligomers to increase its ligand binding affinity. Experimental data revealed that NKp30 homo-oligomerization is facilitated by two interaction sites, which are located within the ligand binding domain as well as the stalk domain. Furthermore, a concentration-dependent equilibrium of monomers, dimers and oligomers was observed, which remarkably shifted to oligomer formation in presence of the stalk domain.

Based on these data, the following modell is proposed: IL-2 stimulation of NK cells leads to a drastic upregulation, and thereby increased local NKp30 receptor concentration on the plasma membrane. This will in turn promote the formation of NKp30 oligomers, which might be a molecular transformer of NK cell activation into enhanced cytotoxicity (Fig. 21). Notably, some targets induce serial killing by one NK cell subset, whereas another NK cell population does not perform killing at all in presence of the same target. Assuming accumulated and equally distributed surface NKp30 on different NK cell surfaces, respectively, different thresholds for NKp30-mediated NK cell killing are suggested. Whereas NK cells with accumulated surface NKp30 are able to form oligomeric complexes immediately upon cytokine activation, much more surface NKp30 has to be presented on the surface of the other NK cell subset to exceed the oligomerization threshold. Accordingly, NKp30 homo-oligomerization might also

induce NKp44- and NKp46-mediated signaling due to the NCR cross-talk, and thereby enhance NK cell cytotoxicity. Hence, pre-assembly of NKp30 receptor molecules prior to ligand binding could result in more efficient signaling events. In addition, an enhanced ligand binding affinity by increased avidity might be induced by NKp30 self-association.

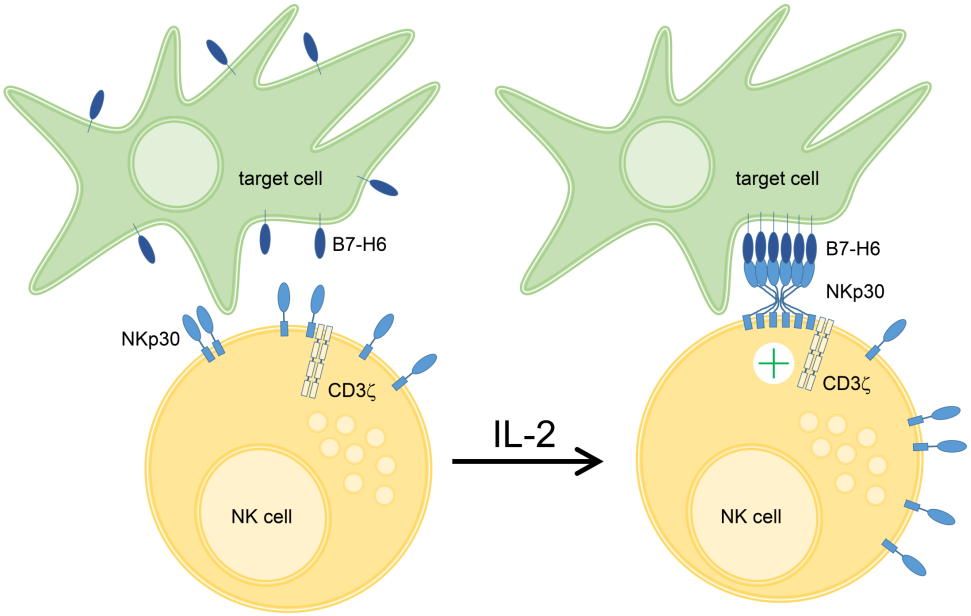

Fig. 21: NKp30 oligomerization drives NK cell cytotoxicity

Upon IL-2 stimulation a variety of activating NK cell receptors including NKp30 are upregulated on the plasma membrane of NK cells. Based on the data, increased plasma membrane NKp30 leads to formation of NKp30 oligomers, which contact cellular ligands in the plasma membrane of target cells. This interaction is mediated by two binding sites within the NKp30 ectodomain resulting in an enhanced ligand binding affinity by increased avidity. Finally, these presumably cooperative receptor-ligand interactions promote robust NKp30-dependent NK cell cytotoxicity. (Modified from [233].)

4.2 Self-Assembly of the NKp30 Ectodomain for Increased Ligand Binding Affinity

Putative interaction sites for ligand binding and NKp30 self-assembly are expected to be located within the extracellular part of the receptor. Investigating the characteristics of single NKp30 ectodomain proteins could raise the potential of finding new interaction partners on both, the NK cell and the target cell. To obtain structural information on the activating NK cell receptors NKp44, NKp46 and NKG2D, respective recombinant ectodomains were produced in *E. coli* strains to obtain large amounts of proteins for biochemical and biophysical approaches [114, 115, 240–242]. Notably, since all of these recombinant receptor ectodomains were found in inclusion bodies, sophisticated refolding protocols were developed to obtain soluble receptor ectodomains. However, this strategy is not only time-consuming, but it also remains unclear if proteins display their native conformation upon refolding. At the beginning of this thesis, the 3D structure of the NKp30 ligand binding domain was unsolved. Therefore, a *de novo* model of the NKp30LBD was calculated using a protein structure prediction service. Based on this predicted model, a C-terminally truncated version (30LBD$_{tr}$, amino acids L19-G120) was used for the expression in *E. coli* and subsequent purification analyses. To circumvent refolding of inclusion body-derived pro-

tein, expression conditions such as tags for affinity purification and host strains were varied to obtain soluble 30LBD$_{tr}$ protein. Although small amounts of soluble MBP-30LBD$_{tr}$ could be purified (Fig. S4), this protein was not able to decorate NKp30 ligand expressing target cells. When compared to the unbound and B7-H6-bound structures of the NKp30LBD, which were solved in 2011 by two independent groups, the predicted model lacked eight amino acids at the C-terminus (unbound NKp30LBD: residues A18-E130 [116], B7-H6-bound NKp30LBD: residues L19-G135 [117]), which might explain its inability to bind on target cells. In accordance, both groups reported the crystallizable NKp30LBD as an Ig-like domain, which displays a two-layer β-sandwich (Fig. S5). The front and back sheets, composed of antiparallel β-strands GFC and ABED, respectively, are linked by a canonical intersheet disulfide bond (C39-C108) [116, 117]. In addition, NKp30 contains two α-helices (α1 and α2) preceding β-strands D and E, respectively. One of these helices (α1) is unique to NKp30 among Ig-like domains [116, 117]. Within both structures, the amino acids N121-E128 represent more than the half G strand. Although there is no direct participation in the interaction with B7-H6, a truncated G strand could influence the arrangement of the opposing A and/or neighboring F strands, thereby causing a conformational change. As a consequence, the respective amino acids within the binding interface would be inaccessible, thus reducing the affinity. Furthermore, the N-terminal MBP-tag (42.5 kDa) is 2.5 fold bigger than the NKp30 ectodomain protein. Although this improves the solubility, it could inhibit ligand binding due to sterical hindrance. However, since the MBP-30LBD$_{tr}$ protein did not recognize the known cellular ligand B7-H6, the overall fold could not be used to investigate NKp30 self-assembly as mechanism to vary receptor-ligand interfaces. Notably, B7-H6 binding activity was demonstrated for the NKp30LBD refolded from *E. coli*-derived inclusion bodies comprising the amino acids L19-G135 [117]. And further, based on the same construct design and refolding protocol, Grave and colleagues [185] reported of higher mass species in size exclusion chromatography and sedimentation velocity analyses probably reflecting the presence of NKp30 ectodomain oligomers.

According to both structures of the NKp30 ectodomain, there is a disulfide bond (C39-C108) that links the front and back sheets of the two-layer β-sandwich. Furthermore, it was shown that NKp30 is *N*-linked glycosylated at three asparagines (N42, N68 and N121) within the LBD. Intensive analyses of the NKp30-B7-H6 interaction clearly demonstrated that glycosylation at residues N42 and N68 is critical for NKp30 function, whereas glycosylation at N121 has little influence on ligand binding and signaling of NKp30 [170]. Additional studies investigated host-specific differences of protein glycosylation. In contrast to NKp30-IgG1-Fc fusion proteins derived from HEK293T cells, those expressed in the human NK cell line NK-92 were resistant to complete enzymatic deglycosylation applying PNGase F or a mixture of glycosidases specific for *N*- and *O*-linked oligosaccharides. Since PNGase F is not able to cleave *N*-linked oligosaccharides when the innermost GlcNAc residue is linked to an α1-3-fucose residue [226], NK cells might modify NKp30 with fucose moieties allowing a different ligand binding mechanism of NKp30 [119]. Studies on glycosylation-dependent receptor-ligand interactions as well as *in vitro* approaches to identify new NKp30 ligands were performed using the well-established NKp30-IgG1-Fc fusion proteins [40, 128, 170, 243–245]. Despite disulfide bond formation and post-translational modification of the NKp30LBD upon expression in mammalian hosts, these bivalent fusion proteins were not suitable for the investigation of NKp30 ectodomain association due to an avidity-mediated increase of the ligand binding affinity, which is induced by the antibody-like architecture. Moreover, the induced dimerization could either induce or prevent further NKp30 self-assembly due to the sterical influence of the C-terminal

Fc part. But even though bivalent proteins were obtained from mammalian expression hosts, NKp30 ectodomain proteins without stabilizing IgG1-Fc part could not be produced.

Beside mammalian cell lines, insect cells are a suitable expression host for human glycoprotein production due to their ability to perform post-translational modifications. Insect cells were already used for the surface expression of individual natural killer cell ligands such as the intercellular adhesion molecule (ICAM)-1 or ULBP1 to analyze granule polarization and degranulation of NK cells within a system of reduced immunological background [246–248]. In addition, glycosylated type I interferon receptor ectodomains were produced in insect cells to analyze the ligand-induced assembling of the ternary complex on a mechanistic level [249]. Along this line, in this thesis, insect cells were used to express a ligand binding receptive NKp30 ectodomain as surface receptor alone or in combination with NKp44 and NKp46 as well as soluble NKp30 ectodomain proteins. While *O*- linked glycosylation of mammalian and insect cell-derived proteins is very similar (i.e. various numbers of sugars including galactose, GlcNAc, N-acetylgalactosamine, and neuramic acids), *N*-linked glycoproteins differ in their branched structures. Mammalian *N*-linked glycoproteins contain standard branched structures, which are composed of mannose, galactose, GlcNAc and neuramic acids, whereas insect cells add oligosaccharides of the high-mannose type. Notably, mimic *Sf* 9 insect cells stably express a variety of mammalian glycosyltransferases, which allow for production of biantennary, terminally sialyated *N*-glycans. Nevertheless, due to very long doubling times, protein production in mimic *Sf* 9 cells was too inefficient (data not shown). By contrast, High Five insect cells produced large amounts of soluble NKp30 ectodomain proteins. Upon enzymatic deglycosylation with PNGase F under varying assay conditions, a distinct pattern of protein bands was observed due to incomplete removal of the oligosaccharides at the positions N42, N68 and/or N121 corresponding to tri-, di-, mono- and non-glycosylated NKp30LBD variants. Since tunicamycin treatment quantitatively blocked *N*-linked glycosylation, insect cell-derived NKp30 ectodomain proteins are most likely α1-3 fucosylated at some or all of the innermost GlcNAc residues dependent on yet unknown conditions. Notably, the exact protein size and glycosylation pattern of NKp30 from primary NK cells remains still elusive since a large protein band (with a molecular mass of 30-45 kDa) detected in a biochemical analysis suggests diverse glycosylation patterns of NKp30 within a polyclonal NK cell population. In addition, even mono-deglycosylation of bivalent NKp30-IgG1-Fc fusion protein derived from the human NK-92 cell line using PNGase F failed almost completely again implying α1-3 fucosylated glycosylation of NKp30 by its natural host. The soluble NKp30 ectodomain produced in insect cells, therefore, represents a molecular equivalent to the ectodomain of human NKp30 which can be employed for further studies.

All of the NCRs consist of a crystallizable extracellular Ig domain, which is connected via a proximal stalk domain to the transmembrane domain followed by a short cytoplasmic tail [114–117]. However, it appears that the NCRs are much more different than anticipated from their domain organization and structure. NKp30 is known to be only *N*-linked-glycosylated, which is important for ligand binding [170], whereas the *O*-glycosylation of NKp46 at position 225 is essential for binding to viral hemagglutinins [243]. Along this line, there are also variations in the contribution of the NCR stalk domains on ligand binding and signaling. Sialic acid moieties attached to the stalk domain of NKp44 bind to viral hemagglutinin proteins [63, 128, 132], whereas the stalk domain of NKp30 displays a completely different mode of action. Previously, the so far neglected stalk domain of NKp30 was identified as an essential component for signal transduction into the effector cell. In addition, it is an important module to

enhance the ligand binding affinity [170]. Hence, the stalk domain could be a feature to provide diversity by induction of NKp30 self-assembly. Notably, the stalk domain has no influence on the physiological role of the different isoforms of NKp30 since alternative splicing results in variations of the LBD and cytoplasmic region without changing the amino acid sequence of the stalk domain (Isoforms a-c: K129-R143, isoforms d-f: K104-R118, Fig. S1). Consistently with the construct design of the above-mentioned study, NKp30 ectodomain proteins were produced in insect cells, which comprised either the entire ectodomain of NKp30 including the stalk domain (30Stalk-His) or the crystallizable ligand binding domain alone (30LBD-His). Molecular and cellular interaction studies of the insect cell-derived NKp30 ectodomain variants with B7-H6 confirmed the beneficial effect of the stalk domain on ligand binding. Moreover, both 30LBD-His and 30Stalk-His mediated a high-affinity interaction when compared to the B7-H6 binding affinities of *E. coli*-derived or bivalent NKp30 ectodomain fusion proteins [117, 170].

To investigate the impact of the stalk domain on ligand binding affinity and putative NKp30 ectodomain self-assembly by different biochemical approaches, it is essential to employ an anti-NKp30 antibody with a defined epitope located within the LBD. This anti-NKp30 antibody should recognize the native or denatured state of both NKp30 ectodomain variants, 30LBD-His and 30Stalk-His, with identical affinity. Since the receptor NKp30 was identified by detection with a mouse monoclonal antibody (clone AZ20) in 1998 [101], further monoclonal and polyclonal anti-NKp30 antibodies were developed. Some of these mouse monoclonal anti-NKp30 antibodies (e.g. clones AZ20, 210845 or P30-15) were able to specifically inhibit NKp30-mediated NK cell cytotoxicity [134, 244]. Their individual epitopes are unknown, but an interaction with the NKp30LBD in its native conformation is most likely since these monoclonal antibodies are recommended for cellular assays or ELISA. Nevertheless, it remains unclear whether the blocking capacity could influence the results by lower ligand decoration efficiencies. The polyclonal goat anti-NKp30 antibody recognizes native and denatured NKp30 in cellular assays, ELISA and immunoblot analyses. The immunogen is denoted with L19-T138 comprising the whole extracellular part of NKp30 including the stalk domain, which could result in recognition of additional binding sites on the 30Stalk-His protein leading most likely to misinterpretations in favor of the stalk domain. Despite a variety of commercially available antibodies recognizing NKp30 in a lot of biochemical and cellular applications, none of these is extensively characterized concerning binding epitopes within the LBD. Therefore, an antibody detecting a defined epitope (amino acids R62-R75) comprising the *N*-linked glycosylation acceptor site N68 as well as the unique α1 helix within the LBD of NKp30 was generated by peptide-immunization of two rabbits. Upon immunoaffinity purification from rabbit serum, a polyclonal pool of different rabbit IgG subtypes was purified, which was suitable in several cellular and molecular approaches. This rabbit anti-NKp30 antibody could bind to a consecutive region of 37 amino acids including R62-R75, thus suggesting the recognition of three or more different epitopes. Furthermore, although the membrane proximal stalk domain is rather flexible, a sterical influence within this region is not assumed, thereby providing identical interaction sites for antibody binding with the same extent on 30LBD-His and 30Stalk-His proteins. Notably, the chosen peptide stretch including the glycosylation acceptor site N68 is located outside of the NKp30-B7-H6 binding pocket, and should therefore not participate in the NKp30-B7-H6 interaction. By contrast, N68 was recently identified to be essential for intracellular signaling upon B7-H6 engagement [170]. Investigations using the anti-NKp30 antibody from peptide immunization thus might shed more light on this discrepance. Along this line, the relevance of the glycosylation at N68 within the epitope sequence of the rabbit anti-NKp30 antibody was inves-

tigated by pre-incubation of soluble NKp30 ectodomain proteins with the anti-NKp30 antibody prior to decoration of B7-H6 expressing target cell lines or ELISA setups with immobilized recombinant B7-H6. Cell decoration efficiencies and ligand binding affinities remained unchanged suggesting no capacity of the rabbit anti-NKp30 antibody to interfere with the receptor-ligand interaction (data not shown). However, NKp30 ectodomain proteins immobilized in ELISA or on target cells could be decorated with the anti-NKp30 antibody from peptide immunization suggesting that the glycosylation at position N68 does not interfere with the recognition of the epitope sequence. It is most likely that the epitope for the anti-NKp30 antibody from peptide-immunization is not accessible in the native, folded and unbound protein. By contrast, pre-incubation with a mouse monoclonal anti-NKp30 antibody (clone 210845) could inhibit NKp30-B7-H6 interaction in equivalent experimental setups. Notably, peptide spot arrays revealed no linear epitope sequence for the binding of this blocking antibody, but further suggested conformational epitopes close to the NKp30-B7-H6 interface (data not shown). Therefore, glycosylation at position N68, at least insect cell-specific, might not be essential for ligand binding. These data support the NKp30-B7-H6 interface of the 3D structure that implies no direct influence of the position N68 on the receptor-ligand interaction [117]. However, pre-incubation of NKp30-functionalized reporter cells with the anti-NKp30 antibody binding in close proximity to N68 could again demonstrate its impact on NKp30-dependent signaling. Association with this antibody could prevent a conformational change within this region containing the unique α1 helix, which might be necessary to induce a yet unknown mechanism for intracellular signal transduction.

Both NKp30 ectodomain proteins exhibited a considerably higher affinity to the recombinant ligand B7-H6-Ig than the bivalent NKp30-Ig fusion proteins [170] or the *E. coli*-derived NKp30 ectodomain employed to determine the structure of the NKp30-B7-H6 complex [117]. This increased affinity might be due to an avidity effect, which is attributed to NKp30 ectodomain oligomerization. Furthermore, 30Stalk-His and 30LBD-His proteins were efficient competitors of NKp30-dependent signaling when bound to B7-H6-expressing target cells with a strong contribution of the stalk domain to quantitative blocking of the NKp30-B7-H6 interaction. Decoration of these target cells with both NKp30 ectodomain variants thereby revealed that the number of clusters was mainly dependent on the ligand concentration on the target cell, but the mean cluster size was significantly increased after binding of 30Stalk-His when compared to 30LBD-His proteins. These observations argued for a stalk-dependent difference in the architecture of the oligomeric self-assembly of the NKp30 ectodomain, which might in turn lead to a different degree of avidity and apparent affinity to B7-H6. In addition, the impact of the stalk domain on NKp30 ectodomain self-assembly was confirmed by size exclusion chromatography. Although an equilibrium of monomers, dimers and oligomers was found for both NKp30 ectodomain variants, the stalk domain definitely induced oligomerization. Whereas 30LBD-His monomers, dimers and oligomers were equally distributed, for 30Stalk-His proteins the ratio shifted tremendously to oligomers with dimers being rather an intermediate state. Based on these data, two distinct sites for NKp30 ectodomain homo-oligomerization are proposed, one present within the Ig domain of NKp30 and one within its membrane proximal stalk domain. Strikingly, all oligomeric forms of both NKp30 ectodomain variants were B7-H6 binding receptive as demonstrated by different ELISA setups with the commercially available polyclonal goat anti-NKp30 and the rabbit anti-NKp30 antibody from peptide immunization. Notably, the polyclonal goat anti-NKp30 cocktail comprises antibodies with specificity for different epitopes within the entire NKp30 ectodomain including the stalk domain. Therefore, more than one antibody molecule might

be able to bind per one 30Stalk-His or 30LBD-His protein. By contrast, the rabbit anti-NKp30 antibody recognizes a distinct epitope sequence, which allows for more quantitative results, but in turn leads to lower signal intensities in ELISA. Along this line, monomeric and dimeric NKp30 ectodomain variants could not be detected by the rabbit anti-NKp30 antibody, whereas subsets of the goat anti-NKp30 pool with different specificity were still able to associate with NKp30 ectodomain monomers and dimers. Most probably the peptide epitope on dimeric and monomeric NKp30 ectodomain proteins was occupied by interacting ligand molecules. By contrast, oligomeric NKp30 ectodomains bound to B7-H6-Ig were detected by both anti-NKp30 antibodies since the respective peptide sequence might be present on multiple NKp30LBDs situated at the outer area of the oligomeric particle, and therefore did not participate in the NKp30-B7-H6 interaction. Thus, oligomers were not quantitatively (equivalent to the respective number of monomers) occupied by B7-H6 ligand molecules. These results do not only confirm ligand binding capacities of the NKp30 ectodomain oligomers, but also provide new access points for the investigation of possible interaction sites for NKp30 dimer and even oligomer formation. On the one hand, NKp30 ectodomain clusters were found on B7-H6 expressing target cells. On the other hand, NKp30 ectodomain monomers and dimers could not be detected by the rabbit anti-NKp30 antibody upon binding to recombinant B7-H6-Ig in ELISA. Therefore, an NKp30 oligomer dissociation upon B7-H6 engagement in respect of providing a certain number of NKp30 monomers for monovalent receptor-ligand interactions can be excluded.

Gel filtration experiments revealed a concentration-dependent increase of 30Stalk-His and 30LBD-His oligomers (reflected by increased peak areas), while the composition of the oligomer particles (reflected by the consistent retention volumes) remained constant. According to their theoretical molecular mass, it was estimated that 30Stalk-His oligomers were assembled by more monomers (e.g. 30Stalk-His: 20 monomers vs. 30LBD-His: 16 monomers). To investigate the impact of the stalk domain on the particle size of the oligomers as well as its influence on the geometric arrangement, negative stain electron microscopy was employed. This method is especially useful for imaging the size and shape of single proteins and larger molecules (especially larger than 100 kDa) with a complex internal structure at the nanometer level [250]. Strikingly, both 30Stalk-His and 30LBD-His particles had an average diameter of 15 nm, although the larger number of monomers within one oligomer would imply a stalk-dependent increase of the particle size. By contrast, most probably, an association of the stalk domain led to formation of a condensed or even the densest packing of monomers, which was further confirmed by the constant retention volumes for the 30Stalk-His and 30LBD-His oligomers at higher protein concentrations. Interestingly, 30LBD-His monomers also were able to assemble suggesting a certain affinity, which might be promoted by close proximity. Notably, no preferred areas or cavities for self-association were identified in this thesis, but biophysical calculations and/or analyses with interfering peptides could help to locate the interfaces of the NKp30LBD-NKp30LBD contact. In addition, oligomer formation was remarkably increased for the 30Stalk-His proteins, thus suggesting a two-step process for NKp30 cluster formation in general. NKp30 self-assembly is mainly characterized by affinity-mediated interaction of the stalk domains, which then in turn induces association of the LBDs due to avidity. Therefore, an ”open flower” configuration is assumed for both 30LBD-His and 30Stalk-His particles in solution (Fig. 22A and B). Since both NKp30 ectodomain variants form particles with similar spherical geometry, a circular arrangement of LBDs and self-assembling stalk domains within the center is most likely. As determined from the 3D structure (using the PyMol software) [116], the two-layer β-sandwich of the NKp30LBD

is approximately 40 Å in length and 20 Å in width. Assuming two opposing LBDs and a diameter of 15 nm for one particle, there would be a residual center of approximately 7 nm in diameter for two stalk domains, each comprising 15 amino acids. Within secondary protein structures, the α-helical conformation reflects the densest packing. As estimated from the pitch of a helix (5.4 Å), which is the product of 3.6 residues per turn with a translation of 1.5 Å the corresponding minimum length for a α-helical stalk domain would be 22.5 Å. By contrast, the distance between two amino acids is about 3.8 Å (determined from the structure of the NKp30 ectodomain [116]) resulting in a maximum length of approximately 53 Å for a totally unstructured sequence of 15 amino acids. Since the stalk domain is very flexible and was therefore not resolved in the structures of the NKp30 ectodomain, an α-helical conformation is excluded. Furthermore, the interaction site for self-assembly is unknown, hence a more detailed analysis of the length of the stalk domain is not possible. However, an association at the C-terminal part of the stalk domain or an influence by the C-terminal His-tags is unlikely due to the diameter of the center.

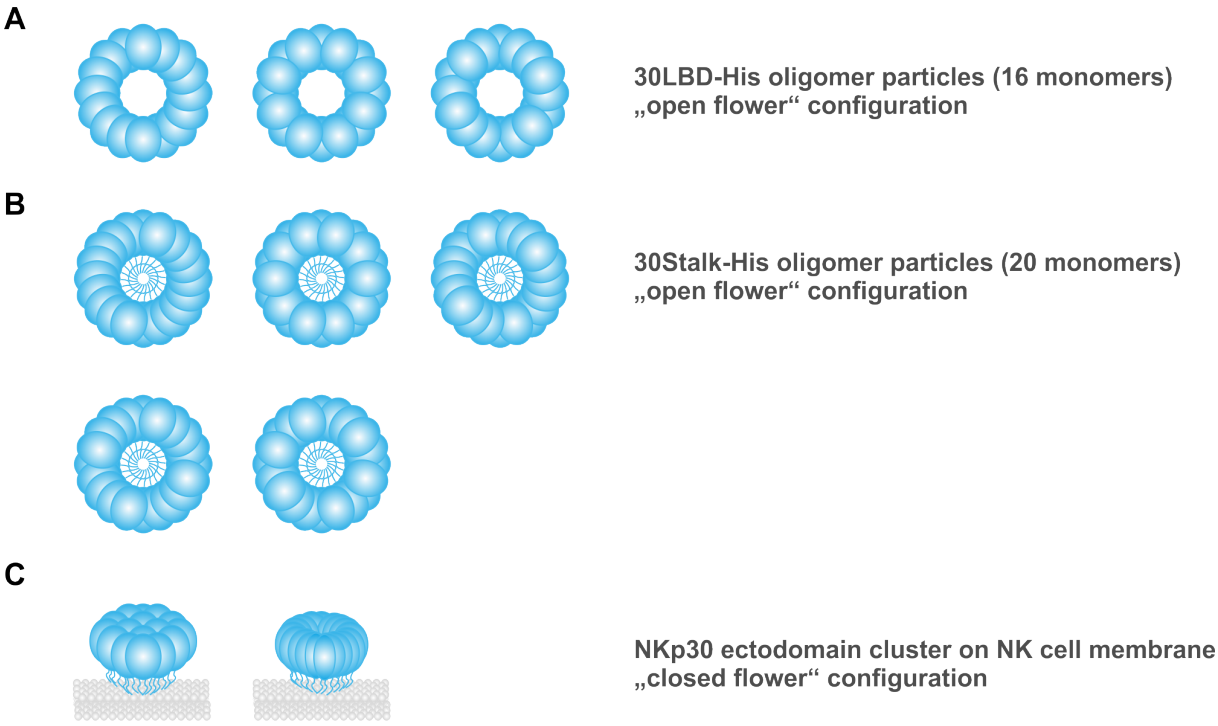

Fig. 22: Putative arrangements of the NKp30 ectodomain within particles and on the NK cell membrane

A selection of symmetric NKp30 ectodomain arrangements suggested from size exclusion chromatography and subsequent electron microscopy analyses of 30LBD-His (A) and 30Stalk-His oligomeric particles. Despite different numbers of monomers within the 30LBD-His and 30Stalk-His oligomers, same particle sizes were observed. (A) 16 globular NKp30 ligand binding domains are ordered exemplarily in three different arrangements to form an ”open flower” configuration. Thus, different interaction sites for ligand binding can be formed. (B) Due to the affinty of the stalk domains, there is a more condensed packing, which allows for 20 monomers to form an ”open flower” configuration within the particle. As demonstrated exemplarily by five different arrangements for 30Stalk-His oligomers, a larger number of monomers results in more variants of symmetric arrangement, thereby increasing the number of different binding interfaces. Notably, different numbers of monomers within the oligomers and asymmetric compositions of 30LBD-His or 30Stalk-His particles further increase variability. (C) On the NK cell membrane, a head-to-head orientation within NKp30 clusters is assumed. Cell decoration experiments of NK cells with NKp30 ectodomain proteins showed that an interaction of the stalk domain is essential for self-assembly since 30LBD-His binding was not detected. Therefore, NKp30 clustering in a ”closed flower” configuration is proposed and shown exemplarily by two different arrangements.

It still remains unclear, how the stalk domain is able to increase ligand recognition and oligomer formation. Suggesting a change of orientation for the interaction within the LBDs, which could be induced by the affinity-mediated self-assembly of multiple stalk domains, there would be space for a few more stalk-containing proteins within the particle, thereby forming additional *de novo* cavities for homo-oligomerization and/or recognition of additional ligands [170]. Notably, this change of orientation would explain the increased number of monomers as well as the unchanged diameter of the particle for the 30Stalk-His when compared to the 30LBD-His oligomers.

As illustrated by the model in Figures 22A and B, one interaction site within the LBD could be situated in close proximity to the stalk domain, which would further foster the hypothesis of "facilited binding" of the NKp30LBD. Since there is a slight conformational reorganization of the NKp30LBD underneath the binding pocket upon interaction with B7-H6, this might be a promising surface stretch for NKp30 ectodomain self-assembly within the LBD. To get more information on the complex internal structure, 2D images of the 30Stalk-His and 30LBD-His oligomeric particles were sorted into classes and averaged. According to the number of classes, both NKp30 ectodomain variants formed a large variety of globular particles with different structural arrangements. A circular or spherical arrangement of several LBDs within one particle implied the presence of more than one binding interface for self-assembly. Due to the number of 2D classes for 30LBD-His particle arrangements, preferred sites for self-interaction within the LBD are assumed. Along this line, multiple putative sites for association might increase the number of possible LBD combinations in solution resulting in heterogeneous surfaces of the oligomeric particles. However, due to an interaction of the stalk domains, more ordered 30Stalk-His oligomers could be expected. By contrast, these particles were even more heterogeneous in their 3D arrangements and geometry. The degrees of freedom might be increased by the flexibility of the stalk domains, which allow for assembly of more monomers within one particle, and a facilited self-assembly of NKp30LBDs suggests interaction sites without strict perference, thus increasing the number of 2D classes. In figures 22A and B the influence of the stalk domain on the 3D geometry heterogeneity is demonstrated by a selection of symmetric NKp30 ectodomain arrangements. Larger numbers of monomers and asymmetric compositions would further increase the variability to form ligand binding receptive cavities. However, a spherical geometry of the oligomeric particles in solution is of no physiological relevance since NKp30 self-assembly in its native environment would be constricted by the anchorage within the NK cell plasma membrane. Based on the identification of two interaction sites, a "closed flower" configuration of NKp30 ectodomain self-assembly on the plasma membrane is proposed (Fig. 22C). Considering the intrinsic potential of the NKp30LBD to homo-oligomerize as well as the rather short stalk domain, which would prevent an alternating dimerization, a head-to-head arrangement of an unknown number of molecules within the NKp30 cluster was most likely. In fact, this type of interaction was strictly dependent on the stalk domain of NKp30 since no decoration of primary NK cells was observed with 30LBD-His proteins. Notably, homo-oligomerization of full-length NKp30 receptors on the NK cell surface would be stabilized by their anchorage within the plasma membrane. Accordingly, interaction of entire NKp30 ectodomains without plasma membrane fixation would lead to faster dissociation when compared to full-length NKp30 interaction. Along this line, self-association of the NKp30 ligand binding domain alone might be too unstable to detect in decoration experiments of primary NK cells. However, a head-to-tail orientation remains an additional possibility, which would be in accordance with the identification of a head-to-tail dimer in the crystal structure of the NKp30 ectodomain derived from *E. coli* [116]. Nev-

ertheless, it remains obscure whether this head-to-tail dimer is of physiological relevance or a product of crystallization. Beside NK cells, NKp30 is expressed by distinct T cell subsets [105–108]. Therefore, a head-to-tail interaction of NKp30 could provide a way for NK cells to bind to other immune cells expressing surface NKp30. This could be important for the regulation of immune responses.

Based on experimental data, mainly obtained from soluble NKp30 ectodomain proteins in solution, individual functions for both subdomains of the NKp30 extracellular part are proposed: i) the major role of the NKp30LBD is to facilitate receptor-ligand interactions, which might be fostered by avidity-induced self-assembly, whereas ii) the receptor-receptor interaction is affinity-mediated by the stalk domain. These mechanistically different steps of a sophisticated process act in concert to allow for high-affinity binding to a multiplicity of diverse ligands as well as subsequent intracellular signal transduction to assure most efficient NKp30-dependent NK cell activity.

4.3 Surface Receptor Oligomerization for Efficient Cellular Cytotoxicity

Cellular cytotoxicity is mediated by lymphocytes of the innate (NK cells) and the adaptive immunity (CTLs) to protect the host from parasites, viral and bacterial infection as well as malignantly transformed cells. In this respect, NK cells and CTLs share a common killing mechanism, which is a form of ”assisted suicide” as the endogenous apoptosis program is activated within the target cell. When a cytotoxic lymphocyte encounters a transformed or infected cell, selectins and integrins (such as L-selectin or lymphocyte function-associated antigen (LFA)-1) are ligated for an effective conjugation between NK cells or CTLs and their targets in the initial adhesion step [251–254]. This adhesion allows for activating receptors (e.g TCR or NCRs and activating KIRs) to focus in the direction of the target cells, which results in formation of a tight interface, the mature immunological synapse. The contact site organizes into three concentric circular zones (bull’s eye pattern) comprising i) the inner circle also known as central supramolecular activation cluster (cSMAC), ii) the peripheral adhesion ring (pSMAC), and iii) the outer (distal) ring (dSMAC). Although it remains unclear how these highly organized ring structure is generated, it is known that T cell costimulation as well as a dynamic filamentous actin (F-actin) cytoskeleton are essential for formation of these protein clusters. Within the cSMAC of a CTL, receptors involved in cell activation and specific signal transduction cascades are concentrated (i.e. TCR/CD3 complex, accessory receptors CD4 and CD28, and protein kinase C θ (PKCθ)), whereas adhesion molecules involved in formation and maintenance of the IS are located in the pSMAC (i.e. LFA-1, LFA-2, and the membrane anchor talin). The dSMAC comprises molecules with a large extracellular part such as CD45 (protein tyrosine phosphatase, receptor type, C, PTPRC) and CD43 (sialophorin or leukosialin). Upon F-actin polymerization and reorganization, the cytotoxic cell is able to focus the activating receptors to the interface and polarize microtubule organizing centers (MTOCs) to transport lytic granules (perforin and granzymes) toward the IS for directed secretion [252, 255–257]. Notably, beside $Ca2^{+}$-dependent killing by the pore-forming molecule perforin and cell-death promoting molecules such as granzymes, NK cells and CTLs are able to kill $Ca2^{+}$-independently by induction of the death receptor pathway via the Fas ligand (FasL) binding to Fas (CD95) on target cells [258–260]. However, there are several important differences between NK cells and CTLs. For example, lytic granules are preformed in resting human NK cells but not in CTLs [261]. Furthermore, the analysis of the NK cell synapse revealed both a cytotoxic synapse and an inhibitory synapse in which the negative regulatory receptors are dominant.

Inhibitory signaling blocks activating receptor clustering and induces cytoskeletal retraction in natural killer cells [262]. However, NK cells readily form cSMAC and pSMAC-like compartments in 1-10 min, regardless of whether the synapses would lead to cytotoxicity or inhibition [260].

There are several studies concerning F-actin polymerization, cytoskeleton organization, lytic granule transport to the synapse and further, but there are no reliable information on activating NK cell receptor migration or clustering within the plasma membrane with respect to IS formation so far. Recently, it has been shown for T cells that kinases, adaptor molecules and antigen receptors accumulate in structures termed microclusters within immunological synapses [263–265]. In addition, small clusters of CD3 were formed prior to concentrating in the cSMAC of the T cell [266], suggesting a clustering of the TCR within the immunological synapse. Along this line, Giurisato and colleagues demonstrated that receptor clustering at the NK-cell lytic synapse is important for the induction of robust signaling in NK cells [267]. Although functional microclusters have been identified in NK cells, these have only been investigated at the supramolecular inhibitory cluster [236, 263]. So, it is unclear whether the level of signaling organization that is observed in T cells can be similarly applied to the NK-cell lytic synapse [71].

The TCR/CD3 complex is an ordered assembly process organized around three trimeric intramembrane interactions: CD3$\delta\epsilon$ associates with TCRα, and CD3$\gamma\epsilon$ with TCRβ through the centrally placed lysine residues, and then the $\zeta\zeta$ module associates with TCRα through an arginine residue in the upper third of the transmembrane domain. The $\zeta\zeta$ dimer is one of four homodimeric modules known to provide the signaling capacity to many activating receptors in the immune system such as the NK cell receptors NKp30 and NKp46 [268, 269]. By contrast to the invariant NK cell receptors, there is a large variety of TCRs due to somatic recombination for recognition of diverse ligands. However, the precise mechanism linking MHC binding outside the cell to early biochemical events inside the cell are controversially discussed. In this respect, triggering models are proposed, which range from receptor clustering and coreceptor recruitment to an array of conformational change models, in which TCR proteins are proposed to physically impinge on the CD3 modules to transmit signals [269–271]. Along this line, it is possible that CD3ζ clustering might also induce NKp30 self-assembly within the NK cell IS. Upon association with CD3ζ, the local concentration of NKp30 receptors might increase up to formation of NKp30 clusters to enhance the NK cell-target cell adhesion by high-affinity receptor-ligand interactions. In addition, *de novo* binding sites for further ligands could be formed. In this respect, NKp30 ectodomain self-assembly in solution might be a first hint to confirm NKp30 clustering within the NK cell membrane for mature IS formation and efficent NK cell cytotoxicity.

Despite less than 30 % sequence similarity, the crystal structure of the NKp30LBD revealed an I-type Ig-like domain which displays significant structural homology with CTLA-4 (cytotoxic T lymphocyte antigen 4, PDB: 1I8L) and CD28 (PDB: 1YJD) [116, 117]. CD28 and CTLA-4 belong to the family of T cell coreceptors, which are type I transmembrane proteins having a single extracellular V-type Ig-like domain [272,273]. Their respective ligands B7-1 (CD80) and B7-2 (CD86) comprise two extracellular Ig domains, which is also known for the cellular ligand of NKp30 belonging to the B7 family (B7-H6). Interestingly, CTLA-4 and CD28 form disulfide-bonded homodimers and, moreover, their ligands B7-1 and B7-2 are also found to be homodimers. On the one hand, covalent dimerization of the receptor CTLA-4 is required for its high avidity binding. On the other hand, oligomerization of the ligands CD80/CD86 is also required for high avidity CTLA-4 binding since CTLA-4 bound with low avidity to monomeric CD86. Therefore, engagement of CD28 and/or CTLA-4 receptors by clustered CD80/CD86 ligands would in-

crease the local receptor concentration. Thus, covalent receptor dimerization and ligand oligomerization are two key features of the CD28/CTLA-4/CD80/CD86 receptor system that control ligand binding and provide a the structural basis for forming unusually stable signaling complexes at the T-cell surface to regulate signal transduction by controlling the duration of receptor occupancy [274–276]. Strikingly, beside a common killing mechanism of NK and T cells, there are also structural similarities of the activating NK cell receptor NKp30 and the T cell coreceptors CD28/CTLA-4 with their respective ligands belonging to the B7 family. Biochemical studies revealed the intrinsic potential of the NKp30LBD to dimerize and even oligomerize to a certain extent. Furthermore, the flexible stalk domain, which is not present in any crystal structure, promoted homo-oligomerization of the NKp30 ectodomain in solution. Although there are no data available for NKp30 clustering on the plasma membrane so far, the potential of NKp30 ectodomain self-assembly was demonstrated. Notably, ligand-induced receptor clustering is a common mechanism for receptor-mediated signaling in immune responses [234–236]. As described for the structurally related CTLA-4, ligand oligomerization on the target cell might therefore be an additional option to increase the local NKp30 concentration on the cell surface to induce NKp30 cluster formation.

Both inhibitory and activating NK cell receptors of the KIR family have been shown to assemble dimers or even oligomers. For instance, inhibitory KIR2DL2 dimerizes with both receptor ectodomain molecules in the same orientation via two different interaction sites. Therefore, Snyder and co-workers [189] suggested formation of KIR2DL2 oligomers within the plasma membrane by alternating dimerization. Moreover, studies with soluble activating KIR2DS1 ectodomain proteins refolded from *E. coli* inclusion bodies demonstrated self-association in rod-like shapes of similar dimensions, suggesting that the KIR2DS1 homo-oligomerization is a well-defined process [190]. By contrast, the activating NK cell receptor NKG2D assembles a composite binding site for the interaction with its corresponding cellular ligands by homo-dimerization [187, 188]. For efficient intracellular signaling, a hexameric complex composed of one NKG2D dimer, which associates with two dimeric DAP10 adaptor molecules, is formed, resembling the structure of the TCR/CD3 complex. Similar to formation of the mature T cell IS, clusters of activating NKG2D were also found in lipid rafts. Along this line, coengagement of the inhibitory receptor NKG2A partially disrupted NKG2D recruitment into rafts [277]. Despite structural diversity of NKG2D and NKp30, both activating NK cell receptors play important roles in immune surveillance. NKG2D is a functional surface receptor in mice and man, whereas functional NKp30 is not found in mice indicating the unique role of NKp30. Considering the longer life span of man, it is conceivable that NKp30 has mainly developed for the defense against constantly changing viruses and malignantly transformed cells. In addition, a phylogenetic study suggests the possibility of a staged appearance of the NCRs with the following progression: NKp46-NKp30-NKp44. This progressive NCR appearance might again reflect an increase in the complexity and in the fine-tuning of the innate immune response [151]. Notably, the phylogenetically youngest NCR NKp44 is expressed only on activated NK cells, possibly providing a supportive function in regulation of NK cell activity. Along this line, NKp30 oligomerization might also act as an activation marker on cytotoxic NK cells, whereas monomeric oder dimeric NKp30 receptors could adopt regulatory functions to identify cognate antigens on the target cell upon the first contact. Indeed, a sharp difference in cytotoxicity against neural tumors was demonstrated between NCR^{bright} and NCR^{dull} NK clones, supporting the notion that the NCRs play a critical role in the induction of cytotoxicity against tumor target cells [278]. In this respect, a strongly increased expression of NKp30, NKp44, NKp46, and NKG2D upon IL-2 stimulation of freshy isolated peripheral blood NK cells was observed,

thereby increasing cellular cytotoxicity [179–182, 184]. Interestingly, IL-2 activated human peripheral blood NK cells were not only more cytotoxic but also twice as big as resting NK cells [72]. Because the degree of oligomerization is dependent on the local receptor concentration, which is upregulated by IL-2 upon NK cell activation, oligomerization of NKp30 might be a molecular transformer of NK cell activation into enhanced cytotoxicity.

As suggested from their structures, monovalent receptor-ligand interactions are expected for the NCRs. Strikingly, within this thesis, it was shown that NKp30 oligomerization might lead to formation of ligand binding competent multivalent complexes. Although this has not been described for the other NCRs, formation of *de novo* binding places by homo-oligomerization of the NKp30 ectodomain could be a mechanism of how the NK cell is able to recognize multiple ligands that are unrelated in sequence and structure. Another way to provide diversity would be a cooperation of NKp30 with the other NCR family members NKp44 and NKp46 [101], further suggested as selective cross-talk between the NCRs [173], but experimental data confirming these hypotheses are scarce. Notably, NKp46 is able to form ligand binding-induced dimers most likely via its membrane proximal domain NKp46D2, which in turn leads to intracellular signaling and target cell lysis [186]. Within this respective study, NKp46 ectodomain dimerization was mediated by a monoclonal antibody and further validated by specific peptide inhibition. However, the precise dimerization interface of NKp46 remains unclear as steric hindrance and a possible direct contribution of the epitope sequence of the antibody to dimerization could not be distinguished in these studies [186].

Oligomerization of proteins is a common principle in nature as illustrated by the fact that 35 % of all proteins within a cell are oligomers [279–281]. Therefore, oligomerization of NKp30 is likely to be of physiological relevance. However, at this point of investigation, the exact process of NKp30 ectodomain self-assembly remains speculation. The intrinsic potential for homo-oligomerization might be enough to assemble pre-formed clusters. An appealing consideration for this hypothesis is that receptor oligomerization prior to ligand interaction would lead to faster activation of signaling. Notably, local concentration and oligomerization might even be fostered by ligand-induced assembly of a condensed immunological synapse between the NK cell and its target cell. Along this line, multivalent interactions with trimeric influenza virus hemagglutinin complexes [63] or multimeric ligand structures such as multimeric N-acetylneuraminic acid (NeuNAc)-containing *N*-glycans binding to NKp44 or NKp46 [282] suggest homo- or heteromeric NCR association [176–178], but to date there is no evidence for neither pre-formed nor ligand-induced receptor oligomerization. However, as mainly demonstrated for T cells so far, ligand-induced receptor clustering is a common mechanism for receptor-mediated signaling in immune responses [234–236]. For instance, approximately 50 % of surface MHC class II protein resided in lipid rafts and this clustering of MHC protein was necessary for presentation of low doses of antigen to T cells [283]. In addition, the NKG2D ligands MICA and the ULBPs were also expressed in lipid rafts at the cell surface, both proteins accumulating at the activating human NK cell immune synapse. Moreover, electron microscopy revealed constitutive clusters of ULBP at the cell surface [284]. This is in line with the dotted decoration pattern upon binding of NKp30 ectodomain proteins on ligands on the target cell surface observed in this thesis. Comparison of the same B7-H6 expressing target cell population decorated with soluble NKp30 oligomers comprising the entire NKp30 ectodomain or only the ligand binding domain revealed a constant number of ligand clusters, suggesting a pre-assembly of B7-H6 monomers on the target cell plasma membrane prior to interaction with NKp30. In any case, NKp30 self-assembly

induced by increased local receptor concentration due to IL-2 activation or upon binding to pre-formed ligand complexes, however, might be a potent instrument to facilitate high-affinity receptor-ligand interaction, stabilization of the immunological synapse as well as extensive amplification of intracellular signal transduction for efficient NK cell-mediated target cell lysis.

4.4 Outlook

Within this thesis, NKp30 homo-oligomerization was identified as important key feature to improve ligand binding affinity for enhanced NK cell cytotoxicity. Based on biochemical data, the beneficial effect of the stalk domain on ligand binding and intracellular signal transduction [170] might be attributed to self-binding following avidity-mediated attraction of the NKp30LBDs. However, despite this obvious intrinsic potential for self-assembly, it remains unclear whether there are pre-existing NKp30 clusters on the plasma membrane of the resting NK cell or cluster formation is induced by IL-2 activation, ligand engagement oder association with its adaptor molecule CD3ζ. To identify putative pre-clustering of functional NKp30 receptors on a cellular background, anti-NKp30 antibody decorated NKp30 expressing cell lines could be analyzed by confocal immunofluorescence microscopy. For this purpose, A5-30FL-His reporter cell lines with and without expression of the accessory protein CD3ζ might be used to identify whether there is any impact of the adaptor molecule on receptor clustering on the A5 cell plasma membrane. Along this line, decoration of these cell lines with recombinant B7-H6 protein could shed more light on the hypothesis of ligand-induced NKp30 homo-oligomerization. There are only few experimantal data on the NKp30-CD3ζ so far. On the one hand, it was shown that NKp30 and CD3ζ are sufficient to mediate intracellular signaling [170]. In addition, stable expression of CD3ζ significantly increased NKp30 surface levels at constant total NKp30 expression level within the cell whereas surface NKp30 full-length expression alone was rather challenging in several cell types. These results suggest that beside its role in signal transduction, CD3ζ might also target NKp30 to the plasma membrane and/or promote the surface retention of NKp30 [238]. As mediator for stable and constant NKp30 surface expression, CD3ζ might further increase the local receptor concentration, thereby promoting NKp30 clustering. However, total internal reflection fluorescence microscopy (TIRFM) of living HeLa cells, which expressed fluorescence-coupled NKp30 receptors alone or in combination with CD3ζ, revealed that the organization status of NKp30 remained unchanged, even upon decoration with its ligand B7-H6. Most probably, the fluorescent tags fused to the N-terminus of NKp30, which had the same size or were even larger, interfered with the NKp30 ectodomain self-assembly. In addition, B7-H6 binding was decreased, which might be attributed to the receptor-ligand binding interface, which is located close to the N-terminus of NKp30. In this respect, both B7-H6 binding as well as NKp30 homo-oligomerization might be hampered by masked residues or even structural rearrangements mediated by the large fluorescence-tags [238]. By contrast, dimerization of NKp46 was observed within this study. Since the dimerization interface of NKp46 is located within the membrane-proximal D2 domain [186] and due to the larger molecular mass of NKp46, less structural influence by the respective tags is suggsted. Therefore, analysis of NKp30 homo-oligomerization by TIRF microscopy might be an option, if there will be smaller fluorescent tags available to prevent conformational changes of the NKp30 ectodomain due to the experimental setup. Another method to investigate lateral mobility of NKp30 within the plasma membrane using TIRFM could be the micropatterning analysis. Fluorescence-coupled NKp30 receptors

situated within the plasma membrane of a living cell would be captured by the respective fluorophore ligand, which was coated in a specific pattern on a solid support. Redistribution of NKp30 coupled to another fluorophore to this ligand-immobilized NKp30 could then be followed by TIRFM. Coating of NKp30 ligands to investige their influence on NKp30 mobility and cluster formation is a further possibility [238]. However, single receptor trafficking experiments in a more physiological context, such as TIRFM of NKp30 receptor expressing A5 reporter cells or NK cell lines, are even more difficult to realize since this sophisticated experimental setup has been established only for HeLa cells so far.

Up to now, it is known that oppositely charged amino acids mediate the association of NKp30 (positive arginine residue) and CD3ζ (negative aspartatic acid residue), but the concrete mechanism and time point of interaction remain elusive. It is possible that ligand binding might induce a conformational rearrangement of the extracellular part of NKp30 and a subsequent shift of the transmembrane domain towards the cytosol. Due to the altered position of the arginine residue within the transmembrane region, a stronger interaction with the aspartatic acid residue might be possible, which in turn could initiate the intracellular signal transduction. Furthermore, the arginine residue could be located outside the transmembrane region and be pushed into the plasma membrane upon ligand binding. Both models suggesting a change in the relative arginine position could be validated by electron spin resonance spectroscopy as introduced spin labels are sensitive to the polarity of their environment [238]. In another approach, R143 could be deleted by point mutation to investigate the crosstalk of the individual NCRs in more detail. Therefore, the NKp30^{dull} NK cell line [119] could be employed to introduce a codon-optimized NKp30 receptor devoid of transmembrane arginine to analyze whether the signal transduction cascade following NKp46 and/or NKp44 triggering could be induced by NKp30 ligand binding. However, based on the data, at least NKp30 homo-oligomerization is mainly mediated by stalk-induced self-binding. To verify the effect on NKp30 ectodomain self-assembly in solution and on the plasma membrane, the stalk-mediated interaction could be inhibited by sterical hindrance employing a specific anti-NKp30Stalk-antibody (CLSM). Pre-incubation of soluble 30Stalk-His proteins and even stalk domain-containing NKp30-IgG1-Fc variants could decrease or even diminish binding on soluble or immobilized ligand molecules in biochemical (ELISA) and cellular assays (cell decoration and signaling reporter assay). Furthermore, the equilibrium of oligomers, dimers and monomers should be shifted completely towards the dimeric (and/or monomeric) state upon pre-incubation with an anti-NKp30Stalk antibody. Moreover, binding of this antibody could further influence the signaling capacity of NKp30 by hampering the flexibility of the stalk domain. Nevertheless, the ligand binding domain of NKp30 has an intrinsic potential to self-associate, which could be further analyzed by bioinformatics identifying putative surface residues suitable for homo-oligomerization. In parallel or subsequently, peptide libraries or peptides calculated for interaction with the respective surface stretches could be used for inhibition assays to further validate distinct surface areas participating in NKp30 ectodomain homo-oligomerization. With these findings, a manipulation of the balance between activation and inhibition could be possible by enhancing NKp30 self-association for improved immunological synapse formation, thereby promoting NK cell activity. Furthermore, deeper insights into the molecular details of ligand recognition and NKp30-dependent NK cell cytotoxicity as well as the identification of new cellular NKp30 ligands can contribute to the future development and improvement of NK cell-based cancer therapies.

5 Summary

5.1 Summary

Natural killer (NK) cells are large granular lymphocytes of the innate immune system that spontaneously kill foreign, tumor and virus-infected cells without prior sensitization. In addition, NK cells act as immune regulators by secretion of chemokines and cytokines as well as direct interaction with other immune cells such as dendritic cells. NK cell function is regulated by a balance between inhibitory and activating signals that are transduced into the cell upon target cell interaction. One of the major activating NK cell receptors is the natural cytotoxicity receptor NKp30. Notably, NKp30 plays a unique role since it is the only NK cell receptor involved in triggering NK cell-mediated cytotoxicity as well as shaping the adaptive immune response. Reduced NKp30 expression has clinical implications in patients with acute myeloid leukemia, cervical cancer, and high grade squamous intraepithelial lesions as well as gastrointestinal sarcoma. Furthermore, downregulation of NKp30 expression resulted in an impaired natural cytotoxicity against leukemia cells and was directly correlated with reduced survival.

NKp30 is a type I transmembrane protein of approximately 30 kDa comprised of an I-type Ig-like ligand binding domain (LBD), a flexible membrane proximal stalk domain, a single transmembrane helix, and a short cytosolic tail. For intracellular signal transduction, NKp30 associates with the immunoreceptor tyrosine-based activating motif (ITAM)-bearing adaptor molecule CD3ζ via oppositely charged amino acid residues within their transmembrane domains. In 2011, the 3D structure of the NKp30LBD was solved in an unbound and a ligand-bound form. However, so far, only few cellular ligands (BAG-6 and B7-H6) have been discovered, and the molecular details of ligand recognition by NKp30 are poorly understood. Recently, it was shown that the membrane proximal stalk domain of NKp30 is important for efficient ligand binding and signaling with respect to its length and amino acid composition. Additionally, it was demonstrated that proper *N*-linked glycosylation of the ligand binding domain is essential for ligand binding. But it is still vague, how this germline-encoded receptor is able to recognize multiple non-related ligands. Interestingly, a crystallographic dimer of the NKp30 ectodomain was observed arguing for potential intrinsic capability to self-assemble. Moreover, a fraction of NKp30 expressed in *E. coli* forms oligomers as detected by size exclusion chromatography.

The aim of this thesis was to identify structural models and mechanisms, which enable variations of the ligand binding interface of NKp30 to recognize a multiplicity of diverse ligands. In this respect, soluble NKp30 ectodomain variants as well as an anti-NKp30 antibody specifically recognizing an epitope within the LBD of NKp30 were generated for molecular and cellular investigation to address the intrinsic ability of NKp30 to form oligomers, which might impact ligand binding affinity and the efficiency of target cell killing by NK cells.

In this thesis, it was demonstrated that baculovirus-infected insect cells were a suitable expression system to produce correctly folded, post-translationally modified and ligand binding-receptive NKp30 proteins, which were functionally equivalent to those derived from human expression hosts. Further-

more, a polyclonal anti-NKp30 antibody, which is specific for an epitope located within the NKp30LBD, was purified from the blood serum of a peptide-immunized rabbit and validated for several molecular and cellular applications. Based on soluble NKp30 proteins comprising either the entire NKp30 ectodomain (LBD and stalk domain) or the ligand binding domain alone, a concentration-dependent formation of NKp30 ectodomain homo-oligomers was found, which was effected by two specific binding sites, one present within the Ig domain of NKp30 and one within its membrane proximal stalk domain. Moreover, both NKp30 ectodomain variant oligomers were functional in ligand binding and contributed to a high-affinity interaction with its cellular ligand B7-H6, which was strongly promoted by the stalk domain. Although both NKp30 ectodomain variant oligomers formed spherical particles of the same diameter in solution, in presence of the stalk domain one oligomer was composed of more monomers. Single particle electron microscopy analyses revealed that the number of calculated 2D classes increased tremendously for the particles of the longer NKp30 ectodomain variant. Therefore, a densest packing of spheres for the monomers within both NKp30 ectodomain variant oligomers is suggested, whereas the flexibility of the stalk domain might allow for a more variable orientation of these monomers within the particle, thereby increasing the heterogeneity of structural arrangements. However, based on decoration experiments with soluble NKp30 ectodomain proteins and primary NK cells facilitating more physiological conditions for NKp30 self-assembly, an ordered arrangement of several NKp30 receptors on the plasma membrane in head-to-head orientation is proposed. Based on these data, oligomerization of the NKp30 ectodomain represents a potent mechanism to modulate the ligand binding affinity of NKp30 for corresponding ligands by increased avidity. Because the degree of oligomerization is dependent on the local receptor concentration, which is upregulated by IL-2 upon NK cell activation, oligomerization of NKp30 might be a molecular transformer of NK cell activation into enhanced cytotoxicity. Future experiments are now focused to investigate NKp30 self-assembly on the plasma membrane of NK cells to enable modulation of the cytotoxicity of NK cell based therapeutics.

5.2 Summary (German)

Natürliche Killerzellen (NK-Zellen) sind große, granuläre Lymphozyten des angeborenen Immunsystems, welche fremdartige, krankhaft veränderte sowie virus-infizierte Zellen spontan und ohne vorherige Sensibilisierung töten. Weiterhin agieren NK-Zellen durch Sekretion von Chemokinen und Zytokinen sowie durch direkte Interaktion mit anderen Immunzellen wie z.B. Dendritischen Zellen als Immunregulatoren. Ihre Funktion wird dabei durch ein Gleichgewicht zwischen inhibierenden und aktivierenden Signalen gesteuert, welche durch die Interaktion mit einer Zielzelle in das NK-Zellinnere übermittelt werden. Einer der wichtigsten aktivierenden NK-Zellrezeptoren ist NKp30, ein Mitglied der Familie der natürlichen Zytotoxizitätsrezeptoren (*natural cytotoxicity receptors*, NCRs). NKp30 ist einmalig unter den aktivierenden NK-Zellrezeptoren, da er als einziger sowohl die NK-Zell-vermittelte Zytotoxizität auslöst als auch die erworbene Immunantwort beeinflusst. Eine verringerte NKp30 Expression hat klinische Folgen für Patienten, die an akuter myeloider Leukämie (AML), Gebärmutterhalskrebs, Plattenepithelkarzinom (*high grade squamous intraepithelial lesions*, HGSIL) oder auch Weichgewebstumoren (*gastrointestinal sarcoma*, GIST) erkrankt sind. Zudem resultiert aus der NKp30 Herunterregulation eine geringere natürliche Zytotoxizität gegenüber Leukämiezellen, welche direkt mit einer verringerten Überlebensrate korreliert.

NKp30 ist ein Typ I Transmembranprotein von etwa 30 kDa, welches aus einer I-Typ Ig-ähnlichen Ligandenbindedomäne (LBD), einer flexiblen membrannahen Stalkdomäne, einer einzelnen Transmembranhelix und einem kurzen zytoplasmatischen Schwanz aufgebaut ist. Um Signale im Zellinneren weiterleiten zu können, assoziiert NKp30 mit dem ITAM (*immunoreceptor tyrosin-based activatin motif*)-enthaltenden Adapterprotein CD3ζ über entgegengesetzt geladene Aminosäurereste innerhalb ihrer Transmembrandomänen. Im Jahr 2011 wurde die 3D-Struktur der Ligangenbindedomäne von NKp30 sowohl in einer ungebunden als auch einer Liganden-gebundenen Form gelöst. Da bisher nur wenige zelluläre Liganden (BAG-6, B7-H6) entdeckt wurden, sind die molekularen Einzelheiten der Ligandenerkennung durch NKp30 weitgehend unbekannt. Vor kurzem konnte jedoch gezeigt werden, dass sowohl die Länge als auch die Aminosäuresequenz der membrannahen Stalkdomäne von NKp30 bedeutsam für eine effiziente Ligandenbindung und Signalweiterleitung sind. Außerdem wurde bewiesen, dass eine korrekte *N*-verknüpfte Glykosylierung der LBD essentiell für die Ligandenbindung ist. Es bleibt aber weiterhin unklar, wodurch dieser keimbahn-kodierte Rezeptor in der Lage ist, verschiedene nicht verwandte Liganden zu erkennen. Interessanterweise wurde ein kristallographisches Dimer der NKp30 Ektodomäne beobachtet, was auf ein intrinsisches Potential zur Selbstassemblierung schließen lässt. Zudem konnte aus einer Präparation von NKp30 Protein, welches aus *E. coli* hergestellt wurde, mittels Größenausschlusschromatographie eine Oligomer-enthaltende Fraktion isoliert werden.

Das Ziel dieser Arbeit war es, strukturelle Modelle und Mechanismen zu identifizieren, welche eine Variabilität der Interaktionsfläche zwischen NKp30 und seinen Liganden ermöglicht, um eine Vielzahl von verschiedenen Liganden zu erkennen. Es wurden lösliche Varianten der NKp30 Ektodomäne sowie ein anti-NKp30 Antikörper, welcher spezifisch ein Epitop innerhalb der LBD von NKp30 erkennt, für molekulare und zelluläre Analysemethoden hergestellt. Mit Hilfe dieser Proteine wurde die intrinsische Fähigkeit von NKp30, Oligomere auszubilden, untersucht, welche die Ligandenbindeaffinität sowie auch die effiziente Zielzelltötung durch NK-Zellen beeinflussen könnte.

In dieser Arbeit konnte gezeigt werden, dass Baculovirus-infizierte Insektenzellen ein geeignetes Expressionssystem zur Herstellung von richtig gefalteten, post-translational modifizierten und ligandenbindungskompetenten NKp30 Proteinen sind, welche in ihrer Funktionalität den in humanen Expressionswirten hergestellten Proteinen gleichgestellt sind. Außerdem wurde ein polyklonaler anti-NKp30 Antikörper aus dem Blutserum eines Peptid-immunisierten Kaninchens gereinigt, welcher spezifisch ein in der NKp30LBD lokalisiertes Epitop erkennt, und für verschiedene molekulare und zelluläre Anwendungen validiert. Basierend auf löslichen NKp30 Proteinen, welche entweder die gesamte NKp30 Ektodomäne (LBD und Stalkdomäne) oder nur die LBD enthielten, wurde eine konzentrationsabhängige Ausbildung von Homo-Oligomeren der NKp30 Ektodomäne gefunden. Die Selbstassemblierung der NKp30 Ektodomäne wird durch zwei spezifische Bindestellen ermöglicht, welche sich in der Ig-Domäne sowie in der membrannahen Stalkdomäne von NKp30 befinden. Diese NKp30 Ektodomänenoligomere waren funktional hinsichtlich der Ligandenbindung und trugen zudem zu einer hoch-affinen Interaktion mit dem zellulären Liganden B7-H6 bei, welche besonders stark durch die Stalkdomäne begünstigt wurde. Obwohl beide NKp30 Ektodomänenoligomere in Lösung sphärische Partikel mit dem gleichen Durchmesser ausbildeten, waren die Oligomere bestehend aus der NKp30 Ektodomänvariante mit Stalkdomäne aus mehr Monomeren aufgebaut. Elektronenmikroskopische Untersuchungen von Einzelpartikeln ergaben zudem eine immens erhöhte Zahl berechneter 2D Klassen für die Oligomerpartikel der vollständigen NKp30 Ektodomäne. Daher wird für die Monomere beider NKp30 Ektodomänvarianten eine Anordnung

in Form der dichtesten Kugelpackung vorgeschlagen. Aufgrund der Flexibilität der Stalkdomäne könnten vielfältigere Orientierungen der Monomere innerhalb der Partikel ermöglicht werden, wodurch sich die Heterogenität der strukturellen Anordnung weiter erhöht. Aufgrund von Dekorationsexperimenten mit löslichen NKp30 Ektodomänenproteinen und primären NK-Zellen, welche physiologischere Bedingungen für die NKp30 Selbstassemblierung widerspiegeln, wird jedoch eine geordnete Aneinanderreihung von NKp30 Rezeptoren in der Plasmamembran mit einer Kopf-an-Kopf-Orientierung zueinander vorgeschlagen. Basierend auf diesen Daten stellt die Oligomerisierung der NKp30 Ektodomäne einen wirksamen Mechanismus dar, um die Ligandenbindeaffinität von NKp30 durch zunehmende Avidität zu verstärken. Da der Grad der Oligomerisierung von der lokalen Rezeptorkonzentration abhängig ist, welche durch IL-2 während der NK-Zellaktivierung hochreguliert wird, könnte die Homo-Oligomerisierung von NKp30 ein molekularer Überträger der NK-Zellaktivierung zu verstärkter Zytotoxizität sein. Zukünftige Experimente sind nun auf die Untersuchung der NKp30 Selbstassemblierung auf der Plasmamembran von NK-Zellen ausgerichtet, um die Regulierung der Zytotoxizität von NK-Zell-basierten Therapien zu ermöglichen.

6 References

[1] Murphy, K., Travers, P., Walport, M., & Janeway, C. (2012) *Janeway's Immunobiology*. (New York: Garland Science), 8th edition.

[2] Cooper, M. D. & Alder, M. N. (2006) The evolution of adaptive immune systems. *Cell* 124, 815–822.

[3] Koch, J., Steinle, A., Watzl, C., & Mandelboim, O. (2013) Activating natural cytotoxicity receptors of natural killer cells in cancer and infection. *Trends Immunol* 34, 182–191.

[4] Marcus, A., Gowen, B. G., Thompson, T. W., Iannello, A., Ardolino, M., Deng, W., Wang, L., Shifrin, N., & Raulet, D. H. (2014) Recognition of tumors by the innate immune system and natural killer cells. *Adv Immunol* 122, 91–128.

[5] Verhoeven, D. H. J., de Hooge, A. S. K., Mooiman, E. C. K., Santos, S. J., ten Dam, M. M., Gelderblom, H., Melief, C. J. M., Hogendoorn, P. C. W., Egeler, R. M., van Tol, M. J. D., Schilham, M. W., & Lankester, A. C. (2008) NK cells recognize and lyse Ewing sarcoma cells through NKG2D and DNAM-1 receptor dependent pathways. *Mol Immunol* 45, 3917–3925.

[6] Hsia, J.-Y., Chen, J.-T., Chen, C.-Y., Hsu, C.-P., Miaw, J., Huang, Y.-S., & Yang, C.-Y. (2005) Prognostic significance of intratumoral natural killer cells in primary resected esophageal squamous cell carcinoma. *Chang Gung Med J* 28, 335–340.

[7] Coca, S., Perez-Piqueras, J., Martinez, D., Colmenarejo, A., Saez, M. A., Vallejo, C., Martos, J. A., & Moreno, M. (1997) The prognostic significance of intratumoral natural killer cells in patients with colorectal carcinoma. *Cancer* 79, 2320–2328.

[8] Ishigami, S., Natsugoe, S., Tokuda, K., Nakajo, A., Che, X., Iwashige, H., Aridome, K., Hokita, S., & Aikou, T. (2000) Prognostic value of intratumoral natural killer cells in gastric carcinoma. *Cancer* 88, 577–583.

[9] Orange, J. S. (2006) Human natural killer cell deficiencies. *Curr Opin Allergy Clin Immunol* 6, 399–409.

[10] Biron, C. A., Byron, K. S., & Sullivan, J. L. (1989) Severe herpesvirus infections in an adolescent without natural killer cells. *N Engl J Med* 320, 1731–1735.

[11] Lopez, C., Kirkpatrick, D., Read, S. E., Fitzgerald, P. A., Pitt, J., Pahwa, S., Ching, C. Y., & Smithwick, E. M. (1983) Correlation between low natural killing of fibroblasts infected with herpes simplex virus type 1 and susceptibility to herpesvirus infections. *J Infect Dis* 147, 1030–1035.

[12] Long, E. O. (2007) Ready for prime time: NK cell priming by dendritic cells. *Immunity* 26, 385–387.

[13] Moretta, A., Marcenaro, E., Parolini, S., Ferlazzo, G., & Moretta, L. (2008) NK cells at the interface between innate and adaptive immunity. *Cell Death Differ* 15, 226–233.

[14] Wehner, R., Dietze, K., Bachmann, M., & Schmitz, M. (2011) The bidirectional crosstalk between human dendritic cells and natural killer cells. *J Innate Immun* 3, 258–263.

[15] Funke, J., Dürr, R., Dietrich, U., & Koch, J. (2011) Natural killer cells in HIV-1 infection: a double-edged sword. *AIDS Rev* 13, 67–76.

[16] Groth, A., Klöss, S., von Strandmann, E. P., Koehl, U., & Koch, J. (2011) Mechanisms of tumor and viral immune escape from natural killer cell-mediated surveillance. *J Innate Immun* 3, 344–354.

[17] Greenberg, A. H. & Playfair, J. H. (1974) Spontaneously arising cytotoxicity to the P-815-Y mastocytoma in NZB mice. *Clin Exp Immunol* 16, 99–109.

[18] Rosenberg, E. B., McCoy, J. L., Green, S. S., Donnelly, F. C., Siwarski, D. F., Levine, P. H., & Herberman, R. B. (1974) Destruction of human lymphoid tissue-culture cell lines by human peripheral lymphocytes in 51Cr-release cellular cytotoxicity assays. *J Natl Cancer Inst* 52, 345–352.

[19] Kiessling, R., Klein, E., & Wigzell, H. (1975) "Natural" killer cells in the mouse. I. Cytotoxic cells with specificity for mouse Moloney leukemia cells. Specificity and distribution according to genotype. *Eur J Immunol* 5, 112–117.

[20] Kiessling, R., Klein, E., Pross, H., & Wigzell, H. (1975) "Natural" killer cells in the mouse. II. Cytotoxic cells with specificity for mouse Moloney leukemia cells. Characteristics of the killer cell. *Eur J Immunol* 5, 117–121.

[21] Jondal, M. & Pross, H. (1975) Surface markers on human b and t lymphocytes. VI. Cytotoxicity against cell lines as a functional marker for lymphocyte subpopulations. *Int J Cancer* 15, 596–605.

[22] Ono, A., Amos, D. B., & Koren, H. S. (1977) Selective cellular natural killing against human leukaemic T cells and thymus. *Nature* 266, 546–548.

[23] Herberman, R. B., Nunn, M. E., & Lavrin, D. H. (1975) Natural cytotoxic reactivity of mouse lymphoid cells against syngeneic acid allogeneic tumors. I. Distribution of reactivity and specificity. *Int J Cancer* 16, 216–229.

[24] Herberman, R. B., Djeu, J., Kay, H. D., Ortaldo, J. R., Riccardi, C., Bonnard, G. D., Holden, H. T., Fagnani, R., Santoni, A., & Puccetti, P. (1979) Natural killer cells: characteristics and regulation of activity. *Immunol Rev* 44, 43–70.

[25] Deniz, G., van de Veen, W., & Akdis, M. (2013) Natural killer cells in patients with allergic diseases. *J Allergy Clin Immunol* 132, 527–535.

[26] Orange, J. S. (2002) Human natural killer cell deficiencies and susceptibility to infection. *Microbes Infect* 4, 1545–1558.

[27] Orange, J. S. (2012) Unraveling human natural killer cell deficiency. *J Clin Invest* 122, 798–801.

[28] Wood, S. M., Ljunggren, H.-G., & Bryceson, Y. T. (2011) Insights into NK cell biology from human genetics and disease associations. *Cell Mol Life Sci* 68, 3479–3493.

[29] Jawahar, S., Moody, C., Chan, M., Finberg, R., Geha, R., & Chatila, T. (1996) Natural Killer (NK) cell deficiency associated with an epitope-deficient Fc receptor type IIIA (CD16-II). *Clin Exp Immunol* 103, 408–413.

[30] Mace, E. M., Hsu, A. P., Monaco-Shawver, L., Makedonas, G., Rosen, J. B., Dropulic, L., Cohen, J. I., Frenkel, E. P., Bagwell, J. C., Sullivan, J. L., Biron, C. A., Spalding, C., Zerbe, C. S., Uzel, G., Holland, S. M., & Orange, J. S. (2013) Mutations in GATA2 cause human NK cell deficiency with specific loss of the CD56(bright) subset. *Blood* 121, 2669–2677.

[31] Notarangelo, L. D. & Mazzolari, E. (2006) Natural killer cell deficiencies and severe varicella infection. *J Pediatr* 148, 563–4; author reply 564.

[32] Gilmour, K. C., Fujii, H., Cranston, T., Davies, E. G., Kinnon, C., & Gaspar, H. B. (2001) Defective expression of the interleukin-2/interleukin-15 receptor beta subunit leads to a natural killer cell-deficient form of severe combined immunodeficiency. *Blood* 98, 877–879.

[33] Caligiuri, M. A. (2008) Human natural killer cells. *Blood* 112, 461–469.

[34] Freud, A. G. & Caligiuri, M. A. (2006) Human natural killer cell development. *Immunol Rev* 214, 56–72.

[35] Di Santo, J. P. (2006) Natural killer cell developmental pathways: a question of balance. *Annu Rev Immunol* 24, 257–286.

[36] Narni-Mancinelli, E., Ugolini, S., & Vivier, E. (2013) Tuning the threshold of natural killer cell responses. *Curr Opin Immunol* 25, 53–58.

[37] Zhang, Y., Wallace, D. L., de Lara, C. M., Ghattas, H., Asquith, B., Worth, A., Griffin, G. E., Taylor, G. P., Tough, D. F., Beverley, P. C. L., & Macallan, D. C. (2007) In vivo kinetics of human natural killer cells: the effects of ageing and acute and chronic viral infection. *Immunology* 121, 258–265.

[38] Montaldo, E., Del Zotto, G., Della Chiesa, M., Mingari, M. C., Moretta, A., De Maria, A., & Moretta, L. (2013) Human NK cell receptors/markers: a tool to analyze NK cell development, subsets and function. *Cytometry A* 83, 702–713.

[39] Cooper, M. A., Fehniger, T. A., Turner, S. C., Chen, K. S., Ghaheri, B. A., Ghayur, T., Carson, W. E., & Caligiuri, M. A. (2001) Human natural killer cells: a unique innate immunoregulatory role for the CD56(bright) subset. *Blood* 97, 3146–3151.

[40] Mandelboim, O., Malik, P., Davis, D. M., Jo, C. H., Boyson, J. E., & Strominger, J. L. (1999) Human CD16 as a lysis receptor mediating direct natural killer cell cytotoxicity. *Proc Natl Acad Sci U S A* 96, 5640–5644.

[41] Leibson, P. J. (1997) Signal transduction during natural killer cell activation: inside the mind of a killer. *Immunity* 6, 655–661.

[42] Schoenborn, J. R. & Wilson, C. B. (2007) Regulation of interferon-gamma during innate and adaptive immune responses. *Adv Immunol* 96, 41–101.

[43] Barreira da Silva, R. & Münz, C. (2011) Natural killer cell activation by dendritic cells: balancing inhibitory and activating signals. *Cell Mol Life Sci* 68, 3505–3518.

[44] Vivier, E., Tomasello, E., Baratin, M., Walzer, T., & Ugolini, S. (2008) Functions of natural killer cells. *Nat Immunol* 9, 503–510.

[45] Orange, J. S. (2013) Natural killer cell deficiency. *J Allergy Clin Immunol* 132, 515–25; quiz 526.

[46] O'Leary, J. G., Goodarzi, M., Drayton, D. L., & von Andrian, U. H. (2006) T cell- and B cell-independent adaptive immunity mediated by natural killer cells. *Nat Immunol* 7, 507–516.

[47] Paust, S., Senman, B., & von Andrian, U. H. (2010) Adaptive immune responses mediated by natural killer cells. *Immunol Rev* 235, 286–296.

[48] Sun, J. C., Beilke, J. N., & Lanier, L. L. (2009) Adaptive immune features of natural killer cells. *Nature* 457, 557–561.

[49] Min-Oo, G., Kamimura, Y., Hendricks, D. W., Nabekura, T., & Lanier, L. L. (2013) Natural killer cells: walking three paths down memory lane. *Trends Immunol* 34, 251–258.

[50] Narni-Mancinelli, E., Ugolini, S., & Vivier, E. (2013) [Natural killer cells: adaptation and memory in innate immunity]. *Med Sci (Paris)* 29, 389–395.

[51] Zamai, L., Ahmad, M., Bennett, I. M., Azzoni, L., Alnemri, E. S., & Perussia, B. (1998) Natural killer (NK) cell-mediated cytotoxicity: differential use of TRAIL and Fas ligand by immature and mature primary human NK cells. *J Exp Med* 188, 2375–2380.

[52] Montel, A. H., Bochan, M. R., Goebel, W. S., & Brahmi, Z. (1995) Fas-mediated cytotoxicity remains intact in perforin and granzyme B antisense transfectants of a human NK-like cell line. *Cell Immunol* 165, 312–317.

[53] Lee, R. K., Spielman, J., Zhao, D. Y., Olsen, K. J., & Podack, E. R. (1996) Perforin, Fas ligand, and tumor necrosis factor are the major cytotoxic molecules used by lymphokine-activated killer cells. *J Immunol* 157, 1919–1925.

[54] Herberman, R. B. & Holden, H. T. (1979) Natural killer cells as antitumor effector cells. *J Natl Cancer Inst* 62, 441–445.

[55] Trapani, J. A., Sutton, V. R., & Smyth, M. J. (1999) CTL granules: evolution of vesicles essential for combating virus infections. *Immunol Today* 20, 351–356.

[56] van den Broek, M. E., Kägi, D., Ossendorp, F., Toes, R., Vamvakas, S., Lutz, W. K., Melief, C. J., Zinkernagel, R. M., & Hengartner, H. (1996) Decreased tumor surveillance in perforin-deficient mice. *J Exp Med* 184, 1781–1790.

[57] Topham, N. J. & Hewitt, E. W. (2009) Natural killer cell cytotoxicity: how do they pull the trigger? *Immunology* 128, 7–15.

[58] Cooper, M. A., Fehniger, T. A., & Caligiuri, M. A. (2001) The biology of human natural killer-cell subsets. *Trends Immunol* 22, 633–640.

[59] Maghazachi, A. A. (2005) Compartmentalization of human natural killer cells. *Mol Immunol* 42, 523–529.

[60] Lanier, L. L. (2005) NK cell recognition. *Annu Rev Immunol* 23, 225–274.

[61] Kärre, K., Ljunggren, H. G., Piontek, G., & Kiessling, R. (1986) Selective rejection of H-2-deficient lymphoma variants suggests alternative immune defence strategy. *Nature* 319, 675–678.

[62] Ljunggren, H. G. & Kärre, K. (1990) In search of the 'missing self': MHC molecules and NK cell recognition. *Immunol Today* 11, 237–244.

[63] Mandelboim, O., Lieberman, N., Lev, M., Paul, L., Arnon, T. I., Bushkin, Y., Davis, D. M., Strominger, J. L., Yewdell, J. W., & Porgador, A. (2001) Recognition of haemagglutinins on virus-infected cells by NKp46 activates lysis by human NK cells. *Nature* 409, 1055–1060.

[64] Bottino, C., Castriconi, R., Moretta, L., & Moretta, A. (2005) Cellular ligands of activating NK receptors. *Trends Immunol* 26, 221–226.

[65] Vivier, E., Raulet, D. H., Moretta, A., Caligiuri, M. A., Zitvogel, L., Lanier, L. L., Yokoyama, W. M., & Ugolini, S. (2011) Innate or adaptive immunity? The example of natural killer cells. *Science* 331, 44–49.

[66] Biassoni, R. (2009) Human natural killer receptors, co-receptors, and their ligands. *Curr Protoc Immunol* Chapter 14, Unit 14.10.

[67] Sivori, S., Carlomagno, S., Pesce, S., Moretta, A., Vitale, M., & Marcenaro, E. (2014) TLR/NCR/KIR: Which One to Use and When? *Front Immunol* 5, 105.

[68] Moretta, A., Bottino, C., Vitale, M., Pende, D., Cantoni, C., Mingari, M. C., Biassoni, R., & Moretta, L. (2001) Activating receptors and coreceptors involved in human natural killer cell-mediated cytolysis. *Annu Rev Immunol* 19, 197–223.

[69] Bottino, C., Biassoni, R., Millo, R., Moretta, L., & Moretta, A. (2000) The human natural cytotoxicity receptors (NCR) that induce HLA class I-independent NK cell triggering. *Hum Immunol* 61, 1–6.

[70] Lanier, L. L. (2008) Up on the tightrope: natural killer cell activation and inhibition. *Nat Immunol* 9, 495–502.

[71] Orange, J. S. (2008) Formation and function of the lytic NK-cell immunological synapse. *Nat Rev Immunol* 8, 713–725.

[72] Olofsson, P. E., Forslund, E., Vanherberghen, B., Chechet, K., Mickelin, O., Ahlin, A. R., Everhorn, T., & Onfelt, B. (2014) Distinct Migration and Contact Dynamics of Resting and IL-2-Activated Human Natural Killer Cells. *Front Immunol* 5, 80.

[73] Bhat, R. & Watzl, C. (2007) Serial killing of tumor cells by human natural killer cells–enhancement by therapeutic antibodies. *PLoS One* 2, e326.

[74] Choi, P. J. & Mitchison, T. J. (2013) Imaging burst kinetics and spatial coordination during serial killing by single natural killer cells. *Proc Natl Acad Sci U S A* 110, 6488–6493.

[75] Vivier, E., Ugolini, S., Blaise, D., Chabannon, C., & Brossay, L. (2012) Targeting natural killer cells and natural killer T cells in cancer. *Nat Rev Immunol* 12, 239–252.

[76] Watzl, C. & Long, E. O. (2010) Signal transduction during activation and inhibition of natural killer cells. *Curr Protoc Immunol* Chapter 11, Unit 11.9B.

[77] Raulet, D. H. & Vance, R. E. (2006) Self-tolerance of natural killer cells. *Nat Rev Immunol* 6, 520–531.

[78] Held, W., Kijima, M., Angelov, G., & Bessoles, S. (2011) The function of natural killer cells: education, reminders and some good memories. *Curr Opin Immunol* 23, 228–233.

[79] Kim, S., Poursine-Laurent, J., Truscott, S. M., Lybarger, L., Song, Y.-J., Yang, L., French, A. R., Sunwoo, J. B., Lemieux, S., Hansen, T. H., & Yokoyama, W. M. (2005) Licensing of natural killer cells by host major histocompatibility complex class I molecules. *Nature* 436, 709–713.

[80] Obeidy, P. & Sharland, A. F. (2009) NKG2D and its ligands. *Int J Biochem Cell Biol* 41, 2364–2367.

[81] Malarkannan, S. (2006) The balancing act: inhibitory Ly49 regulate NKG2D-mediated NK cell functions. *Semin Immunol* 18, 186–192.

[82] Lee, N., Goodlett, D. R., Ishitani, A., Marquardt, H., & Geraghty, D. E. (1998) HLA-E surface expression depends on binding of TAP-dependent peptides derived from certain HLA class I signal sequences. *J Immunol* 160, 4951–4960.

[83] Braud, V. M., Allan, D. S., O'Callaghan, C. A., Söderström, K., D'Andrea, A., Ogg, G. S., Lazetic, S., Young, N. T., Bell, J. I., Phillips, J. H., Lanier, L. L., & McMichael, A. J. (1998) HLA-E binds to natural killer cell receptors CD94/NKG2A, B and C. *Nature* 391, 795–799.

[84] Borrego, F., Ulbrecht, M., Weiss, E. H., Coligan, J. E., & Brooks, A. G. (1998) Recognition of human histocompatibility leukocyte antigen (HLA)-E complexed with HLA class I signal sequence-derived peptides by CD94/NKG2 confers protection from natural killer cell-mediated lysis. *J Exp Med* 187, 813–818.

[85] Wagtmann, N., Biassoni, R., Cantoni, C., Verdiani, S., Malnati, M. S., Vitale, M., Bottino, C., Moretta, L., Moretta, A., & Long, E. O. (1995) Molecular clones of the p58 NK cell receptor reveal immunoglobulin-related molecules with diversity in both the extra- and intracellular domains. *Immunity* 2, 439–449.

[86] Colonna, M. & Samaridis, J. (1995) Cloning of immunoglobulin-superfamily members associated with HLA-C and HLA-B recognition by human natural killer cells. *Science* 268, 405–408.

[87] Vilches, C. & Parham, P. (2002) KIR: diverse, rapidly evolving receptors of innate and adaptive immunity. *Annu Rev Immunol* 20, 217–251.

[88] Borges, L., Hsu, M. L., Fanger, N., Kubin, M., & Cosman, D. (1997) A family of human lymphoid and myeloid Ig-like receptors, some of which bind to MHC class I molecules. *J Immunol* 159, 5192–5196.

[89] Colonna, M., Navarro, F., Bellón, T., Llano, M., García, P., Samaridis, J., Angman, L., Cella, M., & López-Botet, M. (1997) A common inhibitory receptor for major histocompatibility complex class I molecules on human lymphoid and myelomonocytic cells. *J Exp Med* 186, 1809–1818.

[90] Vance, R. E., Kraft, J. R., Altman, J. D., Jensen, P. E., & Raulet, D. H. (1998) Mouse CD94/NKG2A is a natural killer cell receptor for the nonclassical major histocompatibility complex (MHC) class I molecule Qa-1(b). *J Exp Med* 188, 1841–1848.

[91] Raulet, D. H., Held, W., Correa, I., Dorfman, J. R., Wu, M. F., & Corral, L. (1997) Specificity, tolerance and developmental regulation of natural killer cells defined by expression of class I-specific Ly49 receptors. *Immunol Rev* 155, 41–52.

[92] Takei, F., Brennan, J., & Mager, D. L. (1997) The Ly-49 family: genes, proteins and recognition of class I MHC. *Immunol Rev* 155, 67–77.

[93] Hanke, T., Takizawa, H., McMahon, C. W., Busch, D. H., Pamer, E. G., Miller, J. D., Altman, J. D., Liu, Y., Cado, D., Lemonnier, F. A., Bjorkman, P. J., & Raulet, D. H. (1999) Direct assessment of MHC class I binding by seven Ly49 inhibitory NK cell receptors. *Immunity* 11, 67–77.

[94] Daëron, M. & Vivier, E. (1999) Biology of immunoreceptor tyrosine-based inhibition motif-bearing molecules. *Curr Top Microbiol Immunol* 244, 1–12.

[95] Lauzon, N. M., Mian, F., & Ashkar, A. A. (2007) Toll-like receptors, natural killer cells and innate immunity. *Adv Exp Med Biol* 598, 1–11.

[96] Houchins, J. P., Yabe, T., McSherry, C., & Bach, F. H. (1991) DNA sequence analysis of NKG2, a family of related cDNA clones encoding type II integral membrane proteins on human natural killer cells. *J Exp Med* 173, 1017–1020.

[97] Sivori, S., Vitale, M., Morelli, L., Sanseverino, L., Augugliaro, R., Bottino, C., Moretta, L., & Moretta, A. (1997) p46, a novel natural killer cell-specific surface molecule that mediates cell activation. *J Exp Med* 186, 1129–1136.

[98] Pessino, A., Sivori, S., Bottino, C., Malaspina, A., Morelli, L., Moretta, L., Biassoni, R., & Moretta, A. (1998) Molecular cloning of NKp46: a novel member of the immunoglobulin superfamily involved in triggering of natural cytotoxicity. *J Exp Med* 188, 953–960.

[99] Vitale, M., Bottino, C., Sivori, S., Sanseverino, L., Castriconi, R., Marcenaro, E., Augugliaro, R., Moretta, L., & Moretta, A. (1998) NKp44, a novel triggering surface molecule specifically

expressed by activated natural killer cells, is involved in non-major histocompatibility complex-restricted tumor cell lysis. *J Exp Med* 187, 2065–2072.

[100] Cantoni, C., Bottino, C., Vitale, M., Pessino, A., Augugliaro, R., Malaspina, A., Parolini, S., Moretta, L., Moretta, A., & Biassoni, R. (1999) NKp44, a triggering receptor involved in tumor cell lysis by activated human natural killer cells, is a novel member of the immunoglobulin superfamily. *J Exp Med* 189, 787–796.

[101] Pende, D., Parolini, S., Pessino, A., Sivori, S., Augugliaro, R., Morelli, L., Marcenaro, E., Accame, L., Malaspina, A., Biassoni, R., Bottino, C., Moretta, L., & Moretta, A. (1999) Identification and molecular characterization of NKp30, a novel triggering receptor involved in natural cytotoxicity mediated by human natural killer cells. *J Exp Med* 190, 1505–1516.

[102] Rosen, D. B., Araki, M., Hamerman, J. A., Chen, T., Yamamura, T., & Lanier, L. L. (2004) A Structural basis for the association of DAP12 with mouse, but not human, NKG2D. *J Immunol* 173, 2470–2478.

[103] Upshaw, J. L., Arneson, L. N., Schoon, R. A., Dick, C. J., Billadeau, D. D., & Leibson, P. J. (2006) NKG2D-mediated signaling requires a DAP10-bound Grb2-Vav1 intermediate and phosphatidylinositol-3-kinase in human natural killer cells. *Nat Immunol* 7, 524–532.

[104] Srivastava, B. I. S. & Srivastava, M. D. (2006) Expression of natural cytotoxicity receptors NKp30, NKp44, and NKp46 mRNAs and proteins by human hematopoietic and non-hematopoietic cells. *Leuk Res* 30, 37–46.

[105] Tang, Q., Grzywacz, B., Wang, H., Kataria, N., Cao, Q., Wagner, J. E., Blazar, B. R., Miller, J. S., & Verneris, M. R. (2008) Umbilical cord blood T cells express multiple natural cytotoxicity receptors after IL-15 stimulation, but only NKp30 is functional. *J Immunol* 181, 4507–4515.

[106] Correia, D. V., Fogli, M., Hudspeth, K., da Silva, M. G., Mavilio, D., & Silva-Santos, B. (2011) Differentiation of human peripheral blood Vδ1+ T cells expressing the natural cytotoxicity receptor NKp30 for recognition of lymphoid leukemia cells. *Blood* 118, 992–1001.

[107] Hudspeth, K., Fogli, M., Correia, D. V., Mikulak, J., Roberto, A., Della Bella, S., Silva-Santos, B., & Mavilio, D. (2012) Engagement of NKp30 on Vδ1 T cells induces the production of CCL3, CCL4, and CCL5 and suppresses HIV-1 replication. *Blood* 119, 4013–4016.

[108] Hudspeth, K., Silva-Santos, B., & Mavilio, D. (2013) Natural cytotoxicity receptors: broader expression patterns and functions in innate and adaptive immune cells. *Front Immunol* 4, 69.

[109] Bottino, C., Moretta, L., Pende, D., Vitale, M., & Moretta, A. (2004) Learning how to discriminate between friends and enemies, a lesson from Natural Killer cells. *Mol Immunol* 41, 569–575.

[110] Moretta, L., Bottino, C., Cantoni, C., Mingari, M. C., & Moretta, A. (2001) Human natural killer cell function and receptors. *Curr Opin Pharmacol* 1, 387–391.

[111] Middleton, D., Curran, M., & Maxwell, L. (2002) Natural killer cells and their receptors. *Transpl Immunol* 10, 147–164.

[112] Bryceson, Y. T., March, M. E., Ljunggren, H.-G., & Long, E. O. (2006) Activation, coactivation, and costimulation of resting human natural killer cells. *Immunol Rev* 214, 73–91.

[113] Biassoni, R., Pessino, A., Bottino, C., Pende, D., Moretta, L., & Moretta, A. (1999) The murine homologue of the human NKp46, a triggering receptor involved in the induction of natural cytotoxicity. *Eur J Immunol* 29, 1014–1020.

[114] Cantoni, C., Ponassi, M., Biassoni, R., Conte, R., Spallarossa, A., Moretta, A., Moretta, L., Bolognesi, M., & Bordo, D. (2003) The three-dimensional structure of the human NK cell receptor NKp44, a triggering partner in natural cytotoxicity. *Structure* 11, 725–734.

[115] Foster, C. E., Colonna, M., & Sun, P. D. (2003) Crystal structure of the human natural killer (NK) cell activating receptor NKp46 reveals structural relationship to other leukocyte receptor complex immunoreceptors. *J Biol Chem* 278, 46081–46086.

[116] Joyce, M. G., Tran, P., Zhuravleva, M. A., Jaw, J., Colonna, M., & Sun, P. D. (2011) Crystal structure of human natural cytotoxicity receptor NKp30 and identification of its ligand binding site. *Proc Natl Acad Sci U S A* 108, 6223–6228.

[117] Li, Y., Wang, Q., & Mariuzza, R. A. (2011) Structure of the human activating natural cytotoxicity receptor NKp30 bound to its tumor cell ligand B7-H6. *J Exp Med* 208, 703–714.

[118] Lanier, L. L. (2001) On guard–activating NK cell receptors. *Nat Immunol* 2, 23–27.

[119] Hartmann, J. (2012) Influence of the stalk domain and the glycosylation status of the human activating natural killer cell receptor NKp30 on ligand binding. *Dissertation*.

[120] Bloushtain, N., Qimron, U., Bar-Ilan, A., Hershkovitz, O., Gazit, R., Fima, E., Korc, M., Vlodavsky, I., Bovin, N. V., & Porgador, A. (2004) Membrane-associated heparan sulfate proteoglycans are involved in the recognition of cellular targets by NKp30 and NKp46. *J Immunol* 173, 2392–2401.

[121] Zilka, A., Landau, G., Hershkovitz, O., Bloushtain, N., Bar-Ilan, A., Benchetrit, F., Fima, E., van Kuppevelt, T. H., Gallagher, J. T., Elgavish, S., & Porgador, A. (2005) Characterization of the heparin/heparan sulfate binding site of the natural cytotoxicity receptor NKp46. *Biochemistry* 44, 14477–14485.

[122] Hershkovitz, O., Jivov, S., Bloushtain, N., Zilka, A., Landau, G., Bar-Ilan, A., Lichtenstein, R. G., Campbell, K. S., van Kuppevelt, T. H., & Porgador, A. (2007) Characterization of the recognition of tumor cells by the natural cytotoxicity receptor, NKp44. *Biochemistry* 46, 7426–7436.

[123] Hershkovitz, O., Jarahian, M., Zilka, A., Bar-Ilan, A., Landau, G., Jivov, S., Tekoah, Y., Glicklis, R., Gallagher, J. T., Hoffmann, S. C., Zer, H., Mandelboim, O., Watzl, C., Momburg, F., & Porgador, A. (2008) Altered glycosylation of recombinant NKp30 hampers binding to heparan sulfate: a lesson for the use of recombinant immunoreceptors as an immunological tool. *Glycobiology* 18, 28–41.

[124] Hecht, M.-L., Rosental, B., Horlacher, T., Hershkovitz, O., De Paz, J. L., Noti, C., Schauer, S., Porgador, A., & Seeberger, P. H. (2009) Natural cytotoxicity receptors NKp30, NKp44 and NKp46 bind to different heparan sulfate/heparin sequences. *J Proteome Res* 8, 712–720.

[125] Mavoungou, E., Held, J., Mewono, L., & Kremsner, P. G. (2007) A Duffy binding-like domain is involved in the NKp30-mediated recognition of Plasmodium falciparum-parasitized erythrocytes by natural killer cells. *J Infect Dis* 195, 1521–1531.

[126] Esin, S., Batoni, G., Counoupas, C., Stringaro, A., Brancatisano, F. L., Colone, M., Maisetta, G., Florio, W., Arancia, G., & Campa, M. (2008) Direct binding of human NK cell natural cytotoxicity receptor NKp44 to the surfaces of mycobacteria and other bacteria. *Infect Immun* 76, 1719–1727.

[127] Chaushu, S., Wilensky, A., Gur, C., Shapira, L., Elboim, M., Halftek, G., Polak, D., Achdout, H., Bachrach, G., & Mandelboim, O. (2012) Direct recognition of Fusobacterium nucleatum by the NK cell natural cytotoxicity receptor NKp46 aggravates periodontal disease. *PLoS Pathog* 8, e1002601.

[128] Arnon, T. I., Lev, M., Katz, G., Chernobrov, Y., Porgador, A., & Mandelboim, O. (2001) Recognition of viral hemagglutinins by NKp44 but not by NKp30. *Eur J Immunol* 31, 2680–2689.

[129] Draghi, M., Pashine, A., Sanjanwala, B., Gendzekhadze, K., Cantoni, C., Cosman, D., Moretta, A., Valiante, N. M., & Parham, P. (2007) NKp46 and NKG2D recognition of infected dendritic cells is necessary for NK cell activation in the human response to influenza infection. *J Immunol* 178, 2688–2698.

[130] Jarahian, M., Fiedler, M., Cohnen, A., Djandji, D., Hämmerling, G. J., Gati, C., Cerwenka, A., Turner, P. C., Moyer, R. W., Watzl, C., Hengel, H., & Momburg, F. (2011) Modulation of NKp30- and NKp46-mediated natural killer cell responses by poxviral hemagglutinin. *PLoS Pathog* 7, e1002195.

[131] Brusilovsky, M., Rosental, B., Shemesh, A., Appel, M. Y., & Porgador, A. (2012) Human NK cell recognition of target cells in the prism of natural cytotoxicity receptors and their ligands. *J Immunotoxicol* 9, 267–274.

[132] Jarahian, M., Watzl, C., Fournier, P., Arnold, A., Djandji, D., Zahedi, S., Cerwenka, A., Paschen, A., Schirrmacher, V., & Momburg, F. (2009) Activation of natural killer cells by newcastle disease virus hemagglutinin-neuraminidase. *J Virol* 83, 8108–8121.

[133] Arnon, T. I., Achdout, H., Levi, O., Markel, G., Saleh, N., Katz, G., Gazit, R., Gonen-Gross, T., Hanna, J., Nahari, E., Porgador, A., Honigman, A., Plachter, B., Mevorach, D., Wolf, D. G., & Mandelboim, O. (2005) Inhibition of the NKp30 activating receptor by pp65 of human cytomegalovirus. *Nat Immunol* 6, 515–523.

[134] Brandt, C. S., Baratin, M., Yi, E. C., Kennedy, J., Gao, Z., Fox, B., Haldeman, B., Ostrander, C. D., Kaifu, T., Chabannon, C., Moretta, A., West, R., Xu, W., Vivier, E., & Levin, S. D. (2009) The B7 family member B7-H6 is a tumor cell ligand for the activating natural killer cell receptor NKp30 in humans. *J Exp Med* 206, 1495–1503.

[135] Simhadri, V. R., Reiners, K. S., Hansen, H. P., Topolar, D., Simhadri, V. L., Nohroudi, K., Kufer, T. A., Engert, A., & Pogge von Strandmann, E. (2008) Dendritic cells release HLA-B-associated transcript-3 positive exosomes to regulate natural killer function. *PLoS One* 3, e3377.

[136] Pogge von Strandmann, E., Simhadri, V. R., von Tresckow, B., Sasse, S., Reiners, K. S., Hansen, H. P., Rothe, A., Böll, B., Simhadri, V. L., Borchmann, P., McKinnon, P. J., Hallek, M., & Engert, A. (2007) Human leukocyte antigen-B-associated transcript 3 is released from tumor cells and engages the NKp30 receptor on natural killer cells. *Immunity* 27, 965–974.

[137] Rosental, B., Brusilovsky, M., Hadad, U., Oz, D., Appel, M. Y., Afergan, F., Yossef, R., Rosenberg, L. A., Aharoni, A., Cerwenka, A., Campbell, K. S., Braiman, A., & Porgador, A. (2011) Proliferating cell nuclear antigen is a novel inhibitory ligand for the natural cytotoxicity receptor NKp44. *J Immunol* 187, 5693–5702.

[138] Baychelier, F., Sennepin, A., Ermonval, M., Dorgham, K., Debré, P., & Vieillard, V. (2013) Identification of a cellular ligand for the natural cytotoxicity receptor NKp44. *Blood* 122, 2935–2942.

[139] Vieillard, V., Strominger, J. L., & Debré, P. (2005) NK cytotoxicity against CD4+ T cells during HIV-1 infection: a gp41 peptide induces the expression of an NKp44 ligand. *Proc Natl Acad Sci U S A* 102, 10981–10986.

[140] Seidel, E., Glasner, A., & Mandelboim, O. (2012) Virus-mediated inhibition of natural cytotoxicity receptor recognition. *Cell Mol Life Sci*.

[141] Garcia-Iglesias, T., Del Toro-Arreola, A., Albarran-Somoza, B., Del Toro-Arreola, S., Sanchez-Hernandez, P. E., Ramirez-Dueñas, M. G., Balderas-Peña, L. M. A., Bravo-Cuellar, A., Ortiz-Lazareno, P. C., & Daneri-Navarro, A. (2009) Low NKp30, NKp46 and NKG2D expression and reduced cytotoxic activity on NK cells in cervical cancer and precursor lesions. *BMC Cancer* 9, 186.

[142] Mamessier, E., Sylvain, A., Thibult, M.-L., Houvenaeghel, G., Jacquemier, J., Castellano, R., Gonçalves, A., André, P., Romagné, F., Thibault, G., Viens, P., Birnbaum, D., Bertucci, F., Moretta, A., & Olive, D. (2011) Human breast cancer cells enhance self tolerance by promoting evasion from NK cell antitumor immunity. *J Clin Invest* 121, 3609–3622.

[143] Pietra, G., Manzini, C., Rivara, S., Vitale, M., Cantoni, C., Petretto, A., Balsamo, M., Conte, R., Benelli, R., Minghelli, S., Solari, N., Gualco, M., Queirolo, P., Moretta, L., & Mingari, M. C. (2012) Melanoma cells inhibit natural killer cell function by modulating the expression of activating receptors and cytolytic activity. *Cancer Res* 72, 1407–1415.

[144] Fauriat, C., Just-Landi, S., Mallet, F., Arnoulet, C., Sainty, D., Olive, D., & Costello, R. T. (2007) Deficient expression of NCR in NK cells from acute myeloid leukemia: Evolution during leukemia treatment and impact of leukemia cells in NCRdull phenotype induction. *Blood* 109, 323–330.

[145] Sanchez-Correa, B., Morgado, S., Gayoso, I., Bergua, J. M., Casado, J. G., Arcos, M. J., Bengochea, M. L., Duran, E., Solana, R., & Tarazona, R. (2011) Human NK cells in acute myeloid leukaemia patients: analysis of NK cell-activating receptors and their ligands. *Cancer Immunol Immunother* 60, 1195–1205.

[146] Costello, R. T., Sivori, S., Marcenaro, E., Lafage-Pochitaloff, M., Mozziconacci, M.-J., Reviron, D., Gastaut, J.-A., Pende, D., Olive, D., & Moretta, A. (2002) Defective expression and function of natural killer cell-triggering receptors in patients with acute myeloid leukemia. *Blood* 99, 3661–3667.

[147] Delahaye, N. F., Rusakiewicz, S., Martins, I., Ménard, C., Roux, S., Lyonnet, L., Paul, P., Sarabi, M., Chaput, N., Semeraro, M., Minard-Colin, V., Poirier-Colame, V., Chaba, K., Flament, C., Baud, V., Authier, H., Kerdine-Römer, S., Pallardy, M., Cremer, I., Peaudecerf, L., Rocha, B., Valteau-Couanet, D., Gutierrez, J. C., Nunès, J. A., Commo, F., Bonvalot, S., Ibrahim, N., Terrier, P., Opolon, P., Bottino, C., Moretta, A., Tavernier, J., Rihet, P., Coindre, J.-M., Blay, J.-Y., Isambert, N., Emile, J.-F., Vivier, E., Lecesne, A., Kroemer, G., & Zitvogel, L. (2011) Alternatively spliced NKp30 isoforms affect the prognosis of gastrointestinal stromal tumors. *Nat Med* 17, 700–707.

[148] Ferlazzo, G., Tsang, M. L., Moretta, L., Melioli, G., Steinman, R. M., & Münz, C. (2002) Human dendritic cells activate resting natural killer (NK) cells and are recognized via the NKp30 receptor by activated NK cells. *J Exp Med* 195, 343–351.

[149] Vitale, M., Della Chiesa, M., Carlomagno, S., Pende, D., Aricò, M., Moretta, L., & Moretta, A. (2005) NK-dependent DC maturation is mediated by TNFalpha and IFNgamma released upon engagement of the NKp30 triggering receptor. *Blood* 106, 566–571.

[150] Moretta, A., Biassoni, R., Bottino, C., Mingari, M. C., & Moretta, L. (2000) Natural cytotoxicity receptors that trigger human NK-cell-mediated cytolysis. *Immunol Today* 21, 228–234.

[151] De Maria, A., Biassoni, R., Fogli, M., Rizzi, M., Cantoni, C., Costa, P., Conte, R., Mavilio, D., Ensoli, B., Cafaro, A., Moretta, A., & Moretta, L. (2001) Identification, molecular cloning and functional characterization of NKp46 and NKp30 natural cytotoxicity receptors in Macaca fascicularis NK cells. *Eur J Immunol* 31, 3546–3556.

[152] Walzer, T., Bléry, M., Chaix, J., Fuseri, N., Chasson, L., Robbins, S. H., Jaeger, S., André, P., Gauthier, L., Daniel, L., Chemin, K., Morel, Y., Dalod, M., Imbert, J., Pierres, M., Moretta, A., Romagné, F., & Vivier, E. (2007) Identification, activation, and selective in vivo ablation of mouse NK cells via NKp46. *Proc Natl Acad Sci U S A* 104, 3384–3389.

[153] Rutjens, E., Mazza, S., Biassoni, R., Koopman, G., Radic, L., Fogli, M., Costa, P., Mingari, M. C., Moretta, L., Heeney, J., & De Maria, A. (2007) Differential NKp30 inducibility in chimpanzee NK cells and conserved NK cell phenotype and function in long-term HIV-1-infected animals. *J Immunol* 178, 1702–1712.

[154] Bäckman-Petersson, E., Miller, J. R., Hollyoake, M., Aguado, B., & Butcher, G. W. (2003) Molecular characterization of the novel rat NK receptor 1C7. *Eur J Immunol* 33, 342–351.

[155] Hsieh, C. L., Nagasaki, K., Martinez, O. M., & Krams, S. M. (2006) NKp30 is a functional activation receptor on a subset of rat natural killer cells. *Eur J Immunol* 36, 2170–2180.

[156] Hsieh, C. L., Ogura, Y., Obara, H., Ali, U. A., Rodriguez, G. M., Nepomuceno, R. R., Martinez, O. M., & Krams, S. M. (2004) Identification, cloning, and characterization of a novel rat natural killer receptor, RNKP30: a molecule expressed in liver allografts. *Transplantation* 77, 121–128.

[157] Sivakamasundari, R., Raghunathan, A., Zhang, C. Y., Chowdhury, R. R., & Weissman, S. M. (2000) Expression and cellular localization of the protein encoded by the 1C7 gene: a recently described component of the MHC. *Immunogenetics* 51, 723–732.

[158] Xie, T., Rowen, L., Aguado, B., Ahearn, M. E., Madan, A., Qin, S., Campbell, R. D., & Hood, L. (2003) Analysis of the gene-dense major histocompatibility complex class III region and its comparison to mouse. *Genome Res* 13, 2621–2636.

[159] Hollyoake, M., Campbell, R. D., & Aguado, B. (2005) NKp30 (NCR3) is a pseudogene in 12 inbred and wild mouse strains, but an expressed gene in Mus caroli. *Mol Biol Evol* 22, 1661–1672.

[160] Neville, M. J. & Campbell, R. D. (1999) A new member of the Ig superfamily and a V-ATPase G subunit are among the predicted products of novel genes close to the TNF locus in the human MHC. *J Immunol* 162, 4745–4754.

[161] Lanier, L. L. (2003) Natural killer cell receptor signaling. *Curr Opin Immunol* 15, 308–314.

[162] Sasaki, T., Gan, E. C., Wakeham, A., Kornbluth, S., Mak, T. W., & Okada, H. (2007) HLA-B-associated transcript 3 (Bat3)/Scythe is essential for p300-mediated acetylation of p53. *Genes Dev* 21, 848–861.

[163] Wu, Y.-H., Shih, S.-F., & Lin, J.-Y. (2004) Ricin triggers apoptotic morphological changes through caspase-3 cleavage of BAT3. *J Biol Chem* 279, 19264–19275.

[164] Reiners, K. S., Topolar, D., Henke, A., Simhadri, V. R., Kessler, J., Sauer, M., Bessler, M., Hansen, H. P., Tawadros, S., Herling, M., Krönke, M., Hallek, M., & Pogge von Strandmann, E. (2013) Soluble ligands for NK cell receptors promote evasion of chronic lymphocytic leukemia cells from NK cell anti-tumor activity. *Blood* 121, 3658–3665.

[165] Fernández-Messina, L., Ashiru, O., Boutet, P., Agüera-González, S., Skepper, J. N., Reyburn, H. T., & Valés-Gómez, M. (2010) Differential mechanisms of shedding of the glycosylphosphatidylinositol (GPI)-anchored NKG2D ligands. *J Biol Chem* 285, 8543–8551.

[166] Binici, J., Hartmann, J., Herrmann, J., Schreiber, C., Beyer, S., Güler, G., Vogel, V., Tumulka, F., Abele, R., Mäntele, W., & Koch, J. (2013) A soluble fragment of the tumor antigen BCL2-associated athanogene 6 (BAG-6) is essential and sufficient for inhibition of NKp30 receptor-dependent cytotoxicity of natural killer cells. *J Biol Chem* 288, 34295–34303.

[167] Chisholm, S. E. & Reyburn, H. T. (2006) Recognition of vaccinia virus-infected cells by human natural killer cells depends on natural cytotoxicity receptors. *J Virol* 80, 2225–2233.

[168] Kruse, P. H., Matta, J., Ugolini, S., & Vivier, E. (2014) Natural cytotoxicity receptors and their ligands. *Immunol Cell Biol* 92, 221–229.

[169] Warren, H. S., Jones, A. L., Freeman, C., Bettadapura, J., & Parish, C. R. (2005) Evidence that the cellular ligand for the human NK cell activation receptor NKp30 is not a heparan sulfate glycosaminoglycan. *J Immunol* 175, 207–212.

[170] Hartmann, J., Tran, T.-V., Kaudeer, J., Oberle, K., Herrmann, J., Quagliano, I., Abel, T., Cohnen, A., Gatterdam, V., Jacobs, A., Wollscheid, B., Tampé, R., Watzl, C., Diefenbach, A., & Koch, J. (2012) The stalk domain and the glycosylation status of the activating natural killer cell receptor NKp30 are important for ligand binding. *J Biol Chem* 287, 31527–31539.

[171] Schlecker, E., Fiegler, N., Arnold, A., Altevogt, P., Rose-John, S., Moldenhauer, G., Sucker, A., Paschen, A., Pogge von Strandmann, E., Textor, S., & Cerwenka, A. (2014) Metalloprotease-mediated tumor cell shedding of B7-H6, the ligand of the natural killer cell activating receptor NKp30. *Cancer Res*.

[172] Garg, A., Barnes, P. F., Porgador, A., Roy, S., Wu, S., Nanda, J. S., Griffith, D. E., Girard, W. M., Rawal, N., Shetty, S., & Vankayalapati, R. (2006) Vimentin expressed on Mycobacterium tuberculosis-infected human monocytes is involved in binding to the NKp46 receptor. *J Immunol* 177, 6192–6198.

[173] Augugliaro, R., Parolini, S., Castriconi, R., Marcenaro, E., Cantoni, C., Nanni, M., Moretta, L., Moretta, A., & Bottino, C. (2003) Selective cross-talk among natural cytotoxicity receptors in human natural killer cells. *Eur J Immunol* 33, 1235–1241.

[174] Brown, A. C. N., Oddos, S., Dobbie, I. M., Alakoskela, J.-M., Parton, R. M., Eissmann, P., Neil, M. A. A., Dunsby, C., French, P. M. W., Davis, I., & Davis, D. M. (2011) Remodelling of cortical actin where lytic granules dock at natural killer cell immune synapses revealed by super-resolution microscopy. *PLoS Biol* 9, e1001152.

[175] Rak, G. D., Mace, E. M., Banerjee, P. P., Svitkina, T., & Orange, J. S. (2011) Natural killer cell lytic granule secretion occurs through a pervasive actin network at the immune synapse. *PLoS Biol* 9, e1001151.

[176] Morrison, T. G. (1988) Structure, function, and intracellular processing of paramyxovirus membrane proteins. *Virus Res* 10, 113–135.

[177] Sheehan, J. P., Iorio, R. M., Syddall, R. J., Glickman, R. L., & Bratt, M. A. (1987) Reducing agent-sensitive dimerization of the hemagglutinin-neuraminidase glycoprotein of Newcastle disease virus correlates with the presence of cysteine at residue 123. *Virology* 161, 603–606.

[178] Crennell, S., Takimoto, T., Portner, A., & Taylor, G. (2000) Crystal structure of the multifunctional paramyxovirus hemagglutinin-neuraminidase. *Nat Struct Biol* 7, 1068–1074.

[179] Kloess, S., Huenecke, S., Piechulek, D., Esser, R., Koch, J., Brehm, C., Soerensen, J., Gardlowski, T., Brinkmann, A., Bader, P., Passweg, J., Klingebiel, T., Schwabe, D., & Koehl, U. (2010) IL-2-activated haploidentical NK cells restore NKG2D-mediated NK-cell cytotoxicity in neuroblastoma patients by scavenging of plasma MICA. *Eur J Immunol* 40, 3255–3267.

[180] Kajitani, K., Tanaka, Y., Arihiro, K., Kataoka, T., & Ohdan, H. (2012) Mechanistic analysis of the antitumor efficacy of human natural killer cells against breast cancer cells. *Breast Cancer Res Treat* 134, 139–155.

[181] Ferlazzo, G., Thomas, D., Lin, S.-L., Goodman, K., Morandi, B., Muller, W. A., Moretta, A., & Münz, C. (2004) The abundant NK cells in human secondary lymphoid tissues require activation to express killer cell Ig-like receptors and become cytolytic. *J Immunol* 172, 1455–1462.

[182] Mavilio, D., Benjamin, J., Daucher, M., Lombardo, G., Kottilil, S., Planta, M. A., Marcenaro, E., Bottino, C., Moretta, L., Moretta, A., & Fauci, A. S. (2003) Natural killer cells in HIV-1 infection: dichotomous effects of viremia on inhibitory and activating receptors and their functional correlates. *Proc Natl Acad Sci U S A* 100, 15011–15016.

[183] Rosenberg, S. A. & Lotze, M. T. (1986) Cancer immunotherapy using interleukin-2 and interleukin-2-activated lymphocytes. *Annu Rev Immunol* 4, 681–709.

[184] Huenecke, S., Zimmermann, S. Y., Kloess, S., Esser, R., Brinkmann, A., Tramsen, L., Koenig, M., Erben, S., Seidl, C., Tonn, T., Eggert, A., Schramm, A., Bader, P., Klingebiel, T., Lehrnbecher, T., Passweg, J. R., Soerensen, J., Schwabe, D., & Koehl, U. (2010) IL-2-driven regulation of NK cell receptors with regard to the distribution of CD16+ and CD16- subpopulations and in vivo influence after haploidentical NK cell infusion. *J Immunother* 33, 200–210.

[185] Grave, L., Tůmová, L., Mrázek, H., Kavan, D., Chmelík, J., Vaněk, O., Novák, P., & Bezouška, K. (2012) Preparation of soluble isotopically labeled NKp30, a human natural cytotoxicity receptor, for structural studies using NMR. *Protein Expr Purif* 86, 142–150.

[186] Jaron-Mendelson, M., Yossef, R., Appel, M. Y., Zilka, A., Hadad, U., Afergan, F., Rosental, B., Engel, S., Nedvetzki, S., Braiman, A., & Porgador, A. (2012) Dimerization of NKp46 receptor is essential for NKp46-mediated lysis: characterization of the dimerization site by epitope mapping. *J Immunol* 188, 6165–6174.

[187] Garrity, D., Call, M. E., Feng, J., & Wucherpfennig, K. W. (2005) The activating NKG2D receptor assembles in the membrane with two signaling dimers into a hexameric structure. *Proc Natl Acad Sci U S A* 102, 7641–7646.

[188] Steinle, A., Li, P., Morris, D. L., Groh, V., Lanier, L. L., Strong, R. K., & Spies, T. (2001) Interactions of human NKG2D with its ligands MICA, MICB, and homologs of the mouse RAE-1 protein family. *Immunogenetics* 53, 279–287.

[189] Snyder, G. A., Brooks, A. G., & Sun, P. D. (1999) Crystal structure of the HLA-Cw3 allotype-specific killer cell inhibitory receptor KIR2DL2. *Proc Natl Acad Sci U S A* 96, 3864–3869.

[190] Hayley, M., Bourbigot, S., & Booth, V. (2011) Self-association of an activating natural killer cell receptor, KIR2DS1. *PLoS One* 6, e23052.

[191] Wood, W. B. (1966) Host specificity of DNA produced by Escherichia coli: bacterial mutations affecting the restriction and modification of DNA. *J Mol Biol* 16, 118–133.

[192] Haldimann, A., Prahalad, M. K., Fisher, S. L., Kim, S. K., Walsh, C. T., & Wanner, B. L. (1996) Altered recognition mutants of the response regulator PhoB: a new genetic strategy for studying protein-protein interactions. *Proc Natl Acad Sci U S A* 93, 14361–14366.

[193] Haldimann, A., Fisher, S. L., Daniels, L. L., Walsh, C. T., & Wanner, B. L. (1997) Transcriptional regulation of the Enterococcus faecium BM4147 vancomycin resistance gene cluster by the VanS-VanR two-component regulatory system in Escherichia coli K-12. *J Bacteriol* 179, 5903–5913.

[194] Haldimann, A., Daniels, L. L., & Wanner, B. L. (1998) Use of new methods for construction of tightly regulated arabinose and rhamnose promoter fusions in studies of the Escherichia coli phosphate regulon. *J Bacteriol* 180, 1277–1286.

[195] Eastman & Durland. (1998) Manufacturing and quality control of plasmid-based gene expression systems. *Adv Drug Deliv Rev* 30, 33–48.

[196] Ow, D. S.-W., Yap, M. G.-S., & Oh, S. K.-W. (2009) Enhancement of plasmid DNA yields during fed-batch culture of a fruR-knockout Escherichia coli strain. *Biotechnol Appl Biochem* 52, 53–59.

[197] Berger, I., Fitzgerald, D. J., & Richmond, T. J. (2004) Baculovirus expression system for heterologous multiprotein complexes. *Nat Biotechnol* 22, 1583–1587.

[198] Fitzgerald, D. J., Berger, P., Schaffitzel, C., Yamada, K., Richmond, T. J., & Berger, I. (2006) Protein complex expression by using multigene baculoviral vectors. *Nat Methods* 3, 1021–1032.

[199] Prinz, W. A., Aslund, F., Holmgren, A., & Beckwith, J. (1997) The role of the thioredoxin and glutaredoxin pathways in reducing protein disulfide bonds in the Escherichia coli cytoplasm. *J Biol Chem* 272, 15661–15667.

[200] Bessette, P. H., Aslund, F., Beckwith, J., & Georgiou, G. (1999) Efficient folding of proteins with multiple disulfide bonds in the Escherichia coli cytoplasm. *Proc Natl Acad Sci U S A* 96, 13703–13708.

[201] Bertani, G. (1951) Studies on lysogenesis. I. The mode of phage liberation by lysogenic Escherichia coli. *J Bacteriol* 62, 293–300.

[202] Lennox, E. S. (1955) Transduction of linked genetic characters of the host by bacteriophage P1. *Virology* 1, 190–206.

[203] Andersen, P. S., Menné, C., Mariuzza, R. A., Geisler, C., & Karjalainen, K. (2001) A response calculus for immobilized T cell receptor ligands. *J Biol Chem* 276, 49125–49132.

[204] Fiering, S., Northrop, J. P., Nolan, G. P., Mattila, P. S., Crabtree, G. R., & Herzenberg, L. A. (1990) Single cell assay of a transcription factor reveals a threshold in transcription activated by signals emanating from the T-cell antigen receptor. *Genes Dev* 4, 1823–1834.

[205] Weber, K., Bartsch, U., Stocking, C., & Fehse, B. (2008) A multicolor panel of novel lentiviral ”gene ontology” (LeGO) vectors for functional gene analysis. *Mol Ther* 16, 698–706.

[206] Dull, T., Zufferey, R., Kelly, M., Mandel, R. J., Nguyen, M., Trono, D., & Naldini, L. (1998) A third-generation lentivirus vector with a conditional packaging system. *J Virol* 72, 8463–8471.

[207] Zufferey, R., Nagy, D., Mandel, R. J., Naldini, L., & Trono, D. (1997) Multiply attenuated lentiviral vector achieves efficient gene delivery in vivo. *Nat Biotechnol* 15, 871–875.

[208] Hanahan, D., Jessee, J., & Bloom, F. R. (1991) Plasmid transformation of Escherichia coli and other bacteria. *Methods Enzymol* 204, 63–113.

[209] Mullis, K. B. & Faloona, F. A. (1987) Specific synthesis of DNA in vitro via a polymerase-catalyzed chain reaction. *Methods Enzymol* 155, 335–350.

[210] Saiki, R. K., Gelfand, D. H., Stoffel, S., Scharf, S. J., Higuchi, R., Horn, G. T., Mullis, K. B., & Erlich, H. A. (1988) Primer-directed enzymatic amplification of DNA with a thermostable DNA polymerase. *Science* 239, 487–491.

[211] Kost, T. A., Condreay, J. P., & Jarvis, D. L. (2005) Baculovirus as versatile vectors for protein expression in insect and mammalian cells. *Nat Biotechnol* 23, 567–575.

[212] Condreay, J. P. & Kost, T. A. (2007) Baculovirus expression vectors for insect and mammalian cells. *Curr Drug Targets* 8, 1126–1131.

[213] O'Reilly, D. R. (1997) Use of baculovirus expression vectors. *Methods Mol Biol* 62, 235–246.

[214] Luckow, V. A., Lee, S. C., Barry, G. F., & Olins, P. O. (1993) Efficient generation of infectious recombinant baculoviruses by site-specific transposon-mediated insertion of foreign genes into a baculovirus genome propagated in Escherichia coli. *J Virol* 67, 4566–4579.

[215] Sanger, F., Nicklen, S., & Coulson, A. R. (1977) DNA sequencing with chain-terminating inhibitors. *Proc Natl Acad Sci U S A* 74, 5463–5467.

[216] Kelley, L. A. & Sternberg, M. J. E. (2009) Protein structure prediction on the Web: a case study using the Phyre server. *Nat Protoc* 4, 363–371.

[217] Hefferon, K. L., Oomens, A. G., Monsma, S. A., Finnerty, C. M., & Blissard, G. W. (1999) Host cell receptor binding by baculovirus GP64 and kinetics of virion entry. *Virology* 258, 455–468.

[218] Rudolph, C., Lausier, J., Naundorf, S., Müller, R. H., & Rosenecker, J. (2000) In vivo gene delivery to the lung using polyethylenimine and fractured polyamidoamine dendrimers. *J Gene Med* 2, 269–278.

[219] Akinc, A., Thomas, M., Klibanov, A. M., & Langer, R. (2005) Exploring polyethylenimine-mediated DNA transfection and the proton sponge hypothesis. *J Gene Med* 7, 657–663.

[220] Davis, H. E., Rosinski, M., Morgan, J. R., & Yarmush, M. L. (2004) Charged polymers modulate retrovirus transduction via membrane charge neutralization and virus aggregation. *Biophys J* 86, 1234–1242.

[221] Cremer, C. & Cremer, T. (1978) Considerations on a laser-scanning-microscope with high resolution and depth of field. *Microsc Acta* 81, 31–44.

[222] Carpenter, A. E., Jones, T. R., Lamprecht, M. R., Clarke, C., Kang, I. H., Friman, O., Guertin, D. A., Chang, J. H., Lindquist, R. A., Moffat, J., Golland, P., & Sabatini, D. M. (2006) CellProfiler: image analysis software for identifying and quantifying cell phenotypes. *Genome Biol* 7, R100.

[223] Truneh, A., Albert, F., Golstein, P., & Schmitt-Verhulst, A. M. (1985) Early steps of lymphocyte activation bypassed by synergy between calcium ionophores and phorbol ester. *Nature* 313, 318–320.

[224] Lathe, G. H. & Ruthven, C. R. (1956) The separation of substances and estimation of their relative molecular sizes by the use of colums of starch in water. *Biochem J* 62, 665–674.

[225] Maley, F., Trimble, R. B., Tarentino, A. L., & Plummer, Jr, T. (1989) Characterization of glycoproteins and their associated oligosaccharides through the use of endoglycosidases. *Anal Biochem* 180, 195–204.

[226] Tretter, V., Altmann, F., & März, L. (1991) Peptide-N4-(N-acetyl-beta-glucosaminyl)asparagine amidase F cannot release glycans with fucose attached alpha 1—-3 to the asparagine-linked N-acetylglucosamine residue. *Eur J Biochem* 199, 647–652.

[227] Becker, D. J. & Lowe, J. B. (2003) Fucose: biosynthesis and biological function in mammals. *Glycobiology* 13, 41R–53R.

[228] Laemmli, U. K. (1970) Cleavage of structural proteins during the assembly of the head of bacteriophage T4. *Nature* 227, 680–685.

[229] Towbin, H., Staehelin, T., & Gordon, J. (1979) Electrophoretic transfer of proteins from polyacrylamide gels to nitrocellulose sheets: procedure and some applications. *Proc Natl Acad Sci U S A* 76, 4350–4354.

[230] Hilpert, K., Winkler, D. F. H., & Hancock, R. E. W. (2007) Peptide arrays on cellulose support: SPOT synthesis, a time and cost efficient method for synthesis of large numbers of peptides in a parallel and addressable fashion. *Nat Protoc* 2, 1333–1349.

[231] Plewnia, G., Schulze, K., Hunte, C., Tampé, R., & Koch, J. (2007) Modulation of the antigenic peptide transporter TAP by recombinant antibodies binding to the last five residues of TAP1. *J Mol Biol* 369, 95–107.

[232] Nathalie Braun, S. W. (2009) Analyse heterogener Proteinkomplexe. *Biospektrum* 1, 34–36.

[233] Herrmann, J., Berberich, H., Hartmann, J., Beyer, S., Davies, K., & Koch, J. (2014) Homo-oligomerization of the Activating Natural Killer Cell Receptor NKp30 Ectodomain Increases Its Binding Affinity for Cellular Ligands. *J Biol Chem* 289, 765–777.

[234] Germain, R. N. (1997) T-cell signaling: the importance of receptor clustering. *Curr Biol* 7, R640–R644.

[235] Qian, D. & Weiss, A. (1997) T cell antigen receptor signal transduction. *Curr Opin Cell Biol* 9, 205–212.

[236] Faure, M., Barber, D. F., Takahashi, S. M., Jin, T., & Long, E. O. (2003) Spontaneous clustering and tyrosine phosphorylation of NK cell inhibitory receptor induced by ligand binding. *J Immunol* 170, 6107–6114.

[237] Weil, S. (2010) Etablierung eines proteolytischen Fusionsproteins des Natürlichen Killerzellrezeptors NKp30 zur Ligandenidentifizierung. *Diplomarbeit*.

[238] Peters, E. (2013) Oligomerization status of the human activating natural killer cell receptors NKp30 and NKp46.

[239] Berberich, H. (2011) Expression und funktionelle Charakterisierung ligandenbindungsaktiver Teildomänen des NKp30 Rezeptors natürlicher Killerzellen. *Diplomarbeit*.

[240] McFarland, B. J., Kortemme, T., Yu, S. F., Baker, D., & Strong, R. K. (2003) Symmetry recognizing asymmetry: analysis of the interactions between the C-type lectin-like immunoreceptor NKG2D and MHC class I-like ligands. *Structure* 11, 411–422.

[241] Li, P., Morris, D. L., Willcox, B. E., Steinle, A., Spies, T., & Strong, R. K. (2001) Complex structure of the activating immunoreceptor NKG2D and its MHC class I-like ligand MICA. *Nat Immunol* 2, 443–451.

[242] Radaev, S., Rostro, B., Brooks, A. G., Colonna, M., & Sun, P. D. (2001) Conformational plasticity revealed by the cocrystal structure of NKG2D and its class I MHC-like ligand ULBP3. *Immunity* 15, 1039–1049.

[243] Arnon, T. I., Achdout, H., Lieberman, N., Gazit, R., Gonen-Gross, T., Katz, G., Bar-Ilan, A., Bloushtain, N., Lev, M., Joseph, A., Kedar, E., Porgador, A., & Mandelboim, O. (2004) The mechanisms controlling the recognition of tumor- and virus-infected cells by NKp46. *Blood* 103, 664–672.

[244] Byrd, A., Hoffmann, S. C., Jarahian, M., Momburg, F., & Watzl, C. (2007) Expression analysis of the ligands for the Natural Killer cell receptors NKp30 and NKp44. *PLoS One* 2, e1339.

[245] Nowbakht, P., Ionescu, M.-C. S., Rohner, A., Kalberer, C. P., Rossy, E., Mori, L., Cosman, D., De Libero, G., & Wodnar-Filipowicz, A. (2005) Ligands for natural killer cell-activating receptors are expressed upon the maturation of normal myelomonocytic cells but at low levels in acute myeloid leukemias. *Blood* 105, 3615–3622.

[246] Bryceson, Y. T., March, M. E., Barber, D. F., Ljunggren, H.-G., & Long, E. O. (2005) Cytolytic granule polarization and degranulation controlled by different receptors in resting NK cells. *J Exp Med* 202, 1001–1012.

[247] Das, A. & Long, E. O. (2010) Lytic granule polarization, rather than degranulation, is the preferred target of inhibitory receptors in NK cells. *J Immunol* 185, 4698–4704.

[248] March, M. E., Gross, C. C., & Long, E. O. (2010) Use of transfected Drosophila S2 cells to study NK cell activation. *Methods Mol Biol* 612, 67–88.

[249] Lamken, P., Lata, S., Gavutis, M., & Piehler, J. (2004) Ligand-induced assembling of the type I interferon receptor on supported lipid bilayers. *J Mol Biol* 341, 303–318.

[250] Erickson, H. P. (2009) Size and shape of protein molecules at the nanometer level determined by sedimentation, gel filtration, and electron microscopy. *Biol Proced Online* 11, 32–51.

[251] Chen, S., Kawashima, H., Lowe, J. B., Lanier, L. L., & Fukuda, M. (2005) Suppression of tumor formation in lymph nodes by L-selectin-mediated natural killer cell recruitment. *J Exp Med* 202, 1679–1689.

[252] Orange, J. S., Harris, K. E., Andzelm, M. M., Valter, M. M., Geha, R. S., & Strominger, J. L. (2003) The mature activating natural killer cell immunologic synapse is formed in distinct stages. *Proc Natl Acad Sci U S A* 100, 14151–14156.

[253] Davis, D. M., Chiu, I., Fassett, M., Cohen, G. B., Mandelboim, O., & Strominger, J. L. (1999) The human natural killer cell immune synapse. *Proc Natl Acad Sci U S A* 96, 15062–15067.

[254] Vyas, Y. M., Mehta, K. M., Morgan, M., Maniar, H., Butros, L., Jung, S., Burkhardt, J. K., & Dupont, B. (2001) Spatial organization of signal transduction molecules in the NK cell immune synapses during MHC class I-regulated noncytolytic and cytolytic interactions. *J Immunol* 167, 4358–4367.

[255] Carpén, O., Virtanen, I., Lehto, V. P., & Saksela, E. (1983) Polarization of NK cell cytoskeleton upon conjugation with sensitive target cells. *J Immunol* 131, 2695–2698.

[256] Graham, D. B., Cella, M., Giurisato, E., Fujikawa, K., Miletic, A. V., Kloeppel, T., Brim, K., Takai, T., Shaw, A. S., Colonna, M., & Swat, W. (2006) Vav1 controls DAP10-mediated natural cytotoxicity by regulating actin and microtubule dynamics. *J Immunol* 177, 2349–2355.

[257] Wulfing, C., Purtic, B., Klem, J., & Schatzle, J. D. (2003) Stepwise cytoskeletal polarization as a series of checkpoints in innate but not adaptive cytolytic killing. *Proc Natl Acad Sci U S A* 100, 7767–7772.

[258] Weiss, A., Imboden, J., Shoback, D., & Stobo, J. (1984) Role of T3 surface molecules in human T-cell activation: T3-dependent activation results in an increase in cytoplasmic free calcium. *Proc Natl Acad Sci U S A* 81, 4169–4173.

[259] Podack, E. R., Lowrey, D. M., Lichtenheld, M., & Hameed, A. (1988) Function of granule perforin and esterases in T cell-mediated reactions. Components required for delivery of molecules to target cells. *Ann N Y Acad Sci* 532, 292–302.

[260] Dustin, M. L. & Long, E. O. (2010) Cytotoxic immunological synapses. *Immunol Rev* 235, 24–34.

[261] Barber, D. F., Faure, M., & Long, E. O. (2004) LFA-1 contributes an early signal for NK cell cytotoxicity. *J Immunol* 173, 3653–3659.

[262] Abeyweera, T. P., Merino, E., & Huse, M. (2011) Inhibitory signaling blocks activating receptor clustering and induces cytoskeletal retraction in natural killer cells. *J Cell Biol* 192, 675–690.

[263] Treanor, B., Lanigan, P. M. P., Kumar, S., Dunsby, C., Munro, I., Auksorius, E., Culley, F. J., Purbhoo, M. A., Phillips, D., Neil, M. A. A., Burshtyn, D. N., French, P. M. W., & Davis, D. M. (2006) Microclusters of inhibitory killer immunoglobulin-like receptor signaling at natural killer cell immunological synapses. *J Cell Biol* 174, 153–161.

[264] Bunnell, S. C., Hong, D. I., Kardon, J. R., Yamazaki, T., McGlade, C. J., Barr, V. A., & Samelson, L. E. (2002) T cell receptor ligation induces the formation of dynamically regulated signaling assemblies. *J Cell Biol* 158, 1263–1275.

[265] Campi, G., Varma, R., & Dustin, M. L. (2005) Actin and agonist MHC-peptide complex-dependent T cell receptor microclusters as scaffolds for signaling. *J Exp Med* 202, 1031–1036.

[266] Krummel, M. F., Sjaastad, M. D., Wülfing, C., & Davis, M. M. (2000) Differential clustering of CD4 and CD3zeta during T cell recognition. *Science* 289, 1349–1352.

[267] Giurisato, E., Cella, M., Takai, T., Kurosaki, T., Feng, Y., Longmore, G. D., Colonna, M., & Shaw, A. S. (2007) Phosphatidylinositol 3-kinase activation is required to form the NKG2D immunological synapse. *Mol Cell Biol* 27, 8583–8599.

[268] Call, M. E. & Wucherpfennig, K. W. (2007) Common themes in the assembly and architecture of activating immune receptors. *Nat Rev Immunol* 7, 841–850.

[269] Wucherpfennig, K. W., Gagnon, E., Call, M. J., Huseby, E. S., & Call, M. E. (2010) Structural biology of the T-cell receptor: insights into receptor assembly, ligand recognition, and initiation of signaling. *Cold Spring Harb Perspect Biol* 2, a005140.

[270] Kuhns, M. S., Davis, M. M., & Garcia, K. C. (2006) Deconstructing the form and function of the TCR/CD3 complex. *Immunity* 24, 133–139.

[271] Choudhuri, K. & van der Merwe, P. A. (2007) Molecular mechanisms involved in T cell receptor triggering. *Semin Immunol* 19, 255–261.

[272] Chen, L. (2004) Co-inhibitory molecules of the B7-CD28 family in the control of T-cell immunity. *Nat Rev Immunol* 4, 336–347.

[273] Okazaki, T. & Honjo, T. (2007) PD-1 and PD-1 ligands: from discovery to clinical application. *Int Immunol* 19, 813–824.

[274] Greene, J. L., Leytze, G. M., Emswiler, J., Peach, R., Bajorath, J., Cosand, W., & Linsley, P. S. (1996) Covalent dimerization of CD28/CTLA-4 and oligomerization of CD80/CD86 regulate T cell costimulatory interactions. *J Biol Chem* 271, 26762–26771.

[275] Stamper, C. C., Zhang, Y., Tobin, J. F., Erbe, D. V., Ikemizu, S., Davis, S. J., Stahl, M. L., Seehra, J., Somers, W. S., & Mosyak, L. (2001) Crystal structure of the B7-1/CTLA-4 complex that inhibits human immune responses. *Nature* 410, 608–611.

[276] Schwartz, J. C., Zhang, X., Fedorov, A. A., Nathenson, S. G., & Almo, S. C. (2001) Structural basis for co-stimulation by the human CTLA-4/B7-2 complex. *Nature* 410, 604–608.

[277] Serrano-Pertierra, E., Cernuda-Morollón, E., Brdička, T., Hooejši, V., & López-Larrea, C. (2014) L-plastin is involved in NKG2D recruitment into lipid rafts and NKG2D-mediated NK cell migration. *J Leukoc Biol*.

[278] Sivori, S., Parolini, S., Marcenaro, E., Castriconi, R., Pende, D., Millo, R., & Moretta, A. (2000) Involvement of natural cytotoxicity receptors in human natural killer cell-mediated lysis of neuroblastoma and glioblastoma cell lines. *J Neuroimmunol* 107, 220–225.

[279] Goodsell, D. S. (1991) Inside a living cell. *Trends Biochem Sci* 16, 203–206.

[280] Goodsell, D. S. & Olson, A. J. (2000) Structural symmetry and protein function. *Annu Rev Biophys Biomol Struct* 29, 105–153.

[281] Ali, M. H. & Imperiali, B. (2005) Protein oligomerization: how and why. *Bioorg Med Chem* 13, 5013–5020.

[282] Ito, K., Higai, K., Shinoda, C., Sakurai, M., Yanai, K., Azuma, Y., & Matsumoto, K. (2012) Unlike natural killer (NK) p30, natural cytotoxicity receptor NKp44 binds to multimeric α2,3-NeuNAc-containing N-glycans. *Biol Pharm Bull* 35, 594–600.

[283] Davis, D. M. (2002) Assembly of the immunological synapse for T cells and NK cells. *Trends Immunol* 23, 356–363.

[284] Eleme, K., Taner, S. B., Onfelt, B., Collinson, L. M., McCann, F. E., Chalupny, N. J., Cosman, D., Hopkins, C., Magee, A. I., & Davis, D. M. (2004) Cell surface organization of stress-inducible proteins ULBP and MICA that stimulate human NK cells and T cells via NKG2D. *J Exp Med* 199, 1005–1010.

[285] Kaifu, T., Escalière, B., Gastinel, L. N., Vivier, E., & Baratin, M. (2011) B7-H6/NKp30 interaction: a mechanism of alerting NK cells against tumors. *Cell Mol Life Sci* 68, 3531–3539.

7 Appendix

7.1 Supplemental Data

7.1.1 Isoforms of NKp30

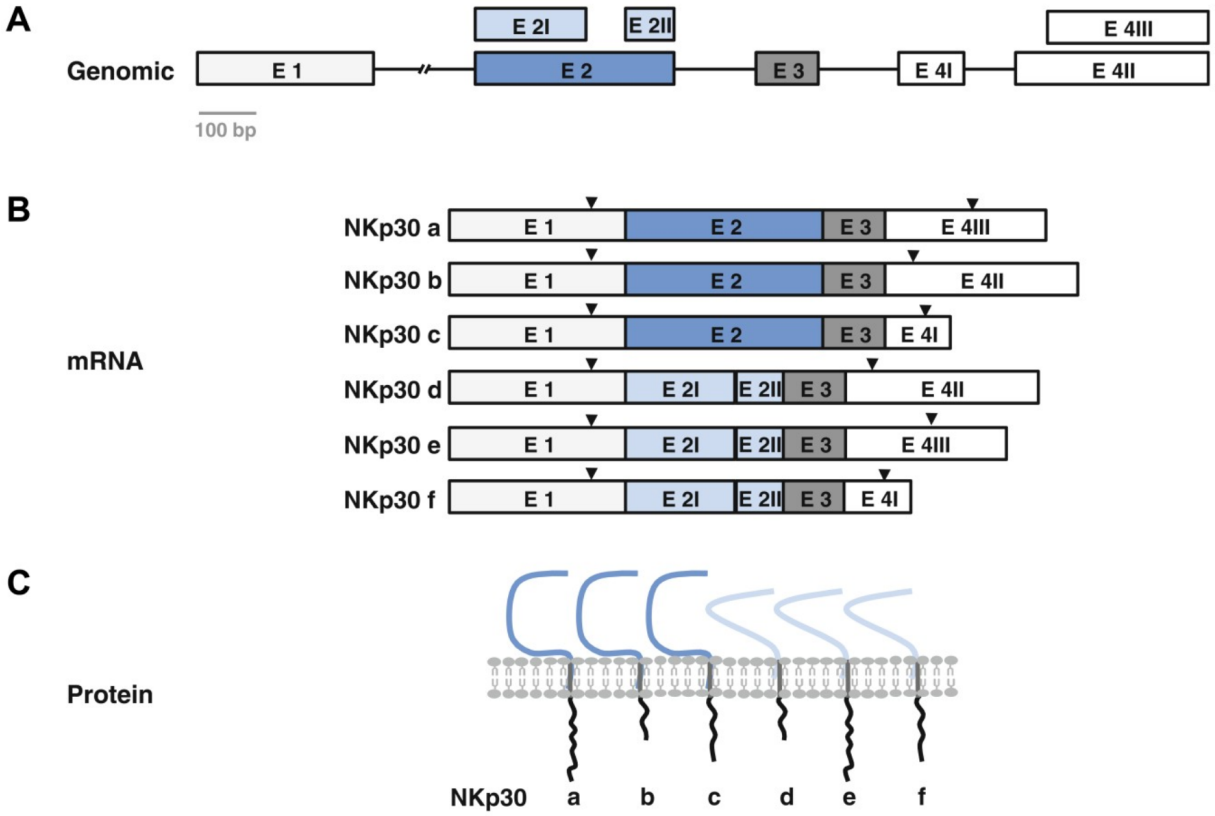

Fig. S1: The human NKp30 gene encodes six splice variants

(A) The genomic organization of the exons contributing to the six transcript variants of NKp30. Exon 1 (E1) encodes the leader sequence, exon 2 (E2) the ectodomain, exon 3 (E3) the transmembrane domain, and exon 4 (E4) the intracellular domain of NKp30. (B) Transcript variants of NKp30. In transcripts a-c, the complete exon 2 is used, whereas in transcripts d-f, exons 2I and 2II are transcribed, resulting in a 75-nucleotide deletion of the extracellular part. In transcripts a and e exon 4III is used, whereas in transcripts b and d exon 4II and in transcripts c and f exon 4I are transcribed. The initiation and stop codons are indicated by the arrowheads. (C) Protein structure of each splice variant of NKp30. Isoform a consists of 201 amino acids and was defined as canonical isoform of NKp30. It harbors the complete ectodomain of NKp30 and the longest intracellular domain (36 amino acids). Isoform b consists of 177 amino acids due to alternative splicing of exon 4. It harbors the complete ectodomain of NKp30 and the shortest intracellular domain (12 amino acids). Isoform c consists of 190 amino acids, harbors the complete ectodomain of NKp30 and an intracellular domain of 25 amino acids. Isoforms d, e and f harbor a partially deleted ectodomain of NKp30, which lacks 25 amino acids within the ligand binding domain. Isoform d, with its intracellular domain corresponding to isoform b, consists of 152 amino acids. Isoform e with the longest intracellular domain consists of 176 and isoform f consists of 165 amino acids due to the intracellular domain corresponding to isoform c with 25 amin acids. (Modified from [285].)

7.1.2 Upregulation of NCR Surface Expression Upon IL-2 Activation

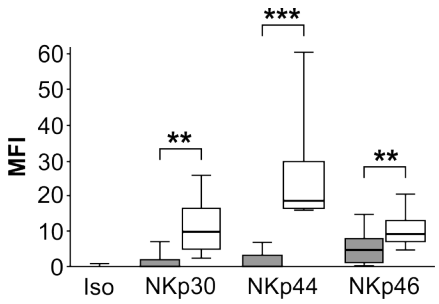

Fig. S2: Induced surface NCR expression upon IL-2 activation of NK cells

In vitro upregulation of the NCRs under the influence of IL-2. Mean fluorescence intensity (MFI) of NCRs (NKp30, NKp44, and NKp46) on $CD56^{+}CD16^{-}CD3^{-}$ NK cells. Notably, the $CD56^{+}CD16^{+}CD3^{-}$ NK cell subset displays comparable NCR surface expressions. Freshly isolated (gray bars) and IL-2 stimulated NK cells (white bars) are shown. Significant differences in up-regulation are marked (**P < 0.005, ***P < 0.001). (Modified from [184].)

7.1.3 Constitutive YFP Expression Upon Transfection and Baculoviral Infection of Insect Cells

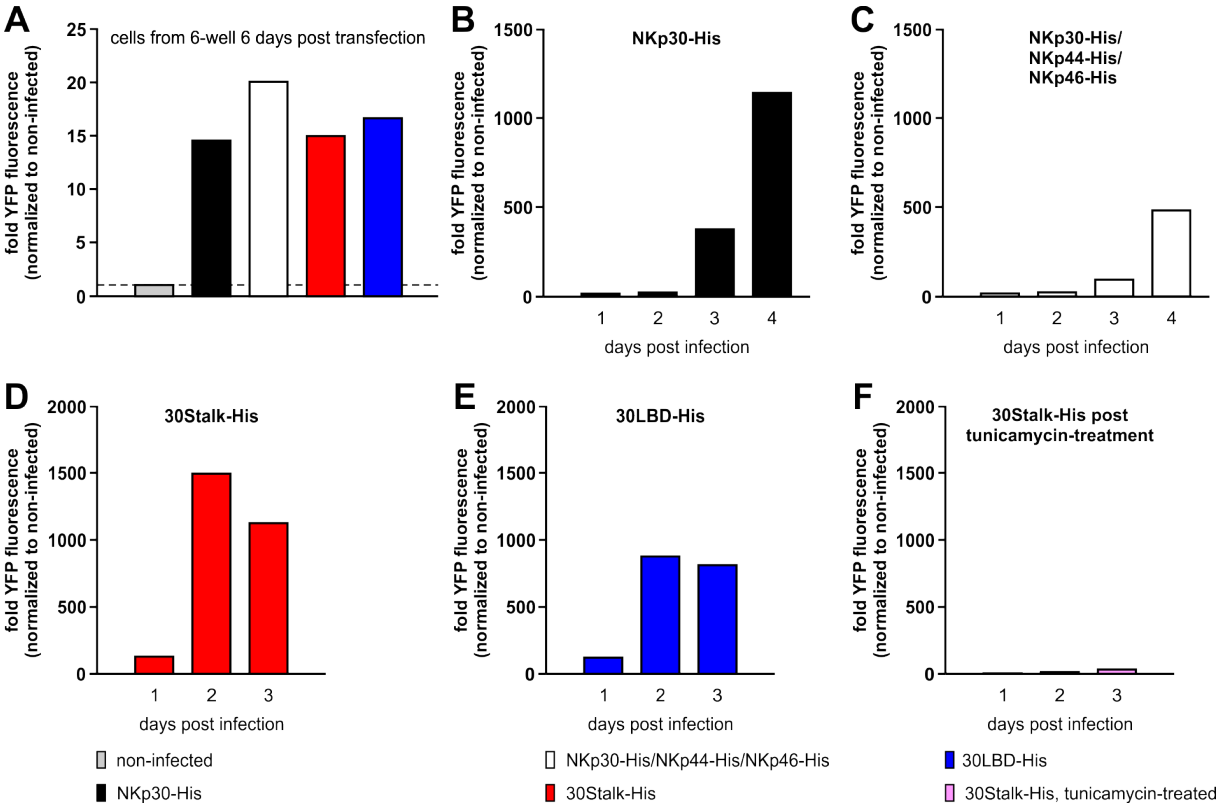

Fig. S3: Normalized YFP fluorescence intensities

Intracellular YFP fluorescence intensities (excitation: 485 nm, emission: 520 nm) of supernatants from centrifugation after sonication of insect cells were measured. To estimate transfection and infection efficiencies, YFP fluorescence intensities were normalized to non-infected insect cells. (A) Fold YFP fluorescence of transfected *Sf* 9 insect cells from one 6-well six days post transfection. (B-F) Fold YFP fluorescence of $1x10^{6}$ infected High Five insect cells one to three/four days post infection (gray: non-infected, black: NKp30-His functionalization, white: NKp30-His/NKp44-His/NKp46-His functionalization, red: 30Stalk-His secretion, blue: 30LBD-His secretion, pink: 30Stalk-His secretion, tunicamycin-treated).

7.1.4 Expression of the NKp30 Ligand Binding Domain in *Escherichia coli*

Since the 3D structure of the NKp30 LBD had not been solved until 2011 [116,117], a *de novo* model of the globular NKp30 LBD was calculated using the protein structure prediction service PHYRE [216]. Therefore, the truncated version of the NKp30 LBD (30LBD$_{tr}$) lacking eight amino acids at the C-terminus (amino acids M1 to G120, see 7.3) was used. To identify the optimal construct design, expression and purification analyses with variants of 30LBD$_{tr}$ fused to an N- or C-terminal deca-histidine tag (His) for affinity purification were performed. Therefore, *E. coli* BL21 cells were transformed with the plasmids pET16b-His10-TEV-NKp30EC or pET16b-NKp30EC-TEV-His10 encoding His-30LBD$_{tr}$ or 30LBD$_{tr}$-His, respectively (2.2.2). Upon inoculation of expression cultures and induction of recombinant gene expression by IPTG at optimized conditions (2.4.1), samples were collected for reducing SDS-PAGE and immunoblot analyses. Though both variants were expressed (Fig. S4A and B), highest recombinant protein levels were obtained for His-30LBD$_{tr}$ as demonstrated by immunoblot analyses (anti-NKp30, polyclonal). At 4 h post induction, recombinant protein levels remained static and bacteria cells were harvested by centrifugation.

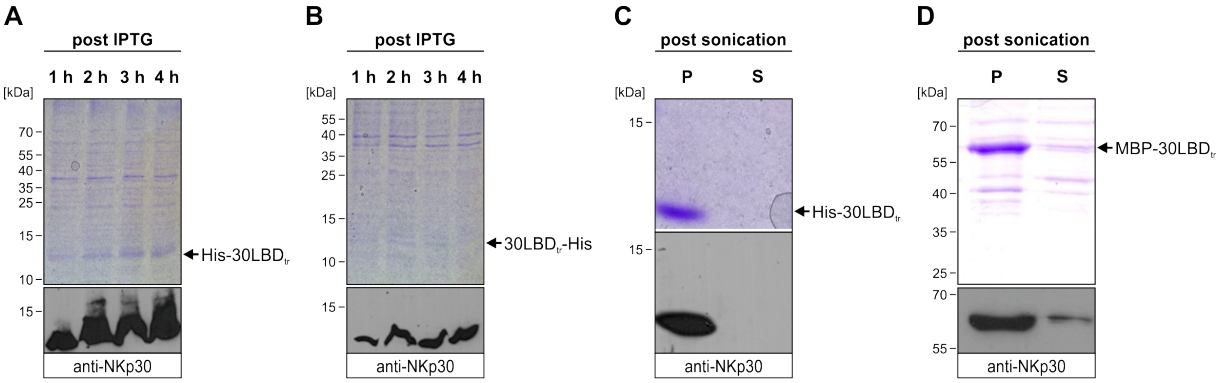

Fig. S4: Production of soluble NKp30 ligand binding domain proteins in *E. coli*

E. coli cells were transformed with plasmids encoding the truncated NKp30 ligand binding domain (30LBD$_{tr}$) fused to different purification tags (His, deca-histidine; MBP, maltose binding protein). Aliquots of bacteria transformed with plasmids encoding for (A) N-terminal and (B) C-terminal His-tagged 30LBD$_{tr}$ were collected post IPTG induction at indicated time points. Optimal conditions for recombinant protein production were identified by reducing SDS-PAGE (coomassie-stained) and immunoblot (anti-NKp30) analyses. Pellet (P) and soluble fraction (S) of sonicated bacteria cells expressing (C) His-30LBD$_{tr}$ or (D) MBP-30LBD$_{tr}$ proteins were analyzed by reducing SDS-PAGE (coomassie-stained) and immunoblot (anti-NKp30).

It is known that *E. coli* derived recombinant proteins are often found in inclusion bodies. Therefore, the bacteria cells were resuspended and sonicated for separation of cytosolic proteins and an insoluble pellet fraction (2.4.1). Reducing SDS-PAGE and corresponding immunoblot (anti-NKp30, polyclonal) analyses revealed complete aggregation of the recombinant His-30LBD$_{tr}$ proteins within inclusion bodies (Fig. S4C). Even expression of His-30LBD$_{tr}$ in *E. coli* Origami (DE3) cells, which facilitate disulfide bond formation and thereby possibly sustaining correct folding of the NKp30 ligand binding domain, did not increase protein solubility (data not shown). To circumvent elaborate refolding screenings, larger purification tags such as GST (plasmid pGEX-4T-1-NKp30EC) or MBP (plasmid pMal-p5X-NKp30EC) were fused at the N-terminus of 30LBD$_{tr}$, which were expressed in *E. coli* BL21 (DE3) upon transformation. Interestingly, immunoblot analysis (anti-NKp30, polyclonal) revealed the presence of soluble MBP-30LBD$_{tr}$ proteins within the cytosolic fraction, at least to some extent (Fig. S4D). However, flow

cytometry analyses of decorated target cells with recombinant MBP-30LBD$_{tr}$ proteins did not demonstrate any ligand binding capacities (data not shown).

7.1.5 B7-H6-Bound Structure of the NKp30 Ligand Binding Domain

Fig. S5: The ligand binding domain of NKp30 is a two-layer β-sandwich

B7-H6 (gray)-bound crystal structure of the NKp30 ectodomain. The Ig-like domain of NKp30 is a two-layer β-sandwich. The front (red) and back sheets (blue) are composed of β-strands GFC and ABED, respectively, are linked by a canonical intersheet disulfide bond (C39-C108, in yellow stick representation). In addition, NKp30 contains two α-helices (α1 and α2) preceding β-strands D and E, respectively. One of these helices (α1) is unique to NKp30 among Ig-like domains. Notably, the predicted model of the NKp30 ligand binding domain lacks eight amino acids at the C-terminus (N121-E128 of the G strand, depicted in brown). (Modified from [117].)

7.2 Plasmid and Vector Maps

7.2.1 Expression Plasmids (*E. coli*)

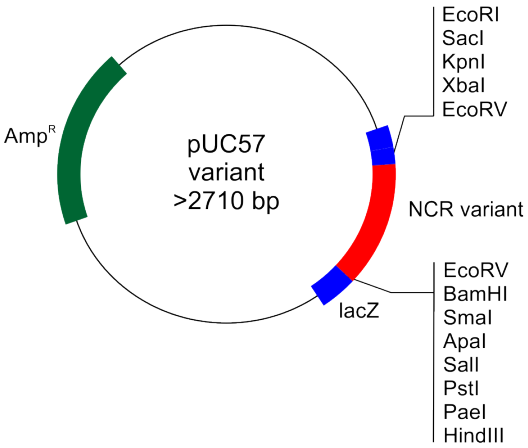

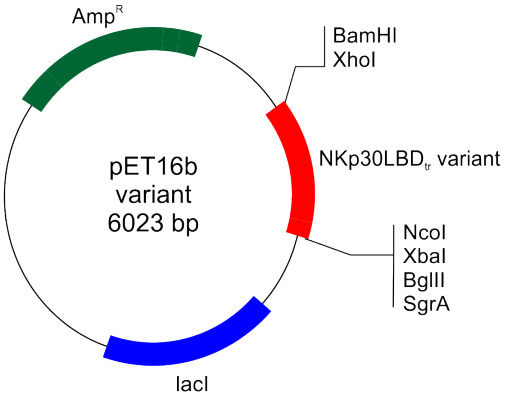

Insert size:

NKp30-His	642 bp	NKp30LBD$_{tr}$-TEV-His	380 bp
NKp44-His	867 bp	His-TEV-NKp30LBD$_{tr}$	380 bp
NKp46-His	951 bp	gp67ss-NKp30LBD-His	531 bp
NKp30-His opt	612 bp	gp67ss-NKp30Stalk-His	576 bp

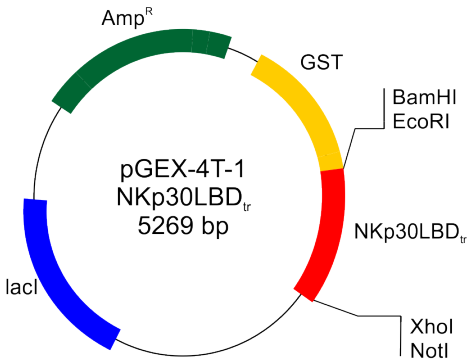

Insert size:
NKp30LBD$_{tr}$ 315 bp

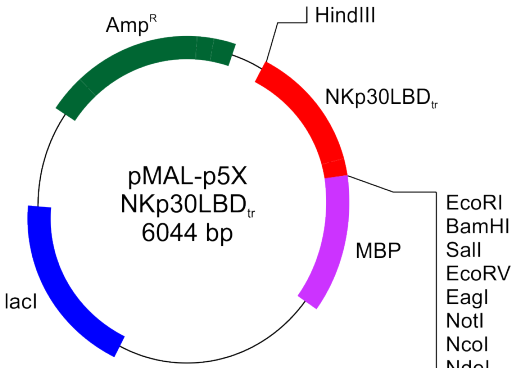

Insert size:
NKp30LBD$_{tr}$ 315 bp

7.2.2 Expression Plasmids (Mammalian Cells)

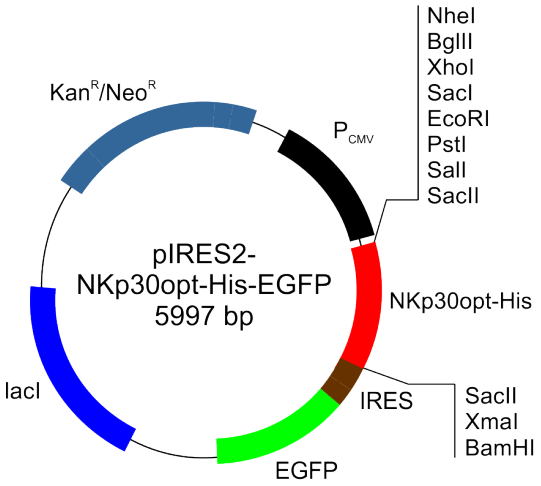

Insert size:
NKp30opt-His 689 bp

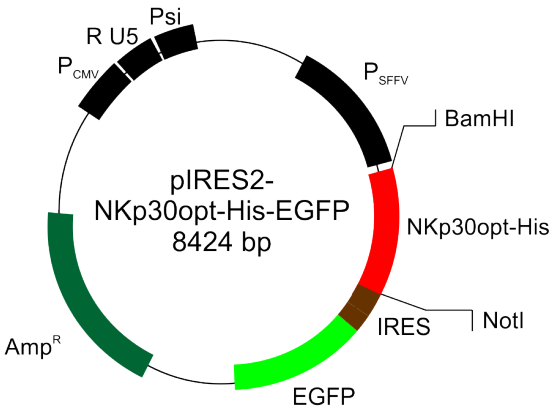

Insert size:
NKp30opt-His 653 bp

7.2.3 Expression Plasmids (Insect Cells)

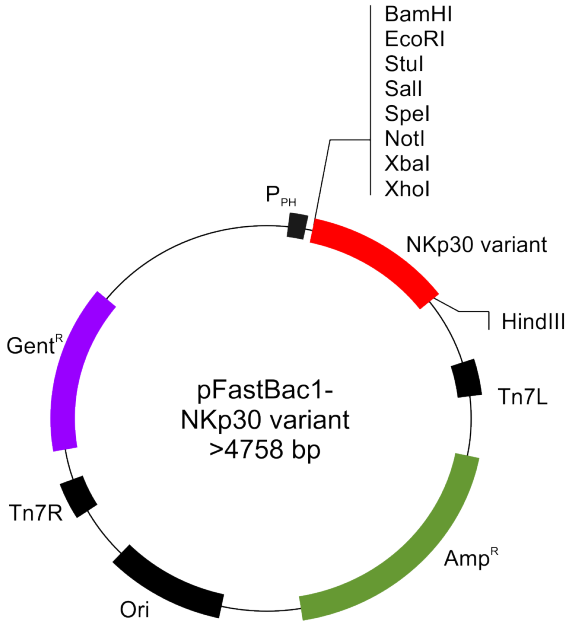

Insert size:
gp67ss-NKp30LBD-His 531 bp
gp67ss-NKp30Stalk-His 576 bp

7.2.4 Multigene Transfer Vectors (Insect Cells)

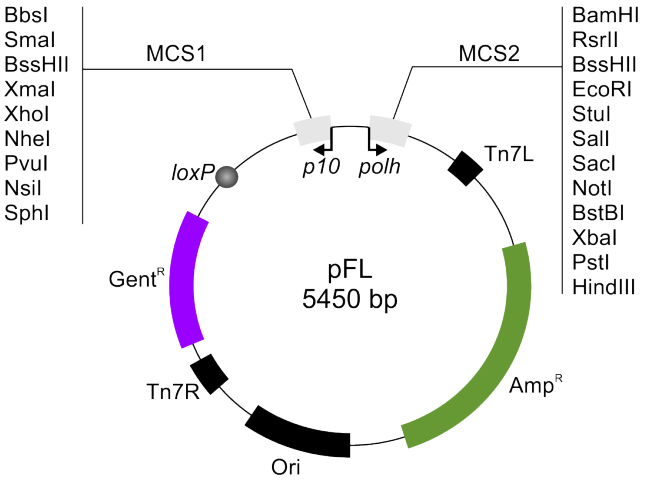

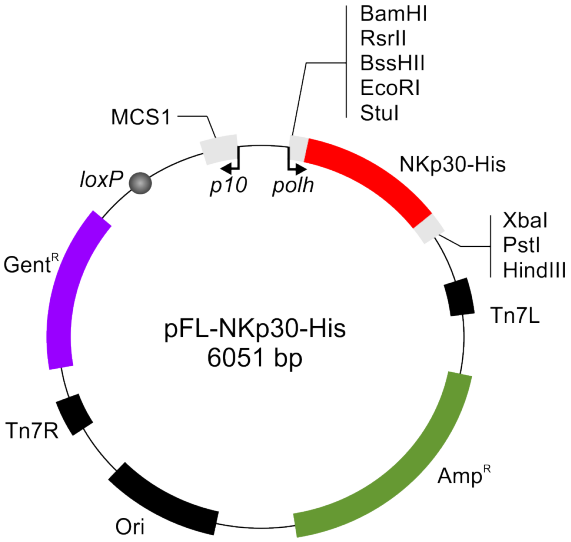

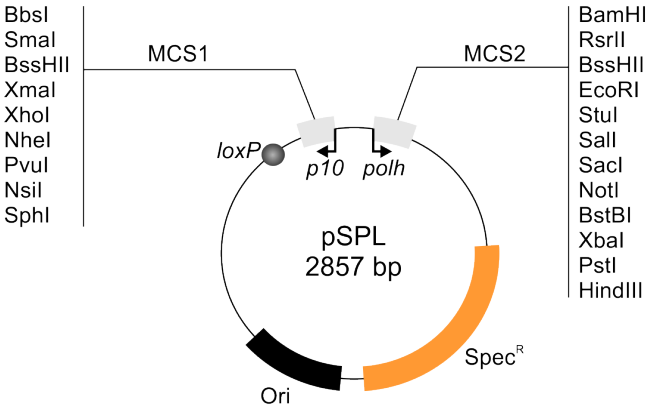

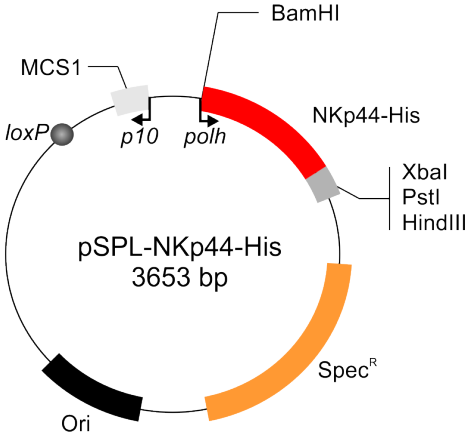

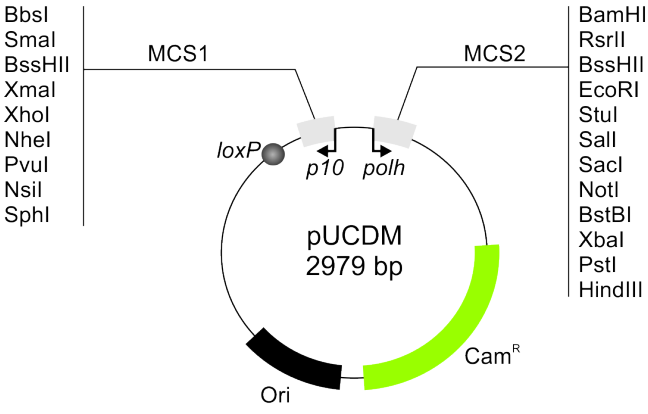

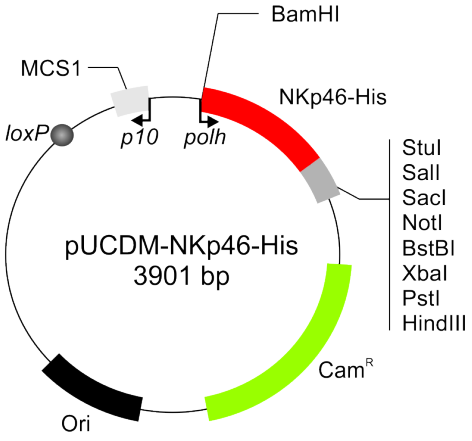

7.3 Protein Sequences

Unless otherwise denoted, nucleotide sequences originate from commercial plasmid vectors or can be found at the NCBI database (www.ncbi.nlm.nih.gov). Respective accession numbers and used base pairs are indicated for each fragment. The color code of the corresponding amino acid sequences refers to the construct scheme. Amino acids depicted in black result from the cloning strategy. Enzymatic cleavage sites for removal of the purification tag are italicized. Domain borders within the amino acid sequence of one fragment (one color) are separated by vertical lines.

Codon-optimized DNA of full-length NKp30 (synthesized by GenScript)

```
  1 ATGGCCTGGA TGCTGCTGCT GATTCTGATT ATGGTCCACC CTGGGTCCTG TGCCCTGTGG
 61 GTCTCTCAGC CTCCCGAAAT TAGAACTCTG GAGGGCAGCT CCGCTTTCCT GCCTTGCTCC
121 TTTAACGCTT CTCAGGGGAG ACTGGCAATC GGAAGTGTGA CATGGTTCAG GGACGAGGTG
181 GTCCCAGGCA AGGAAGTGCG CAATGGGACT CCAGAATTCA GGGGACGCCT GGCCCCTCTG
241 GCTTCTAGTC GGTTTCTGCA CGATCATCAG GCAGAGCTGC ACATCAGAGA CGTGCGGGGC
301 CATGATGCTT CCATCTACGT GTGCAGAGTG GAAGTGCTGG GACTGGGAGT GGGAACAGGA
361 AACGGGACAA GGCTGGTGGT CGAAAAGGAG CACCCACAAT TAGGAGCAGG GACCGTGCTG
421 CTGCTGAGAG CAGGGTTCTA TGCCGTCTCA TTTCTGAGCG TGGCCGTCGG CAGCACCGTG
481 TACTATCAGG GGAAGTGTCT TACTTGGAAG GGCCCACGGC GTCAGCTGCC CGCCGTGGTC
541 CCTGCCCCTC TGCCCCCTCC TTGTGGCTCA TCTGCTCATC TGCTGCCCCC AGTCCCAGGC
601 GGATGA
```

NKp30opt-His/NKp30-His

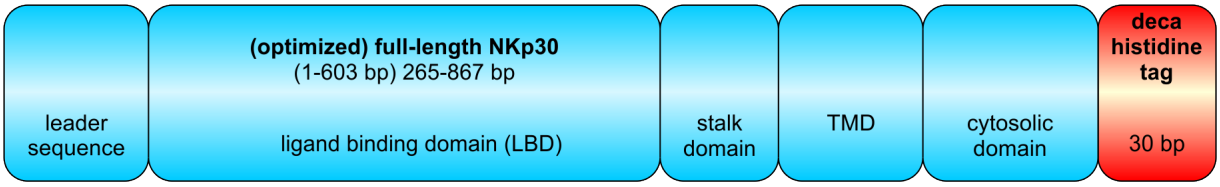

MAWMLLLILIMVHPGSCA|LWVSQPPEIRTLEGSSAFLPCSFNASQGRLAIGSVTWFRDEVVPGKEVRN
GTPEFRGRLAPLASSRFLHDHQAELHIRDVRGHDASIYVCRVEVLGLGVGTGNGTRLVVE|KEHPQLGA
GTVLLLR|AGFYAVSFLSVAVGSTVYYQG|KCLTWKGPRRQLPAVVPAPLPPPCGSSAHLLPPVPGGHH
HHHHHHHHH

NKp44-His

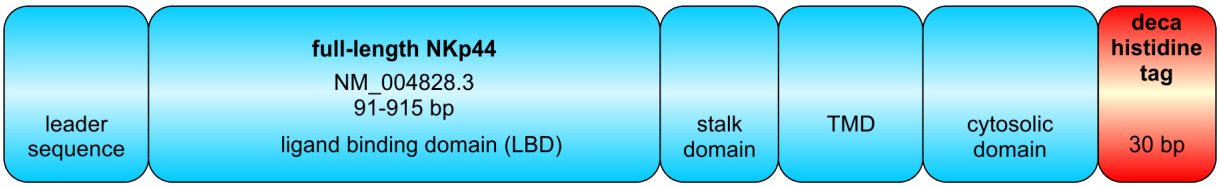

MAWRALHPLLLLLLLFPGSQA|QSKAQVLQSVAGQTLTVRCQYPPTGSLYEKKGWCKEASALVCIRLVT
SSKPRTMAWTSRFTIWDDPDAGFFTVTMTDLREEDSGHYWCRIYRPSDNSVSKSVRFYL|VVSPASAST
QTSWTPRDLVSSQTQTQSCVPPTAGARQAPESPSTIPVPSQPQNSTLRPGPAAPIA|LVPVFCGLLVAK
SLVLSALLV|WWGDIWWKTMMELRSLDTQKATCHLQQVTDLPWTSVSSPVEREILYHTVARTKISDDDD
EHTLHHHHHHHHHH

NKp46-His

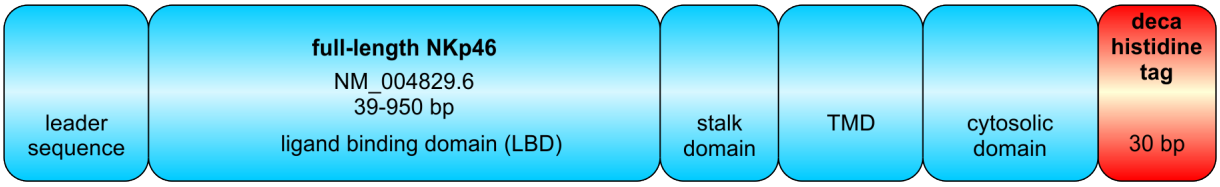

MSSTLPALLCVGLCLSQRISAQQQ|TLPKPFIWAEPHFMVPKEKQVTICCQGNYGAVEYQLHFEGSLFA
VDRPKPPERINKVKFYIPDMNSRMAGQYSCIYRVGELWSEPSNLLDLVVTEMYDTPTLSVHPGPEVISG
EKVTFYCRLDTATSMFLLLKEGRSSHVQRGYGKVQAEFPLGPVTTAHRGTYRCFGSYNNHAWSFPSEPV
KLLV|TGDIENTSLAPEDPTFPADTWGTYLLTTETGLQKDHALWDHTAQNLLR|MGLAFLVLVALVWFL
VEDWLS|RKRTRERASRASTWEGRRRLNTQTLHHHHHHHHHH

His-TEV-NKp30LBD$_{tr}$

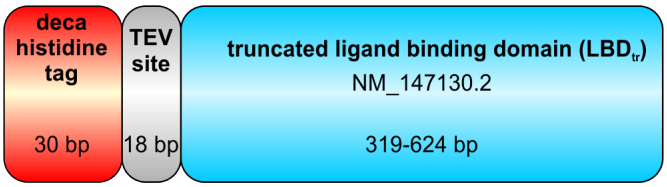

MGHHHHHHHHHHGS*ENLYFQ*GGSLWVSQPPEIRTLEGSSAFLPCSFNASQGRLAIGSVTWFRDEVVPGK
EVRGTPEFRGRLAPLASSRFLHDHQAELHIRDVRGHDASIYVCRVEVLGLGVGTG

NKp30LBD$_{tr}$-TEV-His

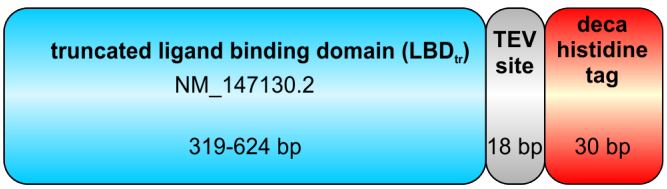

MGLWVSQPPEIRTLEGSSAFLPCSFNASQGRLAIGSVTWFRDEVVPGKEVRNGTPEFRGRLAPLASSRF
LHDHQAELHIRDVRGHDASIYVCRVEVLGLGVGTGGS*ENLYFQ*GGSHHHHHHHHHH

GST-NKp30LBD$_{tr}$

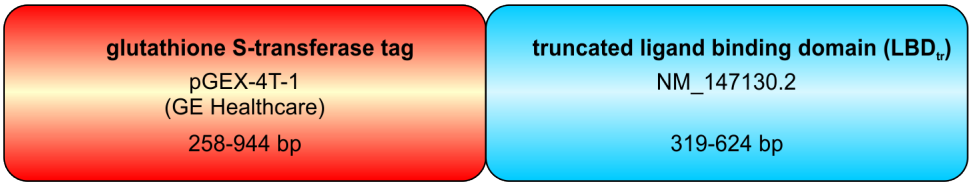

MSPILGYWKIKGLVQPTRLLLEYLEEKYEEHLYERDEGDKWRNKKFELGLEFPNLPYYIDGDVKLTQSM
AIIRYIADKHNMLGGCPKERAEISMLEGAVLDIRYGVSRIAYSKDFETLKVDFLSKLPEMLKMFEDRLC
HKTYLNGDHVTHPDFMLYDALDVVLYMDPMCLDAFPKLVCFKKRIEAIPQIDKYLKSSKYIAWPLQGWQ
ATFGGGDHPPKSDLVPRGSPEFLWVSQPPEIRTLEGSSAFLPCSFNASQGRLAIGSVTWFRDEVVPGKE
VRNGTPEFRGRLAPLASSRFLHDHQAELHIRDVRGHDASIYVCRVEVLGLGVGTG

MBP-NKp30LBD$_{tr}$

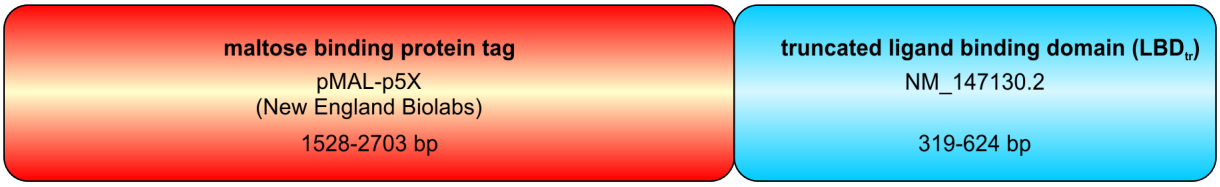

MKIKTGARILALSALTTMMFSASALAKIEEGKLVIWINGDKGYNGLAEVGKKFEKDTGIKVTVEHPDKL
EEKFPQVAATGDGPDIIFWAHDRFGGYAQSGLLAEITPDKAFQDKLYPFTWDAVRYNGKLIAYPIAVEA
LSLIYNKDLLPNPPKTWEEIPALDKELKAKGKSALMFNLQEPYFTWPLIAADGGYAFKYENGKYDIKDV
GVDNAGAKAGLTFLVDLIKNKHMNADTDYSIAEAAFNKGETAMTINGPWAWSNIDTSKVNYGVTVLPTF
KGQPSKPFVGVLSAGINAASPNKELAKEFLENYLLTDEGLEAVNKDKPLGAVALKSYEEELVKDPRIAA
TMENAQKGEIMPNIPQMSAFWYAVRTAVINAASGRQTVDEALKDAQTNSSSNNNNNNNNNNLGIEGRIS
HMSMGGRDIVDGSEFLWVSQPPEIRTLEGSSAFLPCSFNASQGRLAIGSVTWFRDEVVPGKEVRNGTPE
FRGRLAPLASSRFLHDHQAELHIRDVRGHDASIYVCRVEVLGLGVGTG

NKp30LBD-His

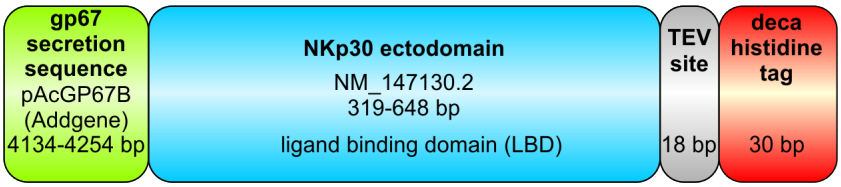

MLLVNQSHQGFNKEHTSKMVSAIVLYVLLAAAAHSAFAADLGSLWVSQPPEIRTLEGSSAFLPCSFNAS
QGRLAIGSVTWFRDEVVPGKEVRNGTPEFRGRLAPLASSRFLHDHQAELHIRDVRGHDASIYVCRVEVL
GLGVGTGNGTRLVVEGS*ENLYFQ*GGSHHHHHHHHHH

NKp30LBD-Stalk-His

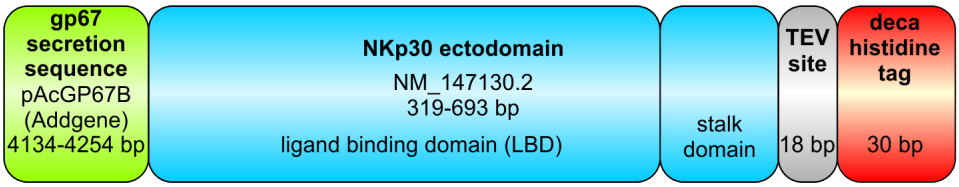

MLLVNQSHQGFNKEHTSKMVSAIVLYVLLAAAAHSAFAADLGSLWVSQPPEIRTLEGSSAFLPCSFNAS
QGRLAIGSVTWFRDEVVPGKEVRNGTPEFRGRLAPLASSRFLHDHQAELHIRDVRGHDASIYVCRVEVL
GLGVGTGNGTRLVVE|KEHPQLGAGTVLLLRGS*ENLYFQ*GGSHHHHHHHHHH

B7-H6-Ig

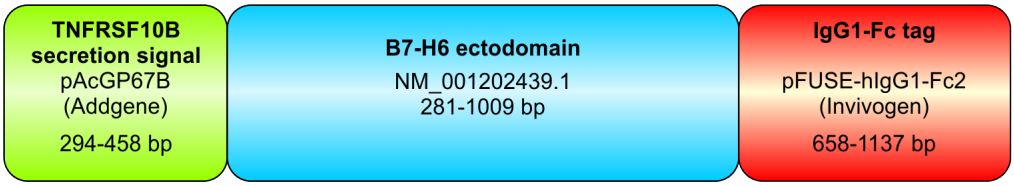

MEQRGQNAPAASGARKRHGPGPREARGARPGPRVPKTLVLVVAAVLLLVSAESALGSDLKVEMMAGGTQ
ITPLNDNVTIFCNIFYSQPLNITSMGITWFWKSLTFDKEVKVFEFFGDHQEAFRPGAIVSPWRLKSGDA
SLRLPGIQLEEAGEYRCEVVVTPLKAQGTVQLEVVASPASRLLLDQVGMKENEDKYMCESSGFYPEAIN
ITWEKQTQKFPHPIEISEDVITGPTIKNMDGTFNVTSCLKLNSSQEDPGTVYQCVVRHASLHTPLRSNF
TLTAARHSLSETEKTDNFSIHWWPDITHTCPPCPAPEAEGAPSVFLFPPKPKDTLMISRTPEVTCVVVD
VSHEDPEVKFNWYVDGVEVHNAKTKPREEQYNSTYRVVSVLTVLHQDWLNGKEYKCKVSNKALPAPIEK
TISKAKGQPREPQVYTLPPSREEMTKNQVSLTCLVKGFYPSDIAVEWESNGQPENNYKTTPPVLDSDGS
FFLYSKLTVDKSRWQQGNVFSCSVMHEALHNHYTQKSLSLSPGK

7.4 Peptide Spot Sequences

NKp30 (18 aa, off-set 1 aa)

A1	MAWMLLLILIMVHPGSCA	B5	FNASQGRLAIGSVTWFRD	C9	ASSRFLHDHQAELHIRDV
A2	AWMLLLILIMVHPGSCAL	B6	NASQGRLAIGSVTWFRDE	C10	SSRFLHDHQAELHIRDVR
A3	WMLLLILIMVHPGSCALW	B7	ASQGRLAIGSVTWFRDEV	C11	SRFLHDHQAELHIRDVRG
A4	MLLLILIMVHPGSCALWV	B8	SQGRLAIGSVTWFRDEVV	C12	RFLHDHQAELHIRDVRGH
A5	LLLILIMVHPGSCALWVS	B9	QGRLAIGSVTWFRDEVVP	C13	FLHDHQAELHIRDVRGHD
A6	LLILIMVHPGSCALWVSQ	B10	GRLAIGSVTWFRDEVVPG	C14	LHDHQAELHIRDVRGHDA
A7	LILIMVHPGSCALWVSQP	B11	RLAIGSVTWFRDEVVPGK	C15	HDHQAELHIRDVRGHDAS
A8	ILIMVHPGSCALWVSQPP	B12	LAIGSVTWFRDEVVPGKE	C16	DHQAELHIRDVRGHDASI
A9	LIMVHPGSCALWVSQPPE	B13	AIGSVTWFRDEVVPGKEV	C17	HQAELHIRDVRGHDASIY
A10	IMVHPGSCALWVSQPPEI	B14	IGSVTWFRDEVVPGKEVR	C18	QAELHIRDVRGHDASIYV
A11	MVHPGSCALWVSQPPEIR	B15	GSVTWFRDEVVPGKEVRN	C19	AELHIRDVRGHDASIYVC
A12	VHPGSCALWVSQPPEIRT	B16	SVTWFRDEVVPGKEVRNG	C20	ELHIRDVRGHDASIYVCR
A13	HPGSCALWVSQPPEIRTL	B17	VTWFRDEVVPGKEVRNGT	C21	LHIRDVRGHDASIYVCRV
A14	PGSCALWVSQPPEIRTLE	B18	TWFRDEVVPGKEVRNGTP	C22	HIRDVRGHDASIYVCRVE
A15	GSCALWVSQPPEIRTLEG	B19	WFRDEVVPGKEVRNGTPE	C23	IRDVRGHDASIYVCRVEV
A16	SCALWVSQPPEIRTLEGS	B20	FRDEVVPGKEVRNGTPEF	C24	RDVRGHDASIYVCRVEVL
A17	CALWVSQPPEIRTLEGSS	B21	RDEVVPGKEVRNGTPEFR	C25	DVRGHDASIYVCRVEVLG
A18	ALWVSQPPEIRTLEGSSA	B22	DEVVPGKEVRNGTPEFRG	C26	VRGHDASIYVCRVEVLGL
A19	LWVSQPPEIRTLEGSSAF	B23	EVVPGKEVRNGTPEFRGR	C27	RGHDASIYVCRVEVLGLG
A20	WVSQPPEIRTLEGSSAFL	B24	VVPGKEVRNGTPEFRGRL	C28	GHDASIYVCRVEVLGLGV
A21	VSQPPEIRTLEGSSAFLP	B25	VPGKEVRNGTPEFRGRLA	C29	HDASIYVCRVEVLGLGVG
A22	SQPPEIRTLEGSSAFLPC	B26	PGKEVRNGTPEFRGRLAP	C30	DASIYVCRVEVLGLGVGT
A23	QPPEIRTLEGSSAFLPCS	B27	GKEVRNGTPEFRGRLAPL	C31	ASIYVCRVEVLGLGVGTG
A24	PPEIRTLEGSSAFLPCSF	B28	KEVRNGTPEFRGRLAPLA	C32	SIYVCRVEVLGLGVGTGN
A25	PEIRTLEGSSAFLPCSFN	B29	EVRNGTPEFRGRLAPLAS	C33	IYVCRVEVLGLGVGTGNG
A26	EIRTLEGSSAFLPCSFNA	B30	VRNGTPEFRGRLAPLASS	C34	YVCRVEVLGLGVGTGNGT
A27	IRTLEGSSAFLPCSFNAS	B31	RNGTPEFRGRLAPLASSR	C35	VCRVEVLGLGVGTGNGTR
A28	RTLEGSSAFLPCSFNASQ	B32	NGTPEFRGRLAPLASSRF	C36	CRVEVLGLGVGTGNGTRL
A29	TLEGSSAFLPCSFNASQG	B33	GTPEFRGRLAPLASSRFL	D1	RVEVLGLGVGTGNGTRLV
A30	LEGSSAFLPCSFNASQGR	B34	TPEFRGRLAPLASSRFLH	D2	VEVLGLGVGTGNGTRLVV
A31	EGSSAFLPCSFNASQGRL	B35	PEFRGRLAPLASSRFLHD	D3	EVLGLGVGTGNGTRLVVE
A32	GSSAFLPCSFNASQGRLA	B36	EFRGRLAPLASSRFLHDH	D4	VLGLGVGTGNGTRLVVEK
A33	SSAFLPCSFNASQGRLAI	C1	FRGRLAPLASSRFLHDHQ	D5	LGLGVGTGNGTRLVVEKE
A34	SAFLPCSFNASQGRLAIG	C2	RGRLAPLASSRFLHDHQA	D6	GLGVGTGNGTRLVVEKEH
A35	AFLPCSFNASQGRLAIGS	C3	GRLAPLASSRFLHDHQAE	D7	LGVGTGNGTRLVVEKEHP
A36	FLPCSFNASQGRLAIGSV	C4	RLAPLASSRFLHDHQAEL	D8	GVGTGNGTRLVVEKEHPQ
B1	LPCSFNASQGRLAIGSVT	C5	LAPLASSRFLHDHQAELH	D9	VGTGNGTRLVVEKEHPQL
B2	PCSFNASQGRLAIGSVTW	C6	APLASSRFLHDHQAELHI	D10	GTGNGTRLVVEKEHPQLG
B3	CSFNASQGRLAIGSVTWF	C7	PLASSRFLHDHQAELHIR	D11	TGNGTRLVVEKEHPQLGA
B4	SFNASQGRLAIGSVTWFR	C8	LASSRFLHDHQAELHIRD	D12	GNGTRLVVEKEHPQLGAG

NKp30 (18 aa, off-set 1 aa)

D13	NGTRLVVEKEHPQLGAGT	D31	VLLLRAGFYAVSFLSVAV	E13	GSTVYYQGKCLTWKGPRR
D14	GTRLVVEKEHPQLGAGTV	D32	LLLRAGFYAVSFLSVAVG	E14	STVYYQGKCLTWKGPRRQ
D15	TRLVVEKEHPQLGAGTVL	D33	LLRAGFYAVSFLSVAVGS	E15	TVYYQGKCLTWKGPRRQL
D16	RLVVEKEHPQLGAGTVLL	D34	LRAGFYAVSFLSVAVGST	E16	VYYQGKCLTWKGPRRQLP
D17	LVVEKEHPQLGAGTVLLL	D35	RAGFYAVSFLSVAVGSTV	E17	YYQGKCLTWKGPRRQLPA
D18	VVEKEHPQLGAGTVLLLR	D36	AGFYAVSFLSVAVGSTVY	E18	YQGKCLTWKGPRRQLPAV
D19	VEKEHPQLGAGTVLLLRA	E1	GFYAVSFLSVAVGSTVYY	E19	QGKCLTWKGPRRQLPAVV
D20	EKEHPQLGAGTVLLLRAG	E2	FYAVSFLSVAVGSTVYYQ	E20	GKCLTWKGPRRQLPAVVP
D21	KEHPQLGAGTVLLLRAGF	E3	YAVSFLSVAVGSTVYYQG	E21	KCLTWKGPRRQLPAVVPA
D22	EHPQLGAGTVLLLRAGFY	E4	AVSFLSVAVGSTVYYQGK	E22	CLTWKGPRRQLPAVVPAP
D23	HPQLGAGTVLLLRAGFYA	E5	VSFLSVAVGSTVYYQGKC	E23	LTWKGPRRQLPAVVPAPL
D24	PQLGAGTVLLLRAGFYAV	E6	SFLSVAVGSTVYYQGKCL	E24	TWKGPRRQLPAVVPAPLP
D25	QLGAGTVLLLRAGFYAVS	E7	FLSVAVGSTVYYQGKCLT	E25	WKGPRRQLPAVVPAPLPP
D26	LGAGTVLLLRAGFYAVSF	E8	LSVAVGSTVYYQGKCLTW	E26	KGPRRQLPAVVPAPLPPP
D27	GAGTVLLLRAGFYAVSFL	E9	SVAVGSTVYYQGKCLTWK	E27	GPRRQLPAVVPAPLPPPC
D28	AGTVLLLRAGFYAVSFLS	E10	VAVGSTVYYQGKCLTWKG	E28	PRRQLPAVVPAPLPPPCG
D29	GTVLLLRAGFYAVSFLSV	E11	AVGSTVYYQGKCLTWKGP	E29	RRQLPAVVPAPLPPPCGS
D30	TVLLLRAGFYAVSFLSVA	E12	VGSTVYYQGKCLTWKGPR	E30	RQLPAVVPAPLPPPCGSS

8 Abbreviations

The table of abbreviations does not contain SI (internationally accepted standard) based units or SI derived units, the one and three letter amino acid code or metric prefixes.

Abbreviation	Description
E. coli	*Escherichia coli*
et al.	*et alii*
Pf EMP1	*Plasmodium falciparum* erythrocyte membrane protein 1
2D	2 dimensional
A	adenine
A_{max}	absorbance maximum
aa	amino acid
AcMNPV	*Autographa californica multicapsid nucleopolyhedrovirus*
ADCC	antibody-dependent cellular cytotoxicity
AML	acute myeloid leukemia
Amp	ampicillin
Amp^R	ampicillin resistence
APC	antigen presenting cell
APC	allophycocyanin
ATCC	American Type Culture Collection
B cell	lymphocyte that matures in the bone marrow
B_{max}	maximum number of binding sites
BAG-6	BCL2-associated anthanogene 6
BCL2	B cell lymphoma 2
BCR	B cell receptor
BEVS	baculovirus expression vector system
bp	base pair
BSA	bovine serum albumin
BV	budded virus
C	cytosine
CAM	chloramphenicole
CD	cluster of differentiation
CLSM	confocal laser scanning microscopy
CMV	cytomegalovirus
conjug.	conjugated
cSMAC	central supramolecular activation cluster
CTL	cytotoxic T lymphocyte

Abbreviation	Description
CTLA-4	cytotoxic T lymphocyte antigen 4
CV	column volume
DAMP	damage-associated molecular pattern
DAP	DNAX-activation protein
DAPI	4',6-diamidino-2-phenylindole
DB	dynabeads
DC	dendritic cell
DMEM	Dulbecco's modified Eagle medium
DMSO	dimethyl sulfoxide
DNA	deoxyribonucleic acid
ds	double-stranded
dSMAC	distal supramolecular activation cluster
DSMZ	*Deutsche Sammlung von Mikroorganismen und Zellkulturen*
DTT	dithiothreitol
ECACC	European Collection of Cell Cultures
ECL	enhanced chemoluminescence
EDTA	ethylene diamine tetra acetic acid
ELISA	enzyme-linked immunosorbent assay
EtBr	ethidium bromide
EtOH	ethyl alcohol
FACS	fluorescence activated cell sorting
FasL	Fas ligand
Fc	fragment, crystallizable
FCS	fetal calf serum
fig.	figure
FITC	fluorescein isothiocyanate
G	guanine
Gent	gentamycin
GFP	green fluorescent protein
GIST	gastrointestinal sarcoma
GlcNAc	*N*-Acetylglucosamine
Gln	L-glutamine
gp	glycoprotein
Grb2	growth factor receptor-bound protein 2
GST	glutathione S-transferase
HA	hemagglutinins
HCMV	human cytomegalovirus
HEK	human embryonic kidney
HEPES	4-(2-hydroxyethyl)-1-piperazineethanesulfonic acid
HGSIL	high grade squamous intraepithelial lesions
His-tag	deca-histidine tag

Abbreviation	Description
HIV	human immunodeficiency virus
HLA	human leukocyte antigen
HMW	high molecular weight
HPV	human papilloma virus
HRP	horseradish peroxidase
ICAM	intercellular adhesion molecule
iDC	immature dendritic cell
IFN	interferon
Ifnar2	type I interferon receptor 2
Ig	immunoglobulin
IL	interleukin
IMAC	immobilized metal ion affinity chromatography
IP	immunoprecipitation
IPTG	isopropyl β-D-1-thiogalactopyranoside
IRES	internal ribosome entry site
IS	immunological synapse
ITAM	immunoreceptor tyrosine-based activation motif
ITIM	immunoreceptor tyrosine-based inhibition motif
JAK	janus kinase
K_D	equilibrium binding constant
Kan	kanamycin
KIR	killer-cell immunoglobulin-like receptor
KLH	Keyhole Limpet Hemocyanin
LB	lysogeny broth
LBD	ligand binding domain
LBD_{tr}	truncated ligand binding domain
LFA	lymphocyte function-associated antigen
LILR	leukocyte Ig-like receptor
LMW	low molecular weight
mAb	monoclonal antibody
MAP	mitogen-activated protein
MBP	maltose binding protein
MEM	modified Eagle medium
MHC	major histocompatibility complex
MICA/B	MHC class I chain-related gene A/B
MLL5	mixed-lineage leukemia-5
MOPS	3-(N-morpholino)propanesulfonic acid
MTOC	microtubule organizing center
MW	molecular mass
MWCO	molecular weight-cut off
NCR	natural cytotoxicity receptor

Abbreviation	Description
NEAA	non-essential amino acids
NeuNAc	N-acetylneuraminic acid
NF-AT	nuclear factor of activated T cells
NK	natural killer
NKG	natural killer group
NKR	natural killer cell receptor
No.	number
NTA	nitrilotriacetic acid
ODV	occlusion-derived virus
opt	codon-optimized
p.a.	*pro analysi*
PAMP	pathogen-associated molecular pattern
PBMC	peripheral blood mononuclear cell
PBS	phosphate-buffered saline
PBS-T	PBS supplemented with Tween20
pCMV	promotor of cytomegalovirus
PCNA	proliferating cell nuclear antigen
PCR	polymerase chain reaction
PDB	protein data bank
PE	phycoerythrin
PEG	polyethylene glycole
PEI	polyethylenimine
Pen	penicillin
pep. immun.	peptide-immunized
PHYRE	**P**rotein **H**omology/Analog**Y** **R**ecognition **E**ngine
PI	protease inhibitor
PI3K	phosphatidylinositol-3-kinase
PKCθ	protein kinase C θ
PNGaseF	Peptide-*N*-Glycosidase F
polh	polyhedrin
polycl.	polyclonal
pRR	pattern recognition receptor
pSMAC	peripheral supramolecular activation cluster
PTM	post-translational modification
PTPRC	protein tyrosine phosphatase, receptor type, C
RNA	ribonucleic acid
RPMI	roswell park memorial institute medium
RT	room temperature
SDS	sodium dodecyl sulfate
SDS-PAGE	SDS polyacrylamide gel electrophoresis
SEC	size exclusion chromatography

Abbreviation	Description
SFFV	spleen focus forming virus
SH	Scr homology domain
SHP-1	SH-1-domain containing protein tyrosine phosphatase
Src	sarcoma
ss	single-stranded
STAT	signal transducers and activators of transcription
Strep	streptomycin
T	thymine
T cell	lymphocyte that matures in the thymus
T_{H1}	T helper cell of subtype 1
T_M	melting temperature
TA	Tobias Abel
tab.	table
TBS	Tris-buffered saline
TBS-T	TBS supplemented with Tween20
TCR	T cell receptor
TEM	molecular transmission electron microscopy
Tet	tetracyclin
TEV	tobacco etch virus
TFB	transformation buffer
TIRFM	total internal reflection fluorescence microscopy
TLR	toll-like receptor
TMB	3,3',5,5'-tetramethylbenzidine
TMD	transmembrane domain
TNF	tumor necrosis factor
TRAIL	TNF-related apoptosis-inducing ligand
Tris	tris(hydroxymethyl)aminomethane
ULBP	unique long 16-binding protein
ultracent.	ultracentrifuged
UV	ultraviolet
V_0	void volume
V_r	retention volume
v/v	volume per volume
Vol	volume
VSV-G	vesicular stomatitis virus
w/v	weigth per volume
wt	wild type
X-gal	5-bromo-4-chloro-3-indolyl-β-D-galactopyranoside
YFP	yellow fluorescent protein
ZAP-70	zeta-chain-associated protein kinase 70

9 Publications and Posters Presentations

9.1 Publications

Herrmann J, Berberich H, Hartmann J, Beyer S, Davies K and Koch J **(2014)** Homo-oligomerization of the activating natural killer cell receptor NKp30 ectodomain increases its binding affinity for cellular ligands. *J Biol Chem* 289(2):765-77.

Binici J, Hartmann J, **Herrmann J**, Schreiber C, Beyer S, Güler G, Vogel V, Tumulka F, Abele R, Mäntele W and Koch J **(2013)** A soluble fragment of the tumor antigen BCL2-associated athanogene 6 (BAG-6) is essential and sufficient for inhibition of NKp30 receptor-dependent cytotoxicity of natural killer cells. *J Biol Chem* 288(48):34295-303.

Hartmann J, Tran TV, Kaudeer J, Oberle K, **Herrmann J**, Quagliano I, Abel T, Cohnen A, Gatterdam V, Jacobs A, Wollscheid B, Tampé R, Watzl C, Diefenbach A and Koch J **(2012)** The stalk domain and the glycosylation status of the activating natural killer cell receptor NKp30 are important for ligand binding. *J Biol Chem* 287(37):31527-39.

Zhu X, De Laurentis W, Leang K, **Herrmann J**, Ihlefeld K, van Pée KH and Naismith JH **(2009)** Structural insights into regioselectivity in the enzymatic chlorination of tryptophan. *J Mol Biol* 391(1):74-85.

9.2 Poster Presentations

Herrmann J, Berberich H, Hartmann J, Beyer S, Davies K and Koch J **(2013)** Homo-oligomerization of the activating natural killer cell receptor NKp30 ectodomain increases its binding affinity for cellular ligands. *14th Meeting of the Society for Natural Immunity*, Heidelberg, Germany

Herrmann J, Berberich H, Hartmann J, Beyer S, Cohnen A, Watzl C and Koch J **(2012)** Investigation of the monovalent interaction of the human activating natural killer cell receptor NKp30 ectodomain (NKp30ECD) and its cellular ligand B7-H6. *Natural Killer Cell Symposium*, Heidelberg, Germany

Herrmann J, Berberich H, Hartmann J, Cohnen A, Watzl C and Koch J **(2012)** Insect cells to analyze the individual interaction between the human activating natural killer cell receptor NKp30 and its ligand B7H6. *14th Meeting of the Society for Natural Immunity*, Asilomar, USA

Herrmann J, Berberich H, Hartmann J, Cohnen A, Watzl C and Koch J **(2012)** Insect cells to analyze the individual interaction between the human activating natural killer cell receptor NKp30 and its ligand B7H6. *Perspectives in Cell- and Gene-Based Medicines*, Frankfurt am Main, Germany

Herrmann J, Berberich H, Hartmann J, Cohnen A, Watzl C and Koch J **(2011)** Generation of a functional monovalent ectodomain of the human NK cell receptor NKp30. *3rd UCT Science Day*, Frankfurt am Main, Germany

10 Acknowledgement

Danksagung

Mein Dank gilt all denjenigen, die durch ihre Anregungen und Unterstützung zum Erfolg meiner Dissertation beigetragen haben:

Professor Dr. Joachim Koch danke ich für die Möglichkeit, meine Doktorarbeit über dieses interessante Thema als eines der ersten Mitglieder seiner Arbeitsgruppe anfertigen zu können. Durch sein großes Engagement und die Vermittlung verschiedener Kooperationspartner durfte ich in den letzten Jahren viele neue Methoden erlernen. Weiterhin danke ich ihm für seine Unterstützung bei der Einarbeitung in das Fachgebiet Immunologie, seine ständige Diskussionsbereitschaft sowie für die Gelegenheit an der Teilnahme vieler spannender Fachtagungen, wodurch ich meinen Horizont stetig erweitern konnte.

Professorin Dr. Beatrix Süß und Professor Dr. Bodo Laube von der TU Darmstadt danke ich für die freundliche und unkomplizierte Übernahme der Begutachtung der vorliegenden Arbeit.

Ich bedanke mich bei all meinen Kooperationspartnern für die tatkräftige Unterstützung bei der Bearbeitung dieses Projekts. Mein besonderer Dank gilt dabei Dr. Imre Berger und Fred Garzoni für ihre Gastfreundschaft und wissenschaftliche Kompetenz. Die Einführung in das baculovirus-basierte Insektenzell-Expressionssystem sowie die freundliche Überlassung des MultiBac Systems machten die Anfertigung dieser Arbeit erst möglich. Weiterhin möchte ich mich bei Professor Dr. Carsten Watzl und André Cohnen für hilfreiche Tipps und vor allem für die Überlassung des B7-H6 Plasmids bedanken, wodurch dieses Projekt eine entscheidende Wendung nahm. Außerdem danke ich recht herzlich Dr. Karen Davies für die EM-Analysen der Oligomerpartikel.

Ich danke allen Mitarbeitern des Georg-Speyer-Hauses, insbesondere meinen Kollegen der Arbeitsgruppe Koch für das angenehme Arbeitsklima, die ständige Hilfsbereitschaft sowie für die hilfreichen fachlichen Diskussionen. Ganz besonders herzlich möchte ich mich bei Dr. Jessica Hartmann für die gemeinsamen Jahre während der Anfertigung unserer Doktorarbeiten und ihre andauernde Freundschaft bedanken. Ihr seid der Grund, warum ich in Phasen der tiefsten Verzweiflung nicht aufgab. Es war mir eine Freude mit euch zu arbeiten.

Ganz herzlich bedanke ich mich bei meinen Praktikanten Hannah Berberich, Viktoria Decker und Isabell Quagliano-Lo Coco, die mich bei der Durchführung der Experimente tatkräftig unterstützt haben. Ein großes Dankeschön geht dabei an Hannah Berberich für die Fachgespräche und dass sie dieses Projekt während der Anfertigung ihrer Diplomarbeit besonders vorangebracht hat.

Meiner gesamten Familie danke ich für ihre Liebe und ihr Vertrauen in mich, ihre ständige Unterstützung in allen Lebenslagen und besonders für ihr Verständnis, wenn diese Arbeit mal wieder Vorrang hatte.

Mein letzter Dank geht an meinen Freund Alexander für seine uneingeschränkte Unterstützung bei der Anfertigung dieser Arbeit, vor allem aber für seine Liebe und seine unendliche Geduld. Danke, dass du immer für mich da bist!

11 Curriculum Vitae

Der Lebenslauf ist in der Online-Verison aus Gründen des Datenschutzes nicht enthalten.

12 Declaration and Affidavit

Ehrenwörtliche Erklärung

Ich erkläre hiermit ehrenwörtlich, dass ich die vorliegende Arbeit entsprechend den Regeln guter wissenschaftlicher Praxis selbstständig und ohne unzulässige Hilfe Dritter angefertigt habe.

Sämtliche aus fremden Quellen direkt oder indirekt übernommenen Gedanken sowie sämtliche von Anderen direkt oder indirekt übernommenen Daten, Techniken und Materialien sind als solche kenntlich gemacht. Die Arbeit wurde bisher bei keiner anderen Hochschule zu Prüfungszwecken eingereicht.

Darmstadt, den 14. August 2014

Julia Herrmann